# Amine/microcrystalline cellulose interactions

Steele, David Fraser

*Award date:*
2002

*Awarding institution:*
University of Bath

# Amine / Microcrystalline Cellulose Interactions

Submitted by

David Fraser Steele B.Sc.(Hons), M.Phil., M.R.S.C.

for the degree of Doctor of Philosophy

of the University of Bath

October 2002







ProQuest LLC
789 East Eisenhower Parkway
P.O. Box 1346
Ann Arbor, MI 48106-1346

*To*

*Sarah Steele*

*and*

*my parents,*
*Bernard and Joan*

## Acknowledgements

First, thanks to my supervisors and those who brought the project together in the first place: Mike Tobyn, Colin Pouton, Anthony Smith and John Staniforth. Stephen Edge deserves a mention for nearly convincing me that polysaccharides could be interesting and for the music and movies banter. The plane was fine...

Thanks also to: Tim Smith and Ken Williams, Renishaw Ltd. (Raman); Gavin Ashton, Perkin-Elmer (DRIFT); David Apperley, University of Durham (SS NMR); Kevin Smith and Don Perry, Dept. Pharmacy & Pharmacology, University of Bath (FTIR); Dan Wolverson, Dept Physics, UoB (UV Raman); Barry Chapman, Dept Physics, UoB (XRD); Ursula Potter, Optical Electronics Group, UoB (SEM); Erin O'Brien, FMC Inc., Stefan Wohlrass, Rettenmaier GmbH. (MCC samples).

This project was funded by Penwest Co, Patterson, NY. Chris Moreton was a source of huge inspiration until he left the company. Afterwards, his shoes were filled by Bob Sherwood, David Schaible and Paul Woodcock at Patterson. Thanks also to Judy Brecht, Ivan Brinkman and the Cedar Rapids crew, for the factory tour and samples.

Special thanks to Edgey (again) for his solidarity, PY for his help with ecumenical matters and to Mo, Magic, Penny, Rachie, Bettina, Robbo and Dany for their friendship. Thank you to all members of the Pharmaceutical Technology Research Group, past and present. Thanks also to Hannah (Buffy fan) and Laura for admin and financial bobbins.

And, of course, huge thanks to my gorgeous wife, Sarah, for her constant love and support.

## Abstract

The effect of variables such as particle size, pulp source, pulping process and silicification of microcrystalline celluloses (MCCs) on the adsorption of an amine drug has been investigated. This adsorption has been shown to affect the *in vitro* analysis of medicines and possibly the bioavailability of such drugs. Previous work has also shown that different MCCs adsorb drugs to different extents.

Analysis of the physical and both bulk and surface chemistry of MCCs obtained from several manufacturers, as well as MCC grades differentiated by bulk density, particle size and inclusion of colloidal silicon dioxide, were used as part of the investigation into possible causes of the variability of adsorption.

Statistically significant differences were observed between the adsorption of tacrine by MCCs and derivative samples marketed as equivalent products and with pharmaceutically improved products. Analysis of adsorption isotherms indicates that this variation is due to different adsorptive capacities, as well as variation in the affinity of dissolved the model drug for the solid. An insight into the effect of manufacturing processes and pulp source can be obtained from these observations. Simple physical differences, for instance non-equivalence in particle size, were unable to explain observed differences. No clear correlation between surface energy and adsorption could be found. Batch to batch variation for selected materials was also quantified.

The capacity of a microcrystalline cellulose product to adsorb the model amine drug is shown to be a function of the route and method of manufacture. Pulp source and pulping processes also play a role in determining the adsorptive capacity of microcrystalline cellulose. Using this data is possible to recommend materials which will adsorb less drug and predict the adsorptive capacities of unknown materials.

## Contents

# 1. Introduction

## 1.1. Background

The adsorption of drugs by excipients during *in vitro* testing is a continuing concern in formulation science. As a result of its multifunctionality, microcrystalline cellulose (MCC) is widely used as an excipient in solid dosage forms; however, the adsorption of some drugs is a barrier to its wider use. Within the pharmaceutical industry it has been observed that drugs containing amine functionalities are prone to adsorption onto MCC, with <100% release observed during *in vitro* dissolution tests. Because MCC is not digestible, the reduced release implies that the total *in vivo* availability will be less than the amount of drug in the formulation.

Microcrystalline cellulose was patented by Battista et al (1961) and was introduced as a pharmaceutical excipient in the US National Formulary in 1966 under the trade name 'Avicel'. Since 1980, there has been an increase in the number of manufacturers marketing pharmaceutical grade MCC. It has been shown that the differences in the source of pulp and the characteristics of the manufacturing processes used result in significant intermanufacturer variations in the observed functionalities of the MCCs (Doelker et al, 1987; Dittgen et al, 1993; Maincent, 1999; Wu et al, 2001). Functionality variations between grades (Doelker, 1993) and between batches (Landín et al, 1993b,c; Rowe et al, 1994) of MCCs have also been reported.

Furthermore, there is an observed variability in the adsorption of drugs by MCCs supplied by different manufacturers (Dittgen et al, 1993; Landín et al, 1993a; Podczeck & Révész, 1993; Iida et al, 1997). This suggests that adsorption depends on certain aspects of MCC manufacture which have not previously been fully elucidated. On the basis of these findings, MCCs supplied by different manufacturers may not be fully interchangeable.

Microcrystalline cellulose is the β-1,4 linked polymer of D-glucopyranose, partially depolymerised to yield a product with a mean degree of polymerisation between 150 and 250. For pharmaceutical grade MCC products, the most commonly used raw material is high-quality timber pulp, as used in paper manufacture. The pulp feedstock is acid depolymerised, neutralised and the resulting slurry is dried to yield

aggregates of MCC fibrils with a volume diameter mean particle size in the range 40 – 200μm.

With this in mind, it is desirable to be able to understand the nature of the interactions between amines and MCC. In order to achieve this, it is necessary to be able to characterise the bulk and surface properties of MCC samples so that differences can be quantified. From the information provided by these analyses a change in MCC grade or supplier may be recommended during formulation. There is also the potential to develop speciality grades for a particular formulation if the compactibility and adsorption of MCC can be controlled and predicted.

The initial approach will be to observe the effect of bulk and surface characteristics on adsorption. Since this approach may be seen as phenomenological in nature, it is also desirable to obtain explicit details on the physical organic chemistry behind the observed interactions. This will assist in tailoring production of MCCs to specific requirements as well as providing a more scientific explanation for the variation in adsorption between MCCs.

The experimental work will involve obtaining MCC samples from several suppliers, characterising the samples for physical and chemical characteristics and then determining the nature and degree of the adsorption of selected amine drugs.

## 1.2. Drug – excipient interactions

Excipients are ingredients added to formulations to assist manufacture. They can provide protection for the active ingredient, aid delivery and improve patient compliance. As part of the work involved in formulating medicines it is necessary to assess the potential for drug – excipient interactions which may affect the stability, solubility, release rate, dissolution and bioavailability of the active drug and formulation (Monkhouse, 1984; Al-Nimry et al, 1997). These interactions are not always detrimental in nature (Crowley, 1999; Kalikanova, 1999) and may be designed in to the formulation.

### *1.2.1. Microcrystalline cellulose as a pharmaceutical excipient*

Microcrystalline cellulose is described as an adsorbant, disintegrant, filler, binder, suspending agent and compaction aid (Kibbe, 2000), and is also used as a flow

enhancement agent for nasal spray delivery (Nagai et al, 1984; Garcia-Areita et al, 2001). For the production of tablets, the multifunctionality of MCC may be exploited, allowing simple dosage forms for direct compression to be formulated with MCC as the only excipient other than possible addition of a lubricant.

Although MCC is a preferred excipient for tabletting (Celik, 1996) it does have disadvantages that prevent its universal use. Due to the extensive hydrogen bonding capability, cellulose is hygroscopic in nature, normally containing 2 - 6% by weight water, which can make it unsuitable for use in conjunction with moisture sensitive drugs. A significant decrease in compactibility has been reported during aqueous wet granulation on drying of the powder mass (Sherwood & Becker, 1998). This loss in functionality has been attributed to a decrease in the water retention capacity of the material (Staniforth & Chatrath, 1996). This is referred to as hornification in the pulp and paper industry and is a result of increased hydrogen bonding between the fibrils in cellulosic material (Weise, 1998). The hydrogen bonding capacity of cellulose is a desirable characteristic of the chemistry of the material, contributing to the bulk physical properties of microcrystalline cellulose materials as well as contributing to the surface chemistry of the product.

This work will concentrate on the adsorptive capacity of MCC, which may be an undesirable property for the majority of pharmaceutical applications. The ability of MCC to adsorb and absorb is a consequence of its surface and bulk chemistry, which in turn may be affected by a number of factors:

*Particle size and surface area:* The specific surface area (area per unit mass), and hence the number of adsorbing sites available, increases as the mean particle size decreases for monolithic materials. Some previous studies have shown an increase in adsorption for MCC grades with smaller particle size (El-Samaligy et al, 1986). The roughness of a surface determines the surface area available for adsorption;

*Porosity:* Pore size distribution is linked to the surface area and may also affect adsorption and desorption rates. Increased tortuosity of the pores in the material will act as a physical retardant to drug release. Small pores, accessible to gaseous probes, may act as steric barriers to drugs of large molecular size;

*Crystal structure:* There are two naturally occurring polymorphs of cellulose, cellulose Iα and cellulose Iβ (Atalla & van der Hart, 1984). In cellulose 1α, the adjacent glucoside chains are parallel, whereas in cellulose 1β the chains are antiparallel. Cellulose II is produced by the action of strong alkaline solutions on either cellulose I polymorph (Raymond et al, 1995). Modelling of the energy profiles of the crystal structure (Sarko, 1976) indicates that cellulose Iα is the most energetic and cellulose II the least energetic and therefore most stable. It is likely, therefore, that the adsorption characteristics of these polymorphs will be different;

*Crystallinity:* Microcrystalline cellulose consists of microcrystals of cellulose linked and hinged with amorphous regions. A balance between the crystalline and amorphous regions, and control of the crystal structures present, are important factors in the production of MCC to conform to Pharmacopoeial requirements. There is evidence that the amorphous content affects both compaction (Suzuki & Nakagami, 1999; Wu et al, 2001) and adsorption, with higher adsorption occurring in more amorphous MCC materials (Nakai et al, 1977). Low crystallinity celluloses were found to be more ductile than standard MCC grades and produced generally weaker tablets (Kumar et al, 2001). For adsorption the more disordered, higher energy amorphous structure has a drive to reduce energy and entropy and so will tend to adsorb more readily;

*Surface energy:* The surface energy of a material depends on both the surface chemistry and the morphology of the surface. Higher energy surfaces are more likely to adsorb molecules from solution. Surface energy may be expressed in terms of the solubility parameter, a function of the cohesive energy density (CED), a measure of the forces that bind together the particles in a system. The solubility parameter is a function of the surface energies due to dispersion (van der Waals' dipolar interactions), polarity and hydrogen bonding capacities. The CED parameter is also of interest in the field of adhesion (Papirer et al, 2000) and compaction technology (Roberts et al, 1991; Roberts & Rowe, 1993) since the CED may be used to quantify particle-particle interactions (Rowe, 1988).

*Degree of polymerisation*: The mean degree of polymerisation (DP) is the number of single glucose units in each chain (see Figure 1.1). The original patent upon which the commercial product is based (Battista et al, 1961) describes the material

on the basis of its DP. In natural cellulose in the cell walls of higher plants a mean DP of up to 10 000 may be found (Krässig, 1993). In the manufacture of MCC, a DP of below 300 is normally achieved by acid depolymerisation using $FeCl_3$ dissolved in sulphuric acid or hydrochloric acid (Battista et al, 1966). This attacks the non-crystalline regions, producing soluble short-chain glucose polymers, raising the crystallinity of the remaining material (see Figure 1.2).

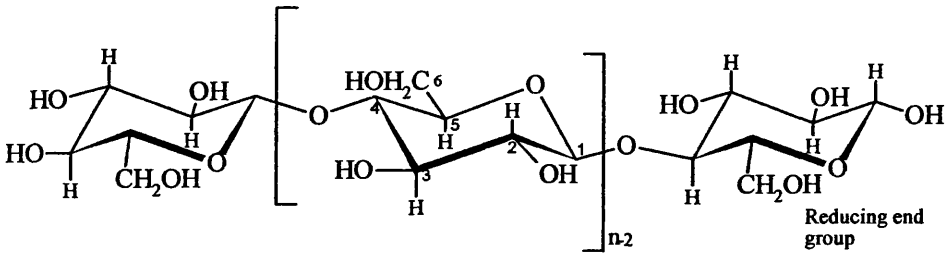


Figure 1.1. Conformational structure of cellulose. The degree of polymerisation, *n*, is the number of glucose residues in a single chain.

Non-commercial low-DP softwood based celluloses have been produced and investigated (Wei et al, 1996; Kumar et al, 2002). A DP 50 to 60 units lower than standard MCC was produced by the action of ≥5 N sodium hydroxide on cotton linter. The product so obtained was found to be less ductile and produced weaker tablets than standard MCC, but had improved disintegration properties. However, the action of the sodium hydroxide solution caused a change in the crystal structure of the low DP material to Cellulose II from predominantly Cellulose Iβ (Kumar et al, 2002). Therefore, any variation ascribed to the lower DP may be a function of the different crystal structures.

### 1.3. Adsorption and interaction studies

Solution phase interactions between compounds of interest and polysaccharide substrates are of interest in both the pharmaceutical and dye industries. Despite the fact that the dye industry is keen to promote irreversible adsorption, in contrast to the general preference in the pharmaceutical industry for minimal adsorption, techniques

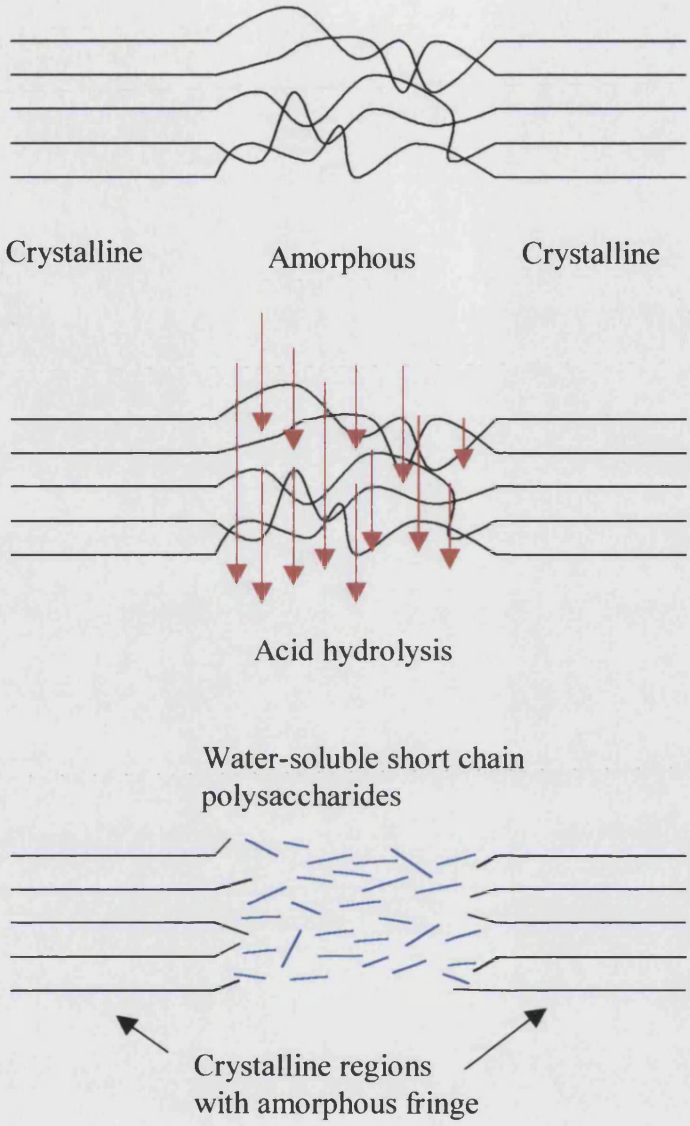


Figure 1.2. Representation of decrease in net mass and increase in crystallinity of cellulose as a result of acid depolymersiation. The acid attacks the amorphous regions, leaving short chain glucose polymers which are removed after neutralisation by washing. Some amorphous content is retained where an amorphous fringe is left after depolymerisation. Diagram after Battista (1950).

developed for investigation of dye-cotton interaction can be transferred to investigate drug-MCC interactions.

Many methodologies are used in the dye and textile industries to assess the efficiency of dye sorption on fabrics. Fast screening of dyes and textiles is possible using a technique based on the principles of liquid chromatography (Ladisch et al, 1992). A textile sample is used as the stationary phase in a column and a concentration gradient of the absorbent under investigation is initiated. This solvent front technique allows faster screening of dyes than can be achieved using the standard batchwise investigations. However, the pumping pressures used in these studies may cause compaction of MCC samples, since MCC is designed to compact readily. Standard HPLC pumps can exert a pressure of 5 kPa. This pressure is too low to form coherent compacts by a factor of over 1000 (Adolfsson et al, 1999), but a levelling-off degree of space filling is evident from the standard tapped density experiments to assess flowability (Carr, 1965; see Chapter 2). Depending on the exact dimensions of the vessel used in the tapped density measurement and the amount of sample used, pressures of up to 400 Pa may be exerted on the powder at the bottom of the vessel. This pressure is sufficient to form dry compacted masses that are difficult to remove from the vessel for some MCCs. It follows, therefore, that higher pressures will also form dense masses. Compaction and the inherent densification of the stationary phase will affect the headspace and bed porosity. This will change the column characteristics during the experiment, resulting in the generation of inconsistent data. Without a potentially lengthy investigation into the behaviour of MCCs under these conditions, it is not feasible to utilise an 'inverse HPLC' method to study drug - MCC interactions.

The principal technique used in this study is the determination of adsorption isotherms. A known mass of solid is equilibrated with a range of solutions of known concentrations of the species of interest. Extraction of the supernatant allows the relationship between the equilibrium concentration and the amount adsorbed to be determined. By analysis of these data, information about the interaction can be obtained.

Other solution phase work, including the determination of the rate at which equilibrium is reached and the dependence of adsorption on temperature, will yield further data for comparing solids and adsorbates quantitatively.

## 1.4. Structure of cellulose and MCC

Cellulose is the most abundant organic chemical in the biosphere (Vincent, 1999). It is the major constituent of the cell walls of all higher plants. A brief summary of the structures of cellulose will be presented here. More detailed discussions are available (e.g. Krässig, 1993; Vincent, 1999). Cellulose structure may be divided into three parts: molecular (composition of the polysaccharide chain), supermolecular (crystal structure and fibril dimensions) and morphological (fibrillar aggregation and cell wall structure).

### *1.4.1. Molecular structure*

There are three hydroxyl groups on each glucose unit, one primary (C6) and two secondary (C2 and C3), all of which are available for hydrogen bonding. The long chains of glucose connected by β–1,4 links are linear and not branched. This allows for increased inter- and intra-chain hydrogen bonding (Krässig, 1993) and gives cellulose a more rigid structure compared with other glucose based, highly branched polysaccharides such as amylose and amylopectin. As well as giving strength to the structure, the extended hydrogen bonding also prevents the dissolution of cellulose in any but the strongest solvents (Garnier & Glasser, 1994; Isogai & Atalla, 1998).

During the manufacture of MCC the material is depolymerised in highly acidic conditions at temperatures of 105 to 145°C for 16 to 60 minutes, depending on the pulp characteristics. This causes oxidation of the hydroxyl groups in the surface which means that the surface of processed MCC is acidic, with carboxyl groups available for ion exchange resulting a pKa of approximately 4 (Krässig, 1993). This is in contrast to glucose, which has a pKa of approximately 12 (Jover et al, 1996), as would be anticipated for a molecule with three hydroxyl groups.

### *1.4.2. Supermolecular structure*

Cellulose has a tendency to form highly organised regions within plant cell walls due to the hydrogen bonding capacity of the molecule. The paracrystalline regions

formed are weakly detectable by X-ray diffractometry in wood pulp, consisting of crystalline regions surrounded by less structured amorphous regions. In nature, chains of cellulose within cell walls pass through both crystalline and amorphous regions.

During processing to obtain MCC the polymer chains are hydrolysed primarily in the amorphous regions (Krässig, 1993). Hydrolysis leaves water-soluble glucose and cellobiose and insoluble microcrystals surrounded and hinged together by much reduced amorphous regions (Figure 1.2). The insoluble residue is of a higher crystallinity than the raw material.

The crystal structure of cellulose is dependent on the conformation of adjacent chains, which in turn is determined by interchain hydrogen bonding. Two allomorphs of cellulose I, the native polymorph, are recognised (Atalla & van der Hart, 1984). Cellulose Iα is the major cellulosic constituent of bacterial cell walls and has a triclinic unit cell. Cellulose Iβ is generally found in higher plants and is monoclinic, differing from cellulose 1α in the alignment of the adjacent cellulose chains. Treatment with strong basic solutions (mercerisation) can break the interchain hydrogen bonds, resulting in the lower energy form, cellulose II (Raymond et al, 1995). This is also a monoclinic structure with the alignment and orientation of the cellulose chains altered to a near minimum energy configuration (Krässig, 1993). The crystal structure affects both the adsorption capacity and the compactibility of the product (Landín et al, 1993a).

### *1.4.3. Morphological structure*

The microscopic structure of MCC powder is a function of the nature of the plant from which the material is manufactured. One of the most important distinctions made between timber sources is that between softwood (coniferous) and hardwood (deciduous) trees. The cellular structure of hardwood trees differs from that of softwood trees (Dinwoodie, 2000). In timber, the cells fill three functions. Thin-walled parenchyma cells store energy as carbohydrates in both hardwood and softwood trees. Support and conduction (transfer of water and minerals) are both functions of thicker-walled tracheids in softwood trees. Softwood tracheid cells vary in cross-sectional size as a function of species and climate, with radii in the range 10

to 60 μm, with cell wall thicknesses between 1 and 8 μm (Savin, 2001). In hardwood trees, tracheid cells are relatively uncommon, support of the tree structure being carried out by very thick-walled fibre cells (10 – 30 μm radius, 1 – 11 μm cell wall thickness (Bodig & Jayne, 1993)). Conduction is carried out by wide, thin-walled vessels in hardwood trees. The density of hardwood timbers is generally higher than that of softwoods.

On pulping, the contribution of the parenchyma and vessels to the porosity of the intact timber is lost; the harsh mechanical processing destroys the thin cell walls. This leaves the tracheid and fibre cells in the softwood and hardwood pulps. Evidence from nitrogen sorption porosimetry suggests that softwood MCCs (Avicel brand) suggests that some porosity due to the plant cell structure remains (Marshall et al, 1972; Westermarck et al, 1999). These pores, in the diameter range 2.5 to 5 nm, will impart a straw-like structure on the MCC particles. An alternative model, that multiple small pores impart a sponge-like morphology to MCC, has been suggested (Ek & Newton, 1998).

As a result of the greater porosity of the tracheid cells, softwood pulp is less dense than hardwood pulp. Microcrystalline celluloses from hardwood trees therefore exhibit a higher bulk density as a result of the relative paucity of capillaries in the cell walls of deciduous trees and a resultant decrease in the porosity of the extracted cellulose portion. Variations in the pulping processes used for softwood and hardwood timber may also have an effect on the final morphology.

### *1.4.4. Manufacture of microcrystalline cellulose*

The timber pulp used as the primary feedstock for the manufacture of pharmaceutical MCC is the same material used in papermaking. The relative density of the timbers can distinguish between softwood and hardwood sources. There is also a distinct difference between the chemistry of the two pulps. Hemicellulose types are significantly different; the ratios of xylose, mannose and arabinose in fully hydrolysed samples are used to discriminate between the two types (Landín et al, 1993a), since the biosynthetic routes for tracheid and fibre cells are different.

Bleaching and mashing of the raw timber removes most of the coloured and 'woody' parts of the timber including lignin, starches and sugars. Previous regulations

permitted the use of chlorite bleaches, but this was phased out with effect from November 2000, in accordance with the Montreal Protocol (1987; 2000), in order to reduce chlorocarbon emissions. This change could affect the characteristics of the resultant MCC product. Trial MCCs manufactured using steam explosion pulps, an alternative to chlorite bleaching, will be investigated along with other commercially available MCCs produced using traditional bleaching methods.

The route used by Penwest Co. (USA) for the manufacture of MCC from the initial pulp feedstock is summarised in Figure 1.3. Processing after the pulp stage involves hot acid hydrolysis using ferric chloride dissolved in 2 to 3 N hydrochloric or sulphuric acid to depolymerise the cellulose, resulting in a product with a mean degree of polymerisation (number of glucose units per chain) of 140 to 300. This is referred to as the level-off degree of polymerisation (Battista, 1950). This is followed by washing and a neutralisation stage using ammonium chloride or other suitable alkaline solution to remove salts and soluble mono and disaccharides released during the acid hydrolysis. Control of the final drying stage, commonly spray- or rotary-drying, yields material of the desired particle size and moisture content.

The method described above is the most common means used to produce commercial grades of MCC. The physical and granulation properties of an experimental MCC manufactured using bacterial culture (Axcent 4000, ICI Ltd, UK) have been investigated (Parker & Rowe, 1991).

Although timber pulp is the preferred source of cellulose for the production of MCC, products suitable for pharmaceutical use have been produced from food waste products such as sugar cane bagasse (Padmadisastra & Gonda, 1989) and soybean husks (Uesu et al, 2000). These lower price feedstocks may be prone to greater variability in functionality as a result of annual or seasonal variations in growing conditions. Such variations are less of a concern for timber-derived MCCs, since the pulp quality will not be as significantly affected by a single year's conditions.

### *1.4.5. Microcrystalline cellulose derivatives*

As mentioned previously there are some problems associated with the use of microcrystalline cellulose (MCC), especially the loss in compactibility during wet

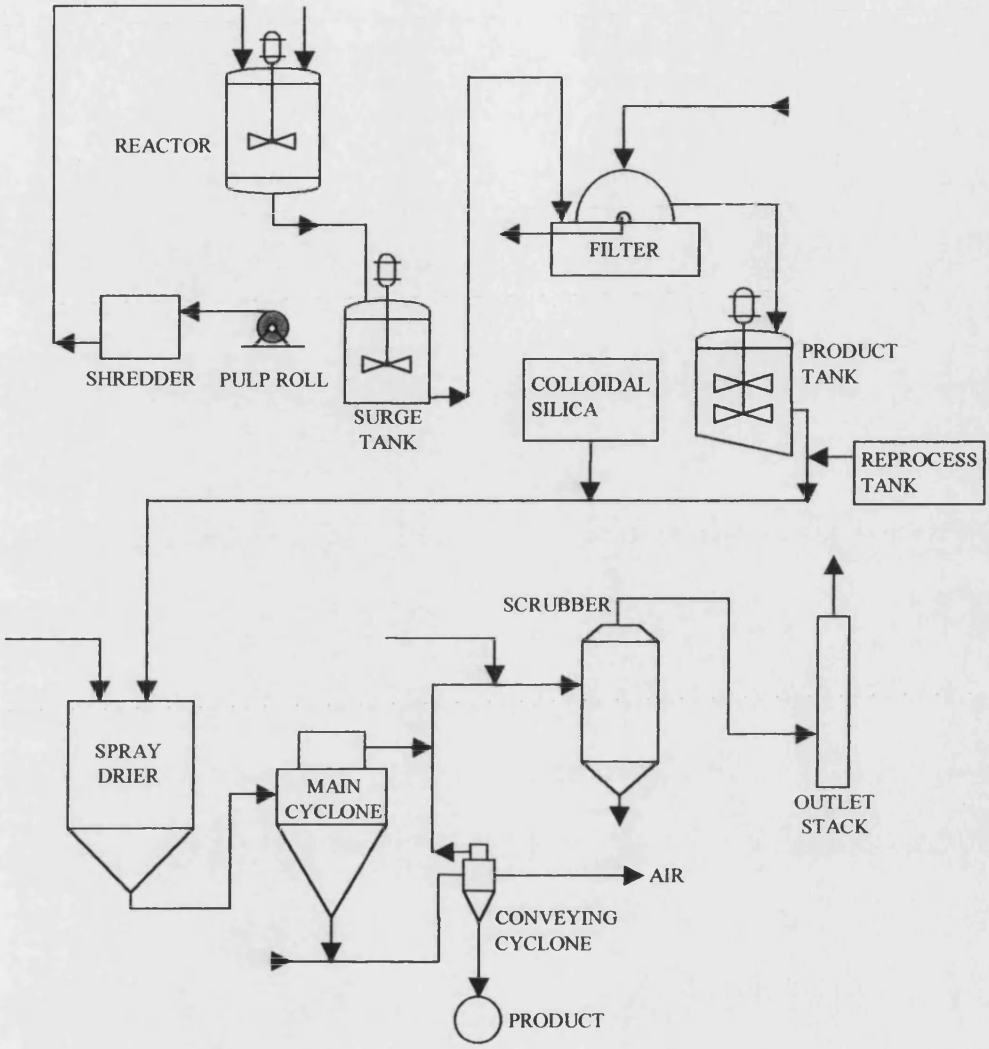


Figure 1.3. Process flow diagram for the production of MCC. The addition of colloidal silica leads to the production of silicified MCC. Diagram reproduced by permission; © Penwest Co., Cedar Rapids, IO, USA.

granulation. Silicified microcrystalline cellulose (SMCC) is a relatively new product designed to be less prone to loss of compactibility due to hornification (Sherwood & Becker, 1998). Hornification is the collapse of the surface hydrogen bonding structure in cellulosic materials (Weise, 1998), resulting in the formation of a hard 'shark skin' surface, which has a reduced water penetration capacity. Materials that have been affected in this way have a reduced elasticity and compactibility.

The introduction of 2% w/w colloidal silicon dioxide into the neutralised cellulose pulp prior to spray-drying results in the production of a material with improved compaction properties (Sherwood & Becker, 1998; Edge et al, 2000). Tobyn et al (1998) showed that there are few discernible differences in the polymorphic or chemical properties of SMCC compared with MCC. MCC and SMCC have comparable particle size distributions and similar infrared spectra, X-ray diffraction spectra and $^{13}C$ SS NMR spectra, which indicate a close similarity in the crystal structures of the two materials. The main exception to the polymorphic similarity is an increased surface area measured for SMCC due to the presence of silicon dioxide in the surface of the material (Edge et al, 1999). Differences in the chemical and compaction properties of these two materials are therefore most likely to be a result of the presence of silicon dioxide in the material.

SMCC is also less sensitive to hydrophobic lubricants such as magnesium stearate (Sherwood & Becker, 1998; Edge et al, 2000). The development of lubricant films over the surface of MCC during mixing precludes MCC particle-particle cohesion, thus hindering the formation of interparticle hydrogen bonds and so reducing the compactibility of the formulation. Variations in the lubricant sensitivity of materials are general indications of differences in the surface properties (Rowe, 1988). The most obvious difference is the presence of silicon dioxide particles intimately associated with the surface of SMCC (Edge et al, 1999).

Since it is clear from this evidence that SMCC possesses different surface properties from MCC, it is desirable, within the context of this work, to study the effect that this surface change has on the adsorption of amines. Therefore, SMCC samples will be studied alongside the standard MCC products to gain additional data for this study.

## 1.5. *In vitro* testing

The dissolution test is one of the standard tests conducted to ensure that a dosage form complies with standards set out in the British Pharmacopoeia (BP). This test provides data describing drug release against time and therefore shows not only the total release, but also release rate. During the test the dosage form under investigation is placed in a thermostatically heated fluid, usually maintained at 37.5°C. Artificial gastric fluids, buffered solutions at pH 2.1 and degassed water are commonly used fluids. In order to comply with BP requirements, agitation of the fluid is required. This may take the form of paddles, spinning basket or vertical agitation of the fluid bath.

## 1.6. *In vitro - in vivo* correlation

The reliability of *in vitro* testing methods in predicting the *in vivo* behaviour is a fundamental concern in formulation science. In the UK, the Animals (Scientific Procedures) Act (1986) requires that animal-based experimentation be kept to a minimum. Therefore, it is not possible to screen all formulations using *in vivo* methods during development. Consequently, a great deal of reliance is placed on *in vitro* methods, which are designed either to mimic the processes undergone by the dosage form when it is used (e.g. tablet dissolution tests) or to provide data that may be used to determine whether the dosage form passes certain minimum requirements (e.g. aerodynamic particle size determined by the twin stage impinger).

In this study the primary concern is the reduction in apparent bioavailability of drugs during dissolution testing. The dissolution test will be discussed more fully in Chapter 3, but a brief summary here will serve to explain where *in vitro – in vivo* correlation may break down. During dissolution tests carried out in accordance with BP and USP recommendations the dosage form under investigation is placed in an agitated bath of suitable medium at 37.5°C. At specified time intervals aliquots of the medium are extracted and the drug concentration determined by a suitable method, normally UV absorption or fluorescence. The main contrast between this technique and the situation *in vivo* is the static nature of the *in vitro* method. During systemic delivery, the dosage form, or its disintegrated components, passes through regions where the drug is absorbed by the body. The reduction in the drug concentration caused by the absorption will drive the system to re-establish

equilibrium, normally by releasing more drug. As mentioned previously, this will result in a greater *in vivo* release compared with static *in vitro* tests. Nevertheless, some reduction in the bioavailability may be anticipated, since a greater percentage of the available adsorbate is adsorbed at low concentrations. Therefore, when the dosage form leaves the absorption site there may still be a significant amount of drug adsorbed.

### 1.7. Adsorption theory - summary

Adsorption is the binding of a foreign molecule onto a solid surface. This process differs from absorption since the binding or capture only occurs at the surface of the solid in adsorption, rather than the foreign molecule penetrating the surface. Adsorption is most conveniently regarded as a static process, wherein the adsorbed molecule is captured in the surface of the adsorbate and remains there for the duration of the experiment. This view of the adsorption process is not the actual situation, since each molecule is temporarily bound to the solid surface and a dynamic equilibrium is established. The binding causes a net reduction in the concentration of the adsorbent in the surrounding matrix. This reduction in concentration is a function of the time each adsorbed moiety remains at the adsorption site.

The temporary nature of the adsorption process is used in the Langmuir (1918) treatment of the adsorption process. Adsorption is taken to occur at specific sites on the surface of the adsorbate. This wholly theoretical treatment of adsorption processes assumes that all adsorption sites are equally energetic and that occupation of a site does not affect the adsorption capabilities of adjacent sites.

Chromatographic techniques exploit the temporary nature of adsorption along with the fact that adsorption between a substrate and the analytes is a function of the molecular structure of the analytes. The interactions between the analytes, the solid phase and the mobile phase determine the retention time of the analyte.

The study and characterisation of the adsorption of foreign materials onto cellulosic materials such as cotton and rayon (wood-pulp derived cellulose) is of great interest in the dying industry. Principals and techniques used in the study of dye-cellulose interactions are suitable for the study of drug-cellulose interactions. For

pharmaceutical applications, the focus is on reducing the interaction to improve delivery of the drug, whereas in the dye industry to drive is the increase interaction as a means to improve dying efficiency and improve the economy of the process.

Structure – affinity studies are of interest in both the dye and pharmaceutics industries. Excellent colour control and efficient uptake are required for dying of materials. The chemical structure of pharmaceuticals is of primary consideration, since this determines the pharmacology of the chemical. It is not, therefore, possible to alter the structure of a drug in order to decrease adsorption, since a different drug with different activity will be formed. A change at a single chiral centre may have little effect on the colour or absorptivity of a chemical, but will alter the pharmacology. Well-known examples include thalidomide, warfarin, and darvon/ novrad, where a change in the chirality of the drug results in a teratogen, a pharmaceutically inactive compound and drugs with different applications, respectively.

Cellulose has been used as a stationary phase for chiral separation in electrophoresis (Huynh et al, 1994). Substituting the hydroxyl groups in the cellulose structure for acetates amplifies the chirality of cellulose and reduces the pressure sensitivity of the material sufficiently for cellulose acetate to be used as a chiral separation stationary phase in high performance liquid chromatography (HPLC) (Hesse & Hagel, 1976; Lindner & Maanschreck, 1980), usually bonded to a silica support in commercial columns.

The study of the dependence of the degree of adsorption on the equilibrium concentration of a solute will form the basis of much of the data collected and discussed in this work (Chapter 3). From such studies, the nature of the adsorption may be determined; factors such as whether the adsorption is mono- or multi-layer over the concentration range studied, the monolayer capacity, and the amount lost to adsorption at a given initial concentration for a given mass may be determined from the data obtained. In addition, the relative affinity of a solid for the solute can be determined and, by performing adsorption studies over a range of temperatures, thermodynamic information may be obtained which will confirm the nature of the adsorption process.

## 1.8. Summary of approach

Characterisation of the physical and chemical nature of the MCCs under investigation is desirable in order to determine whether a link between adsorption and any of the parameters measured exists. The physical characterisation of the MCCs is summarised in Chapter 2. Parameters investigated are: particle size distribution, surface area, porosity and morphology.

The initial aim of this project is to demonstrate differences between MCC products from different manufacturers and MCCs manufactured from different pulp sources. The adsorption studies to be carried out (Chapter 3) will complement previous studies of the adsorption of drugs onto MCC (e.g. Dittgen et al, 1993; Landín et al, 1993a,b,c). This study will expand on these previous studies by using a systematic approach to the relationship between the physical characteristics and chemistry of MCCs and their adsorption of a model amine drug. Experimental grades and MCCs produced from non-chlorite pulps will also be examined. Based on the data from the adsorption studies, an investigation into the effect of the choice of MCC on the *in vitro* drug release of model formulations was undertaken.

In Chapter 4, the crystal structure of the MCCs is explored using X-ray diffractometry, vibrational spectroscopy and solid-state nuclear magnetic resonance spectroscopy (SS NMR). Also, the available carboxyl content of cellulose can be determined by titration to quantify the sites available for ion-exchange interaction and the sugars contents of the MCC can be determined to enable the initial source of the cellulose pulp to be determined. Limitations were placed on the number of some of the chemical characterisation experiments. Not all the techniques were readily available, so samples were selected for analysis with attention being paid to which parameters were shown to be of importance in the aqueous adsorption studies in Chapter 3. A benchmark 'standard' MCC, plus a high density and a silicified MCC were selected as minimum required for such tests. Raman spectroscopy was restricted to these three parameters.

Since adsorption is a surface and interface phenomenon, further characterisation of the surface of MCCs is desirable. To this end, the surface energy, a measure of the stability and reactivity of the surface, of MCC is investigated in Chapter 5. A

comparison of two techniques generally used to determine surface energetics is included in this chapter.

# 2. Physical Characterisation of Microcrystalline Cellulose

## 2.1. Introduction

One of the principal factors known to govern the adsorption capacity of a material is the available surface area. For monolithic materials the specific surface area is inversely proportional to the square of the particle size. Hence, it might be expected that, weight for weight, smaller particle size microcrystalline celluloses (MCCs) will adsorb more of a drug than an otherwise identical MCC.

Many MCCs are marketed on the basis of the mean particle size. Increasing particle size generally improves the flowability of a material, but can lead to poorer compactibility (Doelker et al, 1987) and, in some cases, mixing performance (Swaminathan & Kildsig, 2002) in MCC.

As discussed in Chapter 1, the physical characteristics of samples are important factors to be considered when examining the differences in the adsorption of amines by various MCCs. A difference in the degree of adsorption may be explicable simply in terms of a variation in the surface area of the samples. Five parameters are discussed, with partial data available for some techniques: particle size distribution, surface area, flowability, scanning electron microscopy and pore size distribution.

### *2.1.1. Particle size distribution analysis*

The determination of particle size distribution for samples with particles in the size range 1 to 500 μm may be achieved by a number of techniques. These include sieve analysis, image analysis, time-of-flight determination, mercury porosimetry, sedimentation rate and low angle laser scattering. In this study, the method of choice is that of low angle laser light scattering (LALLS; see Figure 2.1). This is preferred over the other techniques because it is quick, requires a small amount of sample, is not morphology biased and the technique is reproducible for MCC samples in the size range being examined. This is also the technique used by some MCC manufacturers, who use the data to blend size-specific batches and for final characterisation of the batch as given in the product data sheet.

Particle size distribution (Figure 2.2) is obtained through the analysis of the scattering of monochromatic, collimated light by a particle or group of particles. This scattering is described by Mie theory, wherein the diffraction of monochromatic

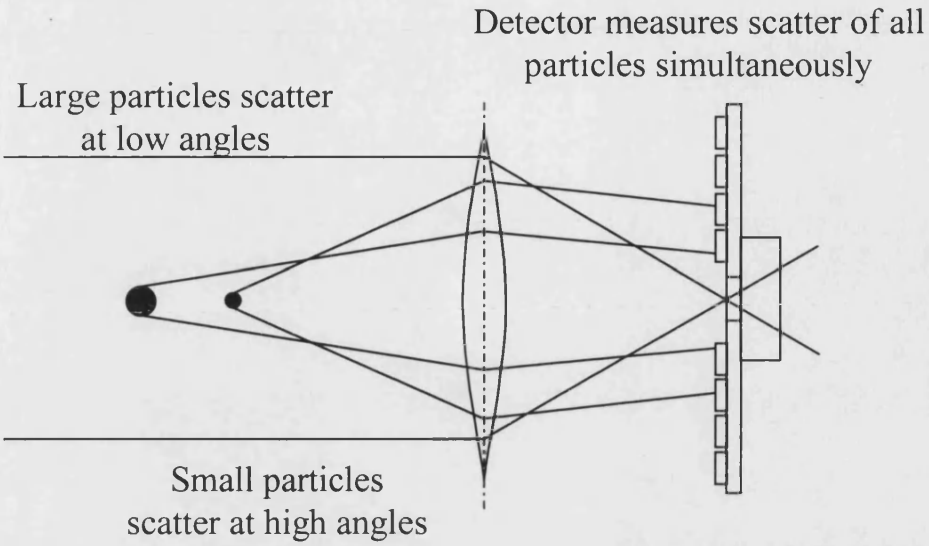


Figure 2.1. Particle size determination by Low Angle Laser Light Scattering (LALLS). The detector array is positioned so that the laser is focussed on its central detector. Concentric detectors on the array yield a diffraction pattern which is deconvoluted to give a projected particle size distribution.

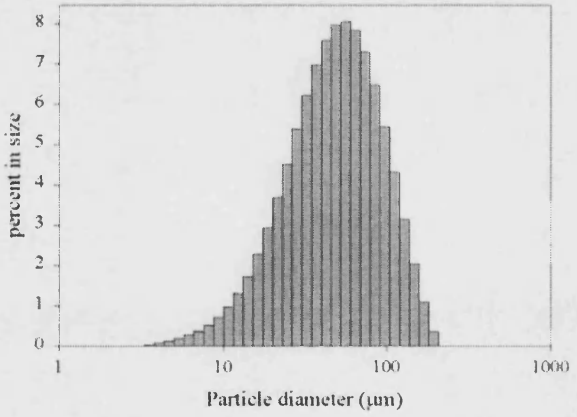


Figure 2.2. Typical particle size distribution histogram obtained by LALLS method.

radiation by particles occurs in a similar manner to Bragg scattering of X-radiation in crystals. According to Mie theory, the scattering is caused by the difference between the refractive indices of the particle and the surrounding medium. The scattering pattern obtained depends on the size of the particle and the wavelength of the light. The particle size determined is the equivalent volume sphere, that is, the radius of a spherical particle of the same volume as the particle analysed.

In practice, samples with a range of particle sizes are presented for analysis. The scatter pattern detected is therefore a summation of the scatter caused by each particle in the sample. The particle size distribution reported is the best fit to an ideal particle size distribution approximated by the measured pattern.

*2.1.2. Surface area by gas adsorption*

Gas adsorption may be used to measure the surface area of materials by condensing the gas onto the surface and determining the amount adsorbed in the monolayer. For a gas of known molecular cross sectional area, the amount adsorbed can easily be converted into a surface area. Measuring the amount of gas adsorbed over a range of relative pressures will enable the monolayer coverage to be determined via the Brunauer, Emmett and Teller (BET) equation (Brunauer et al, 1938). In its linear form the BET equation is:

$$\frac{z}{n(1-z)} = \frac{1}{n_m C} + z\left(\frac{C-1}{n_m C}\right) \qquad \text{Equation 2.1}$$

where $z$ is the relative partial pressure, $n$ is the amount of gas adsorbed at relative pressure $z$, $n_m$ is the monolayer coverage and $C$ is a coefficient that describes the affinity of the gas for the surface. Using the BET equation to measure the surface coverage allows the calculation of the specific surface area ($sa$) by use of the equation:

$$sa = n_m N_A \sigma \qquad \text{Equation 2.2}$$

where $N_A$ is Avogadro's constant (= 6.02 x $10^{23}$) and $\sigma$ is the cross sectional area of the adsorbing species, equal to 0.162 $nm^2$ for $N_2$ (Gemini 2360 Surface Area Analyzer Operator's Manual V5.0, Micromeritics).

Conventionally, nitrogen gas is used as the probe. Cooling the sample to liquid nitrogen temperatures (77 K) reduces thermal effects, enables efficient condensation

of nitrogen onto the surface and gives thermal stability, limiting variations in the saturation vapour pressure. In their original study examining the effect of temperature on the measured surface area, Brunauer et al (1938) found that, for $N_2$, using lower temperatures did not affect the resultant surface area determination. For reasons of economy, therefore, liquid $N_2$ is the preferred cooling medium.

Prior to analysis it is necessary to dry out the sample to remove water from all the pores. Water remaining in the pores during analysis at 77 K will be frozen and so block the access of probe gas to the surface, resulting in a false low surface area being determined. There is evidence that water associated with cellulose is bound to the structure in three distinct ways (Zografi et al, 1984; Weise et al, 1996). Water may be loosely adsorbed on the surface of the material, bound strongly in smaller capillaries and associated with the structure of the amorphous regions. Total dehydration using high temperatures will result in alteration of the amorphous cellulose regions, therefore changing the surface area. Solvent displacement methods have been proposed to try to remove all but the structural water (Nakai et al, 1977), but water miscible solvents such as alcohols may swell the cellulose, resulting in a higher surface area (doRego et al, 1997). Instead, heating under a stream of dry $N_2$ is a preferred method. Zografi et al (1984) determined that such drying regimes did not affect the surface area determined for heating temperatures up to 100°C.

The 'C' constant determined from the adsorption data is related to the affinity of $N_2$ for the surface, being a measure of the heat of adsorption of the first adsorbed layer (Ticehurst et al, 1994). Since $N_2$ is non-polar, it interacts with the material by dispersion forces only. Ticehurst et al (1994) found that 'C' constants determined for two batches of salbutamol sulphate correlated with the results of inverse gas chromatography (IGC) determinations of the dispersive component of the surface energy (see also Chapter 5). Any conclusions drawn from variations in the 'C' value between MCCs must be presented with the caveat that freezing the samples may affect the surface energetics of the sample (R.C. Moreton, personal communication), and so the affinity of $N_2$ for the cellulose may be affected.

Although some morphological change might be expected due to swelling, water can be used as the adsorbate for BET adsorption analysis, yielding information on the availability of cellulose surface for adsorption of water (Zografi & Kontny, 1986; Ek et al, 1994). Using the Dynamic Vapour Sorption apparatus (DVS; Figure 2.3), the

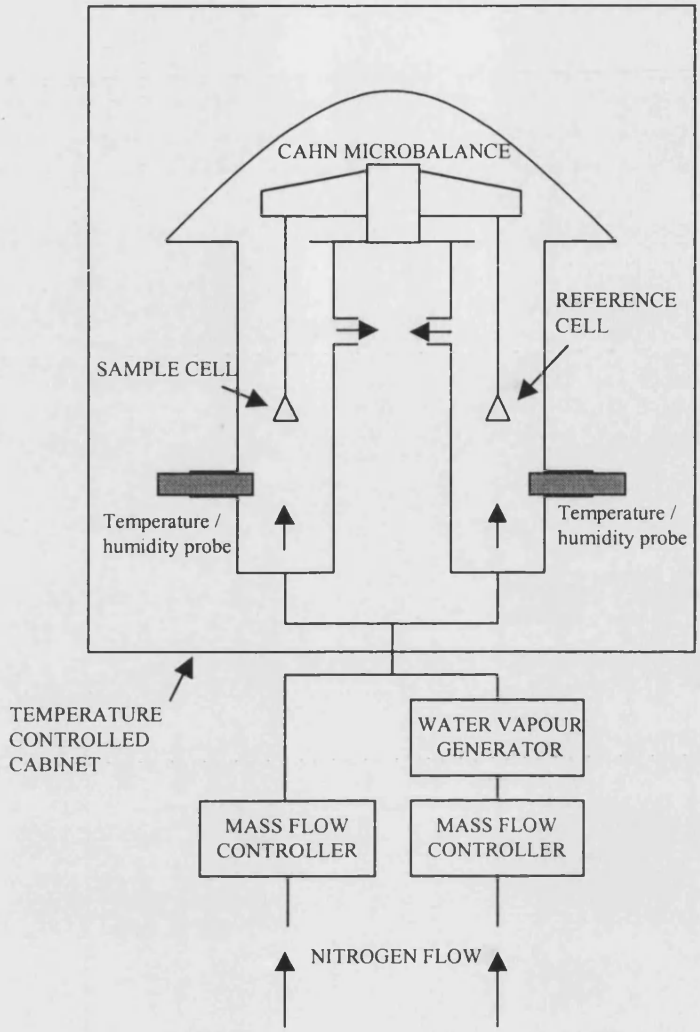


Figure 2.3. Schematic diagram of the Dynamic Vapour Sorption apparatus (DVS) as used to investigate water sorption properties.

amount of water adsorbed over a range of controlled relative humidities can be determined gravimetrically and the surface area determined using the BET equation (Equation 2.1), with a cross-sectional area of 0.111 $nm^2$ (Webster et al, 1998). The relative humidity is substituted for the relative partial pressure, but otherwise the equation may be used as normal. Samples are dried to constant mass prior to analysis by exposing them to a stream of dry nitrogen.

Zografi et al (1984) determined surface areas with water, nitrogen and krypton as probes. They found that the surface area determined using water was a factor of ten higher than that determined using other probes. This was determined to be a result of adsorption of water in the amorphous regions. Suzuki & Nakagami (1999) showed that water sorption increases as crystallinity decreases in the range 63 – 12%, lending weight to the argument put forward by Zografi et al (1984).

### *2.1.3. Flowability*

A primary consideration in the choice of excipients for tabletting is flowability. Good flowability of the blend containing the drug and excipients is required so that the die in the tablet press is filled reproducibly, in order to ensure the drug content of the tablet. Flowability is also an important factor when considering the mixing of powders, since materials that flow well tend to produce mixes with a better degree of order. Several methods are available to measure the flowability of powders, most of which rely on a table by which the measured property is related to a descriptive term for the flowability. Properties such as angle of repose, mean avalanche time (Aeroflow®; Kaye, 1997), compressibility and minimum orifice diameter (Flodex®) are commonly used. In this study, compressibility as measured as a function of bulk and tapped densities (Carr, 1965) will be used to obtain a qualitative measurement of the flowability of the materials.

Several factors affect the flowability of a material. These include bulk density, particle size distribution, aspect ratio, surface roughness and surface energy. In general, dense, smooth, particles with a narrow size distribution, low aspect ratio and low surface energy (e.g. glass beads, steel ball bearings) will have excellent flowability.

### 2.1.4. *Mercury intrusion porosimetry*

Mercury intrusion porosimetry (MIP) is a well-established method that can be used to assess the pore size distribution and the nature of the surface and pore structure (review: León y León, 1998). Briefly, the method involves forcing mercury into the pores of the sample under pressures of up to 400 MPa. Intrusion of mercury into the sample is recorded as a function of pressure with pore radius of a capillary related to pressure by the Washburn equation (León y León, 1998):

$$\mathrm{Pr} = 2\gamma \cos\theta \qquad \text{Equation 2.3}$$

where $P$ is pressure, $r$ is the radius of the cylindrical pore, $\gamma$ is the surface tension of mercury (465 $Nm^{-1}$ at 25°C) and $\theta$ is the contact angle, taken to be 130° (cos = -0.643) for the advancing contact angle on cellulose. A mean value of $\theta$ of 118° (cos = -0.469) may be calculated using the surface energy data obtained in Chapter 5. However, for the purposes of intercomparison, the $\theta$ value of 130° can be used: the absolute values of the pore sizes determined are of less interest than the comparative sizes.

Pore volume is calculated directly from the collected intrusion data. Pore surface area is calculated assuming cylindrical pores, with known radius and volume:

$$sa = \frac{2rv}{r^2} \qquad \text{Equation 2.4}$$

where $r$ is the diameter of the pore and $v$ is the incremental intrusion volume. Incremental intrusion volume is reported in $mlg^{-1}$, hence a specific surface area is calculated.

An estimate of the bulk and true densities of the material may also be obtained from the MIP data. Subtracting the volume of mercury intruded up to the point before the interstitial voids are filled from the volume of the penetrometer gives the bulk volume of the sample, hence the bulk density can be calculated for a known mass of sample. Similarly, the total intrusion volume can be used to obtain the true volume of the material.

### 2.1.5. *Scanning Electron Microscopy*

Scanning electron microscopy (SEM) allows high magnification images of particles to be obtained. For materials such as microcrystalline cellulose with significant

water content the low pressures used in conventional SEM methods cause charging of the samples and damage during imaging as water evaporates into the evacuated sample chamber. Better quality images of hygroscopic materials may be obtained by the use of low temperature SEM (LT-SEM) (Clarke et al, 1998), with images collected at below –80°C. This prevents evaporation of water as well as reducing thermal damage by the electron beam. It is has been shown for fragile, hydrated biological samples such as yeast cells that freezing does not significantly affect the morphology of the samples (Read & Jeffree, 1991).

Particles of approximately 100 μm are difficult to image at ambient temperatures. The highest points on the particles are subject to charging, since these are closest to the electron beam, and this manifests itself as bright spots in the image. Cryogenic imaging prevents this by hindering the evaporation of water from the sample, thereby maintaining the integrity of the conductive coating.

## 2.2. Materials

The twenty six MCC samples used in this work are summarised in Table 2.1. Batch numbers are used to distinguish between samples of the same product manufactured at different times. Where practical, subsamples of approximately 200 g of the MCCs were taken from the supplied sample. A spinning riffler (Microscal Ltd, London) was used to obtain further subsamples for physical analyses and adsorption studies (Chapter 3).

Water was treated by reverse osmosis and ultrafiltration (MilliQ grade, Millipore, UK). Mercury was electronic grade (triple-distilled, Fisher, Loughborough, UK).

## 2.3. Methods

### *2.3.1. Particle size analysis*

Particle size distribution analysis by laser diffraction was performed using the Mastersizer 2000 (Malvern Ltd., Malvern, UK). Samples were presented as dry powders using the Scirocco 2000 automated dry powder feeder set to yield a pressure drop of 3 bar across the sampling chamber. Each analysis is the mean of 10000 scans over ten seconds. Sample feed rate was adjusted to give a laser obscuration of 0.5 to 2.0% during analysis. Results quoted are the means of three analyses. The controlling software averages the scattering patterns obtained from the

Table 2.1. Summary of the twenty-six microcrystalline cellulose samples studied, including multiple batches for Avicel PH101, Emcocel 50M and Vivapur 101. All groupings are based on descriptions from manufacturers' literature.

| MCC | Batch | Supplier | Country | Group |
|---|---|---|---|---|
| Avicel PH101 | 6902C | FMC Inc. | USA | standard grade |
| Avicel PH101 | 1113 | FMC Inc. | USA | standard grade |
| Ceolus KG-802 | H0134 | Asahi Kasei Corp. | Japan | standard grade |
| Emcocel 50M | E5D8C17X | Penwest Co. | USA | standard grade |
| Emcocel 50M | E5D7E21 | Penwest Co. | USA | standard grade |
| Emcocel 50M | E5B1E48 | Penwest Co. | USA | standard grade |
| Pharmacel 101 | 90971 | DMV International | The Netherlands | standard grade |
| Tabulose 101 | 113/99 | Blanver Ltda. | Brazil | standard grade |
| Vivapur 101 | 5610193529 | J. Rettenmeier GmbH | Germany | standard grade |
| Vivapur 101 | 5610104629 | J. Rettenmeier GmbH | Germany | standard grade |
| Vivapur 101 | 5610110714 | J. Rettenmeier GmbH | Germany | standard grade |
| Emcocel 90M | E9B8A01X | Penwest Co. | USA | large particle |
| Emcocel LP200 | 2S6003X | Penwest Co. | USA | large particle |
| Avicel PH302 | Q918C | FMC Inc. | USA | high density |
| Emcocel HD90 | HD9B5K3X | Penwest Co. | USA | high density |
| Multi-Cel N90 | M9B9F43X | Penwest Co. | USA | high density |
| Vivapur 302 | 5630280112 | J. Rettenmeier GmbH. | Germany | high density |
| Prosolv 50 | P5B7D26X | Penwest Co. | USA | silicified |
| Prosolv 90 | P9B9B11X | Penwest Co. | USA | silicified |
| Prosolv HD90 | K9S9040X | Penwest Co. | USA | silicified |
| Avicel PH105 | 5138C | FMC Inc. | USA | treated |
| Emcocel SP15 | SPD7C01X | Penwest Co. | USA | treated |
| Ankit | n/a | Ankit | India | other pulp source |
| RanQ | n/a | RanQ | India | other pulp source |
| Lot #1 | n/a | Penwest Co. | USA | other pulp source |
| Lot #2 | n/a | Penwest Co. | USA | other pulp source |

individual analyses and deconvolutes the averaged pattern to obtain a size distribution histogram (Figure 2.2). All results are quoted as volume distributions; since volume is related to mass this is the most useful means of describing particle size distributions in formulation work.

It has previously been shown that Avicel PH101 is of the form of large (median diameter = 102 μm, determined by sieve fractionation) agglomerates of smaller (median diameter = 27 μm, determined by sedimentation) primary particles (Ek et al, 1994). In order to investigate whether this is the case for other MCCs used in this study, the ultrasonication treatment described by Ek et al (1994) will be used. The same technique, albeit using different sample presentation methods and different instruments, will be used for the determination of the particle size of the agglomerates and the individual particles. This will reduce any possible disparity between the results due to the two different principles used by Ek et al (1994). Approximately 20 mg MCC was suspended in 50 ml water and ultrasonicated (FS 300B Sonic Bath, Decon Labs, Hove, UK) for 20 minutes. The particle size distribution of the resulting slurry was determined using a Mastersizer 2000 (Malvern Instruments, Malvern, UK), with a 100 mm range lens (0.5 – 180 μm). Aliquots of the slurry were introduced into the stirred wet cell sample holder filled with water until a laser obscuration of 10-30% was reached. The results for each of the samples were the mean of 2000 determinations of the agitated sample. The procedure was repeated three times for each MCC.

*2.3.2. Surface area*

Surface area was determined by 5-point BET $N_2$ adsorption using the Gemini 2360 nitrogen adsorption apparatus (Micromeritics, Norcross, USA). After loading into the analysis vessel, the samples were dried at 40°C to constant mass (16 – 20 hours) under a stream of dry nitrogen using the FlowPrep 060 (Micromeritics, Norcross, USA). This drying regime was validated by monitoring the sample mass over drying periods of 1 to 24 hours. The partial pressure of $N_2$ was adjusted by mixing the analysis gas with helium, to a maximum partial pressure of 0.2.

Water BET experiments were conducted at 25°C using the Dynamic Vapour Sorption (DVS) apparatus. Approximately 10 mg MCC sample was placed into one pan of the DVS. The sample was dried to constant mass under a stream of dry

nitrogen (0% RH). The relative humidity was raised in increments of 10% to 90%RH, controlled by the process computer *via* needle valves. Each step in the relative humidity cycle was deemed to be complete when $dm/dt < 0.001$ $mgmin^{-1}$ for three minutes. Partial pressures up to 0.4 were used for the determination of the BET surface area. Because of the low availability of this instrument, a limited number of samples were analysed using this technique.

### *2.3.3. Flowability*

The method proposed by Carr (1965) requires the determination of the bulk and tapped densities of a material. The bulk density was determined by pouring a sample of the powder into a suitable polypropylene measuring cylinder. The mass and volume of the powder were recorded and the bulk density calculated. The same sample was then placed on a jolting volumeter (J. Engelsmann, Ludwigshaven, Germany) and compressed for 500 taps. The volume was recorded and further sets of 500 taps were conducted until a stable volume was reached. The tapped density was calculated from this measurement and Carr's compressibility index (CCI) was calculated from:

$$CCI(\%) = 100\frac{\rho_t - \rho_b}{\rho_t} \qquad \text{Equation 2.5}$$

where $\rho_b$ is the bulk density and $\rho_t$ is the tapped density.

### *2.3.4. Mercury intrusion porosimetry*

Porosimetry data were collected over the pressure range 30 kPa to 414 MPa using the Autopore 9200II (Micromeritics, Norcross, USA). Powder penetrometers with a 1.1 ml stem volume and 5 ml sample volume were used for all samples. Once sealed into the penetrometers, the samples were introduced into the low pressure ports and evacuated to below 5 Pa prior to analysis to remove air and loosely bound surface water. The penetrometers were filled under a pressure of 3 kPa. A program of forty intrusion steps was used for each sample with a five second equilibration time at each pressure point. Pressures up to 350 kPa were achieved using an air pump in the low pressure ports. Higher pressures required sample transfer to a hydraulic port; pressure was transferred to the sample *via* a hydraulic fluid ('High Pressure Fluid',

Micromeritics, Norcross, USA). Seventeen samples were analysed; multiple batches were not analysed since the availability of the porosimeter was restricted.

*2.3.5. Scanning electron microscopy*

Prior to analysis, samples were fixed into carbon discs using Tissue-Tek (Miles Laboratories, Naperville, USA), then frozen using sub-cooled nitrogen (-210°C). After removal of superficial water by sublimation under reduced pressure, samples were coated with colloidal gold before being introduced into the sample chamber. Electron micrographs were collected using the Jeol 6310 (Jeol, Tokyo, Japan) scanning electron microscope with cryogenic facility. Images were collected at or below -170°C using an accelerating voltage of 10 kV at magnifications in the range 100 to 3000. Spot size was adjusted as necessary to obtain clear images without causing visible damage to the sample surface.

## 2.4. Results and discussion

*2.4.1. Particle size analysis*

Particle size distribution data for the untreated MCC samples are summarised in Table 2.2. Data obtained after ultrasonication in water are presented in Table 2.3. All results are presented as volume data, so that half the volume of the sample is smaller than the mean particle size (d (v, 0.5)).

From the data in Table 2.2, it is clear that there is a difference between the particle size distributions of the various grades. Much of this variation is designed into the MCC grade to influence the flow properties, with larger particles generally giving better flow.

The data obtained from the ultrasonicated samples in Table 2.3 show that all the MCCs studied consist of aggregates of 12 – 30 μm particles. These results indicate that each agglomerated particle consists of between 10 and 100 smaller particles, with the drying conditions used in the final stage of MCC manufacture determining the size of the agglomerates and therefore the number of particles in the agglomerates.

Note that the sonicated samples were analysed in the wet state, in contrast to the dry state used for the analysis of the agglomerates. This may affect the results obtained, since cellulose swells slightly in water (Krässig, 1993). It was not possible to

Table 2.2. Summary of particle size distribution data for microcrystalline cellulose samples. Results are volume distributions indicating the diameters of the 10%, 50% and 90% volume ranges.

| MCC | Batch No. | d(v.0.1) | d(v.0.5) | d(v.0.9) |
|---|---|---|---|---|
| Avicel PH101 | 6902C | 19.9 | 53.8 | 123 |
| Avicel PH101 | 1113 | 21.3 | 53.2 | 117 |
| Ceolus KG-802 | H0134 | 17.5 | 51.9 | 138 |
| Emcocel 50M | E5D8C17X | 21.5 | 56.7 | 124 |
| Emcocel 50M | E5D7E21 | 21.4 | 56.4 | 124 |
| Emcocel 50M | E5B1E48 | 21.8 | 56.3 | 126 |
| Pharmacel 101 | 90971 | 13.9 | 56.6 | 153 |
| Tabulose 101 | 113/99 | 23.1 | 70.0 | 164 |
| Vivapur 101 | 5610193529 | 20.6 | 62.8 | 135 |
| Vivapur 101 | 5610104629 | 20.1 | 60.8 | 132 |
| Vivapur 101 | 5610110714 | 19.4 | 60.6 | 134 |
| Emcocel 90M | E9B8A01X | 29.1 | 109 | 263 |
| Emcocel LP200 | 2S6003X | 54.6 | 175 | 379 |
| Avicel PH302 | Q918C | 27.8 | 104 | 255 |
| Emcocel HD90 | HD9B5K3 | 35.5 | 123 | 292 |
| Multi-Cel N90 | M9B9F43X | 31.1 | 117 | 276 |
| Vivapur 302 | 5630280112 | 27.7 | 111 | 258 |
| Prosolv 50 | P5B7D26X | 21.1 | 54.6 | 119 |
| Prosolv 90 | P9B9B11X | 29.0 | 109 | 269 |
| Prosolv HD90 | K9S9040X | 37.8 | 123 | 257 |
| Avicel 105 | 5410C | 6.18 | 18.5 | 41.3 |
| Emcocel SP15 | SPD7C01X | 4.64 | 14.1 | 32.1 |
| Ankit | n/a | 11.9 | 37.4 | 136 |
| RanQ | n/a | 33.8 | 124 | 263 |
| Lot #1 | n/a | 21.7 | 69.0 | 150 |
| Lot #2 | n/a | 28.7 | 91.3 | 197 |

Table 2.3. Summary of particle size distribution data for untreated and ultrasonicated microcrystalline cellulose samples. Results are volume distributions indicating the diameters 50% volume ranges.

| MCC | Batch No. | Untreated (μm) | sonicated (μm) |
|---|---|---|---|
| Avicel PH101 | 6902C | 53.8 | 13.5 |
| Ceolus KG-802 | H0134 | 51.9 | 21.6 |
| Emcocel 50M | E5D8C17X | 56.7 | 18.6 |
| Pharmacel 101 | 90971 | 56.6 | 18.3 |
| Tabulose 101 | 113/99 | 70.0 | 14.2 |
| Vivapur 101 | 5610193529 | 62.8 | 16.8 |
| Emcocel 90M | E9B8A01X | 109 | 17.8 |
| Avicel PH302 | Q918C | 104 | 14.8 |
| Emcocel HD90 | HD9B5K3 | 123 | 12.0 |
| Multi-Cel N90 | M9B9F43X | 117 | 10.3 |
| Vivapur 302 | 5630280112 | 111 | 13.2 |
| Prosolv 50 | P5B7D26X | 54.6 | 17.2 |
| Prosolv HD90 | K9S9040X | 123 | 12.2 |
| Ankit | n/a | 37.4 | 20.8 |
| RanQ | n/a | 124 | 18.2 |
| Lot #1 | n/a | 69.0 | 28.0 |
| Lot #2 | n/a | 91.3 | 17.9 |

analyse the agglomerates using the wet cell because agitation sufficient to maintain a suspension could not be achieved.

*2.4.2. Surface area*

Surface area results are summarized in Table 2.4, together with the particle size data.

Fisher's multiple comparison *post hoc* test was used to distinguish between surface area results obtained by BET $N_2$ adsorption. A level of 95% was selected as significant for the purposes of comparisons.

Similar surface areas were determined for Emcocel 50M and Emcocel 90M. The particle sizes measured by LALLS (section 2.4.1) are of agglomerates of smaller cellulose particles. The measured surface areas are not, therefore, those of monolithic cellulose, but include the internal surface area of aggregates. The results for the standard grades of MCC agree well with previously published data (Zografi et al, 1984; Zografi & Kontny, 1986; Ardizzone et al, 1999).

The silicified MCC samples show a higher specific surface area than the corresponding standard grade MCCs. This is a result of the presence of colloidal silicon dioxide (CSD) in the surface of the material (Edge et al, 1999). The CSD used has a mean particle size of 12 nm and a specific surface area of $200 \pm 15$ $m^2g^{-1}$ (product technical data sheet). The inclusion of 2% w/w CSD as a simple mix with MCC would be expected to increase the specific surface area of MCC by 4 $m^2g^{-1}$. This is approximately the surface area increase observed in these experiments for Prosolv grades compared with the equivalent Emcocel grades. It would appear, therefore, that the CSD is not embedded in the surface of the MCC, but is adsorbed in the surface. This cannot be verified by observation because the available visual techniques do not provide sufficient resolution at the magnifications required.

High surface areas were determined for the limited number of MCC samples investigated using water as the surface probe. Surface area data for the five MCCs analysed yielded values between 108 000 and 115 000 $m^2kg^{-1}$. This is in accordance with previous findings (Zografi et al, 1984; Zografi & Kontny, 1986). The higher surface area is a result of adsorption of water into the amorphous regions of the macromolecule. The adsorption is described well by the BET equation. Despite the differences in the pulp source for these MCCs, there is little difference between the values calculated for the water sorption data.

Table 2.4. Summary of $N_2$ and water BET surface area results obtained for MCC samples.

| MCC | Batch No. | Nitrogen | | Water | |
|---|---|---|---|---|---|
| | | Surface area ($m^2kg^{-1}$) | C coefficient | Surface area ($m^2kg^{-1}$) | C coefficient |
| Avicel PH101 | 6902C | 1220 | 86.0 | 115000 | 20 |
| Avicel PH101 | 1113 | 1070 | 113 | -- | -- |
| Ceolus KG-802 | H0134 | 1250 | 115 | 115000 | 20 |
| Emcocel 50M | E5D8C17X | 1270 | 85.9 | 114000 | 15 |
| Emcocel 50M | E5D7E21 | 1180 | 89.7 | -- | -- |
| Emcocel 50M | E5B1E48 | 1210 | 98.1 | -- | -- |
| Pharmacel 101 | 90971 | 1300 | 87.9 | -- | -- |
| Tabulose 101 | 113/99 | 1340 | 93.3 | -- | -- |
| Vivapur 101 | 5610193529 | 1450 | 90.4 | -- | -- |
| Vivapur 101 | 5610104629 | 1480 | 100 | -- | -- |
| Vivapur 101 | 5610110714 | 1400 | 98.5 | -- | -- |
| Emcocel 90M | E9B8A01X | 1250 | 108 | -- | -- |
| Emcocel LP200 | 2S6003X | 1110 | 96.7 | -- | -- |
| Avicel PH302 | Q918C | 640 | 74.5 | -- | -- |
| Emcocel HD90 | HD9B5K3 | 690 | 79.8 | 108000 | 18 |
| Multi-Cel N90 | M9B9F43X | 1440 | 91.5 | -- | -- |
| Vivapur 302 | 5630280112 | 1220 | 89.0 | -- | -- |
| Prosolv 50 | P5B7D26X | 4910 | 101 | 110000 | 26 |
| Prosolv 90 | P9B9B11X | 5510 | 103 | -- | -- |
| Prosolv HD90 | K9S9040X | 4320 | 96.3 | -- | -- |
| Avicel 105 | 5410C | 2310 | 122 | -- | -- |
| Emcocel SP15 | SPD7C01X | 3320 | 108 | -- | -- |
| Ankit | n/a | 1120 | 83.0 | -- | -- |
| RanQ | n/a | 1130 | 77.8 | -- | -- |
| Lot #1 | n/a | 1690 | 99.2 | -- | -- |
| Lot #2 | n/a | 1130 | 96.6 | -- | -- |

The results obtained here correlate well with previous investigations of water sorption by MCC. Ek et al (1994) equilibrated Avicel PH101 with saturated salt solutions at 33 to 100% RH. Their results are superimposed on the DVS data obtained in this study for Avicel PH101 in Figure 2.4. Note that the results obtained here were achieved in less than 48 hours, compared with at least 20 days for Ek et al (1994), and used smaller samples. Also, the coincidence of the results suggests that the migration of salts frequently observed during extended saturated salt solution equilibrations does not adversely affect the results. Crystallisation of the salts on the sample and container might otherwise be expected to yield false high values for mass increase.

Using the data obtained from the water adsorption experiments, it can be estimated that monolayer coverage occurs at between 20 and 25% RH for all MCCs studied. This includes the silicified MCC analysed, indicating that the colloidal silicon dioxide, although hydrophilic, does not significantly affect the total interaction of the material surface with water.

Using the Fox equation and experimentally determined $T_g$ values (Picker & Hoag, 2002), a $T_g$ at 25°C is predicted when the water content reaches 7% w/w (assuming a 37% amorphous content (Nakai et al, 1977)), at a RH of approximately 70%. However, because the kinetics of cellulose recrystallisation are very slow, even under favourable conditions (Teeäär et al, 1994), no significant change in the sample morphology is anticipated as a consequence of recrystallisation over the 48 hours of the sample run.

### *2.4.3. Flowability*

Data for the bulk and tapped densities and calculated Carr's compressibility indices are summarised in Table 2.5. The MCCs marketed as 'high density' have a generally higher bulk density than the standard grade materials. Vivapur 302 is an exception to this, a bulk density of 0.36 $gcm^{-1}$ being closer to the mean of standard grades (0.32 $gcm^{-1}$) than of the other high density grades (0.46 $gcm^{-1}$).

Podczeck & Miah (1996) reviewed the flowabilities of several pharmaceutical powders and they found that mean particle size, particle size distribution, bulk density and aspect ratio played important roles in determining flowability. This is in

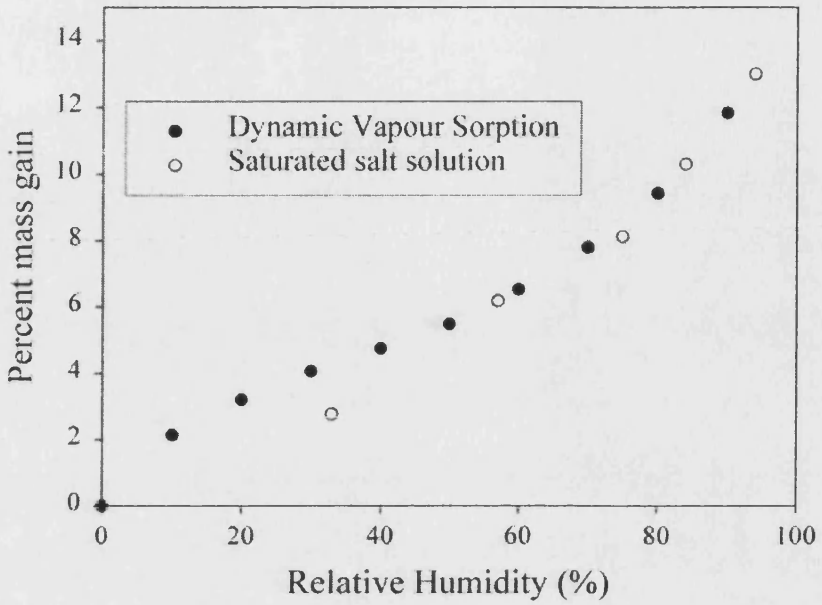


Figure 2.4. Comparison of water sorption profiles of Avicel PH101 determined using dynamic vapour sorption (DVS; this study) and equilibration over saturated salt solutions (data from Ek et al, 1994).

Table 2.5. Summary of the bulk and tapped densities, Carr's compressibility indices and indicated flowability for the MCCs studied. Flowability described with reference to published tables (Carr, 1965).

| MCC | Batch | Bulk density ($gcm^{-3}$) | Tapped density ($gcm^{-3}$) | Carr's index | Flowability |
|---|---|---|---|---|---|
| Ankit | n/a | 0.28 | 0.48 | 41% | v.v. poor |
| Avicel PH101 | 6902C | 0.31 | 0.44 | 30% | poor |
| Avicel PH105 | 5138C | 0.31 | 0.46 | 31% | poor |
| Avicel PH302 | Q918C | 0.48 | 0.62 | 22% | passable |
| Ceolus KG-802 | H0134 | 0.24 | 0.39 | 40% | v.v. poor |
| Emcocel 50M | E5D8C17X | 0.31 | 0.42 | 26% | poor |
| Emcocel 90M | E9B8A01X | 0.31 | 0.40 | 24% | passable |
| Emcocel HD90 | HD9B5K3X | 0.46 | 0.56 | 19% | fair |
| Emcocel LP200 | 2S6003X | 0.34 | 0.43 | 22% | passable |
| Emcocel SP15 | SPD7C01X | 0.22 | 0.35 | 36% | v. poor |
| Lot #1 | n/a | 0.29 | 0.44 | 35% | v. poor |
| Lot #2 | n/a | 0.38 | 0.53 | 29% | poor |
| Multi-Cel N90 | M9B9F43X | 0.34 | 0.43 | 22% | passable |
| Pharmacel 101 | 90971 | 0.34 | 0.51 | 32% | v. poor |
| Prosolv 50 | P9B9B11X | 0.32 | 0.43 | 25% | passable |
| Prosolv 90 | P5B7D26X | 0.34 | 0.45 | 23% | passable |
| Prosolv HD90 | K9S9040X | 0.45 | 0.54 | 16% | fair |
| RanQ | n/a | 0.31 | 0.42 | 26% | poor |
| Tabulose 101 | 113/99 | 0.32 | 0.47 | 32% | v. poor |
| Vivapur 101 | 5610193529 | 0.31 | 0.44 | 29% | poor |
| Vivapur 302 | 5630280112 | 0.36 | 0.55 | 34% | v. poor |

line with both the findings presented here and what would be expected from consideration of the mechanism of flow of solids.

The silicified MCCs (Prosolv™ products) have a slightly improved flowability compared with the equivalent unmodified (Emcocel™) products possibly as a result of the decreased surface to surface contact caused by the presence of silicon dioxide in the surface. This correlates with previous findings (Tobyn et al, 1998; Guo et al, 2002). More important than the flowabilty of SMCCs is the decreased lubricant sensitivity and the ability of the material to flow well at high drug loads (Sherwood & Becker, 1996).

*2.4.4. Mercury intrusion porosimetry*

Mercury intrusion data for seventeen MCCs are presented in Table 2.6. Data for porosity, mean pore size, pore area and tortuosity are calculated from data obtained between 0.1 and 9 μm pore diameter. Larger pores represent the filling of interparticle voids. These data represent a single analysis of each sample and should only be taken as an indication of the general trend for these samples. In the intrusion data, a plateau on the incremental intrusion curve can be used to indicate the completion of interstitial filling prior to pore filling. This general rule assumes that there are no pores of a size approaching the interstitial size; from SEM micrographs, this rule appears to be applicable for MCC samples.

No intrusion was measured below 0.1 μm; some intrusion was detected at high pressures (>300 MPa, pore size less than 10 nm), possibly a result of sample compression (Westermarck et al, 1998). However, nitrogen sorption studies (e.g. Marshall et al, 1972; Westermarck et al, 1999) have suggested that some porosity may be present in this size range. However, such small pores are at the limit of the instrument's design parameters, hence the accuracy of the pressure readings cannot be relied upon. This will result in inaccurate pore diameter determinations and consequent errors in the subsequent calculation of porosity related data. Bulk densities calculated from the MIP data correlate with those determined by volumetric method (Section 2.3.3; $r^2 = 0.75$). The imperfect correlation is a function of inaccuracies inherent in both methodologies. Volumetric determinations of bulk density as performed in section 2.3.3 are subject to errors if the powder column surface is not level, as is frequently the case for poorly flowing materials. The MIP

Table 2.6. Summary of mercury intrusion porosimetry results obtained for seventeen of the MCC samples under investigation.

| MCC | bulk density ($gcm^{-3}$) | envelope density ($gcm^{-3}$) | 'true density' ($gcm^{-3}$) | porosity (%) | pore surface area ($m^2g^{-1}$) |
|---|---|---|---|---|---|
| Ankit | 0.40 | 1.03 | 1.55 | 33.1 | 1.10 |
| Avicel PH101 | 0.39 | 1.02 | 1.48 | 31.4 | 1.38 |
| Emcocel 50M | 0.37 | 0.99 | 1.56 | 36.7 | 1.44 |
| Emcocel 90M | 0.35 | 0.86 | 1.48 | 41.9 | 1.44 |
| Emcocel HD90 | 0.50 | 1.01 | 1.47 | 31.2 | 0.74 |
| Emcocel SP15 | 0.34 | 1.25 | 1.34 | 6.7 | 2.63 |
| Lot #1 | 0.36 | 0.90 | 1.47 | 38.9 | 1.81 |
| Lot #2 | 0.45 | 1.03 | 1.51 | 31.9 | 1.45 |
| MultiCel-N 90 | 0.39 | 0.83 | 1.52 | 45.4 | 1.43 |
| Pharmacel | 0.43 | 0.97 | 1.56 | 37.9 | 1.36 |
| Prosolv 50 | 0.39 | 1.01 | 1.45 | 30.1 | 1.32 |
| Prosolv 90 | 0.38 | 0.88 | 1.45 | 39.2 | 1.32 |
| Prosolv HD90 | 0.50 | 1.02 | 1.49 | 31.6 | 0.76 |
| RanQ | 0.35 | 0.84 | 1.50 | 44.2 | 1.21 |
| Tabulose 101 | 0.39 | 1.11 | 1.52 | 26.9 | 1.05 |
| Vivapur 101 | 0.40 | 1.11 | 1.54 | 27.5 | 1.26 |
| Vivapur 302 | 0.50 | 1.10 | 1.50 | 26.8 | 1.12 |

method may be more accurate, but it is not always possible to guarantee that the powder bed has not been disturbed and compacted prior to evacuation of the penetrometer.

The 'true density' values given in Table 2.6 are calculated with reference to the volume remaining after intrusion up to 0.1 μm. The actual true density of MCC is 1.54 $gcm^{-3}$ (Kibbe, 2001), hence results lower than this value indicate the presence of pores into which mercury has not been intruded at the maximum pressure used. These may be of the order of 2 to 5 nm, as discussed previously. Emcocel SP15 has the lowest measured density, hence the least efficient filling of pores. A possible reason for this is that parts of the material compacted under the intrusion pressure, creating volumes that were unavailable at pressures below 9 MPa.

Figure 2.5 compares incremental intrusion curves for Emcocel 90M and Emcocel HD90, providing a visual confirmation of the intrusion data that can then be related to the morphological features observed in the SEM micrographs (Section 2.4.5).

The porosity profiles of Emcocel 50M and Prosolv 50 are compared in Figure 2.6. The difference between the incremental intrusion porosity profiles, of the order of 10%, is approximately equal to the variability expected for samples of MCC. Because the colloidal silicon dioxide has a mean particle size of 12 nm, it is not possible for any pores present in the silicon dioxide to be observed in the pore size range investigated.

Figure 2.7 compares the MIP data (Table 2.6) with the results obtained by $N_2$ BET analysis (Table 2.4), together with bulk and true density data. Least squares linear regression for the unmodified MCCs yields a regression equation of MIP = 1.267 BET - 376.7, $r^2 = 0.847$. Note, however, that the highest surface area value (Emcocel SP15) has a disproportionately large influence on the regression analysis.

The silicified MCCs do not follow the trend of the unmodified products. MIP does not detect the increase in surface area, detected by $N_2$ BET, due to the inclusion of 2% w/w CSD. Scanning electron micrographs of the surfaces of Prosolv materials (next section; see also Edge et al, 1999) suggest that the distance between the CSD particles are in the range 10 to 500 nm. These gaps would not qualify as pores, since there is no integral wall to define the pore. Furthermore, such very shallow pores (12 nm maximum, equal to the diameter of the CSD particles) are not measurable by

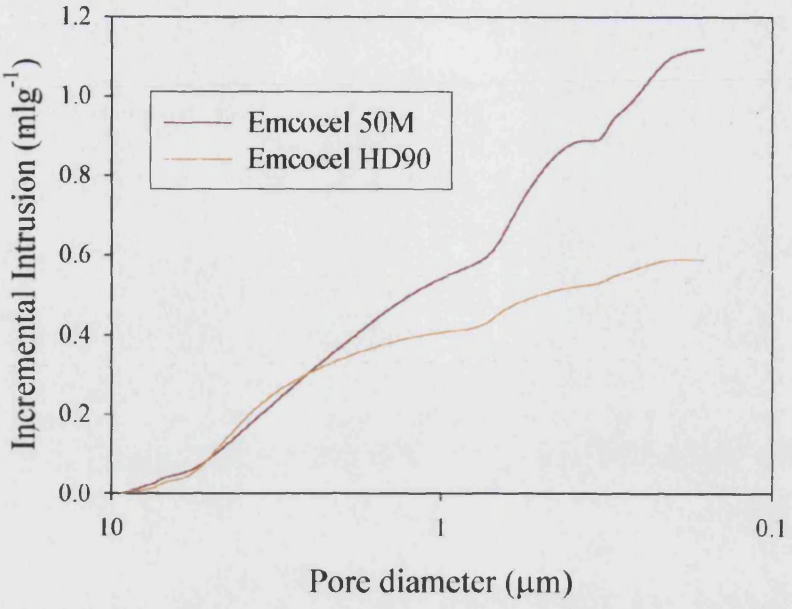


Figure 2.5. Comparison of mercury incremental intrusion profiles for Emcocel 50M and Emcocel HD90. The incremental profiles record the total volume of mercury intruded into the sample.

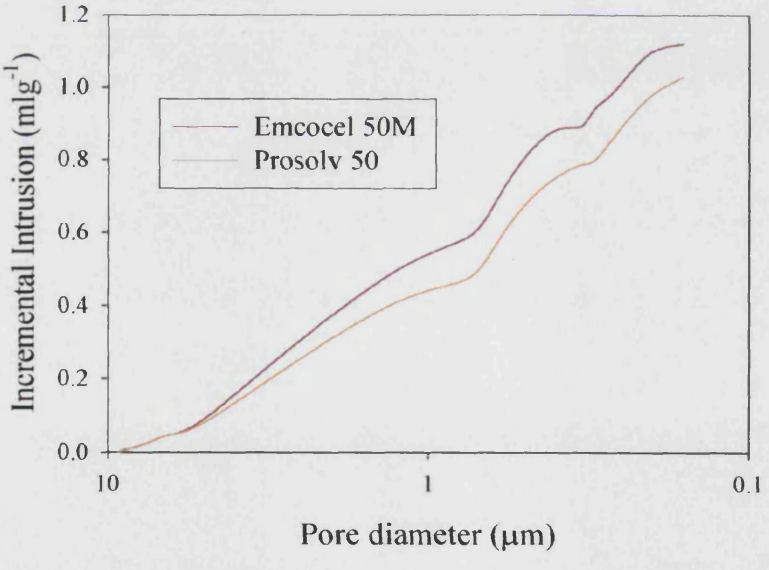


Figure 2.6. Comparison of mercury incremental intrusion profiles for Emcocel 50M and Prosolv 50.

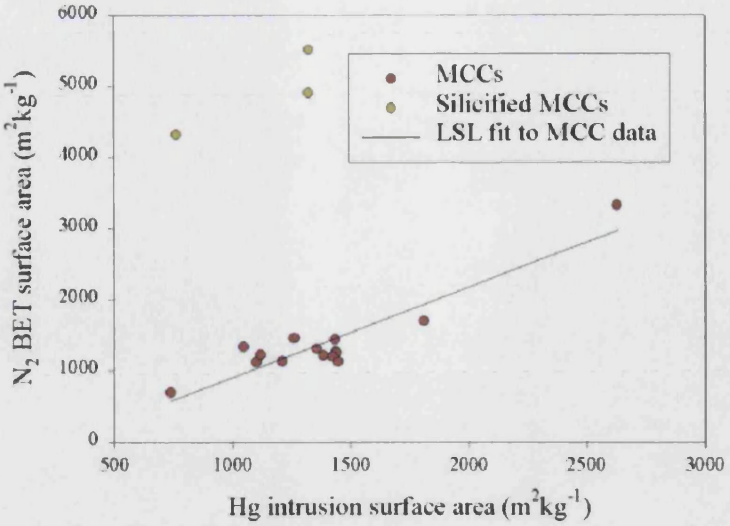


Figure 2.7. Comparison of surface area data calculated for fourteen MCCs and three SMCC samples using mercury intrusion porosimetry (Table 2.6) and 5-point $N_2$ BET analysis (Table 2.4).

MIP. Mercury is a non-wetting liquid for cellulose ($\cos\theta < 0$), therefore the meniscus will partially intrude into the pore at pressures below that required to force mercury into the pore. This decreases the actual volume measured for each pore. Under normal circumstances, this is not a significant source of error, but for very shallow pores the error caused may be highly significant.

*2.4.5. Scanning Electron Microscopy*

Typical images for Avicel PH101, Emcocel 50M, Pharmacel 101 and Vivapur 101 are reproduced in Figures 2.8 and 2.9. These four products show similar general morphologies (Figure 2.8). The images confirm the particle size distribution data obtained in Section 2.4.1 for the size of the MCC agglomerates and also show the smaller, fibrillar cellulose particles which constitute the agglomerates (Figure 2.9). Voids between these smaller particles form the pores measured by MIP, with no pores smaller than approximately 100 nm visible in the SEM images.

The fact that the agglomerates are composed of smaller particles helps to explain why the surface areas of Emcocel 50M and Emcocel 90M are approximately equal. Were these monolithic materials, the specific surface area of Emcocel 50M would be nearly four times (3.6) that of Emcocel 90M, instead of there being no significant difference between the results obtained for these two materials.

The general morphology of Tabulose 101 (Figure 2.10) is different from that of the other standard grades previously discussed. Most noticeable, and of possible interest from an adsorption point of view, is the smoothness of the surfaces of some of the particles. This may be a result of a different drying technique being used; air-stream or spray drying are more commonly used techniques, but it is possible that Tabulose 101 is drum or tray dried and contact with a surface during drying imparts the observed change in morphology.

Emcocel HD90, a high-density MCC, is shown to have smaller and fewer pores than Emcocel 50M (Figure 2.11). This confirms the observed difference in the porosity measured by MIP.

In the micrographs of Prosolv 50 (Figure 2.12), morphologies broadly similar to the unmodified MCCs are observed. The highest resolution images show the presence of sub-micron features in the surface of Prosolv 50 [c], which are absent in the unsilicified product [d]. These features are the colloidal silicon dioxide particles,

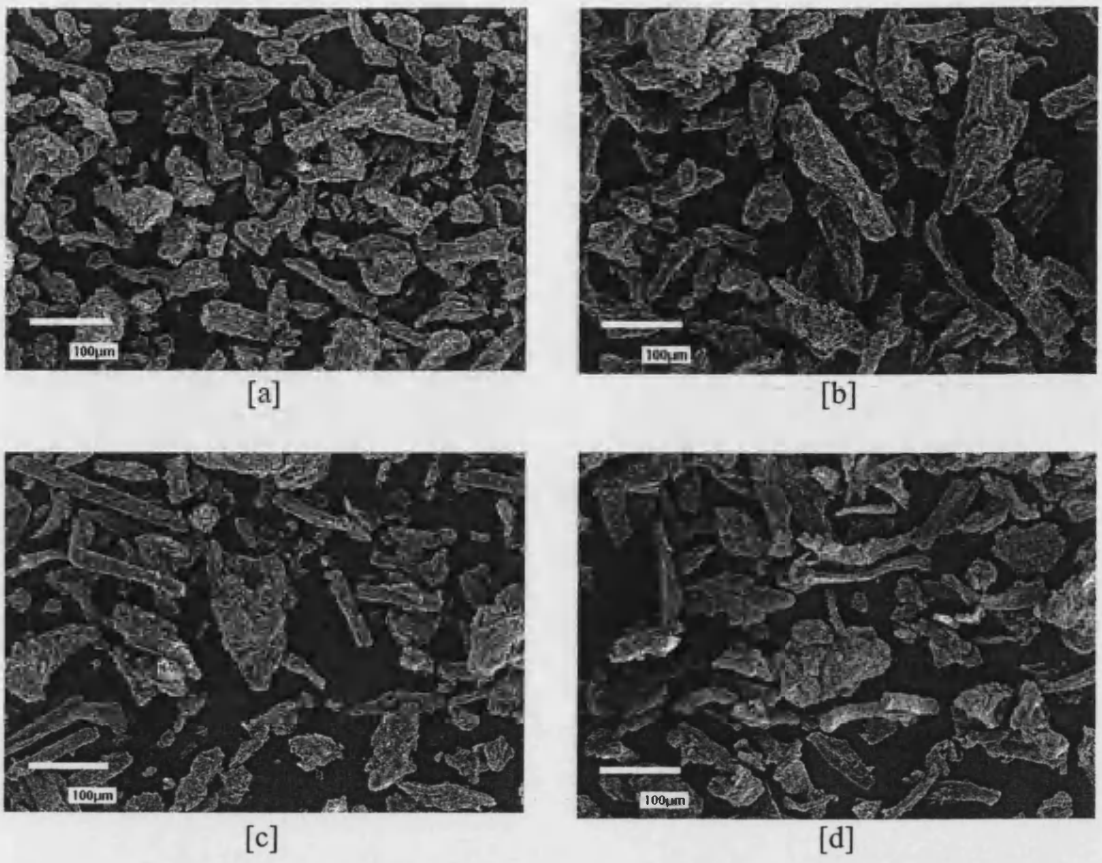


Figure 2.8. Scanning electron micrographs of [a] Avicel PH101, [b] Emcocel 50M, [c] Pharmacel 101 and [d] Vivapur 101. Low magnification images showing the similarity of the general morphology of these MCCs.

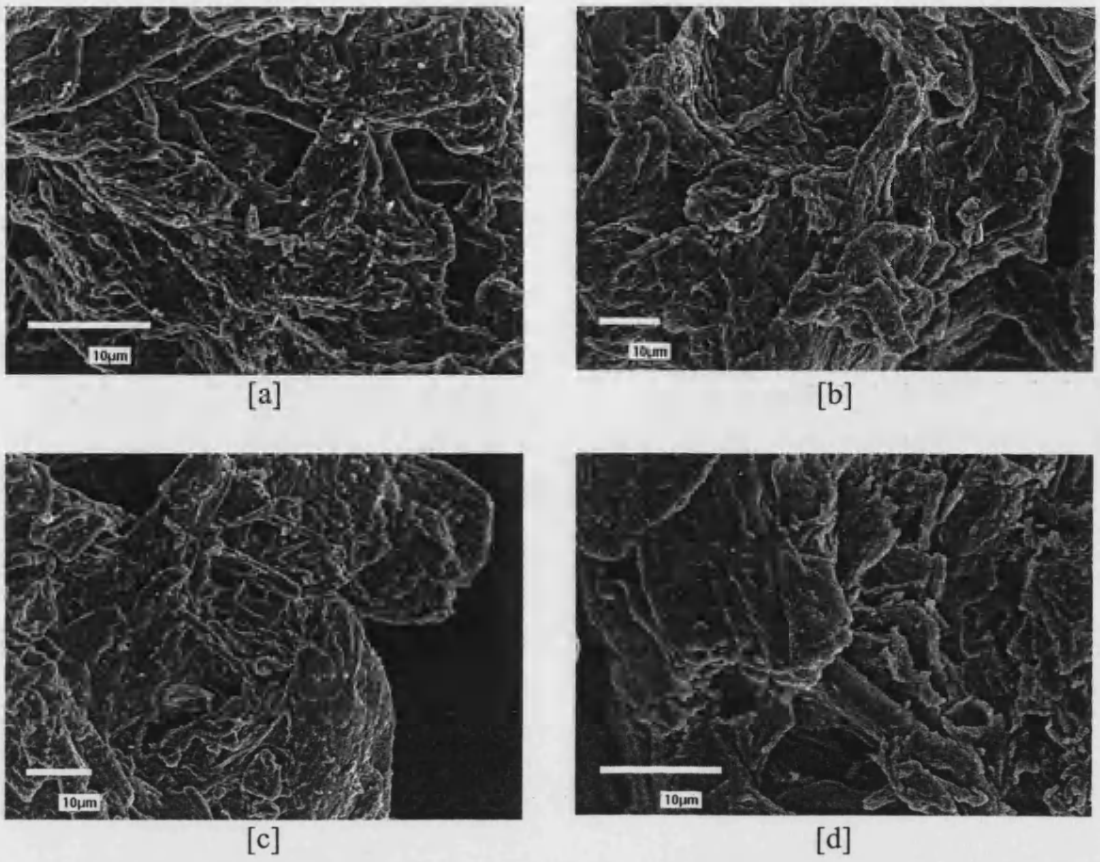


Figure 2.9. Scanning electron micrographs of [a] Avicel PH101, [b] Emcocel 50M, [c] Pharmacel 101 and [d] Vivapur 101. Higher magnification images, showing details of the structure of the agglomerates.

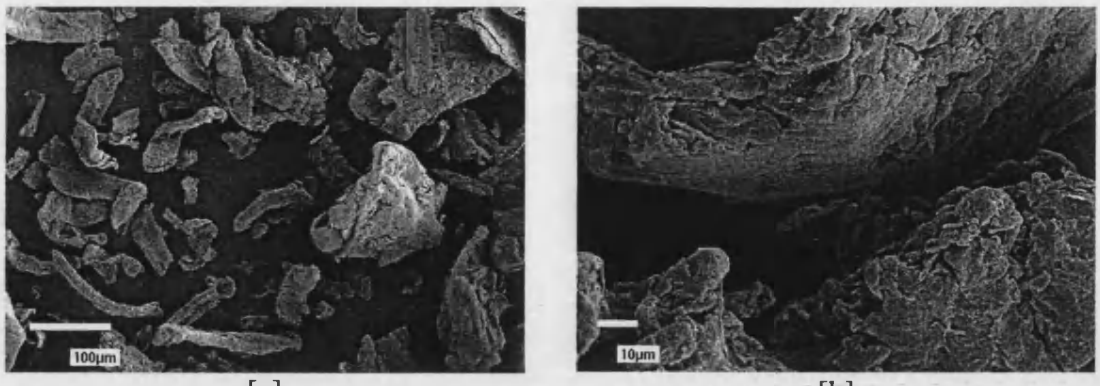


[a] [b]

Figure 2.10. Scanning electron micrographs of Tabulose 101; [a] General view, [b] higher magnification image showing typical smoother particle morphology.

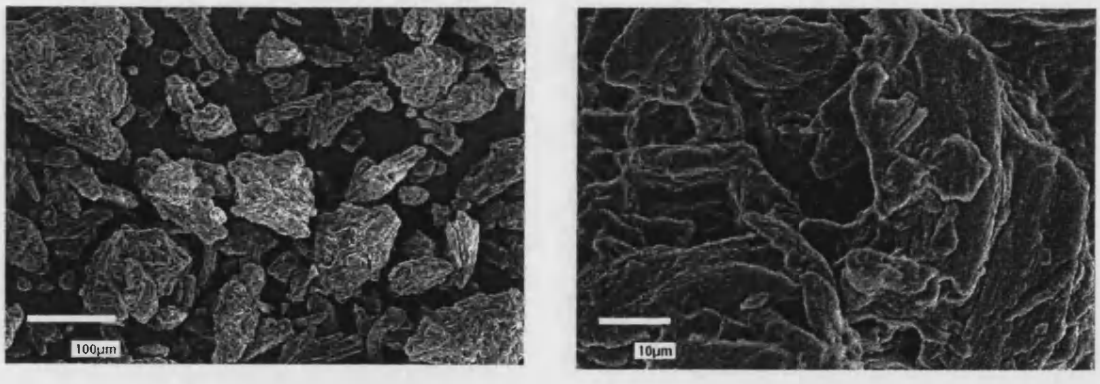


[a] [b]

Figure 2.11. Scanning electron micrographs of Tabulose 101; [a] General view, [b] higher magnification image showing typical smoother particle morphology.

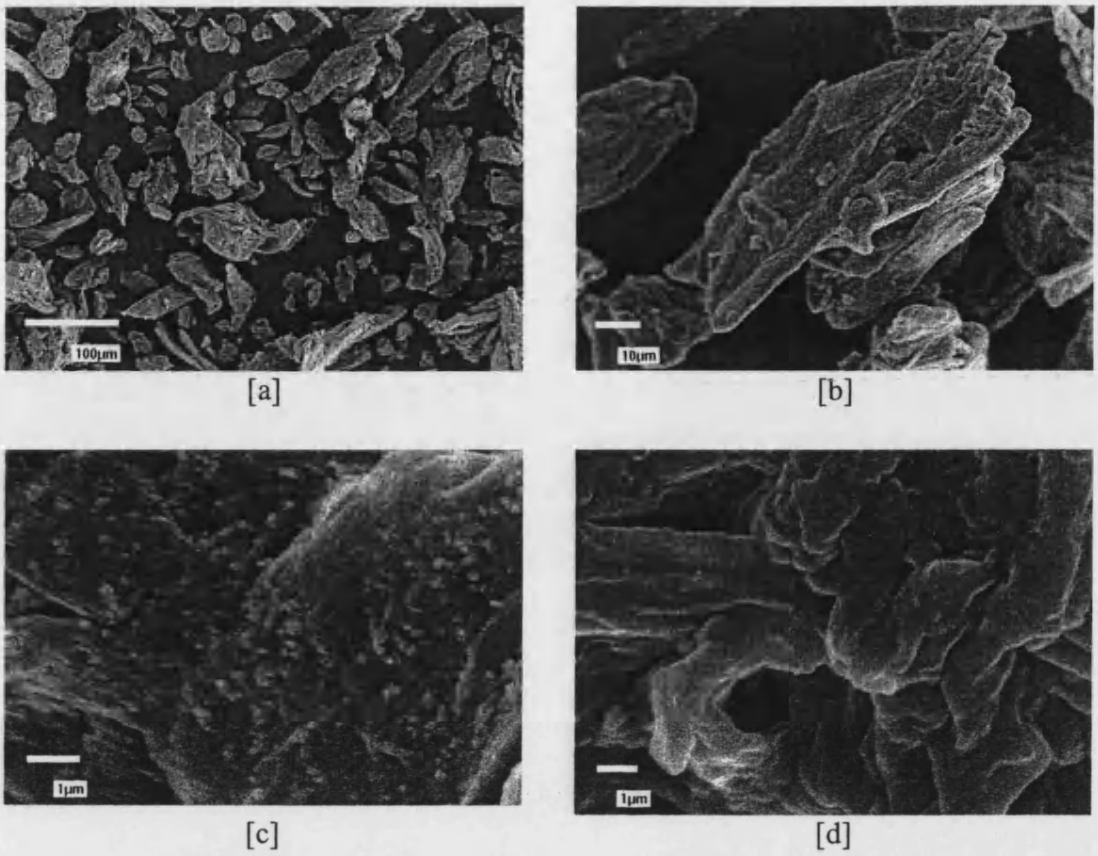


Figure 2.12. Scanning electron micrographs of Prosolv 50; [a] General view, [b] higher magnification image, [c] high magnification and [d] similar magnification view of Emcocel 50M.

which previous work (Edge et al, 1999) has shown concentrates in the surface of SMCC. A particle size of 10 nm may be estimated from the image, in line with the 12 nm stated in the product data sheet for the colloidal silicon dioxide. This can only be an approximation, because the image is not sharply focussed. Some sample damage, evident as cracks between the constituent fibrils in the agglomerate, occurred during the collection of the highest magnification image of Prosolv 50. This prevented the collection of more clearly focussed images.

Morphological considerations of some of the other MCCs illustrate some factors which affect flowability. In Figure 2.13, Ankit, RanQ and Emcocel SP15 are compared. Ankit and RanQ have similar bulk densities (from flowability study), and Ankit has a slightly higher envelope density (from MIP data), a result of the lower porosity, evident from a comparison of the higher magnification images. However, the high aspect ratio of Ankit hinders flow and so the material is more compactible. The smaller particle size of Emcocel SP15 hinders flow because the high surface-to-mass ratio means that there is a much greater friction between the particles, hence reducing the flowability.

## 2.5. Conclusions

The data presented here represent some of the information to be used to explain and explore the differences between MCC grades and manufacturers.

Particle size analysis suggests that all the MCCs studied are supplied as aggregates of smaller individual particles. Information pertaining to the morphology of the individual particles is not available.

Surface area variations may be important in predicting the adsorption capacity of MCC samples. If the samples have similar surfaces then it may be anticipated that a higher surface area will indicate greater adsorption. However, the nitrogen adsorption method of determining surface area may not yield accurate results for microcrystalline cellulose, since the pretreatment could affect the surface and the use of low temperatures might result in water in smaller pores being retained and frozen, thus decreasing the available surface area.

Flowability of the MCCs varies from passable to very poor. The main influence appears to be the morphology of the aggregates, with particle size only influencing the flow of similar shaped materials, such as Emcocel 50M, 90M and LP200.

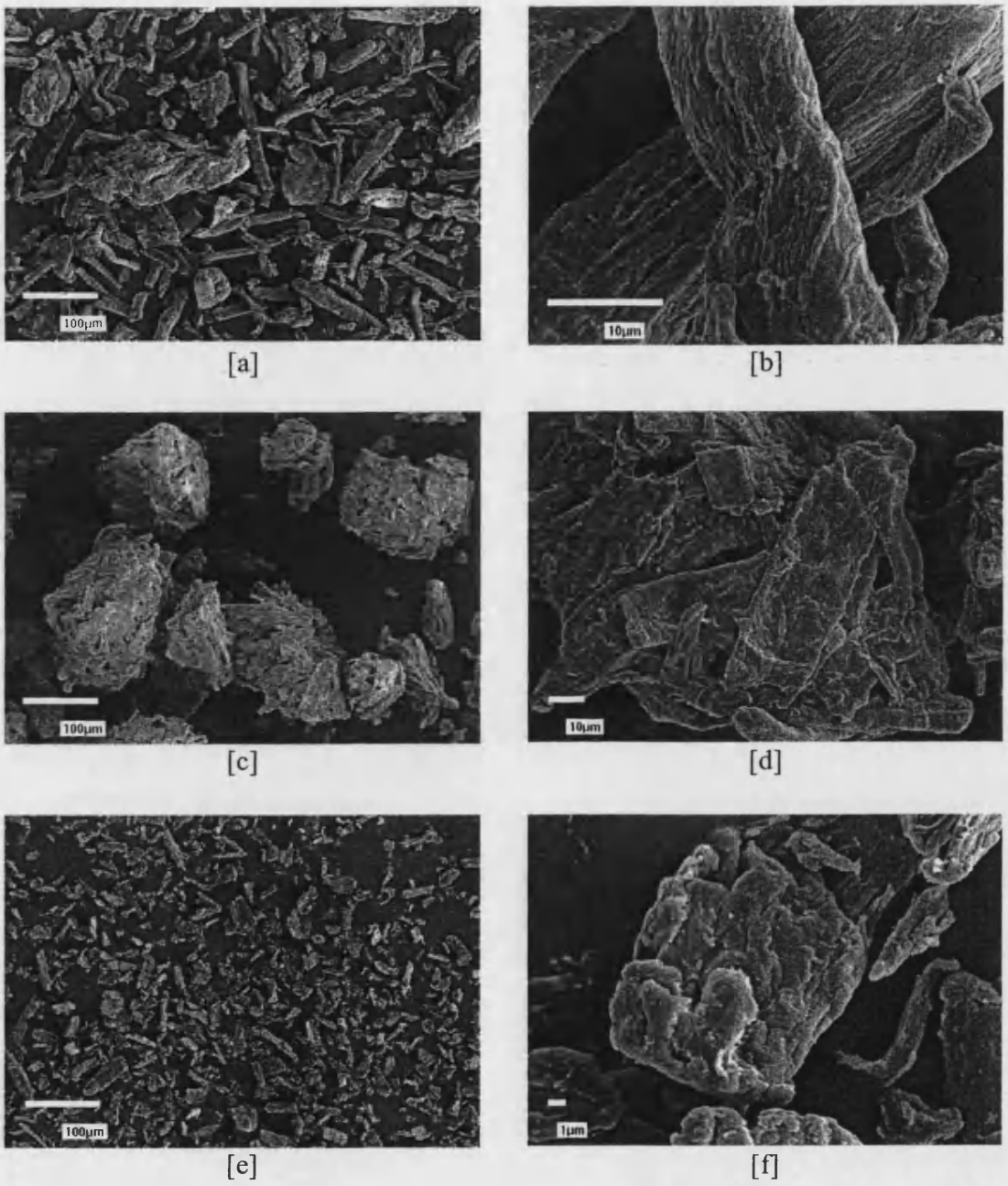


Figure 2.13. Scanning electron micrographs of [a], [b] Ankit; [c],[d] RanQ; [e], [f] Emcocel SP15.

Silicification improves flowability slightly. A higher bulk density also improves flow.

The porosimetry data indicate that the high density grade (Emcocel HD90) has a lower porosity than Emcocel 90M. Figure 2.5 and the data in Table 2.6 show that much of the porosity of Emcocel 90M is in the range 0.1 to 9 μm, in accordance with the observations from the SEM images. Also of interest is a comparison of the data generated for Prosolv 90 with that of Emcocel 90M. A close coincidence in the porosimetry data of these two materials is indicated from the data in Table 2.6. This gives further confirmation of the overall morphological similarity of Emcocel and Prosolv grades previously described (Tobyn et al, 1998).

By comparing the SEM images (Figure 2.8 to Figure 2.13), the following conclusions may be drawn:

all particles in the MCCs studied are agglomerates of smaller particles, approximately 10-30μm in length, up to 10μm wide. This corresponds to fibrillar aggregates, the size of these aggregates being determined by the spray drying conditions employed.

comparison of the images obtained for Emcocel HD90 shows that there are fewer pores in this high density material compared with the standard density grade, Emcocel 90M. The large pores are possibly a legacy of the capillary structures in the original timber sources (Dinwoodie, 2000).

# 3. Adsorption of a Model Amine Drug onto MCC Samples

## 3.1. Introduction

Previous studies of inter-brand and inter-batch variations of MCC have concentrated on comparisons of compactibility (Doelker et al, 1987; Dittgen et al, 1993; Landin et al, 1993c; Hwang & Peck, 2001) and physico-chemical parameters (Landin et al, 1993a; Landin et al, 1993b; Rowe et al, 1994; Ardizzone et al, 1999). Inter-brand and batch-to-batch variations in drug-excipient interactions (Maincent, 1999), drug adsorption (El-Samaligy et al, 1986; Okada et al, 1987; Qtaitat et al, 1988), drug release (Landin et al, 1993c) and water-MCC interactions (Buckton et al, 1999b; Tomer et al, 2001) have also been investigated.

In terms of drug sorption, El-Samaligy et al (1986) and Qtaitat et al (1988) found that the volume diameter mean particle size of the MCC samples influenced the adsorption of the drugs under investigation. A reduced degree of adsorption was observed for larger particle size grades, which the authors linked to the reduced specific surface area of the materials.

Okada et al (1987) compared the adsorption of four basic drugs onto a standard grade MCC with that of a high density grade MCC. They found that the standard grade of MCC had a lower adsorption capacity for three promazine derivatives (Figure 3.1a, b, c) than the high-density grade. In contrast, the adsorption of acrinol (Ethacridine lactate monohydrate; Figure 3.1d), an acridine derivative, was lower for the high-density grade MCC than for the standard grade. Acrinol had the highest affinity for MCC of all the drugs studied.

The promazine derivatives showed capacities in the order chlorpromazine > trifluopromazine > promazine. Although there was no discussion of the effect of the structure of the drugs on the affinity and capacity, the differences observed between the phenothiazine derivatives do not seem to be related to the effect on the chemistry of the molecule of the halogenated ring. The pKas of the drugs are: promazine 9.28; chlorpromazine 9.21; trifluprazine 9.01 (Mannhold et al, 1990). This finding would argue against a simple structure – property relationship for adsorption of a drug onto an excipient; a steric influence is also unlikely because the capacities do not follow a molecular surface area trend.

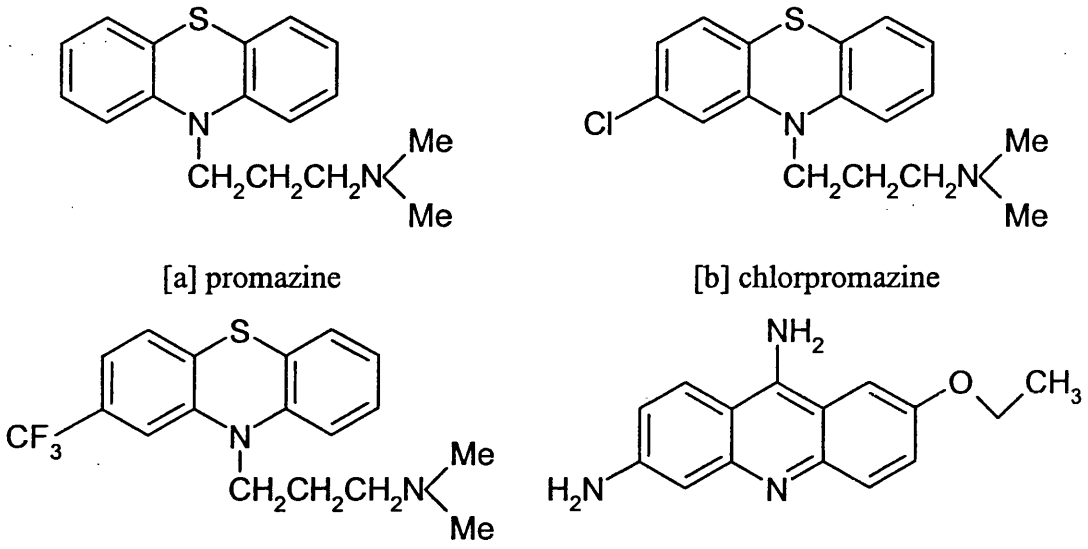


Figure 3.1. Structural formulae of promazine, chlorpromazine, triflupromazine and acrinol.

Qtaitat et al (1988) found that bromhexine HCl (2 - amino - 3, 5 - dibromo - N - cyclohexyl - N - methylbenzylamine HCl; Figure 3.2) adsorption was influenced by particle size, with larger particle size Avicel 102 adsorbing significantly less than Avicel 101 from aqueous solution. Affinity was not significantly affected.

Landín et al (1993c) compared the release profiles of the steroid prednisone (Figure 3.3) formulations using four MCC products and three batches of one MCC. Three batches of Emcocel (unspecified grade, Mendell (now Penwest), Finland), plus Avicel PH101 (FMC Inc, Ireland), Unimac MG101 (Unitika Rayon, Japan) and an unspecified Indian MCC were studied. Analysis of the inter-manufacturer variations showed that Avicel PH101 was similar to all batches of Emcocel, and that Unimac MG101 and the Indian MCC were similar, but different to the other two products, with significantly lower dissolution efficiencies. Significant differences in the dissolution efficiencies of the three batches of Emcocel were found. A positive correlation was determined between lignin content and dissolution efficiency. Also of interest is that the Emcocel batch with the lowest batch number, and therefore the oldest batch used, had a significantly improved dissolution efficiency compared with the other two batches.

Konar & Kim (1997) showed that, in contrast to soluble excipients such as dextrose and lactose, insoluble polysaccharides in general, and cellulose in particular, retarded the rate of release of diclofenac (Figure 3.4) in buffered solutions. This retardation of the release could, in effect, be seen as a net decrease in the bioavailability of the drug, since the release after 8 hours was below 100% (approximately 75%).

The model drug used in this work is an acridine derivative, tacrine hydrochloride (tacrine, 9-amino-1, 2, 3, 4-tetrahydroacridine; Figure 3.5). Tacrine is prescribed as a cholinesterase inhibitor for the alleviation of the symptoms of mild to moderate Alzheimer's type dementia (Cognex®, 10 to 40mg dose). A previous study (Davies, 1999) demonstrated that tacrine adsorbs to a significant degree onto MCC. The flat structure and delocalised aromatic electron structure predicts that the molecule is a fast dye for cellulosic materials (Morita et al, 1985), hence the significant adsorption observed. Tacrine is readily soluble in water with a pKa of 9.3, therefore at pH values below 7, tacrine will be effectively fully protonated. Protonation occurs on the exocyclic nitrogen.

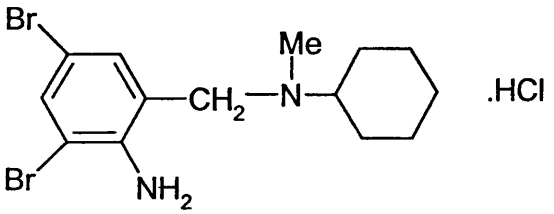


Figure 3.2. Structural formula of bromhexine hydrochloride.

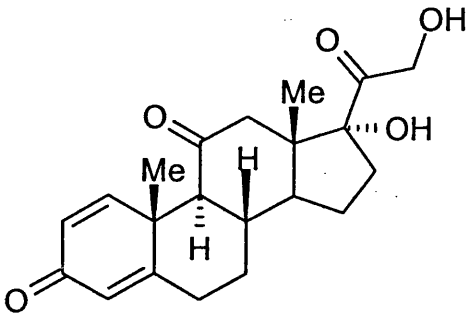


Figure 3.3. Structural formula of prednisone.

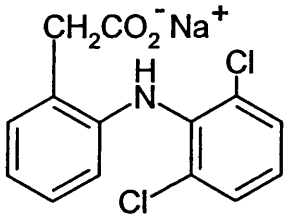


Figure 3.4. Structural formula of diclofenac sodium.

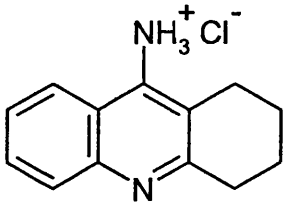


Figure 3.5. Structural formula of tacrine hydrochloride in neutral to acidic pH solution.

It is the purpose of this study to investigate inter-brand variations in the adsorption of the model amine drug and to explore the nature of the drug adsorption onto MCC. A study of the batch-to-batch variation or the potential effect of storage on adsorption for three of the products is possible. In addition, the adsorption of silicified MCC (SMCC), patented MCC derivatives co-processed with 2% w/w colloidal $SiO_2$ (Sherwood & Becker, 1998), will be investigated for the first time.

The methods used to determine adsorption isotherms do not exactly mirror the dissolution tests conducted in accordance with methodologies described in the British, European and US Pharmacopoeias. The dissolution test is one of the standard tests conducted to ensure that a dosage form complies with standards set out in the British Pharmacopoeia (BP) and provides data describing drug release against time and therefore shows not only the total release but also release rate. In order to determine whether the adsorption isotherm data translates into an observable difference in dissolution profiles, dissolution tests on simple formulations containing MCC and tacrine will be undertaken. The MCCs which show the highest and lowest capacities for tacrine adsorption will be selected to improve the probability of successful discrimination.

## 3.2. Materials

### *3.2.1. Microcrystalline cellulose*

Details of the twenty-six MCC samples and derivatives used in this study are given in Table 2.1. The adsorption studies can be divided into ten groups, each group having either a single common feature, which is used to distinguish between the products, or is designed to investigate a particular aspect of MCC manufacture or use. All groupings and descriptions for commercial products are based on the relevant supplier's literature, where available. In order to assess the adsorption of the material as used in general formulation work, samples were not particle size fractionated. The groupings into which the MCCs have been placed can be described thus:

*'Standard' grades from different manufacturers*

These MCCs have a volume diameter mean particle size of approximately 50μm and are marketed as equivalent to Avicel PH101 (FMC Inc, USA). A total of six MCCs were investigated, two US brands, two European, one Brazilian and one Japanese.

These are the most commonly used MCCs in pharmaceutical applications, since they combine generally acceptable flowability with good mixing performance. Multiple batches were acquired for three of the brands (Avicel PH101, Emcocel 50M and Vivapur 101). The most recent batch will be taken as representative of these MCCs.

*Larger particle size grades*

Increased volume diameter mean particle size MCC materials are manufactured by adjustment of the drying conditions. A lower specific surface area is to be expected for larger particle sizes. Three grades, each a commercial product from Penwest Co. (USA) are studied: the 'standard' grade and two large particle grades. According to product literature, the same feedstock as used for the 'standard' grade was used for each of these products, since they are designed to be interchangeable in all respects except for dry flow performance; hence any differences between these products will be due to the final drying conditions.

*High density grades*

Most standard grade MCCs are manufactured using softwood (evergreen) pulp as the feedstock. High density grades are normally manufactured from a hardwood (deciduous) pulp, which have a higher bulk density, reflecting the lower porosity of the source timber (Kotelnikova & Petropavlovsky, 1991).

*Silicified MCC*

The adsorption of SMCCs, patented co-processed MCCs containing 2% w/w colloidal silicon dioxide, were investigated to assess the effect on adsorption of the presence of $SiO_2$ in the particle surface. Standard (50 μm volume diameter mean particle size), large particle (90 μm) and high density grades were investigated.

*Other pulp sources*

These MCCs are manufactured using non-standard pulps, irregular sources and also include a micronised sample. Two Indian products (Ankit and RanQ), a non Pharmacopoeial MCC (Multi-Cel N90) and two experimental pulp source grades from Penwest Co. (Lot#1 and Lot#2) are included in this group. These experimental MCCs are derived from pulps produced using steam explosion pulping. Briefly, the pulp is subjected to high-pressure (1.5 – 3 MPa) steam treatment for up to ten minutes. Explosive decompression discharges the product to atmosphere.

*Treated samples*

Micronised MCC (Emcocel SP15, Penwest Co.) is used to investigate the effect of high-energy milling on the adsorption capacity of MCC.

Samples of Emcocel 50M and Prosolv 50 were heated to 80°C under a stream of dry nitrogen for 16 hours to simulate the drying undergone by formulations during a wet granulation process (Parikh, 1997). It has previously been shown (Sherwood & Becker, 1996) that silicified MCCs do not suffer as great a loss in compactibility on wet granulation as an equivalent standard grade material. It is therefore of interest to test whether there is any effect on adsorption of heating and also whether the silicified material is affected to a greater or lesser extent.

It has also been noted (R.C. Moreton, personal communication) that freezing MCC can affect its compactibility. A batch of MCC accidentally kept at temperatures below 0°C for over 24 hours displayed excessive 'capping' during tablet compaction. Capping is the failure of a tablet in the die due to lamination as a result of air trapped during compaction. Capping is more likely at higher compaction rates, where the elasticity of the material is insufficient to allow trapped air to escape without damaging the tablet. Capping of a material at a lower compaction rate than expected is indicative of a loss of elasticity. To test whether this affects the surface chemistry of MCC, a sample of Emcocel 50M (batch no. E5D8C17X) was frozen for 24 hours at -20°C and allowed to reach ambient temperature before adsorption of tacrine from aqueous solution at 25°C was characterised. This was compared with the more recent adsorption isotherm determined for the untreated material.

### *3.2.2. Batch – to – batch variations*

Multiple batches of Avicel PH101, Emcocel 50M and Vivapur 101 were obtained in order to determine whether any observed inter-product variations fall within the range of batch-to-batch variability.

The adsorption of tacrine from aqueous solution of samples of Avicel PH101, Emcocel 50M and Vivapur 101 were compared when relatively new (3 months after manufacture) and after they had been stored under ambient conditions (30 -55% RH, 16 - 22°C) for 2 years. This was in order to see whether any batch-to-batch variations were a function of the storage time prior to analysis. Note that a different

batch of tacrine was used for the later study, obtained less than one month before the later adsorption experiments were conducted.

### *3.2.3. Process following*

Samples of wet pulp (Temalfa never-dried), dry pulp (Temalfa pulp) and neutralized slurry were obtained from the manufacturers of Emcocel grade MCCs (see Table 3.1). The adsorption of each of these stages was determined in order to observe the effect of the processing on the surface chemistry of the finished product, together with adsorption of the finished product (batch no. E5B1E48).

Table 3.1. Details of 'process following' MCC samples. The pulp and post-neutralisation slurry were taken from the production run to produce Emcocel 50M batch E5B1E48.

| MCC | Batch | Supplier | Country |
|---|---|---|---|
| Temalfa ND | n/a | Penwest Co. | USA |
| Temalfa pulp | PH051999A | Penwest Co. | USA |
| Post-neut slurry | n/a | Penwest Co. | USA |

### *3.2.4. Other chemicals*

Tacrine hydrochloride (BP grade, Aldrich, Gillingham, UK) was used without further purification. Water used was freshly purified by reverse osmosis (Millipore, Watford, UK) with conductivity in the range 650 – 700 μS. Water was de-gassed by helium displacement (minimum 1 hour per litre). Sodium chloride was analytical grade (AR grade, Fisher, Loughborough, UK).

## 3.3. Methods

### *3.3.1. Adsorption of tacrine*

Adsorption isotherms were obtained by batchwise thermostatic equilibration (Richardson, 1973). A 1000 mg sample of MCC was suspended in 40 ml solution at each of fifteen drug concentrations in 50 ml borosilicate volumetric flasks. This was then equilibrated for two hours at the required temperature in a shaking water bath

(Gyrotory®, New Brunswick Scientific, Edison, USA) to ensure thorough mixing, maximum adsorption and thermal equilibrium. The time required for equilibrium adsorption was determined separately by extracting supernatant after equilibration for one half to five hours.

The supernatant was separated by centrifugation (1400 *g*, 10 min) and analysed by UV spectrophotometry (Helios α, Unicam, Cambridge, UK) ($\lambda_{max}$ = 239 nm, $\varepsilon_{tacrine}$ = 39 900 $mol^{-1}cm^{-1}$) after dilution to between 1 and 5 $mgl^{-1}$ (4 – 20 μM). Three controls were analysed: MCC in water, a tacrine solution of an appropriate concentration and water. These determine the UV absorbance of water-soluble extractives, possible thermolytic degradation or adsorption of the drug onto the glassware and levels of contaminants from the glassware. Replicate analyses (n = 5) of the water-soluble extractives indicated that UV absorbing material was released from all the MCC samples. This material may be the protein-like surface active solute previously described (Ardizzone et al, 2001). The UV absorption of these extractives was reproducible to ±0.001 absorbance units at 239 nm for each MCC, therefore the UV absorption of each diluted equilibrium tacrine solution was adjusted to account for the presence of these extractives. No significant thermolytic degradation or adsorption onto the experimental apparatus was found. No significant contamination from the glassware was detected.

### *3.3.2. Tacrine concentration*

Fifteen data points over the initial tacrine concentration range of 0.05 to 1.0 mM were collected for isothermal equilibration studies at 25°C.

### *3.3.3. Temperature Effect*

In order to determine the effect of increased temperature on the adsorption process, and also to obtain thermodynamic information about the adsorption process, adsorption isotherms were measured at 37°C for the MCCs listed in Table 3.2. These were selected as extremes of adsorption affinity and capacity from the experiments at 25°C, a representative standard MCC and a silicified MCC.

Table 3.2. MCC samples used in the study of the effect of temperature on adsorption of tacrine. Justification for the use of each MCC summarises the reasons these MCCs were selected.

| MCC | Justification |
|---|---|
| Pharmacel 101 | Highest capacity at 25°C |
| Emcocel HD90 | Lowest (non-silicified) capacity at 25°C |
| Prosolv HD90 | Lowest capacity at 25°C |
| Emcocel 50M | Representative standard grade MCC |
| Prosolv 50 | Silicified MCC |

Standard free energy, enthalpy and entropy were calculated as follows (Yadava et al, 1991):

$$\Delta G^\circ = -RT \ln K_C \qquad \text{Equation 3.1}$$

$$\Delta H^\circ = R\left(\frac{T_1 T_2}{T_2 - T_1}\right)\ln\left(\frac{K_{C2}}{K_{C1}}\right) \qquad \text{Equation 3.2}$$

$$\Delta S^\circ = \frac{\Delta H^\circ - \Delta G^\circ}{T} \qquad \text{Equation 3.3}$$

where $K_C$, $K_{C1}$ and $K_{C2}$ are the rate constants at temperatures $T$, $T_1$ and $T_2$, respectively. The rate constants are derived from the equilibrium concentrations on the adsorbate and in solution:

$$K_C = \frac{C_{Ae}}{C_{Se}} \qquad \text{Equation 3.4}$$

where $C_{Ae}$ is the equilibrium concentration of adsorbent on the adsorbate ($mgl^{-1}$) and $C_{Se}$ is the equilibrium concentration of adsorbent in solution ($mgl^{-1}$). An average true density of 1.54 $gcm^{-3}$, determined by He Pycnometry (AccuPyc 1330, Micromeritics, Dunstable, UK), was determined for the MCCs under consideration.

### 3.3.4. *Data interpretation*

The Langmuir (L2 (Giles et al, 1960)) isotherm for monolayer adsorption was used to interpret the data obtained in the isotherm studies. The linear form of the Langmuir isotherm is given in equation 3.5:

$$\frac{C_{eq}}{(x/m)} = \frac{1}{k_1 k_2} + \frac{C_{eq}}{k_2} \qquad \text{Equation 3.5}$$

where $C_{eq}$ is the equilibrium concentration, $x$ is the amount of adsorbate adsorbed on $m$ mass of adsorbent, $k_1k_2$ is the affinity constant and $k_2$ is the capacity constant. A plot of $C_{eq}$ against $C_{eq}/(x/m)$ will yield a straight line if ideal adsorption has occurred. This indicates that monolayer adsorption is occurring in the concentration range under investigation. Adsorption sites are assumed to be energetically homogeneous and adsorption is independent of occupancy of adjacent sites.

The adsorption data was also modelled using the Freundlich isotherm, which indicates multi-layer adsorption. Although generally good correlation coefficients were obtained ($r^2 > 0.80$), residuals analysis showed a quadratic trend, indicating that this isotherm does not reliably describe the observed adsorption.

Least squares linear regression analyses were completed using Minitab 12 (Minitab Inc. USA) whereby slope, intercept and the standard deviations of each linear isotherm were computed. In addition to the raw data obtained from these isotherm plots, the surface area available for adsorption may be estimated from the amount of tacrine hydrochloride adsorbed per unit mass. Surface area values are estimated on the basis that the tacrine molecule has a molecular area of 2 $nm^2$, similar to that of anthracene (= 2.05 $nm^2$; Narbonne et al, 1999), using the equation:

$$sa = A.(x/m).N_A \qquad \text{Equation 3.6}$$

where $sa$ is the surface area ($m^2$), $A$ is the area of the molecule (= $2 \times 10^{-18}$ $m^2$), $(x/m)$ is the adsorption capacity in $molkg^{-1}$ and $N_A$ is Avogadro's constant.

### 3.3.5. *Process following*

The total volume of stock solution was adjusted to compensate for the greater volumes of the process-following samples. Both the never-dried pulp and the post-neutralisation slurry contain large volumes (>80% by weight) of water. This contribution to the total volume of the stock solution was compensated for in the

calculation of the initial tacrine concentration. The water content was determined by drying samples at 105°C to constant mass. For the post-neutralisation pulp an additional extraction was required. The fine particle size of the slurry (d v, 0.5 = 5 μm) meant that there were still cellulose particles suspended after centrifugation. Syringe filters (0.2 μm pore size PTFE filters, Whatman, UK) were used to remove the fine particles. These filters were found to have an insignificant adsorption of tacrine, based on tests using tacrine solutions in the concentration range 0.05 to 1.0 mM.

### *3.3.6. Ionic strength*

Experiments to determine the effect of ionic strength on the adsorption of tacrine can provide information about the adsorption mechanism (Okada et al, 1987), since adsorption by ion-exchange will be blocked by the preferential adsorption of the higher charge-density salt ions.

In order to determine the effect of the ionic strength of the tacrine solution on adsorption, adsorption isotherms at 25°C were obtained using Emcocel 50M and Emcocel HD90 as adsorbate. Isotonic solutions of NaCl (0.9% w/v, 0.154 M) over the tacrine concentration range 1.5 to 50 $mgl^{-1}$ were used. Previous investigations (Figure 3.6; see also Okada et al, 1987) had established that adsorption decreased as salinity increased until a plateau of minimum absorption was reached at NaCl concentrations above 0.05M.

A comparison of the effect of saline conditions on the adsorption of four MCCs of interest was also conducted at a single concentration. Triplicate analyses of the adsorption by Tabulose 101, Ceolus KG-802, Ankit and Vivapur 302 of tacrine from 100 $mgl^{-1}$ isotonic NaCl were carried out. The reduction in adsorption from that expected can be used to determine the level of non-ionic adsorption capacity.

### *3.3.7. Reversibility of adsorption*

In order to determine whether the adsorption of the drug is permanent to any degree, a re-equilibration method will be used to determine the amount of tacrine irreversibly adsorbed into the surface of the MCC. Extraction of an aliquot of the supernatant at equilibrium adsorption and replacement with water decreases the amount of drug in the system. Only drug reversibly adsorbed into the solid will be available to establish a new equilibrium between the supernatant and the adsorbed drug.

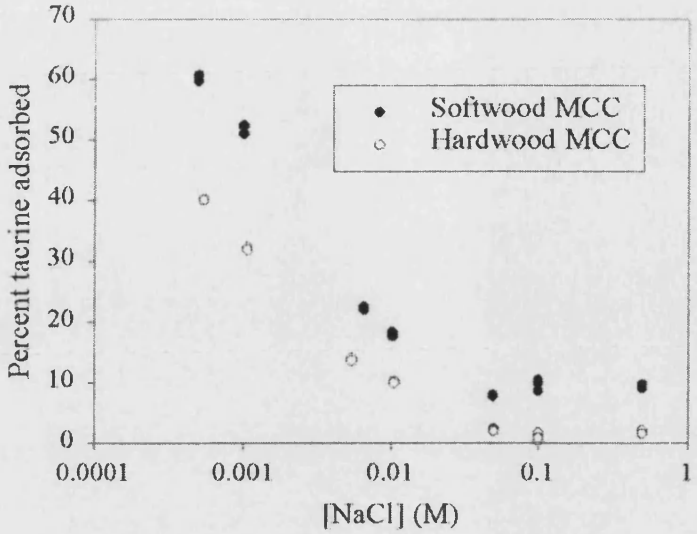


Figure 3.6. Comparison of the effect of salinity on the adsorption of tacrine from aqueous solution of a softwood MCC (Emcocel 50M) and a hardwood MCC (Emcocel HD90). Three repeats at each ionic strength.

Therefore, the second equilibrium concentration will be affected by permanent adsorption of drug onto the solid. The extent of the permanent adsorption can be determined if the adsorption isotherm between the solid and the drug is known.

The extent of the reversibility of the adsorption of tacrine from aqueous solution was assessed for Tabulose 101 and Ceolus KG-802 by a re-equilibration technique. A 1000mg sample of MCC was thermostatically equilibrated with 40 ml of a 150 $mgl^{-1}$ solution of tacrine at 25°C. The sample was then centrifuged as above and 20 ml of the supernatant was removed for UV spectroscopic analysis. The MCC dispersion was then returned to the original volumetric flask by washing with 20 ml of degassed water. The dispersion was then thermostatically equilibrated a second time and the supernatant extracted after centrifugation for UV spectroscopic analysis. From the previously obtained Langmuir isotherm and the equilibrium concentration after the second equilibration, the initial concentration prior to the second equilibration ($C_{in2}$) could be determined:

$$C_{in2} = C_{eq2} + \frac{x_2}{v_t} \qquad \text{Equation 3.7}$$

where $C_{eq2}$ is the second equilibrium concentration, $x_2$ is the amount of tacrine adsorbed in the second equilibration and $v_t$ is the total liquid volume (0.04 l in this study). The value of $x_2$ may be determined from the Langmuir isotherm determined for the MCC used *via* the rearranged equation:

$$x_2 = \frac{C_{eq2} m}{\frac{1}{k_1 k_2} + \frac{C_{eq2}}{k_2}} \qquad \text{Equation 3.8}$$

where $m$ is the mass of MCC used and $k_1k_2$ and $k_2$ are values determined from the Langmuir isotherm (Equation 3.5).

The extent of the reversibility of the adsorption may be determined *via* the equation:

$$f = \frac{v_t}{2x_2}\left(2C_{in2} - C_{eq1}\right) \qquad \text{Equation 3.9}$$

where $f$ is the fraction of tacrine reversibly adsorbed and $C_{eq1}$ is the first equilibrium concentration, determined prior to the re-equilibration step.

This equation is derived as follows; the value for $C_{in2}$ is derived from the mass available in solution, $m_{in2}$. This is determined by:

$$m_{in2} = \frac{v_a m_{eq1}}{v_t} + fx \qquad \text{Equation 3.10}$$

where $m_{eq1}$ is the mass of tacrine in solution after the first equilibration and $v_a$ is the volume of the aliquot of supernatant removed. The quantity $fx$ is the mass of drug that is desorbed when the effective equilibrium concentration is reduced. For the experiments described here, $v_a$ is 20 ml and $v_t$ is 40 ml. Therefore, the concentrations may be determined from:

$$\frac{m_{in2}}{v_t} = \frac{m_{eq1}}{2v_t} + \frac{fx_2}{v_t} \qquad \text{Equation 3.11}$$

$$\therefore C_{in2} = \frac{C_{eq1}}{2} + \frac{fx_2}{v_t} \qquad \text{Equation 3.12}$$

By rearranging Equation 3.12, we obtain Equation 3.9.

### *3.3.8. Mass lost*

The primary aim of this work is to investigate the influence of the observed adsorption on the *in vitro* release of drugs in trial formulations. It is therefore useful to be able to calculate the reduction in dosage reduction resulting from the adsorption. The amount absorbed ($x$) by a known mass of MCC ($m$) with a previously determined affinity ($k_1k_2$) and capacity ($k_2$) at the required equilibrium concentration ($C_{eq}$) may be determined by rearranging the Langmuir isotherm:

$$x = \frac{C_{eq} m}{\frac{1}{k_1 k_2} + \frac{C_{eq}}{k_2}} \qquad \text{Equation 3.13}$$

### *3.3.9. Surface area*

Specific surface area was determined by 5-point BET $N_2$ adsorption (Gemini 2360, Micromeritics, Dunstable, UK) at 77 K in triplicate. Samples were dried at 40°C to constant mass (usually sixteen hours) under a stream of dry nitrogen to remove surface moisture (see Chapter 2).

### *3.3.10. Particle size*

Particle size distribution analysis by laser diffraction was performed using the Mastersizer 2000 (Malvern Ltd., Malvern, UK). Samples were presented as dry powders using the Scirocco 2000 automated dry powder feeder (Malvern Ltd., Malvern, UK) set to yield a pressure drop of 3 bar across the sampling chamber. Each analysis is the mean of 10000 scans over ten seconds. Sample feed rate was adjusted to give a laser obscuration of 0.5 to 2.0% during analysis. Results quoted are the means of three analyses. All results are quoted as volume diameter distributions (see Chapter 2).

### *3.3.11. Dissolution tests*

The adsorption isotherm data indicate that Pharmacel 101 and Prosolv HD90 have the highest and lowest capacities for adsorption of tacrine from aqueous solution. Blends containing 2% w/w of tacrine HCl (BP grade, Aldrich, Gillingham, UK) in MCC were mixed using a Turbula shaker mixer (Type T2 F, Bachhofen AG, Basel, Switzerland) for 3 minutes at 46 rpm. The tacrine HCl was passed through a 125 μm sieve prior to use to remove agglomerates and so improve content uniformity on mixing. Direct compression formulations were compacted using a single station rotary F-press (Manesty, Liverpool) with a gravity-feed hopper. Flat-faced 10 mm diameter stainless steel tooling was used throughout. Lower punch maximum stroke depth was adjusted to obtain tablets of a mass of approximately 250 mg. The upper punch maximum stroke depth was adjusted to obtain tablets with a range of crushing strengths between 50 and 200 N. Tablets much weaker than 50 N had poor integrity, in extreme cases disintegrating during handling. The upper limit of the tablet crushing apparatus used is approximately 200 N. Approximately twenty tablets were produced at each of five upper punch displacements, of which five were used for physical characterisation. At least forty tablets were produced with a crushing strength of approximately 100 N for dissolution testing. Placebo formulations of pure MCC were manufactured to provide controls.

Tablets produced were tested for weight variation, disintegration time, hardness and compaction strength in order to ensure that the tablets produced were acceptable within BP standards. Weight variation for twenty tablets was determined using a 5-figure analytical balance. Disintegration time was determined for six tablets at 37°C

in accordance with the BP test (Appendix XII A (1993)) using an Erweka disintegration tester (Heusenstann, Germany).

Tablet hardness was determined using a diametric tablet tester (Schleuniger-2E, Berne, Switzerland) (n = 5). Tablet tensile strength was determined by using the Fell & Newton (1972) method:

$$\sigma = \frac{2P}{\pi Dt} \qquad \text{Equation 3.14}$$

where $\sigma$ is the tensile strength (MPa), $P$ is the applied load (N), $D$ and $t$ are the diameter and thickness of the specimen, respectively (mm).

Because it is anticipated that there will be less than 100% release from the tacrine formulations, content uniformity may only be implied from a study of the release of drug from the formulation, rather than measuring the actual drug content of the formulation. Total release after 2 hours was determined at 37°C for each tacrine formulation (DC, wet granules, dried granules and compacted granules). A single tablet was placed in 40ml water in a 50ml borosilicate volumetric flask (n = 5). After the equilibration time the supernatant was removed by centrifugation and the UV absorbance and hence the amount released could be determined.

Apparatus conforming to BP specification (Appendix XII D, type 2 (1993)) was used throughout (Pharma-Test PT-DT7, Hainburg, Germany). All tests were conducted at 37.5°C using 900 ml degassed water as the initial dissolution fluid. Paddles rotating at 50 rpm were used to agitate the bath. Aliquots of 10 ml were removed from the supernatant every 30 seconds up to 5 min in order to establish the release profiles of the formulations. A final sample after 120 minutes was taken to establish total release, in line with the adsorption experiments. The concentration of drug in the bath was established using UV detection at 239 nm.

### 3.4. Results and Discussion

The data from the isotherms of all MCCs studied were described well by the Langmuir equation ($r^2 > 0.92$). All data showed a normal distribution (Anderson - Darling test) about the least squares linear regression line. Data for all twenty-five MCC products studied are summarised in Table 3.3. Isotherm plots for Tabulose

Table 3.3. Summary analysis of Langmuir adsorption isotherms measured at 25°C. Abbreviated batch numbers are given for Avicel PH101, Emcocel 50M and Vivapur 101 for the purpose of batch-to-batch comparison and for investigation of the effect of heating and freezing. The affinity constants ($k_1k_2$) and adsorption capacities ($k_2$) are presented together with the 95% confidence intervals of the individual analyses, determined from standard deviation calculations. Tacrine surface areas are based on a molecular surface area of 2 $nm^2$ for tacrine.

| MCC | $k_1k_2$ | $k_2$ ($mmolkg^{-1}$) | Tacrine surface area ($m^2kg^{-1}$) |
|---|---|---|---|
| Avicel PH101 [6902C] | 219 ± 47 | 11.4 ± 0.4 | 13700 ± 500 |
| Avicel PH101 [1113] | 285 ± 11 | 9.27 ± 1.13 | 11200 ± 1400 |
| Avicel PH101 [6902C, 24 months] | 193 ± 7 | 11.6 ± 1.5 | 14000 ± 1800 |
| Ceolus KG-802 | 439 ± 11 | 11.6 ± 0.8 | 14000 ± 700 |
| Emcocel 50M [C17X] | 172 ± 46 | 10.5 ± 0.4 | 12600 ± 400 |
| Emcocel 50M [E21] | 230 ± 4 | 8.43 ± 0.88 | 10200 ± 1100 |
| Emcocel 50M [E48] | 295 ± 7 | 9.39 ± 1.08 | 11300 ± 1300 |
| Emcocel 50M [C17X, 24months] | 250 ± 7 | 8.30 ± 0.82 | 10000 ± 1000 |
| Pharmacel 101 | 219 ± 16 | 12.5 ± 0.2 | 15100 ± 200 |
| Tabulose 101 | 42.4 ± 6.9 | 10.0 ± 1.6 | 12000 ± 1900 |
| Vivapur 101 [3529] | 217 ± 40 | 10.5 ± 0.3 | 12600 ± 300 |
| Vivapur 101 [4629] | 276 ± 6 | 8.72 ± 1.04 | 10500 ± 1300 |
| Vivapur 101 [0714] | 290 ± 5 | 7.84 ± 0.93 | 9400 ± 1100 |
| Vivapur 101 [3529, 24 months] | 236 ± 5 | 10.4 ± 1.0 | 12500 ± 1200 |
| Emcocel 90M | 183 ± 63 | 10.5 ± 0.3 | 12700 ± 400 |
| Emcocel LP200 | 157 ± 73 | 10.5 ± 0.9 | 12700 ± 1000 |
| Avicel 302 | 93.2 ± 35.0 | 6.93 ± 0.46 | 8300 ± 600 |
| Emcocel HD90 | 109 ± 46 | 5.30 ± 0.59 | 6400 ± 700 |
| Vivapur 302 | 220 ± 90 | 8.24 ± 0.44 | 9900 ± 500 |
| Prosolv 50 | 190 ± 79 | 8.30 ± 0.41 | 10000 ± 500 |
| Prosolv 90 | 209 ± 54 | 9.28 ± 0.46 | 11200 ± 600 |
| Prosolv HD90 | 124 ± 31 | 4.33 ± 0.22 | 5200 ± 300 |
| Ankit | 40.8 ± 7.6 | 8.59 ± 0.88 | 10400 ± 1100 |
| RanQ | 90.8 ± 39.3 | 6.24 ± 0.80 | 7500 ± 1000 |
| Avicel PH105 | 165 ± 4 | 8.09 ± 0.63 | 9700 ± 800 |
| Emcocel SP15 | 167 ± 63 | 8.68 ± 0.63 | 10500 ± 800 |
| Lot #1 | 23.2 ± 3.6 | 8.17 ± 1.30 | 9800 ± 1600 |
| Lot #2 | 36.2 ± 8.3 | 8.24 ± 1.32 | 9900 ± 1600 |
| Multi-Cel N90 | 107 ± 31 | 7.75 ± 0.41 | 9300 ± 500 |
| Emcocel 50M [C17X, heated] | 116 ± 47 | 4.76 ± 0.25 | 5800 ± 300 |
| Prosolv 50 [heated] | 67.8 ± 4.0 | 5.78 ± 1.23 | 7000 ± 1500 |
| Emcocel 50M [C17X, frozen] | 280 ± 12 | 8.88 ± 0.67 | 10700 ± 800 |

101, Emcocel 50M and Emcocel HD90 are compared in Figure 3.7 and in the linearised form in Figure 3.8.

### *3.4.1. Statistical treatment of adsorption results*

The initial null hypotheses, that the mean affinities ($\chi^2$ test; $p<0.01$) and the mean capacities ($\chi^2$ test; $p<0.01$) of all MCCs studied were equal, were rejected. Fisher's pairwise multiple comparison test was adapted to establish statistically equivalent groups of MCCs, on the basis of affinity and capacity. This test is based on the standard deviations of the slope and intercept calculated from the linear regression analyses, using a normal distribution for the data points about the linear regression line (see Appendix 1). Using this treatment a critical difference is obtained for affinity and capacity data, determined *via* the calculation of a pooled standard deviation. This means that within sample variations are taken to be equal for each MCC studied, irrespective of the individually calculated 95% confidence limits given in Table 3.3. Differences smaller than 56.5 for affinity constants and 1.04 $mmolkg^{-1}$ for capacities are not significant to within 95% confidence.

The groupings of the MCCs are used to simplify the discussion of the differences and similarities between the affinity constants and capacity values calculated for the adsorption isotherms measured.

### *3.4.2. Standard grades*

Statistical analysis based on Fisher's pairwise comparison shows that there are significant differences ($p < 0.05$) between some of the standard grades.

The affinity constant for Tabulose 101 is significantly lower than the values obtained for the other five MCCs in the standard grade group, and Ceolus KG-802 has a significantly higher affinity than any other MCC sample. The capacities for tacrine of Avicel 101, Ceolus KG-802 and Pharmacel 101 are significantly higher than the other three MCCs, with Pharmacel 101 displaying a significantly higher capacity than Avicel 101 and Ceolus KG-802.

The difference in the affinity constants has a profound effect on the adsorption observed at lower drug concentrations. This is illustrated in Figure 3.9, comparing Tabulose 101 and Ceolous KG-802. The Langmuir isotherms for these products predict that the saturation adsorptions (capacities) differ by 16%. However, in the

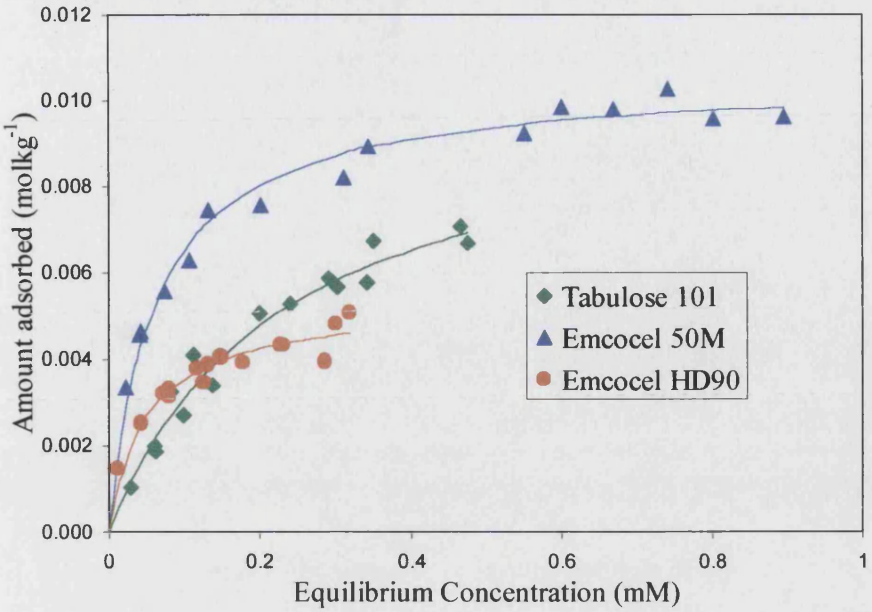


Figure 3.7. Raw data for the adsorption of tacrine from aqueous solution onto Tabulose 101, Emcocel 50M and Emcocel HD90 at 25°C; n = 15 in each case. Fitted lines are the Langmuir isotherms determined from the linearised data (see Figure 3.8 and text).

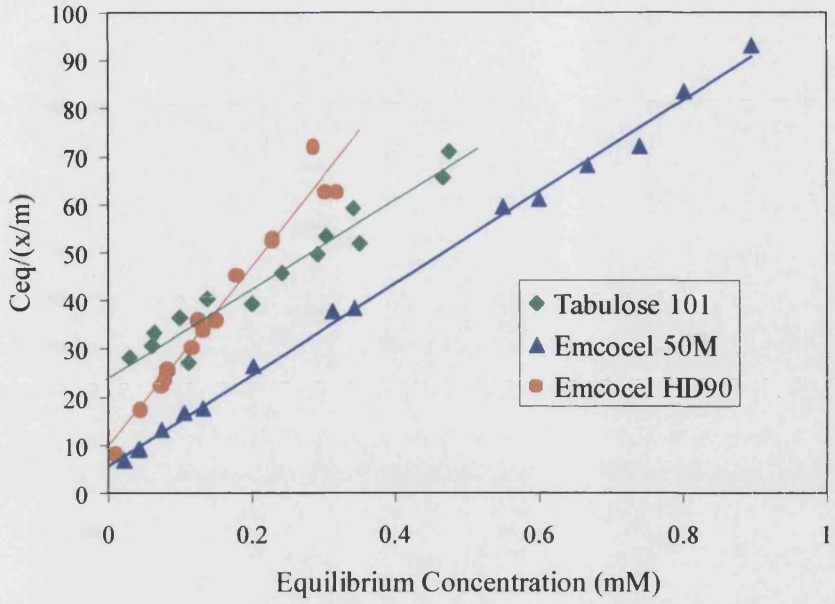


Figure 3.8. Linearised (Langmuir) adsorption data from Figure 3.7. Least squares linear regression lines are the Langmuir isotherm fits, used to calculated affinity and capacity of the solid for the solute. Similar slopes of the Tabulose 101 and Emcocel 50M indicate similar capacities for tacrine. Different affinities are indicated by the dissimilarity of the intercepts.

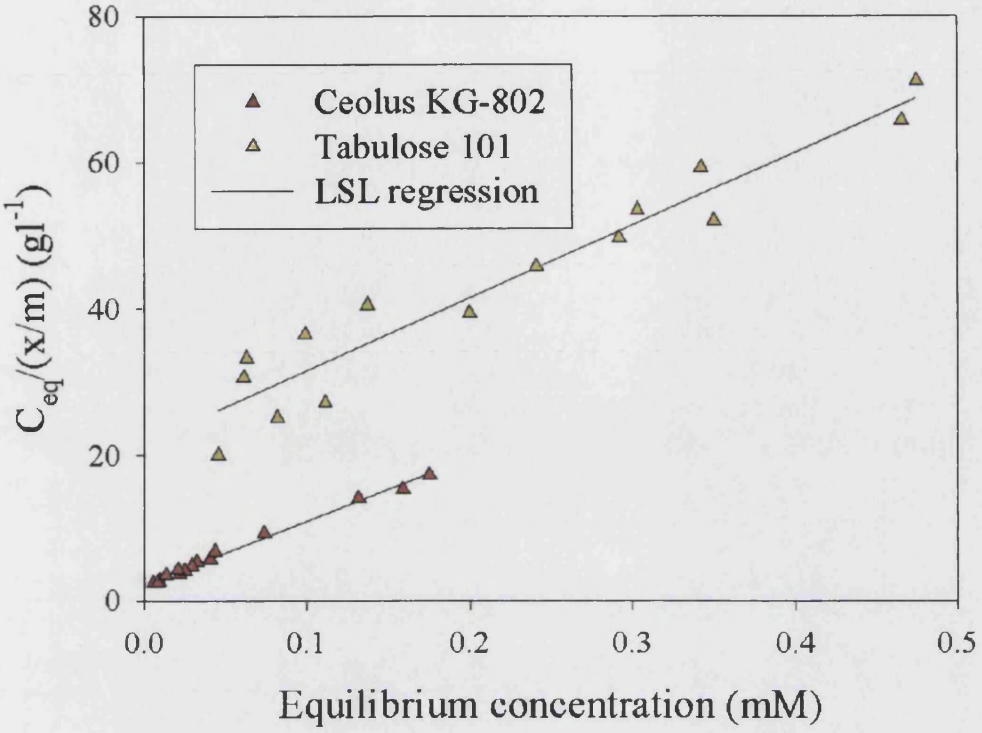


Figure 3.9. Comparison of linearised adsorption data for Tabulose 101 and Ceolus KG-802. Least squares linear regression (LSL) lines show that the capacities are similar (parallel lines), but the affinity of Tabulose 101 for tacrine is much lower (higher intercept).

isothermal equilibration experiments using 1000 mg MCC in 40 ml solution, at a concentration of, for example, 25 $mgl^{-1}$, 88% of the available tacrine will be adsorbed by Ceolus KG-802, compared with 46% by Tabulose 101. Therefore, low affinity MCCs may be suitable for use in cases where a low degree of adsorption is acceptable.

From these results it may be concluded that Vivapur 101 and Emcocel 50M are equivalent products with respect to adsorption of tacrine. Also, the adsorption capacities of Avicel 101 and Ceolus KG-802 are statistically equivalent. The technique used to achieve a lower bulk density for Ceolus KG-802 does not have a significant effect on the adsorption capacity of the material. No correlation between affinity constant and capacity for these products was observed. These results indicate that variables such as pulp source, depolymerisation conditions and neutralisation techniques play an important role. It should be emphasised that these comparisons are made on the basis of single batches from each manufacturer. The differences seen in this study may, therefore, be a reflection of batch-to-batch variations within each manufacturer's product.

Final drying conditions are less likely to play a significant role, since Emcocel 50M is spray dried (Penwest product literature), in contrast to the air-stream drying technique employed in the manufacture of Vivapur 101 (Rettenmaier product literature).

### *3.4.3. Large particle size*

There are no significant differences in either the affinity constants or the capacities of Emcocel 50M, Emcocel 90M and Emcocel LP200 (Figure 3.10). This indicates that the spray drying conditions have no significant effect on the surface chemistry of the MCC products. It may be deduced that the nature of the fibrils forming the aggregates, rather than the size of the aggregates, is a primary determinant of the adsorption capacity. Interestingly, immersion calorimetry studies of a range of particle size grades of Avicel showed that the heat of immersion was not significantly affected by particle size (Rowe et al, 1993).

The reasons for the disagreement of the tacrine adsorption results presented here with the findings of Qtaitat et al (1988) are not immediately explicable, but may be a result of steric factors affecting the ability of the large bromhexine molecules to

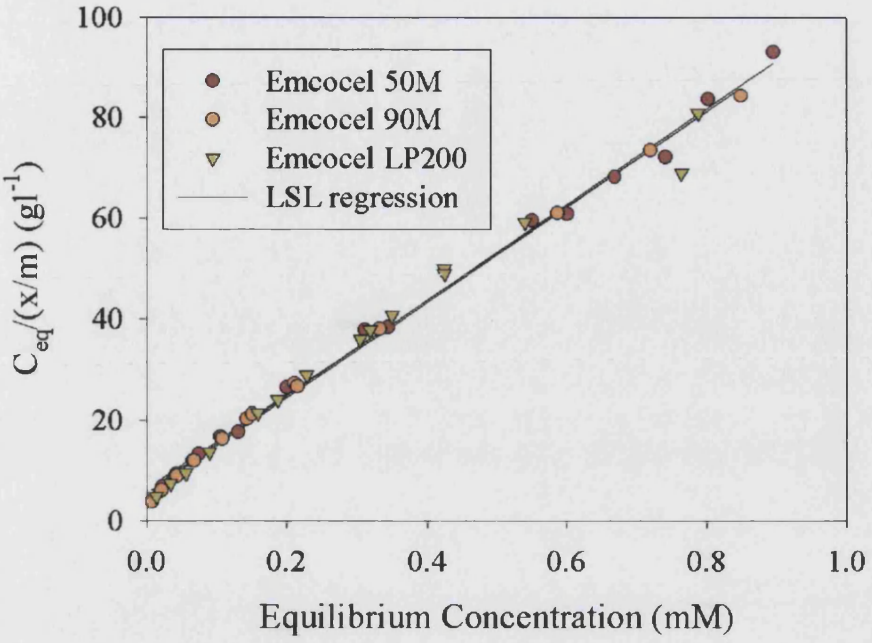


Figure 3.10. Comparison of the effect of MCC particle size against adsorption of tacrine at 25°C. These results suggest than the size of the MCC aggregates does not affect the adsorption of this drug, since there is no significant difference between the affinities or capacities of these three MCCs.

occupy adsorption sites within small pores, which is not a significant factor in tacrine adsorption. Qtaitat et al (1988) presented no porosimetry data, however a difference in the pore size distribution and therefore the accessibility of the internal surfaces may be expected. Microcrystalline cellulose particles as measured by standard particle sizing methods are aggregates of smaller particles of MCC (Chapter 2; see also Ek et al, 1994; Doelker et al, 1995), the size of these aggregates being the measured particle size. On a mass-for-mass basis, less of the interior of the larger particles will be accessible to these larger drug molecules, if it is assumed that there are pores present small enough to block access to the interior of the agglomerate.

### *3.4.4. High density products*

Microcrystalline celluloses manufactured from softwood sources have a significantly higher adsorptive capacity for tacrine than hardwood sourced MCCs. This is best observed when comparing hardwood and softwood products from the same manufacturer, because the same equipment, techniques and manufacturing practices are likely to be used for each product.

Use of a hardwood pulp source for product pairs based on manufacturer and pre-treatment show that there are significant differences in the capacities of these products (Table 3.3). Affinity is not affected for the Rettenmaier GmbH products (Vivapur 101 and Vivapur 302), but the two Penwest Co. pairs (Emcocel 90M and Emcocel HD90; Prosolv90 and Prosolv HD90) and the two FMC Co. products (Avicel PH101 and Avicel PH302) show significant differences within the pairs.

Odaka et al (1987) determined, via Freundlich multiplayer isotherms, a monolayer capacity of 0.218 $mmolkg^{-1}$ for acrinol (Figure 3.1d) on Avicel PH101 and 0.174 $mmolkg^{-1}$ for Avicel 301 at 25°C. These experiments were conducted at pH 6.92 in a solution with an ionic strength of 0.04$moll^{-1}$. No experimental error data were provided, but this difference of 18% is lower than the difference between the adsorption of tacrine from aqueous solution by Avicel PH101 and Avicel PH 302, equal to 39%. The very low adsorption capacity of acrinol may be partly due to the higher ionic strength used by Okada et al (1987).

Okada et al (1987) ascribed the lower capacity of the hardwood derived MCC to variations in the cellulose microcrystallite and cluster structure. The mean size of softwood MCC aggregates is shown to be not significant in this study for tacrine

adsorption (section 3.4.2). Therefore, the known differences in microcrystallite structure between softwood and hardwood products (Landin et al, 1993b) are shown to significantly influence the adsorption capacity of tacrine onto MCC.

The similar capacities for Vivapur 101 and Vivapur 302 suggests that the high density product is not derived from a hardwood pulp source. The batch of Vivapur 302 supplied has a similar capacity to Vivapur 101 batches 4629 and 0714.

### *3.4.5. Silicification*

Silicified MCC products are shown to have a significantly lower capacity, but an unchanged affinity, for tacrine compared with the equivalent unmodified grade (Figure 3.11). This may be a consequence of the presence of $SiO_2$ in the surface of the product (Edge et al, 1999). Silicification reduces the adsorption of tacrine by 21% to 12%, due either to the replacement of cellulosic surface area by non-adsorbing silicon dioxide or the preferential adsorption of silicon dioxide onto active sites in the surface of MCC.

The similarity of the affinity constants of the silicified and unmodified grades indicates that there is not a preferential adsorption of silicon dioxide in the surface. Preferential adsorption would reduce the affinity for tacrine by masking the most active sites, thus making adsorption more difficult. It is more likely that there is a net reduction in the surface available for adsorption, with any masking of adsorption sites occurring randomly.

### *3.4.6. Other pulp sources*

All products based on non-standard pulps display significantly different affinity constants and adsorption capacities compared to Emcocel 50M. The two products from India, Ankit and RanQ, show different capacities but similar affinities. The lower adsorption capacities and affinities may be a result of these products being produced from a hardwood source, as previously determined for Indian MCCs (Landin et al, 1993c). A hardwood source for these samples is suggested by the determination of the degree of polymerisation (DP; see Chapter 4).

The three Penwest Co. special products have similar capacities, but dissimilar affinities with Lot#1 and Lot#2 being equivalent, Lot#2 and MultiCel N-90 equivalent, but Lot#1 and MultiCel N-90 not equivalent. All three have a significantly lower adsorption capacity than Emcocel 50M, used here as a

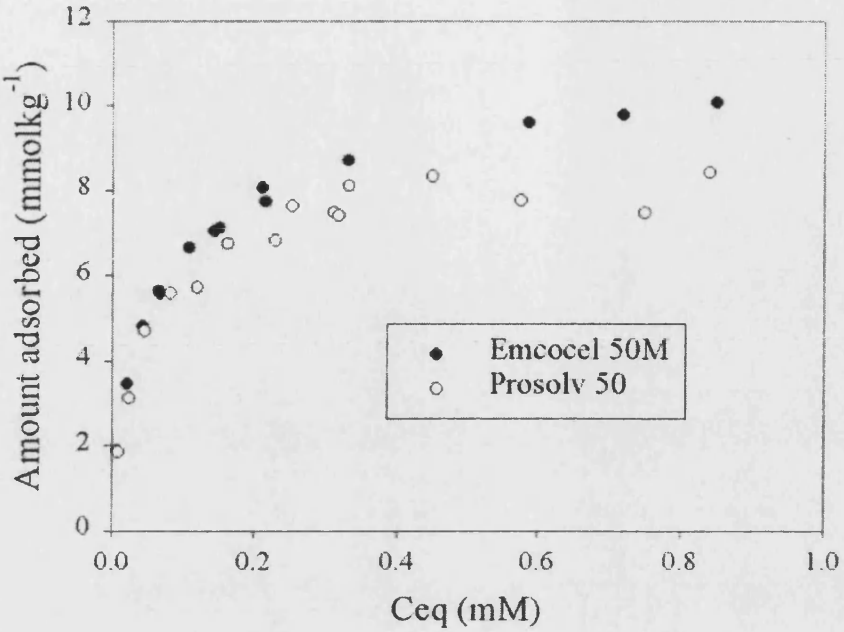


Figure 3.11. Comparison of the adsorption of tacrine from aqueous solution by standard grade MCC (Emcocel 50M) and silicified MCC (Prosolv 50). These results suggest than silicification reduces the adsorption capacity of the material.

benchmark product. These experimental grades are manufactured using different pulps and different bleaching methods. This confirms the importance of pulp source as a determining factor in the adsorption capacity of MCCs. This also shows that the pulping and bleaching methods used to produce the feedstock for MCC production affect the adsorption capacity of the finished product. It is therefore critical that manufacturers carefully control their pulp source, since a change in the feedstock may have a marked affect on the performance of the finished product.

### *3.4.7. Treated samples*

Emcocel SP15 is a micronised (air-jet milled) grade of MCC. This high-energy treatment of the MCC significantly reduces the capacity for adsorption of tacrine compared with Emcocel 50M batch C17X by 17 ± 1%, despite the increase in specific surface area as measured by BET $N_2$ adsorption. The process by which the particle size of Avicel PH105 is reduced is not known. However, the capacity of Avicel PH105 to adsorb tacrine is reduced compared with Avicel PH101 (29 ± 2%). It is not likely that the source of Avicel PH105 is unmodified fine particles recovered during manufacture, since previous work (section 3.4.3) has suggested that the particle size of agglomerates does not affect adsorption significantly. Rather, a milling process may be used to achieve the smaller particle size. The possibility that the process used to comminute the MCCs studied affects the surface properties of the material has previously been suggested from aqueous immersion studies (Rowe et al, 1993). Heats of immersion measured on the basis of energy per unit area found a significantly lower heat of immersion for Avicel 105 compared with other Avicel grades.

Heating significantly reduces the capacity and affinity of Emcocel 50M and Prosolv 50. This may be evidence of mild dry hornification (Weise, 1998), a heat-induced reduction of the water – cellulose interaction. It is therefore possible that the water – cellulose interaction is an important factor in drug adsorption, with the ability of MCC to swell in water a factor in determining the area available for adsorption from aqueous solution. It is interesting to note that, although the SMCC shows evidence of being affected by heating with respect to the adsorption of tacrine from aqueous solution, such surface modification is reported to have a minimal effect of the compactibility of this product (Sherwood & Becker, 1998).

Frozen Emcocel 50M did not have a significantly different adsorption capacity or affinity for tacrine. The reduced elasticity implied by the reported increase in capping of MCC does not affect the surface chemistry of the material in any manner that significantly affects the adsorption of tacrine from aqueous solution.

### *3.4.8. Temperature effect*

Table 3.4 summarises the adsorption results obtain at 37°C for the MCCs listed. In general, a lower adsorption is noted at the increased temperatures, indicative of an exothermic process.

Because different stock solutions were used for each MCC and each temperature, a strictly graphical approach was not suitable. Therefore, at initial concentrations of 1, 10 and 100 $mgl^{-1}$ the predicted adsorption was calculated using the previously determined adsorption isotherms.

For the five MCCs analysed here, a mean standard free energy of $-2.7 \pm 1.2$ $kJmol^{-1}$ and a mean enthalpy of adsorption of $-6.3 \pm 1.6$ $kJmol^{-1}$ is determined. From these results, an entropy change of $-12 \pm 10$ $Jmol^{-1}K^{-1}$ is calculated. The low enthalpy is a strong indication that adsorption occurs by a physical, rather than chemical, process. These result is close to that determined by Acemioglu & Alma (2001) for the adsorption of Cu(II) by cellulose from aqueous solution. It can be anticipated that $Cu^{2+}$ will interact primarily by an ion-exchange mechanism, as has been indicated for the adsorption of some drugs from aqueous solutions by MCC (Okada et al, 1987; see also Section 3.4.13). The close agreement of the results obtained here indicates that a primarily ion-exchanging mechanism is present in this system.

### *3.4.9. Process following*

The pulp supplied as the feedstock for MCC manufacture is in the form of thick (2 mm) paper. For the adsorption experiments, the pulp was shredded by running torn strips through a centrifugal mill (Retsch ZM100, Glen Creston, Stanmore, UK) to obtain particles of approximately 500 μm diameter. It is not anticipated that this treatment will cause a significant change to the surface properties of the pulp. In contrast to the high-energy milling used in the micronisation of MCC to produce Emcocel SP15 (Section 3.4.7), the shredding is a lower energy, single pass technique. This pretreatment mimics the initial step in the MCC manufacture (Chapter 1.4.4), where the pulp is shredded prior to acid depolymerisation.

Table 3.4. Summary analysis of Langmuir adsorption isotherms measured at 37°C.

| MCC | $k_1k_2$ | $k_2$ (mmolkg$^{-1}$) | Tacrine surface area ($m^2kg^{-1}$) |
|---|---|---|---|
| Emcocel 50M | 211 ± 5 | 8.87± 1.00 | 10700 ± 1200 |
| Emcocel HD90 | 167 ± 6 | 3.88 ± 1.31 | 4700 ± 1600 |
| Pharmacel 101 | 212 ± 7 | 12.4 ± 1.1 | 15000 ± 1300 |
| Prosolv 50 | 220 ± 12 | 7.71 ± 1.59 | 9300 ± 1900 |
| Prosolv HD90 | 62.0 ± 4.0 | 5.35 ± 1.07 | 6400 ± 1300 |

During manufacture, MCC undergoes several process steps (see section 1.4.4). Samples of wet pulp (paper mill), dry pulp (MCC feedstock) and post-neutralisation slurry (prior to spray-drying) were obtained for a sample of Emcocel 50M (batch no. E5BIE48) so that the effect of the most drastic manufacturing processes on adsorption could be determined. This, in combination with the previously obtained physical and chemical data (Chapter 2), will give some insight into the factors affecting adsorption.

Adsorption results for the process-following materials are presented in Table 3.5. No conclusions can be drawn from Langmuir analysis of these results, since the large errors associated with the data obscure any differences between the samples. The large errors are most probably due to the high adsorptivity of the Temalfa ND pulp and the consequent increase in the size of the relative errors.

Note that two of the samples (never-dried pulp and post-neutralisation slurry) were supplied with a significant mass of water and were airmailed prior to analysis. The action of ice on the samples may affect the surface chemistry of the samples. Previous work (section 3.4.7) showed that freezing MCC does not significantly affect the adsorption of the final product. However, the MCC used contained approximately 5% moisture, as opposed to being supplied as a 20% w/v cellulose in water slurry. The presence of such a large volume of ice may cause greater physical disruption of the cellulose structure.

### *3.4.10. Reversibility of adsorption*

Quadruplicate analyses of the reversibility of the adsorption of tacrine from aqueous solution onto Tabulose 101 and Ceolus KG-802 indicated that the adsorption is fully reversible ($f = 1.01 \pm 0.01$ for both MCCs). These two MCC types were selected because they display the lowest and highest affinities for tacrine in the adsorption isotherm studies. These results indicate that the affinity of tacrine for MCC and the reversibility of the adsorption are not linked.

This finding confirms some previous work investigating elution of some drugs from MCC using a pH 2.1 HCl solution (El-Samaligy et al, 1986; Franz & Peck, 1982). It was reported to be not possible to fully elute ampicillin, amoxycillin (El- Samaligy et al (1986)), fluphenazine or promethazine (Franz & Peck (1982)) using water as the elution medium. This would tend to confirm the assumptions made by Akaho &

Fukumori (2001) about the adsorption of drugs onto cellulose, who stated that adsorption tends to be irreversible. There is clearly a discrepancy between the results reported here for adsorption of tacrine and the previously published work. It is clear that there are unresolved structure-dependent influences on the reversibility of the adsorption of different drugs.

The observed reversibility of the adsorption of tacrine onto MCC has important consequences for the expected *in vivo* adsorption of this drug, even though *in vitro* dissolution tests may indicate that there is a significant decrease in bioavailability due to adsorption. Constant removal of the drug from the digestive tract will result in the release of adsorbed drug from the dosage form as the equilibrium between the amount adsorbed and the equilibrium concentration of the drug is re-established. Therefore, although adsorption of the drug onto MCC will decrease the *in vivo* bioavailability, the decrease will be less than *in vitro* studies indicate if the adsorption in reversible.

### *3.4.11. Batch-to-batch and time dependence*

More than one batch of Avicel 101, Emcocel 50M and Vivapur 101 were obtained from the manufacturers. These three products are marketed as equivalent products on the basis of particle size. Significant differences were established for all three products on a batch-to-batch basis (Figure 3.12). Some correlation of the time between analysis and manufacture and the adsorption was observed for Emcocel 50M (Figure 3.13). An effect of this type had been suggested by the work of Landín et al (1993c).

In order to test whether storage time effects adsorption capacity, a further analysis of the adsorption of the primary batches of Avicel PH101 (6902C), Emcocel 50M (E5D8C17X) and Vivapur 101 (93529) after a further 24 months storage under ambient conditions was carried out. A significant decrease in the adsorption capacity was determined (2.19 $mmolkg^{-1}$) for Emcocel 50M, but no significant difference for either Avicel PH101 or Vivapur 101 was determined. Also, the affinity of Emcocel 50M for tacrine increased significantly and, again, no significant difference for either Avicel PH101 or Vivapur 101 was observed. Note that the second analysis on both Emcocel 50M and Vivapur 101 were conducted after the recommended 'use by' date. Some microbiological contamination may have

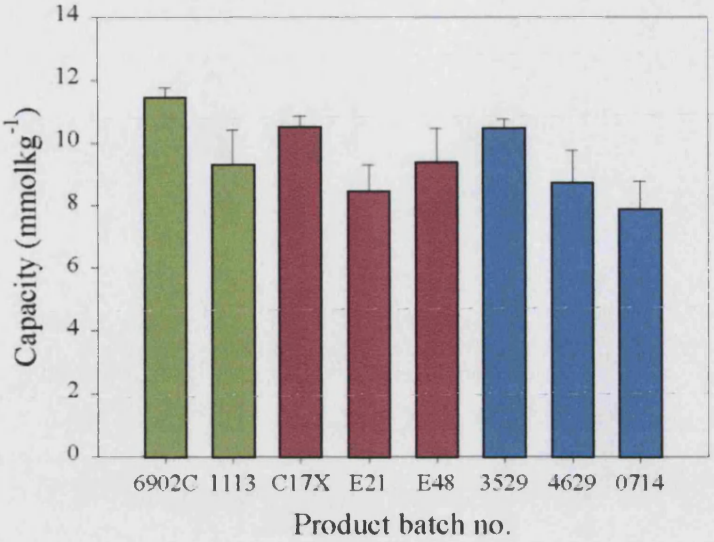


Figure 3.12. Batch-to-batch variation of the capacity of Avicel PH101 (green), Emcocel 50M (red) and Vivapur 101 (blue) for the adsorption of tacrine from aqueous solution at 25°C. Error bars indicate calculated error (see Table 3.3).

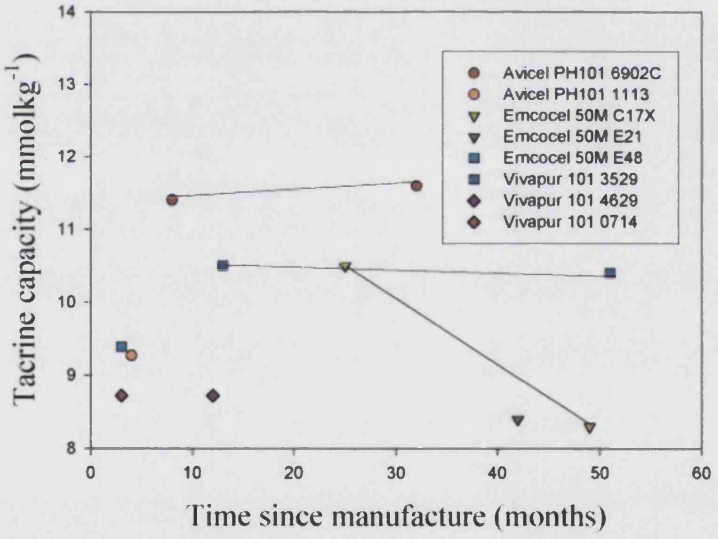


Figure 3.13. Effect of storage time on the capacity of MCCs for adsorption of tacrine from aqueous solution. Three MCC batches were reanalysed at least 24 months after the initial experiments in order to ascertain whether the variations seen in the batch-to-batch study were an effect of storage time, or if there were significant differences between batches.

occurred during previous sample collection, leading to breakdown of the product. There may also be an effect associated with the transport of the product. As with the 'process following' samples, the Emcocel 50M samples were transported by air, whereas the Avicel PH101 and Vivapur 101 samples were surface transported from Ireland and Germany. The exact mechanism is not explicable at present.

### *3.4.12. Correlation of adsorption capacity with surface area*

The correlation of surface area determined by BET $N_2$ adsorption with the capacity to adsorb tacrine from aqueous solution can be determined by examination of the data in Table 3.1. Only standard and large particle grades were considered to avoid the large increase of the BET surface area on silicification and the potential effects of using a hardwood or unknown pulp source. From these data it is observed that there is no apparent correlation between capacity for tacrine and surface area measured by BET $N_2$ adsorption (Table 2.4). The actual correlation coefficient ($r^2$) using the eight MCCs considered was 0.043, a strong indication that no correlation exists.

This finding is explicable with reference to nitrogen adsorption work conducted previously by Nakai et al (1977) and doRego et al (1997). Nakai et al (1977) measured high (80 000 $m^2kg^{-1}$) surface areas of cellulose samples after maceration in water. DoRego et al (1997) measured surface areas in a manner similar to that described here, using cyanine dyes as probes. Working with ethanolic (slightly swelling) and dichloromethane (non-swelling) solutions, they obtained active surface areas of 2400 and 1200 $m^2kg^{-1}$, respectively, for an unspecified cellulose sample.

One possible explanation for these observations is water-induced swelling of the cellulose. In order to investigate the effect of solvent on the apparent surface area, a sample of Emcocel 50M was washed repeatedly with dry ethanol to remove water and then washed with *n*-pentane to remove the ethanol. The resulting powder was analysed using 5-point BET $N_2$ adsorption yielding a surface area of 2300 $m^2kg^{-1}$. By itself, this result could be interpreted as a more complete removal of water from the pores of the sample than is achieved by gentle heating under dry nitrogen. In conjunction with the results of doRego et al (1997) it would appear that swelling of the sample in ethanol is a more valid explanation of the observed increase in surface area than water removal.

### *3.4.13. Effect of Ionic Strength*

Figure 3.6 compares the effect of NaCl concentration on the percentage tacrine adsorbed onto MCC from solutions containing 50 $mgl^{-1}$ (Vivapur 101) and 15 $mgl^{-1}$ (Emcocel HD90) tacrine. The data obtained from this study can be discussed in three different ways:

First, the main mechanism for adsorption onto MCC is by ion exchange. Processing cellulose oxidises the surface hydroxyl groups to carboxyl groups (Michell & Higgins, 1999), resulting in a pKa for cellulosic materials of 4.0 – 4.3 (Krässig, 1993). This means that within the pH range 6 – 7, at which these experiments were conducted, the maximum potential for adsorption by ion exchange is expected for the tacrine – MCC system (Senderoff et al, 1992). The sodium cation, having a smaller radius than the protonated tacrine molecule, has a greater charge density. Therefore, sodium cations preferentially occupy the negative adsorption sites on the surface of MCC, eventually preventing tacrine from adsorbing on these sites. This confirms the findings of Okada et al (1987) and Qtaitat et al (1988) who determined that adsorption was mainly due to an ion-exchange mechanism.

Secondly, there appears to be a second, as yet unassigned, mode of adsorption in the softwood MCC. Approximately 10% of the available tacrine is adsorbed even at high NaCl concentrations. This may be due to a dispersive (Lifschitz – van der Waals) type interaction or H-bonding within the surface (Okada et al, 1987; Jorgensen et al, 2000). Spectroscopic (vibrational and NMR) investigations may be able to resolve this issue (Burhanova et al, 1997). However, it has been shown (Adolfsson et al, 1999) that the primary bonding mechanism in compaction of MCCs is by hydrogen bonding, which would suggest that adsorption can occur by this mechanism for MCCs.

Thirdly, there is a large, significant decrease in the adsorption observed at isotonic salinity (0.154 M NaCl) compared with the adsorption in degassed purified water. As well as providing an insight into the adsorption mechanism, this observation shows that *in vitro* testing conditions will have a marked effect on drug adsorption and the consequent bioavailability determined for a formulation. This last point has implications for the effect of adsorption on *in vivo* release. The higher osmolarity of

physiological systems would decrease the tendency of MCC to adsorb tacrine and other drugs that adsorb through an ion exchange mechanism (Franz & Peck, 1982).

Analysis of the isotherms from the adsorption experiments was complicated by the very low adsorption and the consequent increase in experimental (type 1) error. This error led to a high degree of scatter about the line of best fit, with correlation coefficient ($r^2$) decreasing to 0.8. However, a rank similarity in the calculated adsorption capacities of Emcocel 50M and Emcocel HD90 from saline tacrine solution with the estimated capacities from the single concentration can be established. The 'non-ionic capacities' for these two materials are $0.49 \pm 0.12$ $mmolkg^{-1}$ (Emcocel 50M) and $0.12 \pm 0.58$ $mmolkg^{-1}$ (Emcocel HD90). These results are of the same order of magnitude as those estimated from observation of the effect of the ionic capacity on adsorption at a single initial drug concentration. The 'ionic capacities' of these two materials also correlates well with the carboxyl content determination (see Chapter 4).

The four MCCs investigated for the adsorption from an isotonic 100 $mgml^{-1}$ tacrine solution were chosen partly on the basis of the extremes of affinity observed (Ceolus KG-802 and Tabulose 101) and also because the pulp source was uncertain (Ankit and Vivapur 302). Using the adsorption isotherms in Table 3.3, the decease in adsorption capacity due to the salinity of the solution can be assessed.

### *3.4.14. Decrease in Effective Dosage*

The effect of the adsorption of tacrine on the amount of drug released during a standard *in vitro* dissolution test is summarised for six MCC samples in Figure 3.14. Numbers are limited for clarity, with standard grade, high density, silicified and high-density silicified MCCs being represented. Additionally, the MCCs displaying the highest and lowest affinities (Ceolus KG-802 and Tabulose 101, respectively), are included.

A 250 mg dosage form was used as the example formulation. Drug concentrations of 100, 10, 1 and 0.1 mg were used, with the balance of the 250 mg consisting of MCC. The percent of drug 'lost' increases significantly as the dosage decreases. Interestingly, although Tabulose 101 and Ceolus KG-802 have similar affinities, the amount of drug lost through adsorption for the 0.1mg dose form is not significant for

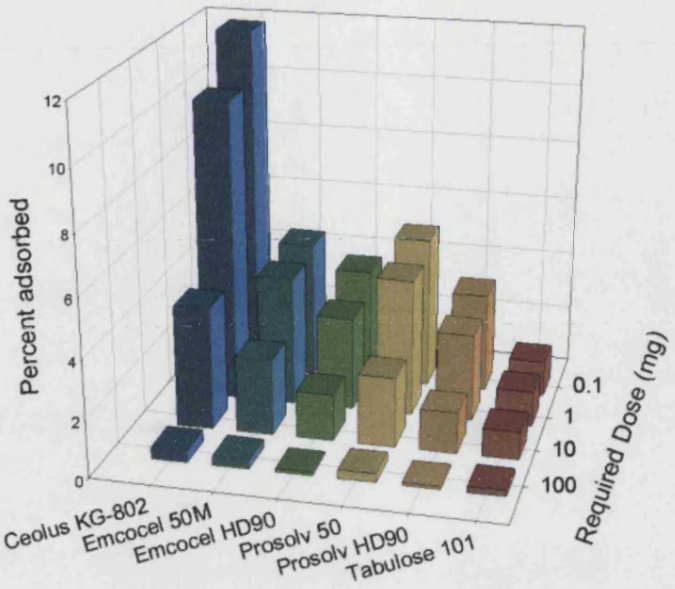


Figure 3.14. Comparison of effect of MCC used against drug adsorbed in a 250mg dosage form required to release 100 to 0.1mg tacrine in a standard tablet dissolution test. Note that, although the capacities of Ceolus KG-802, Emcocel 50M and Tabulose 101 are similar, the difference in affinities has a marked effect on the percent adsorption at low dosages.

Tabulose 101 (0.9%), whereas the 11.7% adsorption by Ceolus KG-802 is sufficient for the dose for to fail BP content uniformity tests.

*3.4.15. Dissolution tests*

All tablets complied with BP guidelines regarding weight uniformity (of 20 tablets, no more than two deviate by >5%, none >10%). The improved weight uniformity of the placebo Prosolv HD90 formulation compared with the placebo Pharmacel 101 formulation is a consequence of the improved flowability of the silicified high density material, as suggested by the Carr's compressibility indices determined in Chapter 2 (see also Tobyn et al, 1998). Disintegration times of less than 20 seconds were recorded for all tablet formulations. All physical parameters for the formulations used in dissolution tests are summarised in Table 3.5.

Drug release from the directly compressed tablets containing an initial 2% w/w tacrine are summarized in Table 3.6. Acceptable content uniformities were determined for all formulations. The predicted release, based on the adsorption characteristics of the two MCCs determined at 37°C in section 3.4.8, are also summarised in Table 3.6.

Results from the dissolution tests are summarized in Table 3.7, together with the predicted release calculated with reference to the adsorption characteristics determined from adsorption isotherms.

Rapid release is observed from all formulations, with greater than 60% release of the label claim mass within two minutes. It was not possible to extract more than four samples from each experiment before 60% release was achieved, therefore release rate and order could not be determined from these experiments. The techniques used to extract information from dissolution tests are generally more suitable for controlled release formulations. Following the dissolution of fast release formulation such as those used here generally requires the use of specialized dissolution equipment, e.g. fibre optic systems.

The theoretical values tend to overestimate the amount released and therefore underestimate the amount adsorbed. Some overlap of the theoretical release with the range of values determined occurs in some cases. As with the content uniformity experiments, there may be some effect on the adsorptivity of the MCC caused by compaction.

Table 3.5. Summary of tablet testing results for the eight tabletted formulations used for dissolution tests.

| MCC | Formulation | Mass (mg) | Hardness (MPa) | Porosity (%) |
|---|---|---|---|---|
| Pharmacel 101 | Placebo dry | 250.7 (2.7) | 1.45 (0.06) | 41.2 (0.5) |
| Pharmacel 101 | Dry blend | 260.0 (2.6) | 1.76 (0.11) | 38.2 (0.7) |
| Pharmacel 101 | Granulated placebo | 255.8 (0.8) | 2.29 (0.08) | 24.4 (0.7) |
| Pharmacel 101 | Granulated | 256.5 (1.6) | 2.85 (0.06) | 11.2 (0.2) |
| Prosolv HD90 | Placebo dry | 251.7 (0.9) | 2.03 (0.07) | 33.3 (0.4) |
| Prosolv HD90 | Dry blend | 250.1 (2.2) | 1.92 (0.09) | 32.9 (0.6) |
| Prosolv HD90 | Granulated placebo | 268.0 (0.8) | 3.17 (0.08) | 11.0 (0.3) |
| Prosolv HD90 | Granulated | 271.8 (3.0) | 2.30 (0.13) | 11.4 (1.0) |

Table 3.6. Content uniformity (drug release from 250mg in 40ml water) and predicted release based on adsorption isotherm data. Predicted release without adsorption is $20 mg g^{-1}$.

| MCC | Formulation | Drug release ($mg g^{-1}$) | Predicted release ($mg g^{-1}$) |
|---|---|---|---|
| Pharmacel 101 | Dry blend | 16.6 (0.7) | 17.8 (0.6) |
| Pharmacel 101 | Granulated, wet | 17.0 (0.3) | 17.8 (0.6) |
| Pharmacel 101 | Granulated, dried | 16.6 (0.7) | 17.8 (0.6) |
| Pharmacel 101 | Granulated, tabletted | 16.5 (0.3) | 17.8 (0.6) |
| Prosolv HD90 | Dry blend | 18.3 (0.8) | 18.9 (1.0) |
| Prosolv HD90 | Granulated, wet | 17.8 (0.3) | 18.9 (1.0) |
| Prosolv HD90 | Granulated, dried | 18.6 (0.4) | 18.9 (1.0) |
| Prosolv HD90 | Granulated, tabletted | 16.5 (0.3) | 18.9 (1.0) |

Table 3.7. Data summary from dissolution tests on DC tablets, dried granules and tabletted granules. Figures in brackets for test release indicate standard deviation (n = 6).

| MCC | Formulation | Dissolution test release (%) | Predicted release (%) |
|---|---|---|---|
| Pharmacel 101 | Dry blend | 81 (4) | 88 |
| Pharmacel 101 | Granulated, dried | 90 (4) | 88 |
| Pharmacel 101 | Granulated, tabletted | 85 (2) | 88 |
| Prosolv HD90 | Dry blend | 90 (3) | 95 |
| Prosolv HD90 | Granulated, dried | 97 (4) | 95 |
| Prosolv HD90 | Granulated, tabletted | 91 (3) | 95 |

Analysis of the dissolution data summarised in Table 3.7 using ANOVA *post hoc* tests does not indicate a significant difference between the formulations made using Pharmacel 101 and Prosolv HD90, with the exception of the directly compressed formulations. Rather than being an indication that the MCCs do not have a significantly different adsorption profile for tacrine, this observed similarity is more likely to be a function of the dissolution test. Differences between dissolutions tests are higher compared with the adsorption isotherm experiments. For the tests described here, two probable sources of variability are the tablet content variability and the mixing of the suspension. For normal dissolution tests the mixing is sufficient to yield acceptable results. However, these experiments were conducted over a time scale which was possibly insufficient to allow complete mixing in the dissolution vessel.

### 3.5. Conclusions

The findings from these studies may be summarised in the following points:

a. Inter-manufacturer differences are demonstrated for the adsorption of tacrine from aqueous solution for the MCC batches used in this investigation. This may be an indication of batch-to-batch variations, with the single batches used being representative of the extremes of variation to be expected between manufacturers' products;

b. The nature of the primary particles that constitute the aggregates of MCC is a critical factor in determining the adsorption capacity of the product. The size of the aggregates is not a significant factor;

c. Negative free energy, enthalpy and entropy are indicated for the adsorption of tacrine onto MCC. The magnitude of the thermodynamic quantities suggests that adsorption occurs by an exothermic physisorption mechanism;

d. Silicified MCC samples show a reduced adsorption capacity due to reduction in the cellulosic surface area, replaced by non-adsorbing $SiO_2$. High density SMCC (Prosolv™ HD90) has the lowest capacity for adsorption of tacrine of all the samples studied;

e. Total capacity and the affinity of the drug for the MCC must both be considered when deciding whether a MCC is suitable for the new formulation;

f. The drug dose required and the mass of MCC to be used in any dosage form must be considered, since adsorption increases as dosage, and therefore concentration, decreases;

g. Significant batch-to-batch variations for three of the standard grade MCC products have been observed;

h. Storage under uncontrolled, ambient conditions over a period of 24 months appears to result in a decreased adsorption capacity for Emcocel 50M, but not for Avicel and Vivapur;

i. Surface area determined by BET $N_2$ adsorption is not an indicator of the adsorption capacity. It is therefore not possible to predict the adsorption of MCC in water from dry state surface area determinations;

j. The adsorption of tacrine onto MCC from an aqueous solution is fully reversible.

k. High-density grades of MCC display a lower adsorption capacity and reduced affinity for tacrine than standard grades;

l. The water – cellulose interaction may be an important factor in determining the adsorption capacity of cellulosic materials from aqueous solution;

m. The main mechanism for adsorption is by ion exchange. A secondary interaction, either hydrogen bonding or a dispersion force interaction, is a minor but significant adsorption mode for softwood MCCs. The ion exchange mode is quickly saturated under test conditions by solubilised ions. Testing conditions for *in vitro* dissolution and bioavailability analyses will, therefore, significantly affect the observed drug release;

n. Dissolution test may not be sufficiently discriminatory to distinguish between MCCs with very different adsorption capacities.

Therefore, a change in the brand of MCC used in a formulation may have a significant effect on the observed *in vitro* adsorption, and potentially affect drug bioavailability.

# 4. Chemical Characterisation of Microcrystalline Cellulose

## 4.1. Introduction

The bulk chemistry of a material is of fundamental interest when considering the type of interactions it undergoes. In cellulose the extensive hydrogen bonding within the polysaccharide structure creates a stable, unreactive molecule. Breakdown of the polysaccharide chain usually only occurs under extreme conditions, such as enzyme hydrolysis by cellulase or with concentrated acid (Kumar et al, 2001). The acid hydrolysis used to depolymerise cellulose during the manufacture of MCC preferentially attacks the amorphous regions, where the hydrogen bonding is somewhat weaker. Even so, highly concentrated acids at elevated temperatures are required for this process. The inter-chain hydrogen bonds in the amorphous regions may be disrupted by polar solvents such as water and ammonia, resulting in swelling of the material. There is strong crystallographic evidence that certain ions such as $Ca^{2+}$ and $Na^{+}$ also promote the swelling of cellulose (Krässig, 1993).

The crystallography of cellulose will be investigated. As mentioned in Chapter 1, more than one polymorph of cellulose is found in manufactured cellulosic materials. Also, the presence of amorphous regions within the material affects the compaction properties and may also affect the adsorption capabilities (Krässig, 1993).

Six techniques are considered here. Certain parameters of interest may be determined by the use of more than one technique, and so the work here will partially be a comparative study.

### *4.1.1. Carboxyl content*

The carboxyl groups on the surface of cellulose dominate the surface chemistry of the material, resulting in a pKa of approximately 4 (Krässig, 1993; Glombitza et al, 1994). Although from its structure (Figure 1.1) it would appear that hydroxyl groups should dominate, there is no evidence that any free hydroxyl groups exist on the surface of cellulose (Michell & Higgins, 1999). The surface hydroxyl groups are oxidised to carboxyl groups during processing. The active carboxyl groups are quantifiable by titration against a suitable base such as sodium hydrogen carbonate. Molecular modelling suggests that unprocessed cellulose has five OH groups per square nanometer (Heiner & Telman, 1997).

### *4.1.2. Mean degree of polymerisation*

The mean degree of polymerisation (DP) is a measure of the length of the α-glucose chains within a cellulose sample. This is of interest because it gives a measure of the number of reducing groups within the sample. The method used here relies on the increase in viscosity measured in a solvent when a long-chain polymer is dissolved in it. The ASTM (1965) method is used here.

Alternative methods have been described. The most comprehensive is that described by Baehr et al (1991), wherein the dissolved sample is analysed by gel permeation chromatography to obtain a spectrum of polymerisation degrees.

### *4.1.3. Infrared spectroscopy*

By scanning absorbance over a range of frequencies in the mid infrared range (400 – 4000 $cm^{-1}$), a spectrum of the type shown in Figure 4.1 (Avicel PH101) is obtained. Each peak (trough in the transmission) in the spectrum corresponds to the energy of a particular vibration within the molecule. Table 4.1 summarises the assignment of vibrational modes detected using infrared and Raman spectroscopy.

Infrared spectroscopy is a standard technique defined in the British Pharmacopoeia as a means by which to identify drugs. More widely, it is used throughout organic chemistry as an aid to identification of synthesised substances. Spectra can be acquired in very short times; therefore IR spectroscopy can be used to follow reactions in real time.

### *4.1.4. Raman spectroscopy*

Raman spectroscopy (Raman, 1928), like infrared spectroscopy, is used to study the molecular vibrations of a sample. A change in the polarisability of the molecule during a vibration results in the vibrational mode being Raman active. Molecular symmetry considerations mean that certain vibrations are more likely to be observed in Raman than in infrared, and vice versa.

Raman spectroscopy is used less frequently than infrared spectroscopy in pharmaceutical investigations. Instruments for this technique are generally more expensive and there is less literature on the use of Raman as opposed to infrared spectroscopy. The primary advantage that Raman spectroscopy has over IR is the relative insensitivity of the technique to water. Water has a very poor Raman

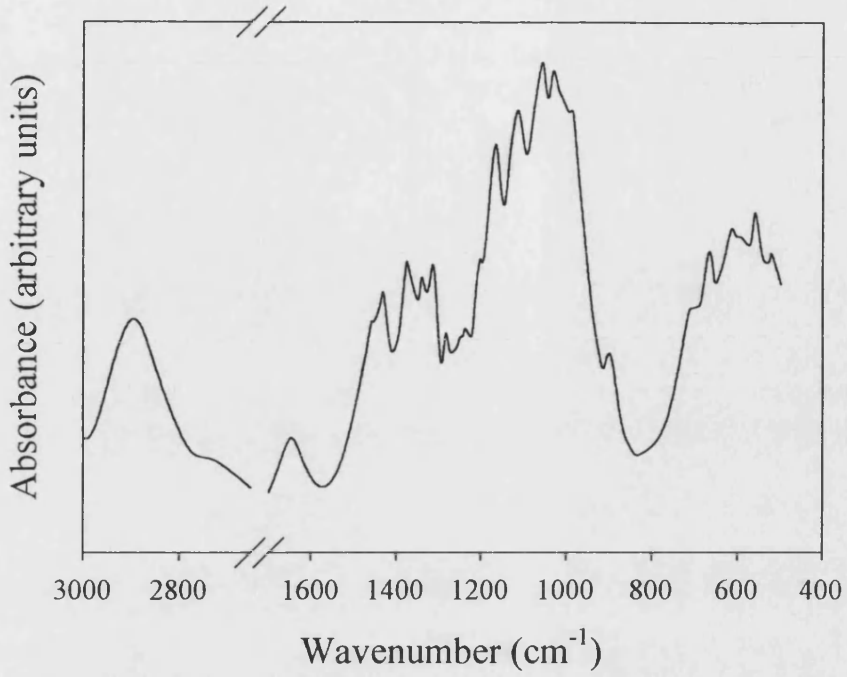


Figure 4.1. Infrared spectrum of cellulose (Avicel PH101). The region between 1700 and 2600 $cm^{-1}$ has been omitted; no peaks are observed in this region for cellulose.

Table 4.1. Summary of band assignments for infrared and Raman spectra of cellulose. All wavenumbers, from Emcocel 50M spectra, rounded to nearest $5cm^{-1}$. Assignment from Blackwell et al (1970), Smith (1979), Wiley & Atalla (1987), Eichhorn et al (2000). Where a band is not listed in both infrared and Raman spectra, the band intensity is generally too weak to be observed.

| Infrared ($cm^{-1}$) | Raman ($cm^{-1}$) | Assignment |
|---|---|---|
| 3345 | 3355 | O-H stretching |
| 2900 | 2900 | C-H stretch |
| 1480 | 1480 | O-H deformation |
| 1430 | | $CH_2$ scissors |
| 1370 | 1380 | C-H deformation |
| 1335 | 1340 | O-H deformation |
| 1315 | | $CH_2$ wagging |
| | 1295 | $CH_2$ twisting |
| 1280 | | $CH_2$ wag |
| 1250 | 1235 | O-H deformation |
| 1200 | | $CH_2$ twist |
| 1160 | | C-O-C stretch, bridge |
| | 1150 | C-O stretch |
| | 1125 | C-O stretch |
| 1105 | 1100 | Ring stretch |
| 1050 | 1060 | C-O stretch |
| 1025 | | C-O deformation, C-6 |
| | 1000 | C-H deformation |
| | 975 | C-OH deformation |
| 900 | 900 | H-C-C bend, C-6 |
| 665 | | O-H torsion |
| 615 | 610 | |
| 560 | 570 | |
| 520 | 520 | Heavy atom stretch |
| 450 | 460 | Ring bend |
| 435 | 440 | Heavy atom stretch |
| | 380 | Heavy atom stretch |
| | 350 | Heavy atom stretch |
| | 330 | Ring bend |

spectrum, and so does not normally interfere with the spectrum derived from the structure of the analyte. An important restriction for Raman is the incompatibility of the method with fluorescent substances. The low efficiency of the Raman effect requires intense incident radiation, usually laser sources. Note, however, that the use of incident radiation of a wavelength outside the range of the excitation frequencies of the fluorophore will allow the Raman signal to be recovered. This may require the use of a different laser, possibly using a different instrument.

A review of the potential of Raman spectroscopy by Alexander et al (1999) noted that, as well as the previously mention fluorescence problems, photodecomposition effect were likely to be a problem for some pharmaceutically active samples. However, the relative ease of use and minimum sample preparation means that Raman spectroscopy has potential for more extensive use in pharmaceutical research.

### *4.1.5. X-ray diffractometry*

X-ray diffractometry (XRD) is the definitive method used to investigate crystal structures. The wavelength of X-rays, from 0.1 to 100 Å, covers the range of molecular and ionic bond lengths. The harder end of the X-ray spectrum (1 to 2 Å) is of most use in investigations of crystal structure. The initial parameter measured is the angle of diffraction, which relates to the dimensions of the interatomic spacing responsible for the diffraction, using the Bragg equation:

$$n\lambda = 2d\sin\theta \qquad \text{Equation 4.1}$$

where $n$ is the integral number of wavelengths, $\lambda$ is the wavelength of the incident radiation, $d$ is the gap and $\theta$ is the diffraction angle.

By determining the interatomic spacings for a known crystal structure, the dimensions of the unit cell may be determined. This is complicated in the case of cellulose by the presence of two cellulose I allomorphs, which differ only in the relative alignment of adjacent cellulose chains. The differences are normally too subtle to be detected in powder XRD experiments.

Because XRD is a means by which to investigate crystal structure, it can be used to determine the presence of different crystal structures and amorphous regions (Nakai et al, 1977; Soltys et al, 1984; Rowe et al, 1994). This method has recently been

approved by the Food and Drug Agency (FDA) in the USA for the determination of the crystallinity of cellulose.

One of the major difficulties in the determination of the crystallinity of polymeric materials such as cellulose is the presence of significant paracrystalline volumes, mostly in the borders between crystalline and amorphous regions. In XRD, such paracrystalline regions will not yield strong diffraction patterns, and will not be quantitatively assessed. However, these regions may not be readily penetrated by water. Therefore, although these paracrystalline regions may be assessed as amorphous, they may not react and adsorb in the same way as amorphous regions.

### *4.1.6. Nuclear magnetic resonance spectroscopy*

In this work solid state nuclear magnetic resonance (SS NMR) spectroscopy is used to measure spectra of the $^{13}C$ atoms in cellulose. The glucose units that comprise the cellulose skeleton each possess six carbon atoms (Figure 1.1). A $^{13}C$ SS NMR spectrum for cellulose is reproduced in Figure 4.2, with the peak assignment for the carbon atoms in the cellulose structure according to Atalla and van der Hart (1984).

Through the use of $^{13}C$ SS NMR Atalla and van der Hart (1984) confirmed the presence of two different cellulose I structures. Cellulose Iβ, the more common structure in higher plants and the more thermodynamically stable, has a different hydrogen bonding structure compared with cellulose Iα. This difference is observed on comparison of NMR spectra. The six signals from the carbon atoms in the anhydroglucose units within the cellulose chain are split through inter- as well as intra-chain interactions. Hence, the splitting observed is characteristic of the cellulose form. In most cellulose samples spectra are complicated by the presence of hemi-celluloses, lignins and pectins. This is less of a problem for purified cellulose samples, such as MCC. However, some post-acquisition processing of the spectra is required so that structural information may be obtained.

From their initial work, Atalla and van der Hart (1984) determined that by band resolution the ratios of the different cellulose types could be determined with reference to the peak areas assigned to the different types. Further work since then has enabled a more sophisticated use of $^{13}C$ SS NMR data. This allows the

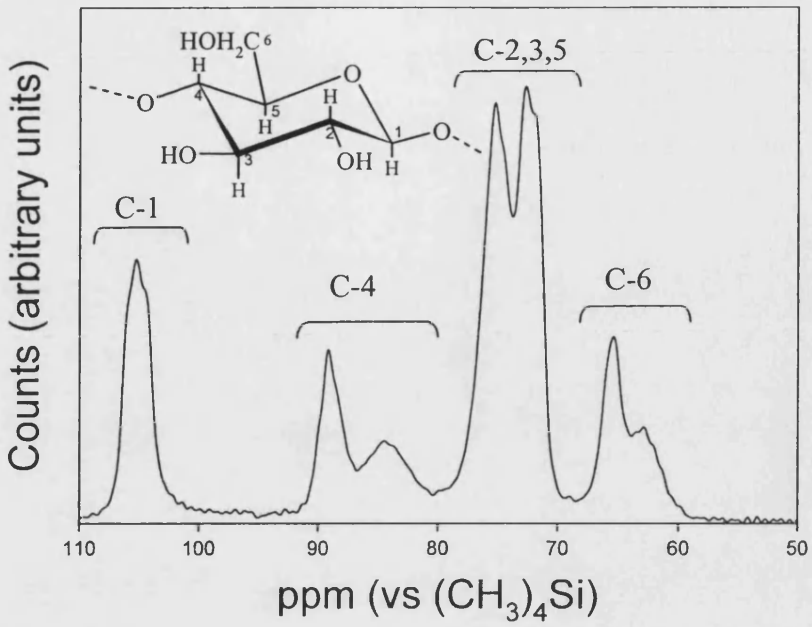


Figure 4.2. Assignment of peaks in the $^{13}C$ SS NMR spectrum of cellulose (Atalla & van der Hart, 1984).

determination of crystallinity as well as determination of ratios of cellulose polymorphs.

The degree of crystallinity may be an important factor in the reactivity and adsorption capacity of microcrystalline cellulose (Zografi et al, 1984) and it has been suggested that the crystal polymorphs have an influence on the compactibility of MCC (Kumar et al, 2002). Therefore, the use of $^{13}C$ SS NMR is a potentially powerful tool for the study of many aspects of the relationship between the functionality and reactivity of MCC and its crystallographic nature.

In an extensive review, Atalla & van der Hart (1999) explored the interpretation of SS NMR spectra obtained from a number of natural and treated cellulose samples. By reference to studies conducted on short chain glucose polymers (cellobiose, oligosaccharides and low DP cellulose) a scheme has been developed whereby the observed peaks can be assigned to the carbon atoms in the glucosidic units of the cellulose polymer (Figure 4.2). Analysis of pure samples of cellulose Iα, Iβ and II allows an estimate of the relative proportions of these polymorphs to be calculated after deconvolution of the spectra.

Schemes to determine the crystallinity of cellulose have been proposed by Sterk et al (1987) and Larsson et al (1999), among others. The method used by Sterk et al (1987) requires the analysis of a highly crystalline cellulose sample as a reference. Larsson's method, used here, relies on the analysis of the relative areas of peaks assigned to crystalline and amorphous character. The peak areas are proportional to the number of atoms in each environment (Sterk et al, 1987), so this method can be used with confidence. The upfield wing of the C-4 and C-6 peaks (Figure 4.2) are assigned to the amorphous region, the upfield position a result of poorer deshielding in the lower density amorphous region.

## 4.2. Materials

All MCC samples (see Table 2.2) were used as supplied.

Hydrochloric acid for titrations was obtained from forty-fold dilution from 0.1N standard solution (Fisher, Loughborough). Each batch was standardised by triplicate titration against dry (120°C, 5 hours, stored over $P_2O_5$) $Na_2CO_3$. Sodium hydrogen carbonate – sodium chloride solution obtained by dissolving 0.42 g $NaHCO_3$ (AR

grade, Fisher, Loughborough) and 0.58 g NaCl (AR grade, Fisher, Loughborough) in 1000ml water. Methyl red indicator (colour change pH 4.2-6.2) was 1% solution in ethanol (Fisher, Loughborough). Purified water (reverse osmosis, Millpore) was used to make up all solutions.

Cupriethylenediamine ('cuen', a solution of $Cu(OH)_2$ in ethylenediamine) was obtained from Smith Chemicals, Powell, OH.

KBr was FTIR grade, (Aldrich, Gillingham, UK) dried at 250°C for 4 hours and stored over $P_2O_5$.

## 4.3. Methods

### *4.3.1. Carboxyl content*

All carboxyl group determinations were carried out in triplicate using TAPPI method T 237. A known amount (approximately 2.500 g) of MCC is suspended in 50 ml of sodium hydrogen carbonate-sodium chloride solution (0.005 N $NaHCO_3$, 0.01 N NaCl) for one hour. This is then filtered and 20 ml of the filtrate is titrated against 0.0025 N HCl using methyl red as indicator. At the first colour change, the solution is boiled to expel dissolved $CO_2$ until the colour change reverses. Titration then continues after cooling until the final endpoint is reached, with additional boiling if necessary. A 20 ml sample of the $NaHCO_3$ / NaCl solution is also titrated as above to determine the reference for the back titration.

The water content of the MCCs was determined on the same day as the titrations in order to reduce effects of varying relative humidity. Approximately 2.500 g from the same batch used for carboxyl content analysis is taken to determine water loss on heating to 105°C for 3 hours. After heating, the sample is placed in a dessicator and allowed to cool over silica gel for 30 minutes prior to final weighing.

The carboxyl content is determined in milliequivalents per kilogram of dry cellulose from:

$$meq/kg = \left\{B - \left[A + \left(A \times \frac{C-D}{50}\right)\right]\right\} \times N \times \left(\frac{2500}{D}\right) \qquad \text{Equation 4.2}$$

where A is the volume of HCl consumed in the titration of MCC filtrate, B is the volume HCl consumed in the titration of $NaHCO_3$ / NaCl solution, C is the mass of

the undried MCC, D is the mass of the oven-dried MCC and N is the normality of the HCl solution.

### *4.3.2. Mean degree of polymerisation*

Mean degree of polymerisation was determined viscometrically (Penwest Co, Patterson , NY). A 125 mg sample of the MCC is dissolved in 12.5 ml 1 M cuen. The viscosity of the solution is determined using a capillary viscometer (Ubbelohde type) at 25°C, where the viscosity of the sample is related to the time taken for the sample to pass through a set length of capillary of known diameter. The mean degree of polymerisation is determined by:

$$DP = 190[\eta] \qquad \text{Equation 4.3}$$

where $[\eta]$ is the intrinsic viscosity of the cellulose solution, measured against a 1 M cuen blank. The presence of adsorbed water is compensated for by previous determination of the water content of the MCC sample using an infrared drying balance.

### *4.3.3. Infrared vibrational spectroscopy*

FTIR spectra were collected using a Perkin-Elmer RX 1 FT-IR system at a spectral resolution of 4 $cm^{-1}$. A total of 64 scans were collected and averaged to obtain the final spectra. Samples were prepared using the KBr disc method. Discs weighing approximately 30 mg were produced in a 13 mm die under 10 tonnes pressure. The sample:salt ratio was adjusted to give peak - to - peak range of at least 50% in transmission.

DRIFT spectra were collected using a Perkin-Elmer Spectrum One FTIR with DRIFT accessory. Samples were gently pressed onto SiC pads and placed directly into the DRIFT accessory. Sixteen spectra were collected and averaged at a resolution of 4 $cm^{-1}$.

Using the method described by Rowe et al (1994), the crystallinity of cellulose may be determined from the relative transmittance of the material at 2900 $cm^{-1}$ (C-H stretch) and 1372 $cm^{-1}$ (C-H deformation):

$$Cryst = \frac{t_{1372}}{t_{2900}} \qquad \text{Equation 4.4}$$

This method relies on the C-H stretch frequency being unaffected by changes in the hydrogen bonding structure, whilst the magnitude of the C-H deformation is proportional to the degree of order of the surrounding H-bonding structure (Ek et al, 1995).

*4.3.4. Raman spectroscopy*

Raman spectra were collected using a Renishaw 785 nm laser Raman microscopy system. The use of UV excitation (244 nm) was also investigated. Stokes radiation was collected to obtain spectra over the Raman shift range 400 – 3000 $cm^{-1}$. A 50x objective lens was used to focus incident light, producing a spot size of approximately 1 μm diameter. Laser intensity, exposure time and the number of spectra co-added to obtain each spectrum were adjusted to yield maximum intensity of the peaks without saturating the detector. Total collection time was under 20 seconds for each of the samples. Sample status was monitored visually to assess any damage caused by the laser excitation.

Spectra for Emcocel 50M, Emcocel HD90, Prosolv 50 and Ankit were collected as representative of the standard, high density, silicified and irregular MCC types.

*4.3.5. X-ray diffractometry*

X-ray powder diffraction spectra were collected using a Phillips X-ray powder diffraction system (Cambridge, UK). All data was gathered at Dept. Physics, University of Bath. The system consisted of the following components: 4 kW X-ray generator (PW 1730/00); long fine-focus Cu target (PW 2273/20; $\lambda = 1.504$ Å) operating at 40 kV and 25 mA; computer-controlled vertical diffractometer goniometer (PW1820/00); Xe proportional counter (PW 1711/10) with a graphite monochromator (PW 1752/00); microprocessor control (PW 1710/00) and diffraction software (PW 1877 PC-APD, version 3.5b). Data was collected in continuous sweep mode, collecting data every 0.02°2$\theta$.

Powder samples were placed in an aluminium sample holder with a 3 mm deep, 4 cm diameter recess. Light tapping of the loaded sample holder enabled a more even sample presentation. Previous validation experiments suggested that a 10% variability in relative peak heights could be expected from this procedure.

The crystallinity index was determined using the method of Nelson & O'Connor (1964). This is defined as the ratio of the area due to the crystalline peaks to the total area, including the amorphous background area, in the region 10 to 35°2$\theta$. A computer program (PeakFit, SPSS Inc.) was used to determine the areas due to amorphous and crystalline regions (Rowe et al, 1994). Using the PeakFit software, it is possible to define the amorphous region as background and fit the crystalline peaks as Gaussian distributions. The areas are calculated by the software, hence the required ratios are obtained.

### *4.3.6. $^{13}C$ CP MAS SS NMR*

All solid state cross polarisation magic angle spinning NMR spectra were collected on a Varian UNITY *Inova* (University of Durham) operating under a static field of 7.05 T. Samples were packed into a 7 mm probe with $Si(CH_3)_4$ as reference. The following conditions were used: Spin rate 4500 Hz; Radio frequency field strength ($\gamma B_1/2\pi$) were 75.43 MHz; 300 acquisitions; 20.0 ms acquisition time; 4 sec relaxation delay; cross polarisation with flip-back.

In order to extract crystallographic information about the samples analysed, it is first necessary to deconvolute the SS NMR spectra. This is achieved by the use of the program PeakFit (SPSS Inc.), wherein the peak shape and fitting parameters may be controlled to achieve the best fit for multiple peaks in the spectrum. Between twelve and fourteen peaks are extracted in the peak-fitting of the MCC samples.

The ratio of cellulose 1$\alpha$ to 1$\beta$ may be assessed with reference to the relative peak areas of the C-1 composite peak (approximately 105 ppm) (see Figure 4.3). The C-1 peak is one of the bridging carbon atoms, its low field position being a function of its bonding to two oxygen atoms, which shield the atom. The large shift amplifies changes in the magnetic environment of the atom due to alteration of the surrounding environment. The change from cellulose 1$\alpha$ to 1$\beta$ is subtle, being a shift in the orientation of adjacent glucose chains from parallel to anti-parallel. This results in an effective doubling of the unit cell for cellulose 1$\beta$, which contains two repeating glucose units. This change is sufficient to mean that the C-1 carbon in cellulose 1$\beta$ can be in one of two environments, with a sufficient difference to be detected by SS NMR techniques (Atalla & van der Hart, 1984). In contrast, the unit cell of cellulose

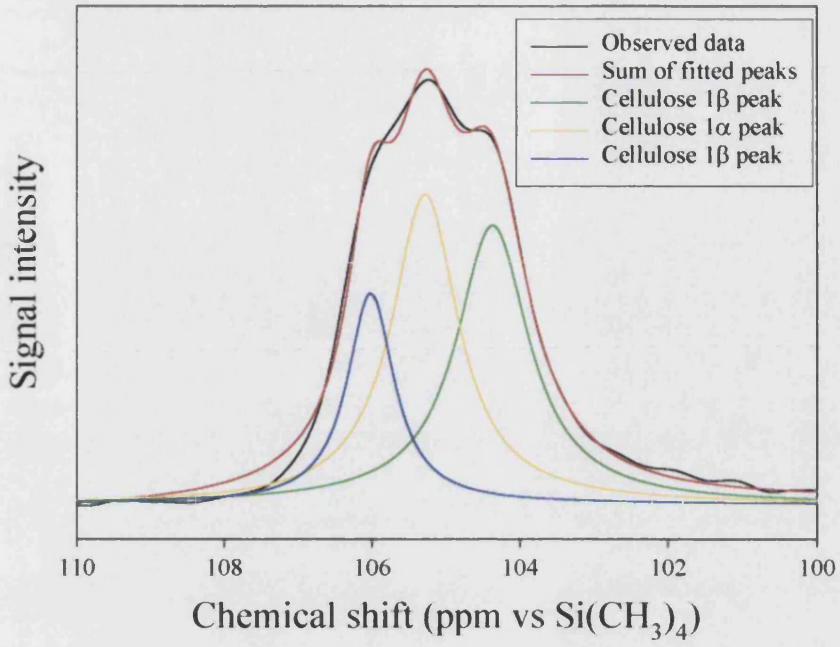


Figure 4.3. Deconvolution of C1 peak of Avicel PH101. The ratio of the area of the central peak to the total areas of the other two peaks is an indication of the ratio of cellulose 1α to cellulose 1β. Peaks at 104.4, 105.3 and 106.0ppm were observed. Correlation coefficient ($r^2$) of the fit = 0.9985.

1α is only one repeating unit long about the c-axis, so there is only one possible environment for the C-1 carbon.

The C-1 carbon atom does not appear to be affected by the amorphous content of the cellulose. In contrast to the C-4 and C-6 atoms, no significant shift in the positions of the C-1 atoms is observed. Broadening of the peaks is an indication of an increasing amorphous content (Ek et al, 1995). The broadening is quantifiable, but not necessarily easily correlated to the amorphous content.

The amorphous content of the analysed MCCs may be determined though measurement of the relative intensities of the crystalline (90 ppm) and amorphous (85 ppm) C-4 peaks in the spectra. The upfield shift observed for the carbon atoms in the amorphous region is a result of deshielding of the C-4 carbon, which is one of the bridging carbons. Using the method of Ek et al (1995), the crystallinity index (*CI*) is determined by:

$$CI = \frac{a}{a+b} \qquad \text{Equation 4.5}$$

where $a$ is the area of the crystalline C-4 peaks (86 – 93 ppm) and $b$ is the area of the amorphous peaks (80 – 86 ppm) (see Figure 4.4). The areas were determined via deconvolution of the C-4 signal using PeakFit.

Most samples were analysed in the dry state, but one sample of Emcocel 50M was analysed with 50% w/w added water. This can improve peak sharpness (Horii et al, 1985; Newman, 1987), but the presence of water may reduce the intensity of the radio frequency signals across the sample in some instruments.

An investigation in to the potential use of $^{13}C$ Solid State Nuclear Magnetic Resonance Spectroscopy ($^{13}C$ SS NMR) to determine the nature of the tacrine adsorption mechanism was conducted. Pharmacel 101, the MCC with the highest capacity for tacrine (Table 3.3), was used in order to maximise the potential signal from adsorbed drug. A one gram sample of Pharmacel 101 was equilibrated with 40 ml of a 200 $mgl^{-1}$ tacrine solution as described in Chapter 3. At the same time, a sample of Pharmacel 101 was equilibrated with 40 ml water. The samples were centrifuged and the supernatant was decanted off. The wet solids were then dried using a centrifugal filter (VectaSpin 20, Whatman Co., Maidstone, UK) before submission for analysis.

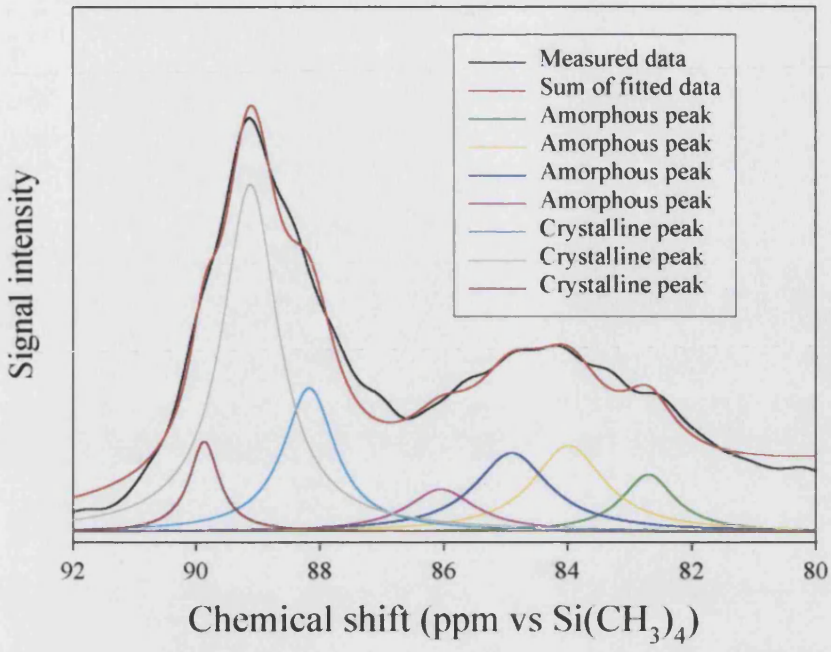


Figure 4.4. Deconvolution of C4 peak of Avicel PH101. The ratio of the total area of the amorphous peaks (upfield of 87ppm) to the total areas of the crystalline peaks (downfield of 87ppm) is an indication of the amorphous content of the material. Correlation coefficient ($r^2$) of the fit = 0.9860.

## 4.4. Results and discussion

### *4.4.1. Carboxyl content*

Carboxyl contents determined for Ceolus KG-802, Emcocel 50M, Emcocel HD90, Pharmacel 101, Prosolv 50 and Tabulose 101 are given in Table 4.2. The carboxyl titration results are compared with the tacrine capacities determined in Chapter 3 in Table 4.2 and in Figure 4.5.

Taking the data as a whole, the correlation coefficient of the carboxyl content data with the tacrine capacity data is poor ($r^2 = 0.59$). However, in Chapter 3, it was indicated that there are at least two modes of adsorption, one of which is significantly affected by the presence of ionic species in the supernatant. Taking into account the variable, unmeasured, contribution by the non-ionic mode, the carboxyl content closely matches the tacrine capacity of the materials, which indicates that the carboxyl groups in the surface of MCC are the major contributing factor to the adsorption capacity.

Examination of the graph in Figure 4.5 reveals the possibility of two separate data sets: Tabulose 101 and Ceolus KG-802 fall below the trend line of the three other softwood MCCs. The assignment of Emcocel HD90 is ambiguous, since it could belong to either set. This suggests that the mechanism of adsorption of tacrine by Tabulose 101 and Ceolus KG-802 has a significant non-ionic component.

### *4.4.2. Mean degree of polymerisation*

Values for DP are summarised in Table 4.3. For the known hardwoods, a lower degree of polymerisation is measured than for the softwood MCCs. A two-sample t-test comparing softwood and hardwood MCCs indicates that softwood and hardwood MCCs yield different DP values, to greater than 95% confidence.

The mean value for the softwood MCCs is 231 ± 23 (n = 17; ± std dev); the data set is normally distributed (Anderson-Darling test). Testing for outliers using the Grubbs test (see Appendix 1) indicates that Tabulose 101 (DP = 305) is an outlier to greater than 99% confidence ($G_{1\%, 17} = 2.785$; calculated G = 3.30). Similarly, the value determined for Vivapur 302 (DP = 234) may be regarded as an outlier for the hardwood MCCs to greater than 99% confidence ($G_{1\%, 5} = 1.749$; calculated G = 1.77).

Table 4.2. Carboxyl content (n = 3) and tacrine capacity of six MCCs. Errors in brackets represent standard deviations.

| MCC | Carboxyl ($meqkg^{-1}$) | Tacrine capacity ($mmolkg^{-1}$) |
|---|---|---|
| Ceolus KG-802 | 7.3 (1.1) | 11.6 (0.8) |
| Emcocel 50M | 9.7 (0.5) | 10.5 (0.4) |
| Emcocel HD90 | 5.3 (0.2) | 5.3 (0.6) |
| Pharmacel 101 | 11.3 (0.8) | 12.5 (0.2) |
| Prosolv 50 | 7.5 (0.6) | 8.3 (0.4) |
| Tabulose 101 | 6.4 (0.5) | 10.0 (1.6) |

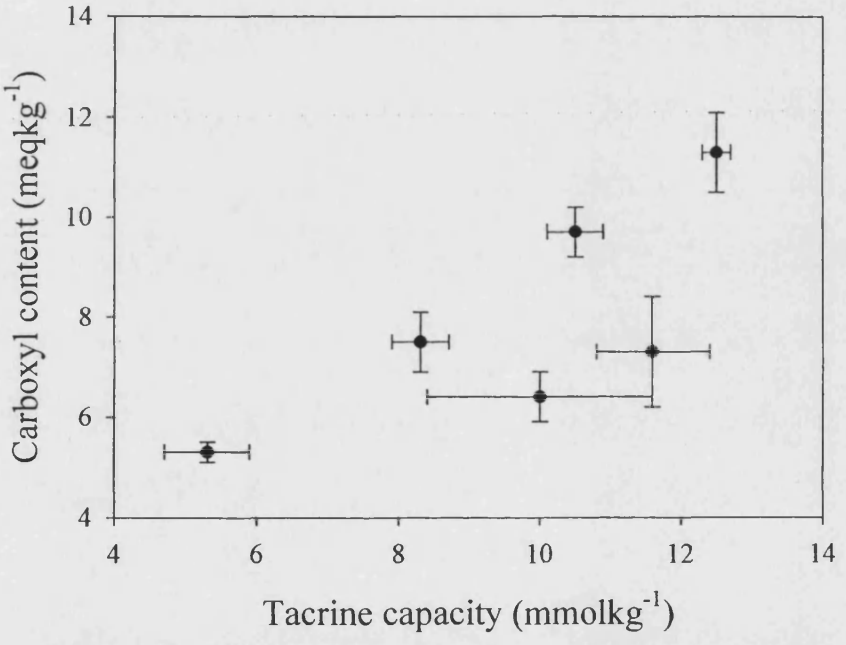


Figure 4.5. Comparison of tacrine capacity at 25°C and carboxyl content for six MCC samples (data in Table 4.2).

Table 4.3. Summary of the mean degree of polymerisation determined for nineteen samples of MCC and derivative products, plus heated Emcocel 90M, determined by viscometry. All values presented with an error of ± 5 DP units (technique reproducibility). Values for Penwest samples from certificate of analysis supplied. Loss on drying values not available for Lot#1 and Lot#2, since small sample lots were provided.

| Sample | Batch no. | LOD (%) | DP |
|---|---|---|---|
| Ankit | n/a | 5.3 | 166 |
| Avicel PH 101 | 6902C | 4.9 | 228 |
| Avicel PH 101 | 1113 | 4.9 | 220 |
| Avicel PH 105 | 5410C | 5.3 | 226 |
| Avicel PH 302 | Q918C | 5.4 | 158 |
| Ceolus KG-802 | H0134 | 4.3 | 265 |
| Emcocel 50M | E5D8C17X | 4.4 | 228 |
| Emcocel 90M | E9B8A01X | 4.3 | 227 |
| Emcocel 90M heated | E9B8A01X | 1.9 | 224 |
| Emcocel HD90 | HD9B5K3X | 4.8 | 156 |
| Emcocel LP200 | 2S6003X | 4.3 | 211 |
| Emcocel SP15 | SPD7C01X | 5.3 | 227 |
| Lot#1 | n/a | -- | 221 |
| Lot#2 | n/a | -- | 210 |
| MultiCel-N 90 | M9B9F43X | 4.2 | 175 |
| Pharmacel 101 | 90971 | 5.1 | 228 |
| Prosolv 50 | P5B7D26X | 4.9 | 215 |
| Prosolv 90 | P9B9B11X | 4.3 | 221 |
| Prosolv HD90 | K9S9040X | 4.7 | 154 |
| RanQ | n/a | 4.7 | 188 |
| Tabulose 101 | 113/99 | 5.6 | 305 |
| Vivapur 101 | 5610193529 | 6.0 | 228 |
| Vivapur 302 | 5630280112 | 4.5 | 234 |

Excluding Tabulose 101, the mean values for the softwood MCCs is 226 ± 12 (n = 16; ± std dev), and for the high density MCCs excluding Vivapur 302 the mean value is 161 (n = 4; range = 154 - 175). The higher mean DP measured for Tabulose 101 compared with the other softwood MCCs suggests a shorter acid depolymerisation step during manufacture. The high DP measured for Vivapur 302 suggests that a softwood source is used for this MCC. Vivapur 302 has a lower bulk density than the other high density MCCs (Section 2.4.3), which also suggests that a softwood source is used, with control of the drying conditions, rather than a change in the pulp source, yielding a slightly higher bulk density than the other standard grades.

These results suggest that the original timber source for the unknown MCCs can be identified. Ankit MCC (mean DP = 166) is within the range of known hardwood MCCs and RanQ MCC (mean DP = 188) is closer to the hardwood MCCs than to the softwood range.

It should be noted that the values obtained for silicified MCCs (Prosolv grades) are close to those for the equivalent MCC grades. The presence of colloidal $SiO_2$ at 0.02% w/w in the cellulose / cuen solution does not affect the measured viscosity. The Einstein equation for low phase volumes predicts an increase in viscosity of 0.05%, equivalent to an error of less than one polymer unit.

### *4.4.3. Infrared spectroscopy*

FTIR (KBr disc) absorption spectra between 500 and 1500 $cm^{-1}$ for Emcocel 50M and Emcocel HD90 are compared in Figure 4.6. This part of the vibrational spectrum contains modes due to intra- and extra-cyclic C-O stretching and the mode due to the bending of the extracylic alcohol group. These groups are sensitive to variations in the hydrogen bonding network in cellulose, itself dependent on the crystal structure in the system (Maréchal & Chanzy, 2000).

The FTIR spectra of Emcocel 50M and Prosolv 50 are indistinguishable from each other. This indicates that the $SiO_2$, present at a level of 2% w/w, is not detectable by the vibrational spectroscopic methodologies used in this study. It also confirms previous work (Tobyn et al, 1998), which suggests that there are no significant differences in the chemistry of standard and silicified MCCs.

No significant differences were observed between the DRIFT spectra and those collected using the KBr disc method (spectra not reproduced here). Therefore, any

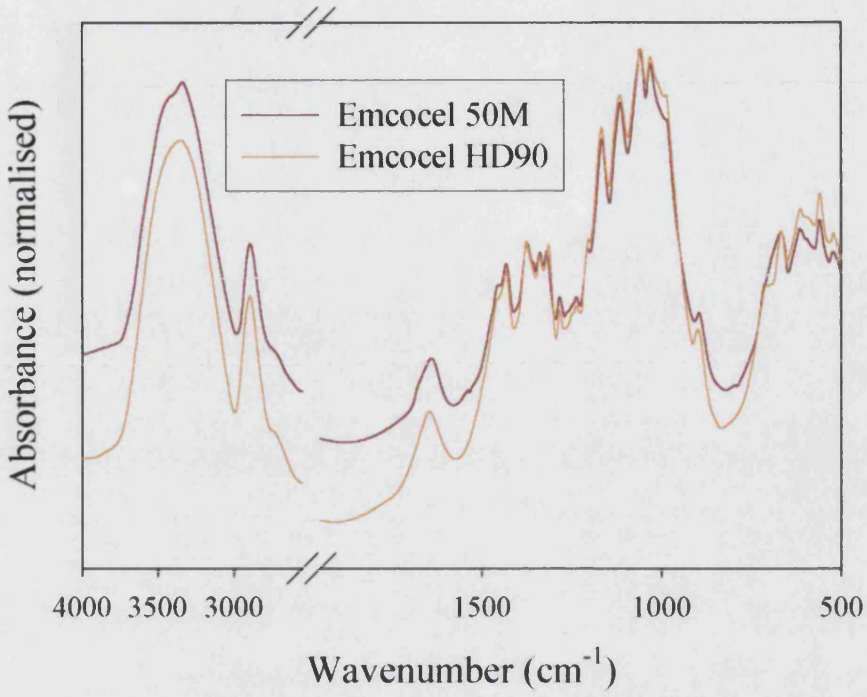


Figure 4.6. Comparison of infrared spectra of Emcocel 50M and Emcocel HD90. Peaks in the absorbance indicate frequencies of vibrational modes. There are no significant differences between the peak positions of the vibrational modes of the two samples. This suggests that the two materials have very similar chemistry.

possible change in the crystallography of the MCCs caused by the sample preparation cannot be detected using this technique.

Table 4.4 summarises the crystallinity indices determined from the FTIR spectra of the MCCs studied. The results obtained here do not agree well with previously published data obtained using infrared techniques, where crystallinities in the range 58 – 69% were determined (Rowe et al, 1994; Ek et al, 1995). The presence of small amounts of infrared adsorbing contaminants appears to affect the crystallinity indices obtained for some materials, most notably RanQ and Tabulose 101. Note also that Rowe et al (1994) and Ek et al (1995) used a consistent sample concentration on the KBr discs. No discussion was presented with respect to the potential variation of the measured crystallinity index with MCC concentration in the solid solution.

The Raman and infrared spectra of Emcocel 50M are compared in Figure 4.7. Cellulose has no centre of symmetry; therefore all molecular vibrational modes are both infrared and Raman active. The absence of some infrared active modes in the Raman spectrum can be attributed to the relative weakness of these modes in the Raman spectrum.

### *4.4.4. Raman spectroscopy*

The use of the UV excitation laser was found to be unsuitable for MCC samples. Sample damage (see Figure 4.8) was evident at higher incident energies; hence low excitation power was required. This necessitated extended collection times up to one hour, but poor spectra compared with those obtained using infrared excitation resulted (Figure 4.9). The Tyndall effect should result in much stronger scattering at lower wavelengths. However, the spectra obtained using a UV source were poorer than those obtained at 785 nm. Note that, as well as there being more detail in the 785 nm excitation spectrum, collection time was much shorter (20 seconds compared with 1 hour). Additionally, filtration of the scattered radiation prior to detection in the UV system removes scattered radiation up to 500 $cm^{-1}$, compared with the removal of the first 200 $cm^{-1}$ in the IR excitation spectrum. Useful information from the 'fingerprint' region is therefore lost in the UV excitation experiment.

A green light (634 nm) laser gave generally reasonable spectra, but a high fluorescent background was evident which may obscure some of the weaker Raman signals. Since fluorescence is dependent on the excitation wavelength, it is to be

Table 4.4. Crystallinity (%) of MCC samples determined by FTIR and $^{13}C$ SS NMR. Details of methodologies in main text.

| MCC | FTIR | XRD | $^{13}C$ SS NMR |
|---|---|---|---|
| Ankit | 89 | 89 | 58 |
| Avicel PH101 | 76 | 89 | 63 |
| Ceolus KG-802 | 82 | 86 | 50 |
| Emcocel 50M | 72 | 88 | 59 |
| Emcocel HD90 | 88 | 88 | 64 |
| MultiCel N90 | 68 | 86 | 59 |
| Pharmacel 101 | 86 | 87 | 73 |
| Prosolv 50 | 80 | 87 | 59 |
| Prosolv HD90 | 84 | 86 | 61 |
| RanQ | (102) | 87 | 61 |
| Tabulose 101 | 96 | 86 | 66 |
| Vivapur 101 | 80 | 88 | 60 |
| Vivapur 302 | 82 | 87 | 50 |

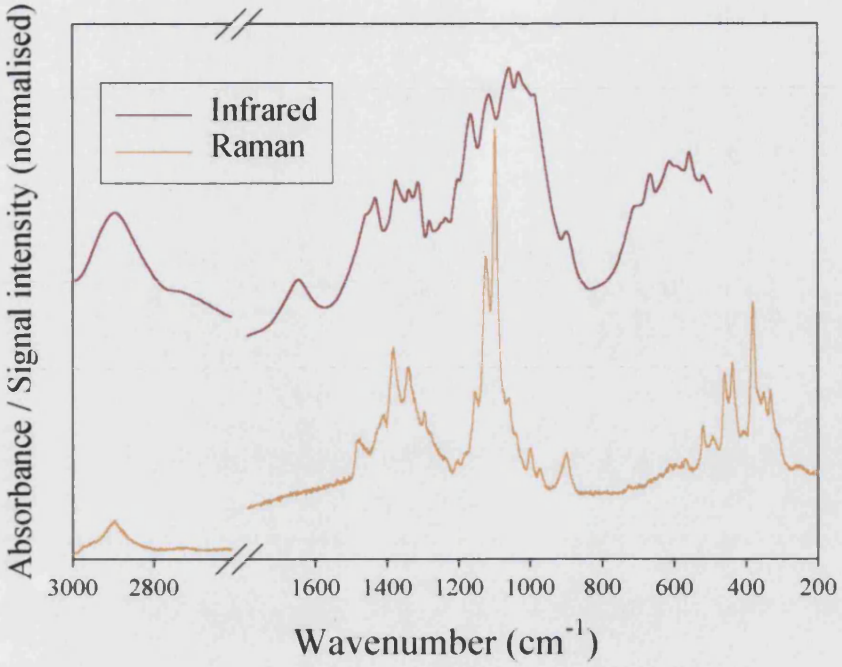


Figure 4.7. Comparison of infrared and Raman spectra of Emcocel 50M. Peaks in both the absorbance (infrared) and the signal intensity (Raman) indicate frequencies of vibrational modes.

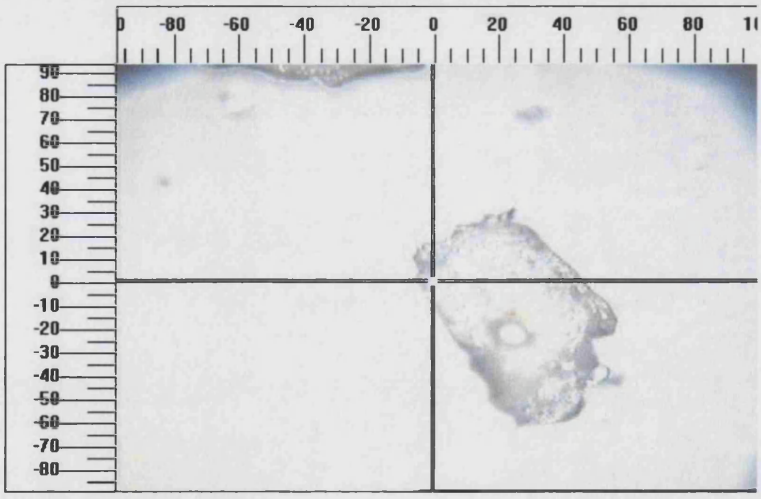


Figure 4.8. The hole at (20, -25) is due to damage caused by UV laser to a MCC particle during collection of a Raman spectrum. This damage is a result of the thermolytic oxidation. This will cause the chemistry of the analyte to change during the analysis. As a result, the spectrum recorded is not representative of the original material. Scale bars in μm.

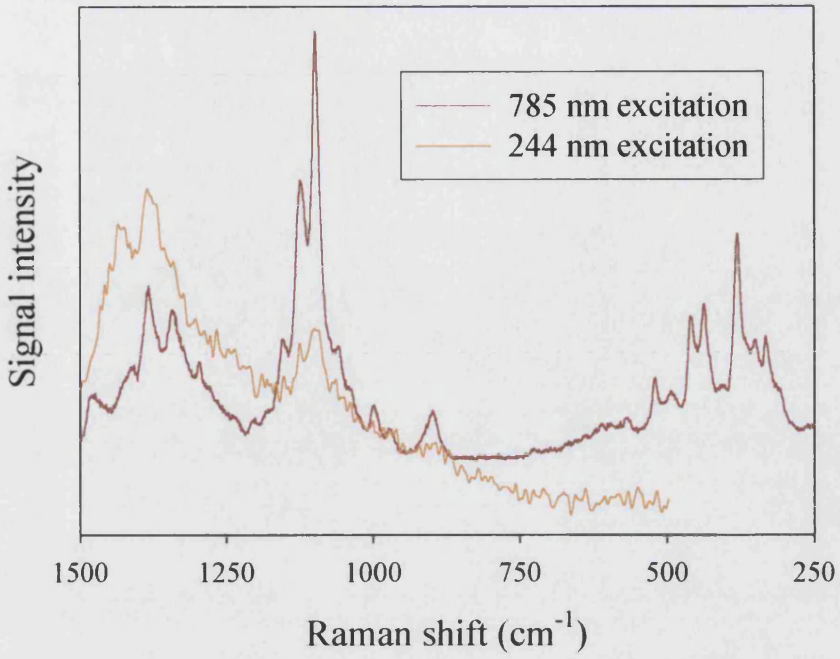


Figure 4.9. Comparison of Raman spectra obtained by infra red (785 nm) and ultraviolet (244 nm) excitation. Filtration of the UV Raman detected radiation means that no spectral data are collected below 500cm$^{-1}$.

expected that using a different laser source will affect, and hopefully reduce or eliminate, the fluorescence observed.

The best spectra, with no discernible fluorescence, were obtained using the 785 nm excitation source. Raman spectra comparing Emcocel 50M and Emcocel HD90 in the region 1000 to 1500 $cm^{-1}$ are shown in Figure 4.10. As with the infrared measurements, there are no significant differences between the spectra. An increase in the intensity of the peak at 520 $cm^{-1}$ in the spectrum of Emcocel HD90, assigned to heavy atom stretch, may be indicative of a variation in the crystal structure. However, no other significant differences were noted between these spectra, so the peak may be a result of contamination.

*4.4.5. X-ray diffractometry*

A comparison of the X-ray diffraction spectra of Emcocel 50M and Emcocel HD90 is given in Figure 4.11. Note that the hardwood MCC has a noticeable peak at approximately 21°2$\theta$ on the shoulder of the main peak at 22.5°2θ. This has been assigned to the 110 plane in cellulose II (Isogai, 1994), but other evidence (see below) suggests that the observed reflection may be due to an anisotropic crystal structure, since cellulose II could not be detected using other methodologies (Edge et al, 2001). A rising baseline can be observed for all the XRD spectra obtained (see Figure 4.11). This is indicative of poor calibration, therefore the crystallinity results obtained here may not be reliable.

The crystallinity values (Table 4.4) determined are somewhat higher than those previously determined for MCCs (Nakai et al, 1977; Rowe et al, 1994). Comparing the XRD results with those obtained using the FTIR methodology (section 4.3.3), no correlation between the results using the two methods is observed. Previous investigations (Rowe et al, 1994) were able to obtain good correlation between FTIR and XRD methodologies. The previously mentioned possibility that some of the FTIR spectra are significantly affected by the presence of IR absorbing contaminants may partially explain this. Also, the results obtained using the XRD method give a very narrow spread of results and, with the methodologies used, are not sufficiently discriminatory.

The rising baselines observed in the XRD spectra (Figure 4.11) will result in false low values for the amorphous content. Removal of the background may cause a

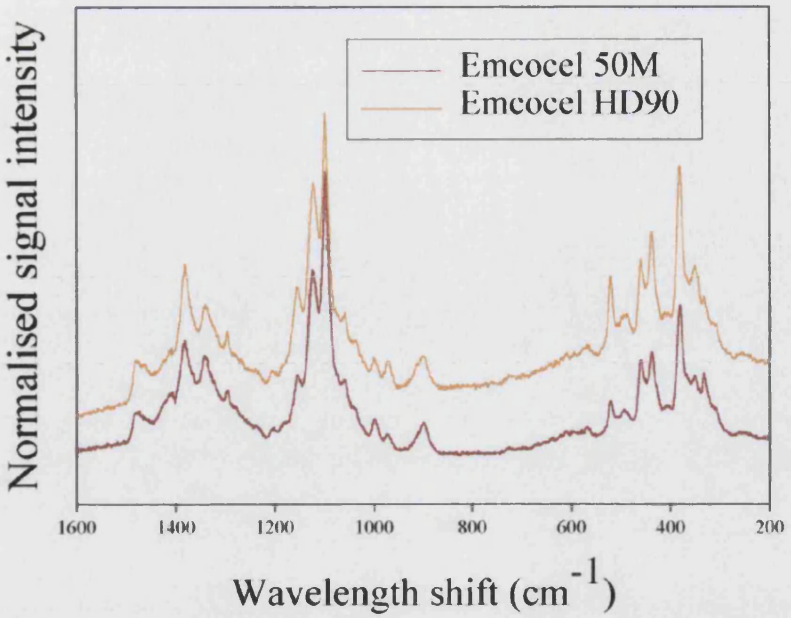


Figure 4.10. Comparison of Raman spectra for Emcocel 50M and Emcocel HD90. The Emcocel HD90 spectrum has been offset for clarity.

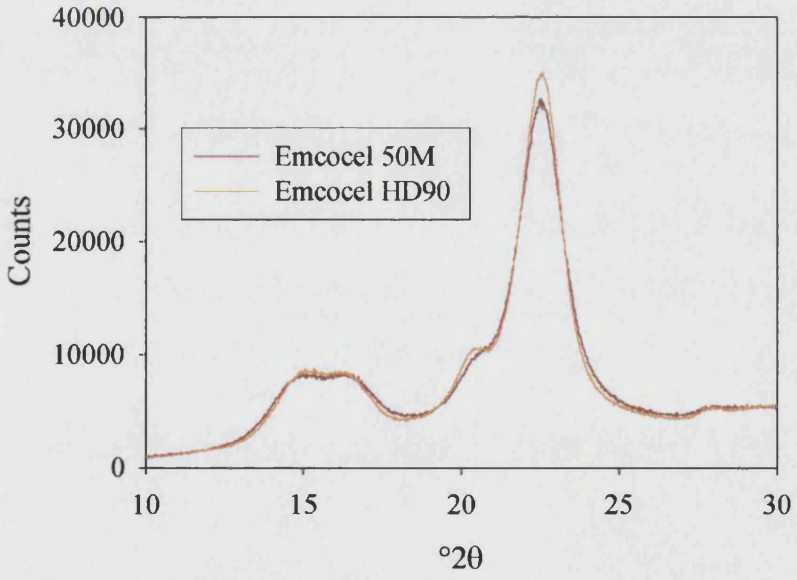


Figure 4.11. Comparison of X-ray diffraction spectra obtained for softwood (Emcocel 50M) and hardwood (Emcocel HD90) derived MCCs. Note that there are rising baselines in both the spectra; the trough at approximately 27°2θ should be level with the line at 10°2θ.

significant reduction in the area to be assigned to the amorphous region, resulting in the calculation of crystallinity values that are too high. This may be a machine-based fault, a consequence of the equipment used being preferentially employed in studies concentrating on °2θ angles above 30°.

### *4.4.6. $^{13}C$ CP MAS SS NMR spectroscopy*

The ratio of cellulose 1α to 1β determined from the relative ratios of the parts of the C-1 composite peak at 105 ppm are summarised in Table 4.5. The $^{13}C$ SS NMR spectra of cellulose 1β and cellulose II are quite similar (van der Hart & Atalla, 1984). However, the absence of a C-4 doublet and the close spacing of the C-6 doublet (< 2 ppm) suggest that there is no significant cellulose II component in any of the MCCs studied (van der Hart & Atalla, 1984).

Figure 4.12 compares the spectra of dry and 'wet' (50% w/w water) Emcocel 50M. It is clear that, contrary to previous reports (Horii et al, 1984; Newman, 1987), moistening the cellulosic samples does not result in a narrowing of the spectral signals. This is probably an instrument-specific problem; any improvement in resolution is offset by poorer decoupling performance as a result of attenuation of the RF signal in the spectrometer.

A two-sample t-test indicates that hardwood MCCs have a significantly lower mean cellulose 1α level (28.3, sd = 4.3) than softwood MCCs (46.5, sd = 5.0). These results further indicate (see mean DP results, section 4.4.2) that the high density MCC Vivapur 302 is derived from a softwood source, rather than hardwood as is the case for other high density MCCs.

The crystallinity values determined from analysis of the C-4 peaks are summarised in Table 4.4 and compared with values from infrared analyses. There is a poor correlation between these results. However, it may be expected that the values obtained from $^{13}C$ SS NMR data are more reliable than those from FTIR data. Sterk et al (1987) noted that the area of a NMR peak is proportional to the number of nuclei contributing to the signal; this fact is routinely exploited in solution phase NMR analyses as part of the determination of molecular structure. The FTIR values are based on empirical observation (Nelson & O'Connor, 1964); a simple ratio of the peak intensities from an infrared spectrum may be subject to errors due to band broadening and the presence of IR absorbing impurities.

Table 4.5. Cellulose 1α to 1β ratio for MCCs, determined from $^{13}C$ SS NMR data. Details of methodologies in main text.

| MCC | Percent 1α |
|---|---|
| Ankit | 24 |
| Avicel PH101 | 51 |
| Avicel PH302 | 26 |
| Ceolus KG-802 | 51 |
| Emcocel 50M | 40 |
| Emcocel HD90 | 32 |
| MultiCel N90 | 42 |
| Pharmacel 101 | 51 |
| Prosolv 50 | 47 |
| Prosolv HD90 | 32 |
| RanQ | 47 |
| Tabulose 101 | 40 |
| Vivapur 101 | 45 |
| Vivapur 302 | 50 |

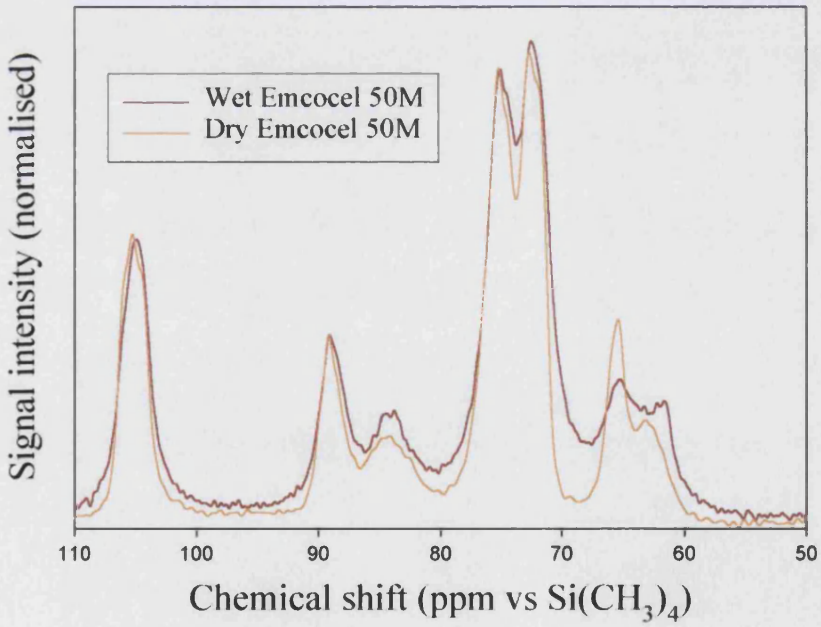


Figure 4.12. Comparison of $^{13}C$ SS NMR spectra of wet (50% w/w water) and dry Emcocel 50M. Loss of definition indicates that moistened samples do not yield improved spectral resolution for the instrumentation used.

Spectra obtained for the $^{13}C$ SS NMR experiments with adsorbed tacrine are compared in Figure 4.13. The presence of tacrine in the sample could not be established from a difference spectrum, subtracting the wet Pharmacel 101 spectrum from the Pharmacel 101 with tacrine spectrum. The concentration of tacrine in the surface of Pharmacel 101 appears to be too low to be detected using the technique and instruments available.

### *4.4.7. Correlation of chemical properties with adsorption capacity*

Since it was not possible to unequivocally link any physical property to the adsorption capacity of MCCs, a review of possible links between chemical properties and tacrine capacity will be undertaken.

Using crystallinity values obtained from the $^{13}C$ SS NMR data, no correlation between amorphous content and tacrine capacity or affinity was found ($r^2 < 0.18$).

From product literature and previous discussions, DP and $^{13}C$ SS NMR results may be used to indicate the pulp source (softwood or hardwood). Figure 4.14 shows the correlation of adsorption capacity with 1α content. A poor correlation ($r^2 = 0.34$) is observed for the fourteen MCCs considered. Similarly, the DP of the MCCs cannot be correlated with the affinity or capacity of the materials. However, the graph in Figure 4.14 does appear to lead to an improved differentiation between softwood and hardwood sourced MCCs.

The lack of correlation between the adsorption capacity and the crystallinity may be due to the relative availability of the amorphous regions. Some amorphous regions may be surrounded by impenetrable crystalline regions. Furthermore, large amorphous regions may not be fully accessible throughout the volume; migration of the large drug molecules will be hindered by the hydrogen bonding between cellulose chains.

## 4.5. Conclusions

Differences between softwood and hardwood MCCs are evident from the chemical characterisation work described here. With the exception of the carboxyl content determinations, it was not possible to readily identify a parameter which could be linked to the adsorption capacity of the MCCs investigated. Previous data (Chapter 3) suggest that the primary mode of adsorption of tacrine onto MCC is by ion

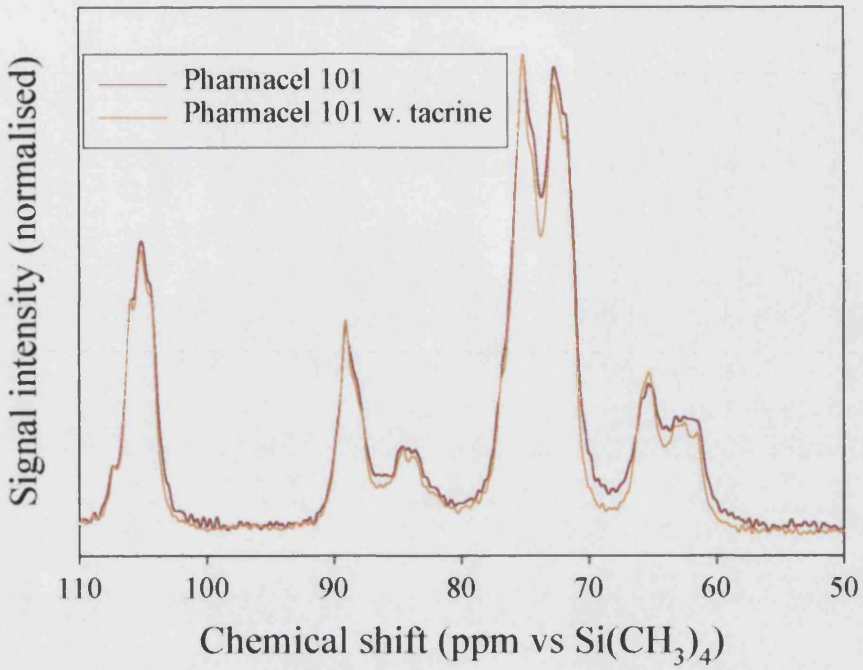


Figure 4.13. Comparison of $^{13}C$ SS NMR spectra of moist Pharmacel 101 with and without adsorbed tacrine.

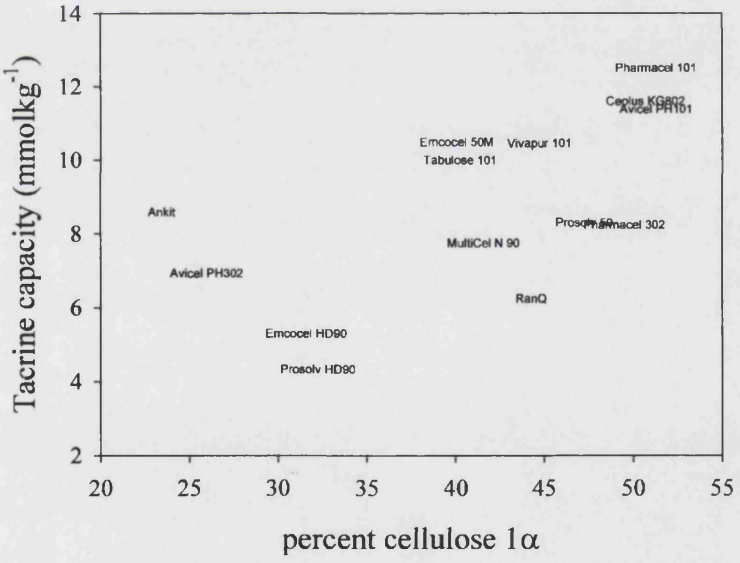


Figure 4.14. Correlation of percent cellulose 1α, determined by 13C SS NMR, with capacity for adsorption of tacrine from aqueous solution at 25°C.

exchange. Together with previously published data which determined that the pKa of processed cellulose is approximately 4, the importance of the carboxyl content to the adsorption process can be established. The secondary mode of adsorption, of significant interest for softwood MCCs, has not been identified.

The general statement implicit from the results in Chapter 3, that hardwood MCCs adsorb less tacrine from aqueous solution than softwood MCCs, is confirmed here, with evidence that the cellulose 1α content has a weak influence on adsorption capacity.

Crystallinity indices determined using XRD and FTIR methods do not correlate with each other, nor do the results agree with the $^{13}C$ SS NMR determinations of crystalline content. As mentioned previously, definition of amorphous regions is complicated by the presence of paracrystalline regions. Furthermore, since the strength of the signal in a NMR spectrum is proportional to the number of nuclei in the magnetic environment of interest, the $^{13}C$ SS NMR method used here may be expected to yield the most reliable estimate of the amorphous content.

# 5. Surface Energy Determination

## 5.1. Introduction

Surface free energy measurements are commonly used in polymer sciences to investigate wettability and adhesion characteristics (Good, 1992; Desai et al, 2001). In pharmaceutical science, surface free energy is used to investigate specific interactions such as adsorption, cohesion, adhesion, dispersion stability and lubricant sensitivity in pharmaceutical dosage forms (Hancock et al, 1987; Buckton, 1992; Dourado et al, 1998; Pepin et al, 1999). Furthermore, Ahfat et al (1997) showed that the mixing performance of binary and ternary blends could be predicted *via* surface energy data. More specifically, the water - solid interaction may also be of interest in the investigation of excipients designed to facilitate tablet disintegration, such as microcrystalline cellulose. With reference to the previously discussed adsorption of drugs from aqueous solution (Chapter 3), the water - solid interaction may be linked to adsorption capacity or affinity.

The surface free energy of a solid is defined as the reversible work required to form a unit area of new surface under constant temperature, mass, pressure and volume. A number of techniques are available for the direct measurement of this quantity, such as Griffith's brittle fracture method (Lawn, 1993) and the sub-melting point zero creep technique (Hayward & Greenough, 1960). However, these methods require samples that are thermally stable, either plastically deform or display brittle fracture and are isotropic, and preferably consist of single crystals. Therefore these techniques are not suitable for most pharmaceutical materials.

An alternative definition, that the surface free energy is equal to the sum of the free energy of all adsorption sites over unit area, may be exploited (Jacob & Berg, 1994). By establishing secondary properties based on interactions of probe materials, the surface free energy of the solid may be calculated.

### *5.1.1. Liquid surface energy*

Determination of solid surface energy relies on the knowledge of surface energetics of liquids and empirical comparisons of the interactions between solids and liquids. The surface energy of a liquid is the interfacial tension between the liquid and

surrounding medium (usually air). This interfacial tension is a function of the intermolecular forces within the liquid. Highly polar liquids such as water display a high degree of intermolecular interaction, both dipole-dipole and dispersion interactions. As a consequence, such liquids have a high surface tension (water = 72.8 $mNm^{-1}$). Liquids such as *n*-hexane interact by dispersion forces alone, and so tend to have a low surface tension (*n*-hexane = 18 $mNm^{-1}$).

Determination of the air – liquid interfacial tension ($\gamma_L$), or surface tension, is a well-established procedure. Briefly, a probe of known geometry is raised from contact with the surface of the liquid sample. The maximum force measured prior to the breaking of the liquid film is a function of the probe geometry and the surface energy of the liquid.

### *5.1.2. Wetting*

Wetting of a solid is a function of the liquid-solid interaction. The extent of the interaction is determined by the relative surface energies of the solid and liquid. If the liquid molecules have a greater attraction for the solid molecules than for each other, then the liquid will wet the solid to some extent. In general, therefore, if the surface energy of the liquid is less than that of the solid, wetting will occur. Non-polar surfaces such as PTFE with a low surface energy are not wetted by water, since the water-water cohesive forces are greater than the water-PTFE adhesive forces.

The degree of wetting can be determined by contact angle measurements. In Figure 5.1a, a liquid droplet is in contact with a smooth surface. The contact angle is a function of the degree of interaction between the liquid and the solid. If the liquid-liquid interaction is greater than the solid-liquid interaction, then the contact angle $\theta$ is greater than 90° and wetting does not occur. For low surface energy liquids on high surface energy solids $\theta = 0°$ and perfect wetting occurs. At the point where $\theta$ just equals 0°, the solid surface energy equals the liquid surface energy (Zisman, 1964). However, it is not possible to change the surface energy of a liquid during an experiment, since it is best practice to measure contact angles using pure materials and thorough mixing could not be guaranteed.

Contact angles between the extremes of non-wetting and perfect wetting ($0° < \theta < 90°$) are used to indirectly measure solid surface energies. In this region of non-

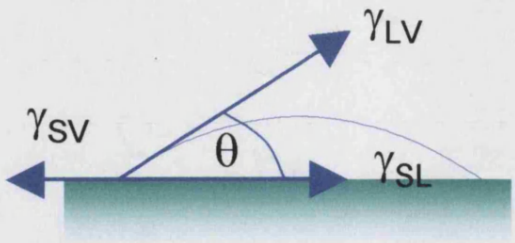


$$\gamma_{LV} \cos\theta = \gamma_{SV} - \gamma_{SL}$$

Figure 5.1a. Contact angle of a liquid on a smooth, non-porous material. The contact angle can be determined by visual means, and so surface energy information can be obtained.

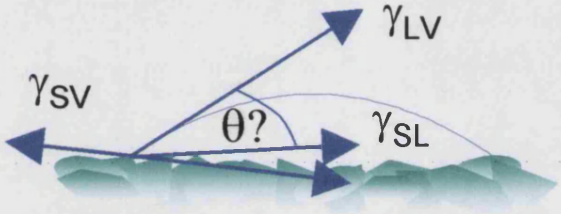


Figure 5.1b. Contact angle of a liquid on a rough surface. The contact angle cannot be measured accurately by visual methods, since a reference line cannot be assigned with any confidence.

spontaneous wetting, Young's equation may be used to explain the relationship between the contact angle and the three interfacial tensions.

$$\gamma_L \cos\theta = \gamma_S - \gamma_{SL} \qquad \text{Equation 5.1}$$

Therefore, the contact angle is a function of the surface energies of the solid and the liquid and also of the nature of the surrounding medium. This latter factor is not a consideration here, since all measurements are conducted in a normal atmosphere.

For polymer films and other smooth non-porous surfaces, the contact angle may be accurately determined by the use of a goniometer. This apparatus uses a magnifying lens and movable crosshairs in an eyepiece attached to a Vernier protractor which allows the user to determine contact angles.

Contact angles on porous materials and powders cannot be determined accurately using a goniometer, since the powder surface will not present an even surface to the liquid (see Figure 5.1b). Compacts of powders are not suitable for measurement, since the sample will be porous and hence a stable drop will not form. Also, the compaction itself may affect the surfaces of the particles, with pressure-induced changes in crystallography (Kumar & Kothari, 1999) and anisotropy of compacted MCC (Edge et al, 2001) potentially leading to orientation-specific results. Variations in the surface energy properties of compacts as a function of compaction force (compact strength) have also been observed (Buckton & Newton, 1986; Khan et al, 2001).

In this study, two techniques will be used to determine and compare the surface energies of MCCs, previously investigated for their ability to adsorb tacrine hydrochloride (Chapter 3). This will not only serve to establish the presence or absence of a link between adsorption capacity and affinity, but also enable a comparison to be made between the techniques for their ease of use, comparability and suitability for polysaccharides such as cellulose. The techniques under investigation both use secondary methods to determine the degree of interaction between a well-characterised solvent and the unknown solid.

### *5.1.3. Water-cellulose interactions*

It has previously been suggested (Chapter 3) that the water-cellulose interaction may be of importance in determining the ability of cellulose to adsorb drugs from

aqueous solution. Therefore, the use of surface energy studies to determine the ability of water to wet cellulose will be of interest. Calorimetric immersion studies have suggested that there are some variations in the MCC-water interactions depending on sample pre-treatment (Rowe et al, 1993; see also Chapter 3.4.3).

### *5.1.4. Capillary intrusion*

The spontaneous filling of a void by a liquid is due to the capillary force. In porous monolithic samples contact angles may be determined *via* the rate of liquid uptake through capillary action. This capillary intrusion (CI) method may also be used as an alternative to direct measurement of contact angles in powders, where a powder column is analogous to a packed column of capillaries (Buckton, 1993).

Measurement of liquid uptake rate relates to contact angle *via* the Washburn equation for the spontaneous uptake of liquid due to capillary action:

$$t = Am^2 \qquad \text{Equation 5.2}$$

where $t$ is time, $m$ is the mass of liquid adsorbed and $A$ is a constant:

$$A = \frac{\eta}{c\rho^2\gamma\cos\theta} \qquad \text{Equation 5.3}$$

where $\eta$ is the viscosity of the liquid, $c$ is the material constant, $\rho$ is the density of the liquid, $\gamma$ is the surface tension and $\theta$ is the contact angle. The material constant is dependent on the porous architecture of the sample. The two equations above may be combined and rearranged:

$$\cos\theta = \frac{m^2}{t}\frac{\eta}{\rho^2\gamma c} \qquad \text{Equation 5.4}$$

Therefore, monitoring $m^2/t$ as experimental data for liquid uptake will enable measurement of the contact angle. The value $c$ remains unknown and may be determined for a reproducible sample using a liquid with a 0° contact angle ($\cos\theta = 1$). For many materials such as cellulose (surface energy > 30 $mNm^{-1}$, the approximate limit of wetting by water), *n*-hexane ($\sigma = 18.4$ $mNm^{-1}$) may be used to determine the value of $c$. Theoretically the value of $c$ is (Rulison, 1996):

$$c = \tfrac{1}{2}\pi^2 r^5 n^2 \qquad \text{Equation 5.5}$$

where $r$ is the mean capillary radius and $n$ is the number of capillaries in the sample. Since $c$ is dependent on $r^5$, it is essential that a reproducible sample be used for these experiments. This is a non-trivial task for powders where packing of the powder column will affect the radius and number of capillaries in the sample. However, for free-flowing powders a reproducible powder column may be achieved by controlled tapping of the loaded sample holder, provided the initial loading is carried out reproducibly (Desai et al, 2001).

Several methods for calculating the total surface energy and contributions of polar and disperse contributions to the total surface energy of a solid have been published (review: Gindl et al, 2001). The method to be used here is the generally preferred acid-base approach (Good, 1992).

#### 5.1.4.1 Surface energy characterisation

The surface energy of a solid may be calculated from contact angle measurements using different liquids (e.g. Li & Neumann, 1992). Further information is gained by the use of liquids having known dispersive and polar character. The specific interactions dictate the surface contact angle between the surface and the liquid. These are a composite of the dispersive (Lifschitz-van der Waals, $\gamma_L^{LW}$), acid-base ($\gamma_L^{AB}$) and individual positive and negative polar ($\gamma_L^+, \gamma_L^-$) components of the liquid surface tension.

For capillary intrusion, the liquids used must not react with the solid, nor may the solid be soluble in the liquid. Several solvents are suitable for this type of study, but four liquids are commonly used. Water, *n*-hexane and ethylene glycol are readily available liquids with known acid-base and dispersive surface tension components. Diiodomethane is used to determine the dispersive contribution of the solid surface energy, since it possesses negligible acid-base character (Sharma et al, 2001) and a high surface energy (50.8 $mNm^{-1}$). Table 5.1 summarises the component contributions for the four solvents used, together with other necessary physical data.

Using liquids with known acid-base and Lifschitz – van der Waals character means that the contact angle determinations may be extended to provide further information about the solid surface. The surface free energy components are calculated according to equations 5.6 to 5.10 (de Meijer et al, 2000). The contact angles of

Table 5.1. Summary of physical data and surface tension parameters for the five liquids used at 20°C. Surface tension parameters from van Oss, 1993; Wu et al, 1996; van Oss et al., 1997.

| liquid | density ($kgm^{-3}$) | viscosity (mPas) | $\gamma_L$ ($mJm^{-2}$) | $\gamma_L^{LW}$ ($mJm^{-2}$) | $\gamma_L^{+}$ ($mJm^{-2}$) | $\gamma_L^{-}$ ($mJm^{-2}$) | $\gamma_L^{AB}$ ($mJm^{-2}$) |
|---|---|---|---|---|---|---|---|
| *n*-hexane | 659 | 0.31 | 18.4 | 18.4 | 0 | 0 | 0 |
| ethylene glycol | 1113 | 15.4 | 48.0 | 29.0 | 1.9 | 47.0 | 19.0 |
| diiodomethane | 3325 | 2.6 | 50.8 | 50.8 | 0 | 0 | 0 |
| water | 1000 | 1.00 | 72.3 | 21.8 | 25.5 | 25.5 | 51.0 |

three liquids are required to calculate the dispersion, positive and negative contributions.

The Lifschitz-van der Waals component of the surface energy of the solid ($\gamma_s^{LW}$) is calculated from the contact angle of diiodomethane:

$$\gamma_s^{LW} = 0.25\gamma_l^{LW}(1+\cos\theta)^2 \qquad \text{Equation 5.6}$$

With $\gamma_s^{LW}$ known, the acid ($\gamma_s^+$) and base ($\gamma_s^-$) components of the surface energy may be calculated from the contact angles of water (denoted W) and ethylene glycol (denoted EG).

$$\sqrt{\gamma_s^+} = (AF - BD)/(CF - CE) \qquad \text{Equation 5.7}$$

$$\sqrt{\gamma_s^-} = (BC - AE)/(CF - CE) \qquad \text{Equation 5.8}$$

$$A = \gamma_W(1+\cos\theta) - 2\sqrt{(\gamma_s^{LW}\gamma_W^{LW})} \qquad \text{Equation 5.9}$$

$$B = \gamma_{EG}(1+\cos\theta) - 2\sqrt{(\gamma_s^{LW}\gamma_{EG}^{LW})} \qquad \text{Equation 5.10}$$

$$C = 2\sqrt{\gamma_W^-} \quad D = 2\sqrt{\gamma_W^+} \quad E = 2\sqrt{\gamma_{EG}^-} \quad F = 2\sqrt{\gamma_{EG}^+}$$

The total acid-base component of the solid surface energy, $\gamma_s^{AB}$, is given by:

$$\gamma_s^{AB} = 2\sqrt{\gamma_s^+\gamma_s^-} \qquad \text{Equation 5.11}$$

The total surface free energy of the solid is given by:

$$\gamma_s = \gamma_s^{LW} + \gamma_s^{AB} \qquad \text{Equation 5.12}$$

### 5.1.4.2 Work of spreading (hydrophobicity and hydrophilicity)

The bulk hydrophobic or hydrophilic nature of a material may be summarised by the interfacial free energy ($\Delta G^{IF}_{sls}$) and the work of spreading ($W_s$). The interfacial free energy between two distinct condensed phases can be expressed as:

$$\Delta G_{sls}^{IF} = -2\gamma_s \qquad \text{Equation 5.13}$$

When $\Delta G^{IF}_{sls}$ is negative, there is an attraction between the surfaces of the solid *l* immersed in a liquid, hence a higher cohesive attraction, indicating that the material is generally not wetted by the liquid. Conversely, a positive value for $\Delta G^{IF}_{sls}$ indicates that the solid is fully wetted by the liquid, having a greater attraction for the liquid than for itself.

The work of spreading is the difference between the work of adhesion between the solid and liquid and the work of cohesion of the liquid (Dourado et al, 1998):

$$W_s = W_a - W_c = 2\left(\left(\gamma_s^{LW}\gamma_l^{LW}\right)^{0.5} + \left(\gamma_s^{+}\gamma_l^{-}\right)^{0.5} + \left(\gamma_s^{-}\gamma_l^{+}\right)^{0.5}\right) - 2\gamma \qquad \text{Equation 5.14}$$

If the liquid used is water, then the work of spreading will indicate the hydrophilicity or hydrophobicity of the material, with a negative value indicating a hydrophobic material. Similarly, the lipophilicity of the material with respect to any known lipid may be determined if the surface energy properties are known.

Spreading coefficients have successfully been applied to the study of tablet coatings. The importance of the properties of both the coating formulation and the tablet in determining the adhesion of the film to the tablet has long been recognised (Rowe, 1977). A significant correlation between the spreading coefficients and the maximum adhesive strength of formulations on a placebo formulation has been observed (Khan et al, 2001).

#### 5.1.4.3 Dry powder interactions

The concept of work of spreading has been extended to the investigation of mixing performance for binary and ternary blends (Ahfat et al, 1997; Hancock et al, 1997; Barra et al, 1998). The balance between the cohesive and adhesive forces between solids in binary and ternary mixes has been shown to be an indicator of mixing performance (e.g. Rowe, 1988; Rowe, 1992). Ahfat et al (1997) predicted the mixing of coloured powders using contact angle measurements and spreading coefficients. The spreading of binary blends over glass, effectively a ternary system, was also predicted using the same coloured powders.

### *5.1.5. Inverse gas chromatography*

Inverse Gas Chromatography (IGC) is based on the well-established technique of Gas Chromatography (GC). In GC a mixture of components is injected into a stream

of gas and is carried over a stationary phase in a column (see Figure 5.2). Separation of the components will occur if the interactions between each component and the stationary phase are sufficiently different to cause some components to be retained for a longer time and hence retarded in their passage through the column. A chromatogram of the signal from a suitable detector against time can be used to identify and quantify the components in the mixture.

For GC a solid phase is selected and the unknown gas phase components are analysed with reference to the stationary phase. Conversely, in IGC the surface chemistry of the stationary phase is investigated using gases with known characteristics (Figure 5.2). The fundamental quantity determined in IGC is the retention time of the probe. This, together with information pertaining to the surface energetics of the liquid, is used to characterise the surface energy of the solid.

Solid surface energetics may be determined through the measurement of retention time of non-polar (*n*-alkanes) and polar probes (e.g. ethanol, acetone) to obtain details of specific interactions. For a minimum amount of probe vapour, the retention time in the column is a function of the degree of interaction between the gas and the column packing. More specifically, the Gibbs free energy of adsorption is related to the adsorption equilibrium constant ($K$) and the retention volume ($V_R$) according to:

$$-\Delta G_A = RT \ln K + C_1 = RT \ln V_R + C_2 \qquad \text{Equation 5.15}$$

where $C_1$ and $C_2$ are constants that depend on the standard states of the gaseous and adsorbed states and the solid surface area, respectively, $R$ is the gas constant, $T$ is the temperature. The retention volume is related to the retention time by instrument-specific parameters such as gas flow rate and pressure drop through the instrument. The work of adhesion ($W_A$) between a vapour probe and the solid may be approximated as (Gutierrez et al, 1999):

$$-\Delta G_A = N_A a W \qquad \text{Equation 5.16}$$

where $N_A$ is Avogadro's constant and $a$ is the area of interaction of the probe. Fowkes (1982) stated that the total $W_A$ is the sum of two terms; the ubiquitous dispersive Lifschitz-van der Waals' type ($W_A^{LW}$) and specific ($W_A^{SP}$) interactions. The latter term covers all non-dispersive interaction such as acid-base, hydrogen

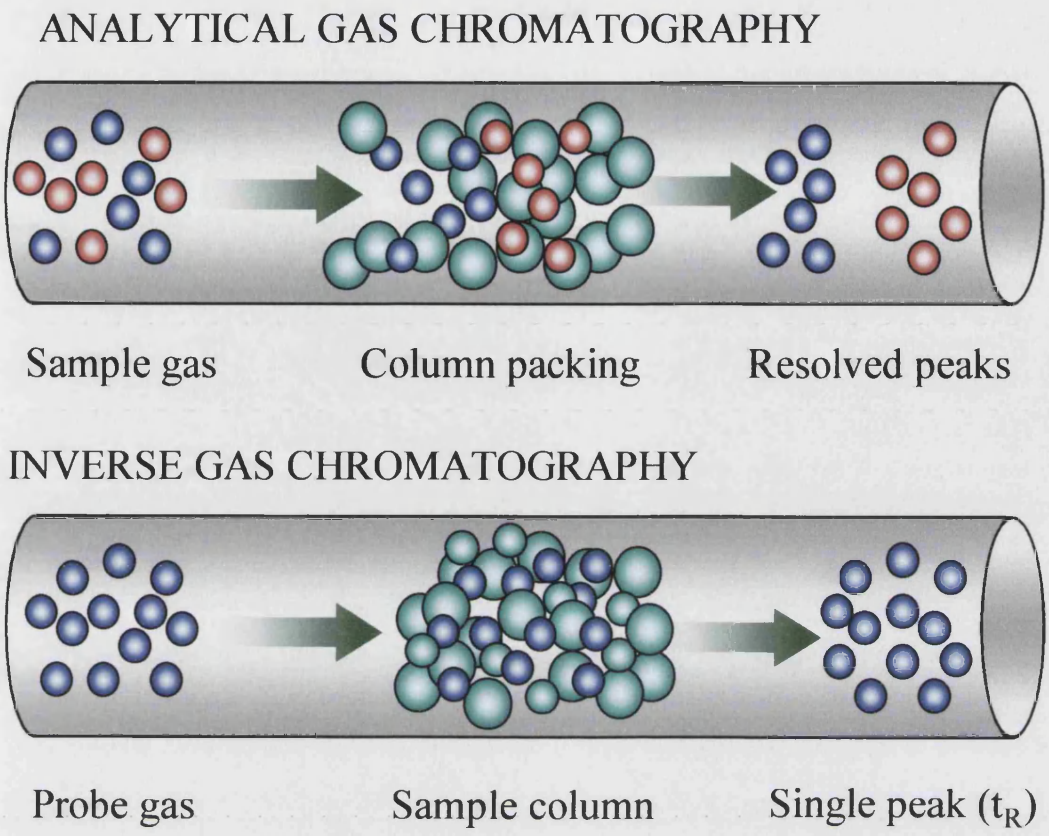


Figure 5.2. Comparison of analytical gas chromatography and inverse gas chromatography.

bonding and $\pi$ bonding. It follows that the free energy of adsorption may be similarly split and, if the surface energy of the solid is the sum of the free energy over all the sites, the surface energy may be split:

$$\gamma_S = \gamma_S^d + \gamma_S^{sp} \qquad \text{Equation 5.17}$$

where $\gamma_S^d$ is the dispersive component of the surface energy and $\gamma_S^{sp}$ is the component of the surface energy due to all specifically active sites, equivalent to the polar contributions to the surface energy.

Using a probe that has no discernable polar characteristics, equation 5.17 may be expressed as $W_A = W_A^D$. In this circumstance, the work of adhesion may be expressed as:

$$W_A = 2\left(\gamma_S^d \gamma_L^d\right)^{1/2} \qquad \text{Equation 5.18}$$

where $\gamma_L^d$ is the dispersive component of the surface energy of the liquid, equal to the surface energy or interfacial tension for non-polar liquids, such as *n*-alkanes. Combining equations 5.15, 5.17 and 5.18 the surface energy of a solid is linked to the retention time of a probe by (Schultz et al, 1987):

$$RT \ln V_R = 2N_A(\gamma_S^d)^{1/2} a(\gamma_L^d)^{1/2} + C \qquad \text{Equation 5.19}$$

Therefore, the slope of a linear plot of $a(\gamma_L)^{1/2}$ against $RT\ln V_R$ using *n*-alkanes may be used to obtain the non-polar contribution of the solid surface energy ($\gamma_S^d$) (Figure 5.3).

Specific interactions (e.g. acid-base) can be determined using suitable probes, with the deviation of the measured $RT\ln V_N$ from the alkane baseline giving the Gibb's free energy of the acid-base contribution to the total surface energy (Figure 5.3). The abscissa of the polar probe is situated on the basis of the molecular area of the probe, so that the drop-down to the alkane baseline can be made.

Values for the acid-base contributions to the surface energy are obtained using a comparative system relating to the ability of materials to donate and accept electrons is standard in IGC (Gutmann, 1978). Liquids are characterised as Lewis bases (electron donors) or Lewis acids (electron acceptors). The donor number and corrected acceptor number (DN and AN*, respectively) are used to calculate the acid

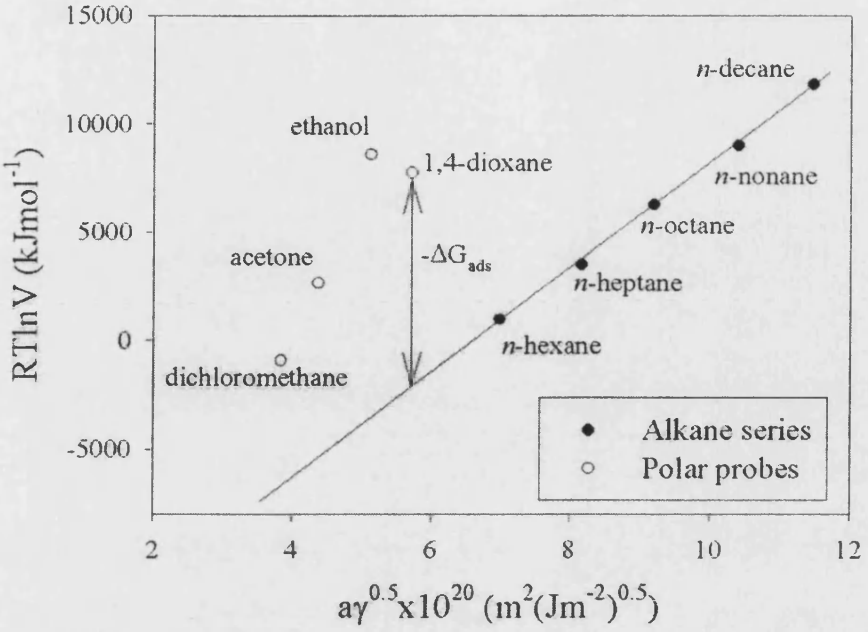


Figure 5.3. Raw data obtained from IGC experiments using Emcocel HD90 as stationary phase. The alkane series is used to calculate the dispersive component of the solid surface energy. The energies of specific interactions of polar probes are calculated with reference to the alkane baseline.

and basic parameters of the solid by referencing published values of DN and AN* of the probe solvents:

$$\Delta G_{abs}^{AB} = K_A \cdot DN + K_D \cdot AN^* \qquad \text{Equation 5.20}$$

This can be rearranged to give:

$$\frac{\Delta G_{abs}^{AB}}{AN^*} = \left(\frac{DN}{AN^*}\right) \cdot K_A + K_D \qquad \text{Equation 5.21}$$

Hence, a linear plot of $\Delta G^{AB}_{abs}$ against DN/AN* will yield values for $K_A$ and $K_D$. The values calculated assume zero entropic contribution. The entropic contribution may safely be ignored because the measurements are conducted at infinite dilution, hence such a contribution will be negligible (Papirer et al, 1988).

The value of DN is the energy of a co-ordinate bond between a donor atom and the antimony atom of $SbCl_3$ (Gutmann, 1978). The values of DN are given in kcalmol, hence the conversion factor of 1 cal = 4.184 J must be applied before reporting results. The values of AN, corrected by Riddle & Fowkes (1990), are derived from the relative chemical shift in the $^{31}P$ NMR spectrum of $Et_3PO$ when dissolved in the acid species of interest. This is normally a dimensionless quantity, but may be converted using the DN number of $Et_3PO$ of 167.4 $kJmol^{-1}$.

### *5.1.6. Previous investigations*

Microcrystalline cellulose has previously been investigated using the CI method (Rulison, 1996), with an unspecified MCC yielding a total surface energy ($\gamma_S$) of 40 $mJm^{-2}$, determined by the Zisman (1964) method. This is comparable with literature values for total surface free energy of wood of 40.0 to 55.5 $mJm^{-2}$ determined by contact angle measurements (de Maijer et al, 2000). Dourado et al (1996) obtained similar results using a thin-layer wicking technique.

Buckton et al (1999a) used IGC to determine the dispersive component of the surface energy of an active drug (saquinavir mesylate) in its 'as received' state and after three drying regimes. Aliquots of a 25% w/v slurry of the sparingly soluble drug was dried in a vacuum oven (80°C, 200 mbar, 4 hr) and tray-dried at 160°C for 2 hr. A dry batch was also heated to 160°C for 2 hr. All three regimes appeared to affect the surface energy, vacuum drying and heating of the dry sample causing less

of a difference than tray drying the wet mass. The tray-dried material had the lowest surface energy, and is therefore the most stable. The higher surface energy of the 'as received' sample was shown to be a function of the higher amorphous content of the sample, indicated by differences in the water sorption thermodynamics.

Dourado et al (1998) used a thin-layer wicking technique to characterise the surface energy of three microcrystalline cellulose types. They determined a total free energy of 51.8 $mJm^{-2}$ for Avicel PH101 (FMC Co., USA) and 57.2 and 59.0 $mJm^{-2}$ for two MCCs supplied by Sigma Co. (UK). By using a total of four contact liquids, they were also able to determine polar and dispersive contributions to the total surface energy. For Avicel PH101, a negative contribution equal to 50.1 $mJm^{-2}$ was determined, but zero positive polar contribution was determined (Ek et al, 1994).

Most previous investigations into the surface chemistry of MCC by IGC may not be suitable for comparison with the results reported here. Huu-Phuoc et al (1987), Jacob & Berg (1994), Garnier & Glasser (1994), Czeremuszkin et al (1997) and Papirer et al (2000) all heated cellulosic samples to greater than 80°C prior to analysis. It has been shown that heating to these temperatures affects the surface chemistry of cellulose with respect to adsorption capacity (Chapter 3) and water - cellulose interactions (Weisse, 1998). Therefore, these results may not be comparable with those reported here. Values of the dispersive component of the surface energy determined for cellulosic samples lie in the range 32 to 52 $mJm^{-2}$.

Tshabalala (1997), as part of an investigation into the surface chemistry of wood, used untreated cellulose powder as the stationary phase in IGC experiments. A generally acidic surface was suggested by the results obtained for cellulose powder, in comparison to the amphoteric nature indicated after analysis of washed and dried wood samples.

## 5.2. Materials

All microcrystalline cellulose samples were used as supplied; see list in Chapter 2.

For the capillary intrusion experiments, water was purified by reverse osmosis and ultrafiltration (MilliQ grade, Millipore, UK), *n*-hexane (AR grade, Fisher, Loughborough, UK), diiodomethane (analytical grade, Aldrich, Gillingham, UK)

Solvents used for IGC measurements were: *n*-hexane, *n*-heptane, *n*-octane, *n*-nonane, *n*-decane, acetone, 1,4-dioxane, dichloromethane and ethanol (all HPLC grade). All surface area, surface tension and donor / acceptor data from Guttman (1978), Belgacem et al (1995) and Riddle & Fowkes (1990); see Table 5.2.

## 5.3. Methods

Density was determined in triplicate using an individually calibrated 25 ml density bottle (Grade A, Fisher, Loughborough) at 20°C.

Viscosity was determined using cone and plate geometry on a controlled stress rheometer (CSL, TA Instruments, Leatherhead, UK) at 20°C. Newtonian behaviour was assumed for all solvents, since the variable solvent front velocity cannot easily be incorporated into the model. The assumption of Newtonian behaviour was shown to be valid for all solvents over the strain rate range 1 to 200 $s^{-1}$, approximately the strain rate under which the intrusion occurs.

Although liquid surface tension data was obtained from the literature, the total surface tension was monitored during experimental runs to ensure that no surface-active materials were introduced into the solvent either by atmospheric contamination or by leaching of soluble components from the test solids through the frit. Surface tension was determined using the rod method. A clean rod is suspended under the analytical balance and in contact with the liquid. The maximum force as the liquid bath is lowered is related to the surface tension. Any decrease in the surface tension between measurements is indicative of contamination and the liquid is replaced.

The rate of uptake of liquid by a packed powder column was determined gravimetrically. Powders and solvents were stored in an air-conditioned room maintained at 20°C. All measurements were performed in the same room. Pyrex tubes with a porous frit (in-house designed; Figure 5.4) were reproducibly packed by pouring 1000 ± 10 mg of powder into the tube and tapping using a jolting volumeter (J. Engelsmann, Ludwigshaven, Germany: 3 mm movement, 240 $min^{-1}$) for 50 taps. This was then suspended under an analytical balance (HM-120 5-figure balance, A & D Instruments, Abingdon, UK) over a bath of the liquid being used. A bath with a diameter of 10 cm was used, a wide bath being preferred because the liquid level will not be significantly affected by uptake of the liquid into the sample. A significant

Table 5.2. Characteristics of probe molecule used for IGC experiments. Data from Guttman (1978); Belgacem et al (1995); Riddle & Fowkes (1990).

| probe | a(Å$^2$) | $\gamma_L^d$ (mJm$^{-2}$) | a$(\gamma_L^d)^{0.5}$ (Jm$^{0.5}$ x 10$^{-20}$) | DN | AN | Lewis characteristics |
|---|---|---|---|---|---|---|
| *n*-hexane | 51.5 | 18.4 | 6.99 | -- | -- | neutral |
| *n*-heptane | 57.0 | 20.3 | 8.12 | -- | -- | neutral |
| *n*-octane | 62.8 | 21.3 | 9.17 | -- | -- | neutral |
| *n*-nonane | 68.9 | 22.7 | 10.4 | -- | -- | neutral |
| *n*-decane | 75.0 | 23.4 | 11.5 | -- | -- | neutral |
| acetone | 34.0 | 16.5 | 4.37 | 17.0 | 2.5 | amphoteric |
| $CH_2Cl_2$ | 24.5 | 24.5 | 3.83 | 0.0 | 3.9 | acidic |
| ethanol | 21.1 | 35.3 | 5.13 | 20.0 | 10.3 | amphoteric |
| 1,4-dioxane | 31.4 | 33.2 | 5.72 | 14.8 | 0.0 | basic |

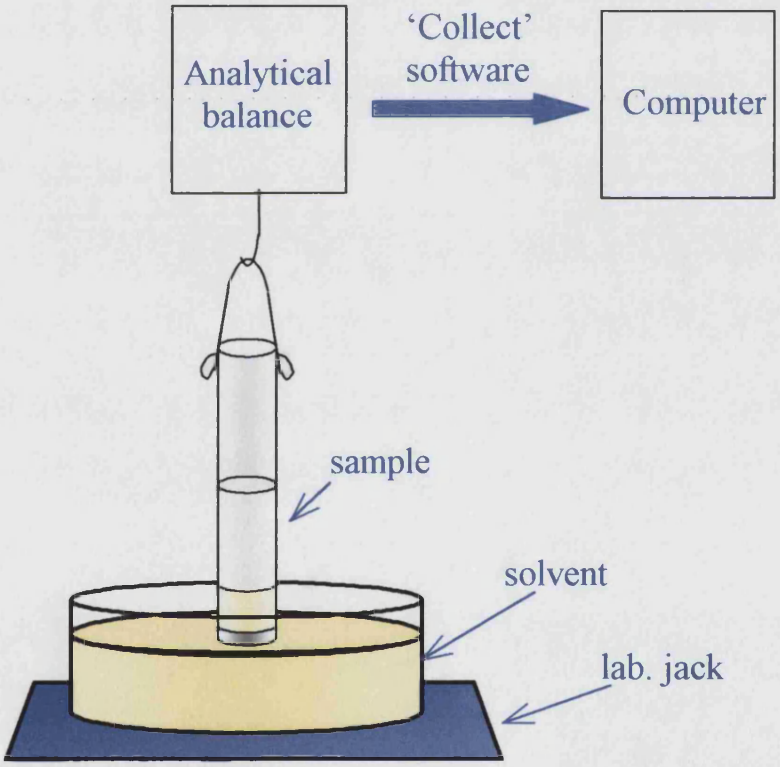


Figure 5.4. Apparatus used for the capillary intrusion work. The sample is reproducibly packed into an in-house designed borosilicate tube with a frit at the base. This is suspended from an analytical balance above a wide solvent bath. The bath is raised until the solvent just contacts the frit and the mass change is collected automatically.

& D Instruments, Abingdon, UK) over a bath of the liquid being used. A bath with a diameter of 10 cm was used, a wide bath being preferred because the liquid level will not be significantly affected by uptake of the liquid into the sample. A significant decrease in the liquid level would change the force that the surface tension exerts on the sample tube, and so affect the readings from the balance.

The bath was then raised manually until the bottom of the tube just contacted the liquid surface and capillary rise could be seen to have begun. The reproducibility of the *n*-hexane blank indicated that there was no error induced due to the buoyancy of the loaded tube. Raw data was collected automatically at a rate of one point per second over no more than 30 seconds of the intrusion. Swelling of the MCC samples by water or ethylene glycol affects the intrusion rate higher up the powder column by restricting the capillaries at the base of the column.

Each MCC was analysed in the same tube used to determine the 'c' constant. Variations in the diameter of the tubes were shown to affect the calculated 'c' constant, since the porous architecture is affected by the tube profile.

Blank runs (n = 5) were conducted using each intrusion tube in order to determine the contribution of the solvent adsorbed in the frit and surface tension to the mass reported. This value, which remains constant throughout the experiment, was subtracted from the raw data prior to plotting the $m^2$ against time curve.

Each MCC type was analysed in the same tube used to determine the 'c' constant. Least squares linear regression analysis was used to obtain the slope over the straight part of the $m^2$ against time curve.

Inverse gas chromatography experiments were conducted at infinite dilution using an SMS iGC 2000 (SMS UK, London), column oven maintained at a constant temperature of 303 K. All MCC samples were used as supplied. Approximately 2 g of each MCC was loaded into 3 mm ID glass columns, previously treated with dimethlydichlorosilane (BDH, Poole) to passivate the glass surface. A vibratory bed was used for sample loading to ensure full packing. Experiments were conducted at 44% and 0% RH, peak detection was by flame ionisation detection. A flow rate of 10 $mlmin^{-1}$ was used throughout. Samples were equilibrated for 12 hours at the required relative humidity. The same loaded sample column was used for both the 44%RH and the 0%RH runs, with the 44%RH run completed before conditioning for

the run at 0%RH. This was to avoid any possible permanent damage to the sample caused by drying affecting the 44%RH results.

## 5.4. Results and Discussion

### *5.4.1. Capillary intrusion*

Contact angle data for the ten MCC samples investigated using the CI method are summarised in Table 5.3. The acid-base method summarised in section 5.1.4.1 was used to translate the contact angle measurements into values for the components of the surface energy.

Determination of contact angles, and therefore surface energy data, by the CI method is dependent on the reproducible determination of the material constant 'c' in Equation 5.4. For each MCC except Emcocel SP15 the relative standard deviation of the calculated material constant (n = 5) was less than 5%, indicating good reproducibility (Table 5.4).

The very poor flowability of Emcocel SP15, a result of its small particle size, was the most probable contributing factor to the poor reproducibility of the material constant. Results obtained for Emcocel SP15 will not be considered further for the purposes of intercomparison. Note that a thin-layer wicking method, whereby the sample is attached to a glass slide using glue or by evaporation of a suspension of the sample, may be used for fine powders (Dourado et al, 1998). However, soluble components in the glue may affect the characteristics of the solvent used and the use of a suspension prior to analysis may affect the surface characteristics of the solid.

Values for the specific components of the surface energy of the ten MCCs studied are summarised in Table 5.5. These data suggest that the MCC samples have a predominantly negative surface. This confirms the generally acidic nature of the MCC surface (pKa = 4.0 – 4.3), a result of the presence of titratable carboxyl groups in the surface (Chapter 4). Silyl groups in the surface of the silicified MCC would not be expected to contribute significantly to the negative part of the surface energy, because the CSM used has a similar pKa to MCC (4.40; product data sheet).

Significant positive contributions to the total surface energy were indicated from the results obtained for Emcocel HD90 and Pharmacel 101. These may be artefacts

Table 5.3. Summary of cos θ and contact angle (°) values for three solvents on ten MCC samples. Standard deviations (sd) values calculated by error propagation for contact angles.

| MCC | Diiodomethane | | | | Ethylene Glycol | | | | Water | | | |
|---|---|---|---|---|---|---|---|---|---|---|---|---|
| | cos θ | sd | Angle | sd | cos θ | sd | Angle(°) | sd | cos θ | sd | Angle(°) | sd |
| Ankit | 0.673 | 0.032 | 47.7° | 2.0 | 0.751 | 0.111 | 41.3° | 6.9 | 0.567 | 0.046 | 55.4° | 3.1 |
| Avicel PH101 | 0.694 | 0.010 | 46.1° | 0.7 | 0.660 | 0.183 | 48.7° | 11.9 | 0.434 | 0.016 | 64.3° | 1.1 |
| Ceolus KG802 | 0.686 | 0.051 | 46.7° | 3.3 | 0.512 | 0.157 | 59.2° | 10.8 | 0.537 | 0.027 | 57.5° | 1.8 |
| Emcocel 50M | 0.785 | 0.023 | 38.3° | 1.4 | 0.776 | 0.076 | 39.1° | 4.7 | 0.552 | 0.021 | 56.5° | 1.4 |
| Emcocel HD90 | 0.636 | 0.036 | 50.5° | 2.4 | 0.880 | 0.071 | 28.4° | 4.2 | 0.363 | 0.077 | 68.7° | 5.7 |
| Emcocel SP15 | 0.580 | 0.068 | 54.5° | 4.6 | 0.878 | 0.549 | 28.6° | 32.8 | 0.992 | 0.091 | 7.3° | 5.2 |
| Prosolv 50 | 0.806 | 0.027 | 36.3° | 1.7 | 0.826 | 0.062 | 34.3° | 3.8 | 0.624 | 0.057 | 51.4° | 3.7 |
| Pharmacel 101 | 0.640 | 0.021 | 50.2° | 1.4 | 0.896 | 0.015 | 26.4° | 0.9 | 0.412 | 0.003 | 65.7° | 0.2 |
| Tabulose 101 | 0.733 | 0.014 | 42.9° | 0.9 | 0.780 | 0.081 | 38.7° | 5.0 | 0.564 | 0.096 | 55.7° | 6.5 |
| Vivapur 101 | 0.628 | 0.057 | 51.1° | 3.8 | 0.676 | 0.045 | 47.5° | 2.9 | 0.414 | 0.016 | 65.5° | 1.1 |

Table 5.4. Material constant determination for ten MCC samples. Standard deviations, calculated by error propagation, in brackets.

| MCC | Constant ($x10^{-15}$ $m^5$) |
|---|---|
| Ankit | 2.624 (0.053) |
| Avicel PH101 | 4.246 (0.215) |
| Ceolus KG-802 | 4.289 (0.234) |
| Emcocel 50M | 4.267 (0.245) |
| Emcocel HD90 | 2.722 (0.085) |
| Emcocel SP15 | 1.033 (0.025) |
| Pharmacel 101 | 2.616 (0.047) |
| Prosolv 50 | 3.938 (0.088) |
| Tabulose 101 | 4.065 (0.014) |
| Vivapur 101 | 4.239 (0.165) |

Table 5.5. Summary of solid surface energy ($\gamma_S$) ($mJm^{-2}$) determined by the acid-base method using data in Table 5.3. Errors in brackets.

| MCC | dispersive ($\gamma_s^d$) | positive ($\gamma_s^+$) | negative ($\gamma_s^-$) | acid-base ($\gamma_s^{AB}$) | total ($\gamma_s$) |
|---|---|---|---|---|---|
| Ankit | 35.6 (2.3) | 0.1 (0.0) | 29.5 (4.0) | 3.8 (1.2) | 39.4 (2.5) |
| Avicel PH101 | 36.4 (0.8) | 0.0 (0.0) | 21.3 (4.9) | 1.3 (0.4) | 37.7 (0.9) |
| Ceolus KG-802 | 36.1 (3.7) | 0.5 (0.0) | 38.4 (4.4) | 8.3 (1.2) | 44.4 (3.9) |
| Emcocel 50M | 40.5 (1.9) | 0.0 (0.0) | 26.1 (2.6) | 2.0 (0.5) | 42.4 (1.9) |
| Emcocel HD90 | 34.0 (2.5) | 1.9 (0.1) | 9.3 (1.7) | 8.5 (1.6) | 42.5 (3.0) |
| Emcocel SP15 | 31.7 (4.3) | 0.2 (0.1) | 76.8 (37.1) | 6.9 (6.6) | 38.6 (7.9) |
| Pharmacel 101 | 34.2 (1.5) | 1.9 (0.0) | 11.7 (0.4) | 9.3 (0.3) | 43.4 (1.5) |
| Prosolv 50 | 41.4 (2.2) | 0.1 (0.0) | 30.6 (2.5) | 2.5 (1.4) | 43.9 (2.7) |
| Tabulose 101 | 38.1 (1.1) | 0.1 (0.1) | 27.4 (2.9) | 3.4 (2.1) | 41.6 (2.4) |
| Vivapur 101 | 33.7 (3.9) | 0.2 (0.0) | 19.4 (1.2) | 3.7 (0.3) | 37.4 (3.9) |

resulting from the low contact angle determined for ethylene glycol. However, previous surface energy measurements of wood suggested an amphoteric nature (Tchabalala, 1997; de Meijer et al, 2000). Species absent in most forms of purified cellulose, but still apparent in these two products, may be responsible.

ANOVA of the surface energy values calculated for the nine MCC samples (Emcocel SP15 results disregarded; see above) suggests that there is no significant difference between the dispersive components or the total surface energies of the samples ($p<0.05$). For the acid-base contributions, significant differences are observed. Using Fisher's pairwise comparison test at a 5% significance level, two groups are suggested. Ceolus KG-802, Emcocel HD90 and Pharmacel 101 all possess 'high' acid-base (> 8.3 $mJm^{-2}$), all of which have a significantly higher acid-base component than the other six MCCs considered (max = 3.8 $mJm^{-2}$).

As discussed in Chapter 2.1.2, it has been suggested that the 'C' parameter determined from $N_2$ BET adsorption experiments may be related to the dispersive component of the surface energy of a material (Ticehurst et al, 1994). However, no correlation ($R^2 = 0.001$) was found between the 'C' values listed in Table 2.2 and the $\gamma_d$ values calculated here (Table 5.5). This may be a result of alteration of the cellulose surface during freezing with liquid $N_2$.

The lower surface energy of the high density MCC may also contribute to the generally lower strength of compacts made from these materials, since the cohesive energy density of a compact is related to the surface energy of the material (Vachon & Chulia, 1999). There is no significant difference (ANOVA, Fisher's test, $p<0.05$) between either the dispersive, positive or negative components of the surface energies of Emcocel 50M and Prosolv 50. The generally improved compactibility and lubricant sensitivity of the silicified MCC (Sherwood & Becker, 1998) cannot be explained simply in terms of surface energetics. The improved compactibility may be a result of a physical keying effect, due to the presence of the CSD (Guo et al, 2002).

From the surface energy data calculated here, together with the surface area data collected in Chapter 2, it is possible to determine the energy per gram of a material. In Table 5.6, the product of the $N_2$ adsorption BET surface area ($mJm^{-2}$) and the specific surface area ($m^2kg^{-1}$) yields a specific surface energy (SSE, $mJkg^{-1}$). This

Table 5.6. Specific surface energy for ten MCC samples.

| MCC | Surface energy ($\gamma_s$) ($mJm^{-2}$) | $N_2$ BET surface area ($m^2kg^{-1}$) | Specific energy ($Jkg^{-1}$) |
|---|---|---|---|
| Ankit | 39.4 (2.5) | 1120 | 44.1 |
| Avicel PH101 | 37.7 (0.9) | 1220 | 46.0 |
| Ceolus KG-802 | 44.4 (3.9) | 1250 | 55.5 |
| Emcocel 50M | 42.4 (1.9) | 1270 | 53.8 |
| Emcocel HD90 | 42.5 (3.0) | 690 | 29.3 |
| Emcocel SP15 | 38.6 (7.9) | 3320 | 128 |
| Pharmacel 101 | 43.4 (1.5) | 1300 | 56.4 |
| Prosolv 50 | 43.9 (2.7) | 4910 | 216 |
| Tabulose 101 | 41.6 (2.4) | 1340 | 55.7 |
| Vivapur 101 | 37.4 (3.9) | 1450 | 54.2 |

may be related to the potential bonding energy between the MCC particles, with a higher SSE indicative of potentially stronger compacts. A cursory review shows that Prosolv 50 should make stronger compacts than the unmodified grades, and Emcocel HD90 should make weaker compacts than standard MCCs. This has been shown to be true in general for SMCC (Guo et al, 2002) and high-density MCCs (Tobyn et al, 2002). No linear correlation between compact strength and specific surface energy can be expected using such a simple relationship. Other factors, especially particle size, plasticity and surface roughness, must be considered when attempting to predict the relative compactibilities of materials.

The value calculated for Emcocel SP15 is somewhat misleading, in that practical experience argues against strong compacts being made of the small particle size grade of MCC. However, the poor compacts made with Emcocel SP15 are a function of the physical processes involved in tablet compaction. Poor die filling, a consequence of the poor flowability of the material, can leave voids in the powder column. Depending on the speed of the tablet press, air may be trapped in the powder bed during the compaction cycle, which reduce the number of MCC – MCC bonds in the tablet, thus reducing the overall strength of the compact.

### *5.4.2. Inverse gas chromatography*

Three MCC samples were analysed by IGC. Dispersive contributions at 0% and 44% RH are summarised in Table 5.7. Dispersive, electron donor and electron acceptor values are summarised in Table 5.8. Errors are based on the computed standard deviation determined by error propagation. These were selected to investigate the two important aspects of the nature of MCCs shown to be of importance for adsorption of tacrine from aqueous solution (Chapter 3). Emcocel 50M was used as a control MCC. Emcocel HD90 was used to represent hardwood derived MCCs and Prosolv50 was used to investigate the effect of silicification.

The values of the dispersive components of the surface energies determined here compare well with previous values determined by IGC. Papirer et al (2000) determined a $\gamma_s^d$ of 52.3 $mJm^{-2}$ for an Avicel sample. Jacob & Berg (1994), using the same method for the determination of the surface area of alkane probes as used here, determined $\gamma_s^d$ of 45.9 $mJm^{-2}$. As mentioned previously, both these authors dried MCC samples under high temperature prior to analysis.

Table 5.7. Summary of dispersive component value ($\gamma_s^d$) parameters calculated for three MCC samples by IGC at 0% and 44% RH; calculated errors in brackets.

| MCC | $\gamma_s^d$ at 0% RH ($mJm^{-2}$) | $\gamma_s^d$ at 44% RH ($mJm^{-2}$) |
|---|---|---|
| Emcocel 50M | 55.5 (0.6) | 44.9 (0.5) |
| Emcocel HD90 | 45.6 (0.4) | 40.5 (0.4) |
| Prosolv 50 | 70.2 (0.5) | 45.6 (0.4) |

Table 5.8. Summary of acidic (KA) and basic (KD) parameters calculated for three MCC samples by IGC at 44% RH; calculated errors in brackets. Note that these results indicate a basic surface for Emcocel HD90.

| MCC | $\gamma_s^d$ ($mJm^{-2}$) | $K_A$ ($Jmol^{-1}$) | $K_D$ ($Jmol^{-1}$) | $K_D/K_A$ |
|---|---|---|---|---|
| Emcocel 50M | 44.9 (0.5) | 67 (56) | 184 (56) | 2.75 (2.56) |
| Emcocel HD90 | 40.5 (0.4) | 167 (56) | 92 (56) | 0.55 (0.40) |
| Prosolv 50 | 45.6 (0.4) | 113 (134) | 134 (134) | 1.19 (1.84) |

The dispersive components of the surface energies of the three MCCs determined at 44%RH are similar to the results obtained in the CI experiments. At 44% RH the IGC data is 5 to 6 $mJm^{-2}$ higher than that determined using CI, but the same rank order is observed; Prosolv 50 > Emcocel 50M > Emcocel HD90.

The higher values determined at 0% RH may be a result of the availability of higher energy adsorption sites, which, at 44% RH, are preferentially occupied by water molecules. From water adsorption studies conducted using Dynamic Vapour Sorption (DVS; see Chapter 2) it is known that the monolayer coverage of MCC is exceeded at 44% RH (monolayer coverage at approximately 28% RH for most MCCs studied). However, Marshall et al (1972), using immersion calorimetry measurements found that the surfaces of the MCCs they studied (Avicel brand) were energetically homogeneous. Therefore, the observed variation at 0% RH may be a result of the retention of polar probes, which are not completely eluted from the previous experiment.

In Table 5.8, it is clear that large errors are associated with the IGC data as used to determine the acid and base parameters (electron donor and acceptor numbers) of the surface energy. Previous work using acid / base probes (e.g. Czeremuszkin et al, 1997) attributed these errors to retention of the probes, which were elutable after the injection of water. In this study, the use of moist carrier gas did not appear to improve the accuracy of this technique, previously used successfully for synthetic polymers and inorganic materials. More useful, readily interpretable data are obtained from CI experiments on these materials. However, a smaller sample is required for the IGC experiments and the technique is less laborious than CI.

Comparison of the data obtained for the high-density MCC, Emcocel HD90, and the standard grade product indicates that the high-density grade has a lower dispersive surface energy. This may have consequences for lubricant sensitivity and mixing, with a lower degree of interaction with other materials in a mix.

Calculated acid and base parameters for the three MCCs analysed by IGC are summarised in Table 5.8. The very large errors associated with these results reduce the value of these data, but general conclusions may be drawn. Of interest is the general positive nature of the surface of Emcocel HD90. Determination of the surface energy components of Emcocel HD90 by CI suggested that there are positive

sites in the surface of Emcocel HD90. The presence of positively charged groups detected using IGC suggests that he positive groups detected using CI are real, rather than being a result of experimental error.

### *5.4.3. Work of spreading*

Table 5.9 compares the calculated work of spreading for water and magnesium stearate the MCCs studied. The approximate equivalence of the surface energetics of the MCCs results in similar general hydrophobicity, lipophilicity and magnesium strearate interaction values for all MCCs. From the data presented here it is determined that MCCs are generally hydrophobic in nature. This may seem at odds with the observation that MCCs appear to disperse in water, but is in accord with molecular modeling investigations, which determined that the surface of cellulose is non-hydrophilic (Heiner & Teleman, 1997; Heiner et al, 1998). Molecular modeling suggests that water is not attracted to cellulose surfaces, having the same chemical potential and density at a modeled cellulose surface as that found in bulk water. Therefore, a negative work of spreading may be expected.

However, the ability of MCC to disperse in water will be affected by the release of surface-active material (Ardizzone et al, 2001). The stability of suspensions is affected both by the surface tension between the liquid and the solid and by the particle size of the solids. In Chapter 3, stirred 0.025 $gml^{-1}$ suspensions of MCC in tacrine solution were used in the investigation of adsorption from aqueous solution. From the data provided by Arizzone et al (2001), a reduction in the surface tension of the suspension could be expected. This may be enough to increase the spreading coefficient to a value greater than zero, indicative of a stable suspension (Douardo et al, 1998). Without further data, such as the effect the released surfactants have on the specific components of the surface energy of the surfactant solution and the critical micelle concentration of the surfactant mix released from each MCC, it is not possible to calculate the surface energy of a given MCC in water suspension. Therefore, it is not possible to obtain an estimate of the spreading coefficient of the system.

Table 5.9. Calculated work of spreading ($mJm^{-2}$) values of water and magnesium stearate for nine MCCs studied. Because of the large errors in the calculated surface energy values for Emcocel SP15, this MCC was not included in this part of the study.

| MCC | Water | Mg stearate |
|---|---|---|
| Ankit | -31.6 (4.1) | 29.8 (1.4) |
| Avicel PH101 | -41.2 (5.4) | 26.6 (0.5) |
| Ceolus KG-802 | -20.2 (4.6) | 34.2 (2.3) |
| Emcocel 50M | -32.5 (3.0) | 31.3 (1.1) |
| Emcocel HD90 | -46.4 (3.4) | 23.7 (1.6) |
| Pharmacel 101 | -42.8 (1.3) | 25.1 (0.9) |
| Prosolv 50 | -27.4 (2.9) | 33.6 (1.3) |
| Tabulose 101 | -31.7 (3.1) | 30.8 (0.7) |
| Vivapur 101 | -42.7 (3.4) | 25.0 (2.5) |

### *5.4.4. Correlation with adsorption results*

As with the chemical characterisation work, the results from the surface energy values determined here are compared with the adsorption of tacrine from aqueous solution, as determined in Chapter 3. The dispersive, negative, total acid-base and total surface energies of nine of the MCCs (Emcocel SP15 excluded; see above) were compared with the affinity and capacity for adsorption of tacrine from an aqueous solution (Chapter 3). The positive contributions were not included because these are subject to high relative errors for most of the MCCs studied. The Pearson's correlation coefficient ($r^2$) is below 0.25 for all eight interactions.

However, using the specific surface energy an improved correlation ($r^2 = 0.77$) between the specific energy and tacrine adsorption capacity is observed (Figure 5.5). Values calculated for Prosolv 50 were excluded from this study, since previous discussions suggest that the CSD in the surface of MCC does not influence the surface energy of MCC, but does 'block' a proportion of adsorption sites (Chapter 3). The low value obtained for Emcocel HD90 has a significant influence on the data; excluding this data point results in a Pearson's correlation coefficient of 0.43. Obtaining further data, using more MCC samples with low surface areas, will allow this correlation to be tested more robustly.

It has previously been suggested that the water-cellulose interaction may affect the ability of MCC to adsorb tacrine from aqueous solution. However, a poorer correlation between the water spreading coefficient and tacrine adsorption capacity is observed than between the tacrine adsorption capacity and the total surface energy.

## 5.5. Conclusions

The Capillary Intrusion method has been shown to be of value for measuring the surface energy characteristics of MCC samples, provided the flowability of the materials does not hinder the production of reproducible samples.

Approximately equivalent values for the dispersive contribution to the surface energy of the three MCCs used for the purpose of comparing the two techniques were calculated from the data collected.

A direct comparison of the magnitudes of the specific interactions is not possible, because the treatment of the IGC data yields surface energy data based on a molar

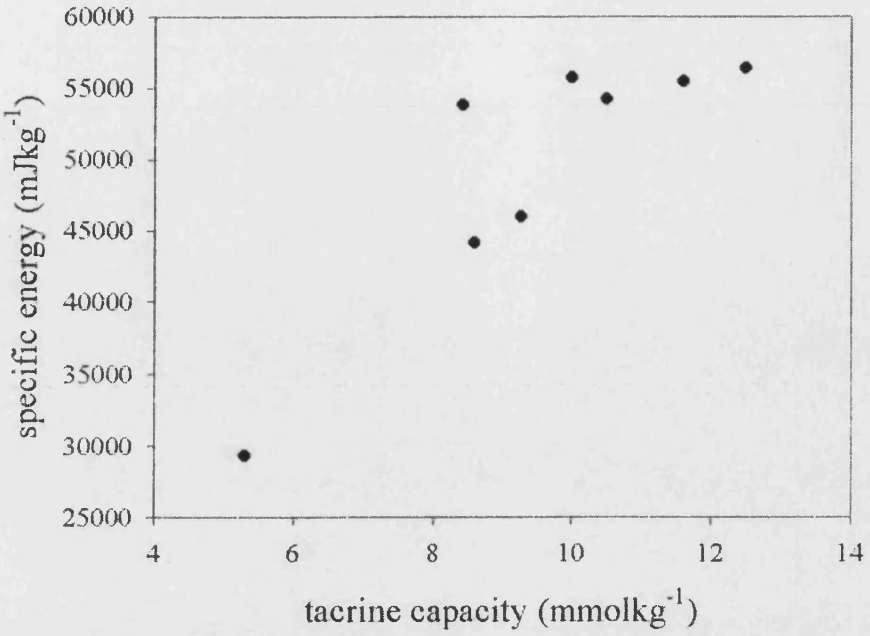


Figure 5.5. Correlation of specific surface energy ($mJkg^{-1}$) with tacrine capacity ($mmolkg^{-1}$).

energy, rather than energy per unit area. With the exception of Emcocel HD90, all MCCs are described as having predominantly negative (acidic) surfaces on analysis using IGC. However, IGC measurements disagree with the CI data in characterising the surface of Emcocel HD90, although some positive character is in evidence for Emcocel HD90 from CI measurements.

From work of spreading calculations, all MCC surfaces are described as predominantly non-hydrophilic. This confirms molecular modelling investigations of the surface, where few hydrophilic sites were determined and a predominantly lipophilic surface was computed (Heiner & Teleman, 1997). The general lipophilicity of the MCC surface may be a factor in the sensitivity of MCC to lubricants such as magnesium stearate.

The differences between the IGC and CI data are explicable in terms of what the two techniques measure. In IGC, there is a tendency to selectively measure the highest energy sites in the surface, which have a greater influence on the surface characteristics. Using moistened carrier gas will cause a small reduction in the measured surface energy by the preferential adsorption of water at high-energy hydrophilic sites which may hinder adsorption at adjacent lipophilic sites.

Results obtained using CI suggest that the powder column approach used here may be applicable to powders and granules in a restricted particle size range. Smaller particle size samples may be difficult to load reproducibly and swelling of the particles will change the capillary structure more quickly than in larger particle size samples. Very large particles (not studied here) are less suitable, since the capillary effect is restricted by the diameter of the pores in the sample, therefore low surface energy liquids may not be able to penetrate large pores.

## 5.6. Summary

The objective of this study was to investigate the factors affecting the adsorption of amine drugs onto MCC products. To this end, the adsorption characteristics of a model drug, tacrine hydrochloride, were characterised for twenty six MCC samples, the majority of which are commercially available. Physical and chemical characterisation work was also undertaken, including a study of the surface energetics of MCC samples.

Particle size analysis (Chapter 2.4.2) and scanning electron microscopy (Chapter 2.4.5) suggests that all the MCCs studied are supplied as aggregates of smaller individual particles (see also Ek et al, 1994).

Determination of adsorption isotherms for the adsorption of tacrine on MCCs from aqueous solution has been shown to be a valuable tool for investigating interactions at surfaces (Chapter 3; Franz & Peck, 1982).

It was shown that the adsorption characteristics varied between MCC products produced by different manufacturers (Chapter 3.4.2; Landín et al, 1993a).

Particle size of the MCC agglomerates was not found to have a significant effect on the adsorption characteristics (Chapter 3.4.3).

For the drug studied, tacrine hydrochloride, the most important influence on the adsorption characteristics of the 'as received' samples was the original pulp source (Chapter 3.4.4). Softwood derived MCCs had a higher adsorption capacity than hardwood derived MCCs.

For the first time, the effect of the silicification of MCCs (Prosolv® grades) has been investigated (Chapter 3.4.5). Silicified MCCs had a significantly lower adsorption capacity than the equivalent MCCs from the same manufacturer.

Sample pre-treatment was also shown to be of importance, with both heating and milling having a significant affect on the adsorption characteristics (Chapter 3.4.7).

Investigations into the nature of the adsorption process suggested that the adsorption of tacrine onto MCC is a fully reversible (Chapter 3.4.10) and the primary mode of adsorption is by an ion pairing process (Chapter 3.4.13).

Significant batch-to-batch variations were determined for three 'standard grade' MCC products (Chapter 3.4.11).

Dissolution testing of simple model formulations failed to show differences in the adsorption of the two MCCs with the highest and lowest adsorption capacities (Chapter 3.4.15).

Differences between softwood and hardwood MCCs are evident from the chemical characterisation work described in Chapter 4.

Carboxyl content determinations were found to yield data which could be correlated with the tacrine capacity (Chapter 4.4.1). This relates to the finding in Chapter 3.4.13, that the predominant mode of adsorption is by ion exchange (Okada et al, 1987).

Surface energetics were investigated using two techniques in Chapter 5, capillary intrusion and inverse gas chromatography. These yielded equivalent values for the surface energetics of the three MCCs studied using both methods.

The surfaces of all MCCs were found to be predominantly negative (Chapter 5.4.1, 5.4.2; Dourado et al, 1996; de Maijer et al, 2000).

A combination of the surface energy data determined in Chapter 5.4.1 and the surface area data in Chapter 2.3.2 suggested that there is a maximum specific surface energy of MCCs.

A generally hydrophilic surface for MCCs was determined by modeling the spreading pressure of water (Chapter 5.4.3).

In conclusion, in this thesis we have characterised the adsorption of tacrine hydrochloride from aqueous solution onto MCC. The adsorption varies between MCC products, with the most important influence being the pulp source, adsorption is fully reversible and may be affected by the ionic strength of the surrounding medium (Steele et al, 2003). We have also established that silicified MCCs form stronger compacts than the unsilicified material (Edge et al, 2000), that compaction imparts directionality into the strength of MCC compacts (Edge et al, 2001) and that surface energetics of MCCs may be characterised using a capillary intrusion method.

# A1. Errors and Statistical Analysis

Knowledge of the errors associated with analytical measurements is required so that intercomparisons can be made between samples and techniques. Using the errors associated with a set of data, it is possible to state the confidence that points in the set readings are similar or different. The main points considered here are: error propagation, linear regression and comparisons.

## A1.1. Error propagation

The general form for the determination of errors propagated due to arithmetic operations is of the form:

$$s(F(x_0)) = \left|\frac{dF}{dx}\right|_{x=x_0} s_{x_0} \qquad \text{Equation A1.1}$$

Common error propagation functions are summarised in Table A1.1. In addition, two functions used in this work that are not commonly listed are given in Table A1.1; $e^x$ and acos($x$).

Error propagated by complex arithmetic relationships, particularly those used in Chapter 5 to obtain surface energy data, were calculated using Excel™ spreadsheets.

## A1.2. Linear regression

Least squares linear regression analysis was used to obtain capacity and affinity data from the adsorption data collected in Chapter 3. In this technique, the sum of the residuals (the deviation of the observed value from the predicted value) is minimised. The linear equation of the general form $y = mx + c$ is obtained from the data by determining the minimum sums of squares. The sum of squares is a minimum when:

$$m = \frac{SP}{SS_X} \text{ and } c = \overline{Y} - m\overline{X} \qquad \text{Equation A1.2}$$

where $SP$ is the sum of products ( $= \sum (X - \overline{X})(Y - \overline{Y})$ ) and $SS_X$ is the sum of squares of the $X$ values ( $= \sum (X - \overline{X})^2$ ).

The least squares linear regression can then be defined from the calculated values of $m$ and $c$.

Table A1.1. Error Propagation in common arithmetic calculations.

| Type of calculation | Example | Standard deviation of y |
|---|---|---|
| Addition or subtraction | $y = a + b - c$ | $s_y = \sqrt{s_a^2 + s_b^2 + s_c^2}$ |
| Multiplication or division | $y = \frac{ab}{c}$ | $\frac{s_y}{y} = \sqrt{\left(\frac{s_a}{a}\right)^2 + \left(\frac{s_b}{b}\right)^2 + \left(\frac{s_c}{c}\right)^2}$ |
| Exponentiation | $y = a^x$ | $\frac{s_y}{y} = x\frac{s_a}{a}$ |
| Logarithm | $y = \log_{10} a$ | $s_y = 0.434\frac{s_a}{a}$ |
| Antilogarithm | $y = 10^a$ | $\frac{s_y}{y} = 2.303 s_a$ |
| Natural exponentiation | $y = e^x$ | $s_y = e^x s_x$ |
| anticosine | $y = a\cos(x)$ | $s_y = \frac{s_x}{\sqrt{1 - x^2}}$ |

The standard deviation of a population is obtained from:

$$\sqrt{\sum(x-\bar{x})^2/(n-1)} \qquad \text{Equation A1.3}$$

where $x$ is the value of an individual reading, $\bar{x}$ is the sample mean and $n$ is the number of reading for that sample.

For a linear regression, the value of the standard deviations of the residuals, slope and intercept are calculated as follows:

Residuals:

$$s_y = \sqrt{\frac{\sum(y_i-\bar{y})^2 - m^2\sum(x_i-\bar{x})^2}{N-2}} \qquad \text{Equation A1.4}$$

Intercept:

$$s_c = s_y\sqrt{\frac{1}{N-\frac{(\sum x_i)^2}{\sum x_i^2}}} \qquad \text{Equation A1.5}$$

Slope:

$$s_m = \frac{s_y}{\sqrt{\sum(x_i-\bar{x})^2}} \qquad \text{Equation A1.6}$$

*A1.2.1. Autocorrelation*

The test used to detect autocorrelation is the Durbin-Watson test (Durbin & Watson, 1950). The residuals from a regression analysis are analysed to test whether they exhibit a trend. The $d$ statistic is defined with reference to the residuals of the points about the least squares linear regression line:

$$d = \frac{\sum_{i=2}^{n}(z_i - z_{i-1})^2}{\sum_{i=1}^{n} z_i^2} \qquad \text{Equation A1.7}$$

where $z_i$ is the residual of the $i$th of $n$ points .

Upper and lower boundaries $d_L$ and $d_U$ are defined such that where $d_L < d < d_U$, no autocorrelation is suggested. The upper and lower boundaries are dependent on the number of regression variables ($k = 2$ for straight line regression) and the number of

samples ($n$ = 15 for the adsorption tests detailed in Chapter 3). These are tabulated in Durbin & Watson (1971).

### A1.3. Comparisons

If an F-test on all samples rejects the null hypothesis $H_0$; $\mu_1 = \mu_2 = \ldots = \mu_i$, then comparisons may be used to determine inter-sample differences.

The estimate of the pooled standard deviation of the $i$ samples in the $j$ groups under consideration ($s_p$) for comparison:

$$s_p = \sqrt{\left[\sum_i \sum_j (x_{ij} - \bar{x}_i)^2\right] \Big/ \left[\sum_i (n_i - 1)\right]} \qquad \text{Equation A1.8}$$

The method adapted for the determination of pairwise comparisons is that developed by Fisher (1956). This was developed for intercomparison of three or more groups with normal distribution about the mean. The method uses a family error rate, wherein the confidence bounds for each pair are determined with reference to the errors in all experiments under consideration. This method can be applied to the data under discussion because the data are normally distributed about the predicted line (Anderson-Darling test on residuals, $P > 0.1$) and the samples sizes are the same in all groups. Recent techniques developed to determine exact confidence bounds, and hence enable intercomparisons, require identical design matrices (e.g. Spurrier, 1999). Identical design matrices are not possible using the adsorption techniques detailed in Chapter 3, because for each point on the isotherm the mantissa and ordinate are interdependent and are both functions of the initial concentration, hence the matrices are necessarily different in all experiments.

However, the determination of confidence bounds between three or more regression lines is an ongoing area of research within statistics, and the further development of these techniques is beyond the scope of this work.

For Fisher's comparison, confidence limit, $F$, is determined from:

$$F = s_{pj} t_{\alpha,n-2} \sqrt{\frac{2}{n_i + n_j - 2}} \qquad \text{Equation A1.9}$$

where $t_{\alpha,n-2}$ is the critical $t$ interval at a significance level $\alpha$ for $n-2$ observations, $s_p$ is the pooled standard deviation and $n_i$ and $n_j$ are the number of observations in each pair under consideration.

For each pairwise comparison the pairs are considered unequal if the confidence limits do not include zero within their range.

*A1.3.1. Comparisons of linear regression data*

For g groups of linear regression data, where $y_g = m_g x_g + c_g$, the regression equation for the $m$th group may be expressed as:

$M_{y.x} = A_m + B_m x \qquad m = 1,2,\ldots,g.$

Three questions may be asked by the statistics:

Are the slopes equal? $M_{y.x} = A_m + Bx$

Are the intercepts equal? $M_{y.x} = A + B_m x$

Are the lines the same? $M_{y.x} = A + Bx$

For the adsorption isotherm data (Chapter 3), the first two translate into questions about the equivalence of the capacity and affinity of the materials for the drug. Equal slopes and intercept for the two lines indicate equivalent materials fort he adsorption of the drug.

Multiple comparisons for linear regressions usually assume either identical design matrices (Spurrier, 1999) or that the comparisons are to be made with respect to an unknown mean (Miller, 1982). These were not suitable for the work conducted here, since the design matrices for the adsorption studies cannot be made to be identical and a mean value has no meaning for this study.

For the adsorption isotherm data, standard deviations were obtained *via* least squares linear regression analysis using SigmaPlot 2001 (SPSS Inc., Chicago, USA). The sum of the squares of each sample was calculated from:

$$ss_i = \sqrt{s_i^2 \cdot (n-1)} \qquad \text{Equation A1.10}$$

where $ss_i$ is the sum of squares, $s_i$ is the standard deviation of the sample and $n_i$ is the number of observations in the sample. The pooled standard deviation for $j$ samples each of $i$ observations is calculated from:

$$s_{pj} = \sqrt{\frac{\left(\sum_j ss_i\right)^2}{\sum_j n_i - 1}}$$ Equation A1.11

The Fisher critical difference is:

$$F = s_{pj} t_{\alpha,n-2} \sqrt{\frac{2}{n_i + n_j - 2}}$$ Equation A1.12

where $t_{\alpha,n-2}$ is the critical $t$ interval at a significance for $n-2$ observations.

An Excel spreadsheet was used to calculate the pooled standard deviation of the whole population from the standard deviations calculated by SigmaPlot. The six family groupings (Table 2.1) and each of the 351 ($= {}_{27}C^2$) pairs of affinity and capacity data considered in the adsorption experiments in Chapter 3.

By analogy with the pooled standard deviation for a population sample (Equation A1.8) each with $i$ samples may be expressed by:

$$s_{pf} = \sqrt{\frac{ss^2}{\sum_j n_i - 1}}$$ Equation A1.13

The Fisher critical difference is calculated as in Equation A1.9. The simplicity of the calculation of the critical differences between pair and the validity of the Fisher test are both improved if the data sets are equal.

### A1.4. Test for outliers

The test for a single outlier used is that developed by Grubbs (1969). This method relies on the calculation of the standard deviation of the population, which gives information about the spread of the data about the mean for a normally distributed population. The risk that an observation is not an outlier is a function of the position of the observation with respect to the normal distribution curve and the number of observations in the data set. Tabulated criteria at 5% and 1% levels are referenced against calculated risk factors determined from the test data. If the specified criterion is exceeded then the datum under consideration may be an outlier. The statistic calculated is dependent on the number of observations. The Grubbs statistic is calculated by:

$$G = \frac{|\bar{x} - x_1|}{s(x)}$$ Equation A1.14

where $x_1$ is the result under investigation and $s(x)$ is the standard deviation of the whole data set. If the Grubbs statistic exceeds the tabulated value for the number of observations, then the measured observation may be rejected as an outlier to the stated degree of confidence.

## References


Acemioglu, B., Alma, M.H., 2001. Equilibrium studies on adsorption of Cu(II) from aqueous solution onto cellulose. J. Colloid Interf. Sci. 243, 81-84.

Adolfsson, Å., Gustafsson, C., Nyström, C., 1999. Use of tablet tensile strength adjusted for surface area and mean interparticle distance to evaluate dominating bonding mechanisms. Drug Dev. Ind. Pharm. 25, 753-764.

Ahfat, N.M., Buckton, G., Burrows, R., Ticehurst, M.D., 1997. Predicting mixing performance using surface energy measurements. Int. J. Pharm. 156, 89-95.

Akaho, E., Fukumori, Y., 2001. Studies on adsorption characteristics and mechanism of adsorption of chlorhexidine mainly by carbon black. J. Pharm. Sci. 90, 1288-1297.

Alexander, R., Clements, J.A., Guest, R., Hailey, P., Leiper, K., Moffat, A.C., Pugh, K., 1999. New Technologies Forum spotlights Raman spectroscopy. Eur. Pharm. Rev. 1999, 6, 41-46.

Al-Nimry, S.S., Assaf, S.M., Jalal, I.M., Najib, N.M., 1997. Adsorption of ketotifen onto some pharmaceutical excipients. Int. J. Pharm. 149, 115-121.

Ardizzone, S., Dioguardi, F.S., Mussini, P.R., Mussini, T., Rondinini, S., Vercelli, B., Vertova, A., 1999. Batch effects, water content and aqueous/organic solvent reactivity of microcrystalline cellulose samples. Int. J. Biol. Macromolecules 26, 269-277.

Ardizzone, S., Dioguardi, F.S., Quagliotto, P., Vercelli, B., Viscardi, G., 2001. Microcrystalline cellulose suspensions: effects on the surface tension at the air-water boundary. Colloids Surfaces A: Physicochem. Engin. Aspects 176, 239-244.

Atalla, R.H., van der Hart, D.L., 1984. Native cellulose: A composite of two distinct crystalline forms. Science 233, 283-285.

Atalla, R.H., van der Hart, D.L., 1999. The role of solid state $^{13}C$ NMR spectroscopy in studies of the nature of native celluloses. Solid State Nuclear Magnetic Resonance 15, 1-19.

Baehr, M., Fuhrer, C., Puls, J., 1991. Molecular weight distribution, hemicellulose content and batch conformity of pharmaceutical cellulose powders. Eur. J. Pharm Biopharm. 37, 136-141.

Barra, J., Lescure, F., Falson-Rieg, F., Doelker, E., 1998. Can the organization of a binary mix be predicted from the surface energy, cohesion parameter and particle size of its components? Pharm. Res. 15, 1727-1736.

Battista, O.A., 1950. Hydrolysis and crystallization of cellulose. Ind. Eng. Chem. 42, 502-507.

Battista, O.A., Hill, D., Smith, P.A., 1961. Level-off D.P. cellulose products. US Patent 2 978 446.

Battista, O.A., Hill, D., Smith, P.A., 1966. Formed products of cellulose crystallite aggregates. US Patent 3 278 519.

Belgacem, M.N., Czeremuszkin, G., Sapieha, S., 1995. Surface characterisation of cellulose fibres by XPS and inverse gas chromatography. Cellulose 2, 145-157.

Blackwell, J., Vasko, P.D., Koenig, J.L., 1970. Infrared and Raman spectra of the cellulose from cell wall of valonia ventricosa. J. App. Phys. 41, 4375-4379.

Bodig, J., Jayne, B.A., 1993. Mechanics of Wood and Wood Composite. Krieger Publishing, Florida. 712pp.

Brunauer, S., Emmett, P.H., Teller, E., 1938. Adsorption of gasses in multimolecular layers. J. Am. Chem. Soc. 60, 309-319.

Buckton, G., 1992. The estimation and application of surface-energy data for powdered systems. Drug Dev. Ind. Pharm. 18, 1149-1167.

Buckton, G., 1993. Assessment of the wettability of pharmaceutical powders. In: Contact Angle, Wettability and Adhesion Ed: K.L. Mittal 437-451.

Buckton, G., Newton, J.M. 1986. Assessment of the wettability of powders by the use of compressed powder discs. Powder Technol. 46, 201-208.

Buckton, G., Dove, J.W., Davies, P., 1999a. Isothermal microcalorimetry and inverse gas chromatography to study small changes in powder surface properties. Int. J. Pharm. 193, 13-19.

Buckton, G., Yonemochi, E., Yoon, W.L., Moffat, A.C., 1999b. Water sorption and near IR spectroscopy to study the differences between microcrystalline cellulose and silicified microcrystalline cellulose before and after wet granulation. Int. J. Pharm. 181, 41-47.

Burkhanova, N.D., Yugai, S.M., Khalikov, S.S., Turganov, M.M., Muratova, S.A., Nikonovich, G.V., Aripov, K.N., 1997. Interaction of drugs with microcrystalline cellulose at the molecular and supermolecular levels. Chem. Nat. Compounds 33, 340-346.

Carr, R.L., 1965. Evaluating flow properties of solids. Chem. Eng. 1965, 163-168.

Celik, E., 1996. The past, present and future of tabletting technology. Drug Dev. Ind. Pharm. 22, 1-10.

Clarke, M.J., Potter, U.J., Gilpin, C., Tobyn, M.J., Staniforth, J.N., 1998. Imaging of hygroscopic ultrafine pharmaceutical powders using low temperature and environmental scanning electron microscopy. Pharm. Pharmacol. Commun. 4, 419-425.

Crowley, P.J., 1999. Excipients as stabilizers. Pharm. Sci. Technol. Today 2, 237-243.

Czeremuszkin, G., Mukhopadhyay, P., Sapieha, S., 1997. Elution behavior of chemically different probes on the evaluation surface properties cellulose by inverse gas chromatography. J. Colloid Interface Sci. 194, 127-137.

Davies, J.L., 1999. PhD Thesis, Electrorheological fluids as smart medicines with potential in controllable drug delivery, University of Bath.

de Meijer, M., Haemers, S., Cobben, W., Militz, H. 2000. Surface energy determinations of wood: Comparison of methods and wood species. Langmuir 16, 9352-9359.

Desai, T.R., Li, D., Finlay, W.H., Wong, J.P., 2001. Determination of surface free energy of interactive dry powder liposome formulations using capillary penetration technique. Colloids Surfaces B: Biointerfaces 22, 107-113.

Dinwoodie, J.M., 2000. Timber: its nature and behaviour. Van Nostrand Reinhold Co. Ltd., London. 256pp.

Dittgen, M., Fricke, S., Gerecke, H., 1993. Microcrystalline cellulose in direct tabletting. Manuf. Chem. 64, 17-21.

Doelker E., 1993. Comparative compaction properties of various microcrystalline cellulose types and generic products. Drug Dev. Ind. Pharm. 19, 2399-2471.

Doelker, E., Mordier, D., Iten, H., Humbert-Droz, P., 1987. Comparative tableting properties of sixteen microcrystalline celluloses. Drug Dev. Ind. Pharm. 13, 1847-1875.

doRego, A.M., Pendo Pereira, L., Reis, M.J., Oliveira, A.S., Vieira Ferreira, L.F., 1997. X-ray photoelectron, UV-vis adsorption and luminescence spectrophotometric studies of 2,2'-cyanines adsorbed onto microcrystalline cellulose. Langmuir 13, 6787-6794.

Dourado, F., Gama, F.M., Chibowski, E., Mota, M., 1998. Characterization of cellulose free energy. J. Adhesion Sci. Technol. 12, 1081-1090.

Durbin, J., Watson, G.S., 1950. Testing for serial correlation in least squares regression I. Biometrika 37, 409-428.

Durbin, J., Watson, G.S., 1971. Testing for serial correlation in least squares regression III. Biometrika 58, 1-19.

Edelson, M.R., Hermans, J., 1963. Flow of gels of cellulose microcrystals. II. Effect of added electrolyte. J. Polymer Sci. C 145-152.

Edge, S., Potter, U.J., Steele, D.F., Tobyn, M.J., Chen, A., Staniforth, J.N., 1999. The location of silicon dioxide in silicified microcrystalline cellulose. Pharm. Pharmacol. Commun. 5, 371-376.

Edge, S., Steele, D.F., Chen, A., Tobyn, M.J., Staniforth, J.N., 2000. The mechanical properties of compacts of microcrystalline cellulose and silicified microcrystalline cellulose. Int. J. Pharm. 200, 67-72.

Edge, S., Steele, D.F., Tobyn, M.J., Staniforth, J.N., Chen, A., 2001. Directional bonding in compacted microcrystalline cellulose. Drug Dev. Ind. Pharm. 27, 613-621.

Eichhorn, S.J., Huges, M., Snell, R., Mott, L., 2000. Strain induced shifts in the Raman spectra of natural cellulose fibers. J. Mat. Sci. Lett. 19, 721-723.

Ek, R., Alderborn, G., Nyström, C., 1994. Particle analysis of microcrystalline cellulose: Differentiation between individual particles and their agglomerates. Int. J. Pharm. 111, 43-50.

Ek, R., Wormald, P., Östelius, J., Iversen, T., Nyström, C., 1995. Crystallinity index of microcrystalline cellulose particles compressed into tablets. Int. J. Pharm. 125, 257-264

El-Samaligy, M.S., El-Mahrouk, G.M., El-Kirsh, T.A., 1986. Adsorption - desorption effect of microcrystalline cellulose on ampicillin and amoxycillin. Int. J. Pharm. 31, 137-144.

Fell, J.T, Newton, J.M., 1972. Determination of tablet strength by diametrical compression test. J. Pharm. Sci. 59, 688-691.

Fisher, R.A., 1956. Statistical Methods and Scientific Inferences. Oliver & Boyd, Edinburgh.

Fowkes, F.M., 1982. Characterization of solid-surfaces by wet chemical techniques. ACS Symposium Series 199, 69-88.

Franz, R.M., Peck, G.E., 1982. In vitro adsorption – desorption of fluphenazine dihydrochloride and promethazine hydrochloride by microcrystalline cellulose. J. Pharm. Sci. 71, 1193-1199.

Garcia-Arieta, A., Torrado-Santiago S., Goya, L., Torrado, J.J., 2001. Spray-dried powders as nasal absorption enhancers of cyanocobalamin. Biol. Pharm. Bull. 24, 1411-1416.

Garnier, G., Glasser, W.G., 1994. Measurement of the surface free energy of amorphous cellulose by alkane adsorption: A critical evaluation of inverse gas chromatography. J. Adhesion 46, 165-180.

Giles, C.H., MacEwan, T.H., Nakhwa, S.N., Smith, D., 1960. Studies in adsorption. Part XI. A system of classification of solution adsorption isotherms, and its use in diagnosis of adsorption mechanisms and in measurement of specific surface areas of solids. J. Chem. Soc. 3973-3993.

Gindl, M., Sinn, G., Gindl, W., Reiterer, A., Tschegg, S., 2001. A comparison of different methods to calculate the surface free energy of wood using contact angle measurements. Colloids Surfaces A: Physicochem. Engineering Aspects 181, 279-287.

Glombitza, B.W., Oelkrug, D., Schmidt, P.C., 1994. Surface acidity of solid pharmaceutical excipients I. Determination of the surface acidity. Eur. J. Pharm. Biopharm. 40, 289-293.

Good, R.J., 1992. Contact angle, wetting and adhesion: a critical review. J. Adhesion Sci. Technol. 6, 1269-1302.

Grubbs, F.E., 1969. Procedures for detecting outlying observations in samples. Technometrics 11, 1-21.

Guo, M., Muller, F.X., Augsburger, L.L., 2002. Evaluation of the plug formation process of silicified microcrystalline cellulose. Int. J. Pharm. 233, 99-109.

Gutierrez, M.C., Rubio, J., Rubio, F., Oteo, J.L., 1999. Inverse gas chromatography: a new approach to the estimation of specific interactions. J. Chrom. 845, 53-66.

Gutmann, V., 1978. The donor-acceptor approach to molecular interactions. Plenum Press, NY. 17-33.

Habib, Y.S., Abramowitz, R., Jerzewski, R.L., Jain, N.B., Agharkar, S.N., 1999. Is silicified wet-granulated microcrystalline cellulose better than original wet-granulated microcrystalline cellulose? Pharm. Dev. Tech. 4, 431-437.

Hancock, B.C., York, P., Rowe, R.C., 1997. The use of solubility parameters in pharmaceutical dosage form design. Int. J. Pharm. 148, 1-21.

Hayward, E.R., Greenough, 1960. The surface energy of solid nickel. J. Inst. Metals 88, 217-245.

Heiner, A.P., Teleman, O., 1997. Interface between monolithic crystalline cellulose and water: breakdown of the odd/even duplicity. Langmuir 13, 511-518.

Heiner, A.P., Kuutti, L., Teleman, O., 1998. Comparison of the interface between water and four surfaces of native crystalline cellulose by molecular dynamics simulations. Carbohydrate Res. 306, 205-220.

Hesse, G., Hagel, R., 1976. Die chromatographische racemattrenung. Liebigs Ann. Chem. 1976, 996-1008.

Horii, F., Hirai, A., Kitamaru, R., 1984. CP MAS C-13 NMR-study of spin relaxation phenomena of cellulose containing crystalline and noncrystalline components. J. Carbohyd. Chem. 3, 641-662.

Huu-Phuoc, N., Nam-Tran, H., Buchmann, M., Kesselring, U.W., 1987. Experimentally optimized determination of the partial and total cohesion parameters of an insoluble polymer, microcrystalline cellulose, by gas-solid chromatography. Int. J. Pharm. 34, 217-223.

Huynh, T.K.X., Ossicini, L., Polcaro, C., 1994. Chiral separations on cellulose in electrophoresis. J. Chrom. A 663, 264-266.

Hwang, R.-C., Peck, G.R., 2001. A systematic evaluation of the compression and tablet characteristics of various types of microcrystalline cellulose. Pharm. Tech. 3, 112-122.

Iida, K., Aoki, K., Danjo, A., Chen, C.Y., Horisawa, E., 1997. A comparative evaluation of the mechanical properties of various celluloses. Chem. Pharm. Bull. 45, 217-220.

Isogai, A., Atalla, R.H., 1998. Dissolution of cellulose in aqueous NaOH solutions. Cellulose 5, 309-319.

Jacob, P.N., Berg, J.C., 1994. Acid-base surface energy characterization of microcrystalline cellulose and two wood pulp fiber types using inverse gas chromatography. Langmuir 10, 3086-3093.

Johansson, B., Alderborn, G., 2001. The effect of shape and porosity on the compression behaviour and tablet forming ability of granular materials formed from microcrystalline cellulose. Eur. J. Pharm. Biopharm. 52, 347-357.

Jover, I., Podczeck, F., Newton, M., 1996. Evaluation, by a statically designed experiment, of an experimental grade of microcrystalline cellulose, Avicel 955, as a technology to aid the production of pellets with high drug loading. J. Pharm. Sci. 85, 700-705.

Kalinkova, G.N., 1999. Studies of beneficial interactions between active medicaments and excipients in pharmaceutical formulations. Int. J. Pharm. 187, 1-15.

Kaye, B.H., 1997. Characterizing the flowability of a powder using the concepts of fractal geometry and chaos theory. Part. Part. Sys. Characterization 14, 53-66.

Khan, H., Fell, J.T., MacLeod, G.S., 2001. The influence of additives on the spreading coefficient and adhesion of a film coating formulation to a model tablet surface. Int. J. Pharm. 227, 113-119.

Kibbe, A.H., 2000. Handbook of Pharmaceutical Excipients. American Pharmaceutical Association.

Konar, N., Kim, C., 1997. Water soluble polycations as oral drug carriers (tablets). J. Pharm. Sci. 86, 1339-1344.

Kotelnikova, N.E., Petropavlovsky, G.A., 1991. Preparation of microcrystalline cellulose from cellulose of deciduous wood species and its properties. *In* Cellulose Sources and Explotation, Kennedy, J.F., Phillips, G.O., Williams, P.A. Eds., Ellis Horwood, London. 21-31.

Krässig, H.A., 1993. Cellulose. Structure, Accessibility and Reactivity. Gordon and Breach Science Publishers, Amsterdam. 360pp.

Kucera, P., Moros, S.A., Mlodozeniec, A.R., 1981. Differential frontal analysis of carboxylic acids. J. Chrom. 210, 373-388.

Kumar, V., Kothari, S.H., 1999. Effect of compressional force on the crystallinity of directly compressible cellulose excipients. Int. J. Pharm. 177, 173-182.

Kumar, V., Kothari, S.H., Banker, G.S., 2001. Compression, compaction, and disintegration properties of low crystallinity celluloses produced using different agitation rates during their regeneration from phosphoric acid. AAPS PharmSciTech. 2, article 7.

Kumar, V., Reus-Medina, M.D.L., Yang, D., 2002. Preparation, characterization, and tabletting properties of a new cellulose-based pharmaceutical aid. Int. J. Pharm. 235, 129-140.

Ladisch, C.M., Yang, Y., Velayudhan, A., Ladisch, M.R., 1992. A new approach to the study of textile properties with liquid chromatography. Comparison of void volume and surface area of cotton and ramie using a rolled fabric stationary phase. Textile Res. J. 62, 361-369.

Landín, M., Martínez-Pacheco, R., Gómez-Amoza, J.L., Souto, C., Concheiro, A., Rowe, R.C., 1993a. Effect of country of origin on the properties microcrystalline cellulose. Int. J. Pharm. 91, 123-131.

Landín, M., Martínez-Pacheco, R., Gómez-Amoza, J.L., Souto, C., Concheiro, A., Rowe, R.C., 1993b. Effect of batch variation and pulp source on the properties of microcrystalline cellulose. Int. J. Pharm. 91, 133-141.

Landín, M., Martínez-Pacheco, R., Gómez-Amoza, J.L., Souto, C., Concheiro, A., Rowe, R.C., 1993c. Influence of microcrystalline cellulose source and batch variation on the tabletting behaviour and stability of prednisone formulations. Int. J. Pharm. 91, 143-149.

Langmuir, I., 1918. Adsorption of gasses on glass, mica and platinum. J. Am. Chem. Soc. 40, 1361-1403.

Larsson, P.T., Hult, E.L., Wickholm, K., Pettersson, E., Iversen, T., 1999. CP/MAS C-13-NMR spectroscopy applied to structure and interaction studies on cellulose I. Solid State Nucl. Mag. 15, 31-40.

Lawn, B., 1993. Fracture of Brittle Solids, Cambridge University Press. 378pp.

León y León, C.A., 1998. New perspectives in mercury porosimetry. Adv. Colloid Interface Sci. 76-77, 341-372.

Li, D., Neumann, A.W., 1992. Contact angles on hydrophobic solid surfaces and their interpretation. J. Colloids Interface Sci. 148, 190-200.

Lindner, K.R., Mannschreck, A., 1980. Separation of enantiomers by high-performance liquid chromatography on triacetylcellulose. J. Chrom. 193, 308-310.

Luaungtana-Anan, M., Fell, J.T., 1987. Surface free-energy determinations on powders.
Powder Technol. 215-218.

Maincent, P., 1999. L'interchangeabilité des excipients en formulation et ses consequences éventuelles. Thérapie 54, 5-10.

Mannhold, R., Dross, K.P., Rekker, R.F., 1990. Drug lipophilicity in QSAR practice. 1. A comparison of experimental with calculative approaches. Quant. Structure-Activity Relationships 9, 21-28.

Maréchal, Y., Chanzy, H., 2000. The hydrogen bond network in Iβ cellulose as observed by infrared spectroscopy. J. Mol. Struct. 523, 183-196.

Marshall, K., Sixsmith, D., Stanley-Wood, N.G., 1972. Surface geometry of some microcrystalline celluloses. J. Pharm. Pharmacol. Supp. 24 138P.

Michell, A.J., Higgins, H.G., 1999. The absence of free hydroxyl groups in cellulose. Cellulose 6, 89-91.

Monkhouse, D.C., 1984. Stability of preformulation and formulation of solid pharmaceuticals. Drug Dev. Ind. Pharm. 10, 1373-1412.

Morita, Z., Tanaka, T., Motomura, H., 1985. Diffusion/adsorption model of cellulose dyeing II. Ordinary cellulose-direct dye system. J. App. Polym. Sci. 30, 3697-3705.

Nagai, T., Nishimoto, Y., Nambu, N., Suzuki, Y., Sekine, K., 1984. Powder dosage form of insulin for nasal administration. J. Control. Release 1, 15-22.

Nakai, Y., Fukuoka, E., Nakajima, S., Hasegawa, J., 1977. Crystallinity and physical characteristics of microcrystalline cellulose. Chem. Pharm. Bull. 25, 96-101.

Nelson, M.L., O'Connor, R.T., 1964. Relation of certain infrared bands to cellulose crystallinity and crystal lattice type. Part II. A new infrared ratio for estimation of crystallinity in cellulose I and II. J. Appl. Polym. Sci. 8, 1325-1341.

Newman, R.H., 1987. Effect of finite preparation-pulse power on carbon-13 cross-polarization NMR of heterogeneous samples. J. Magn. Reson. 72, 337-340.

Okada, S., Nakahara, H., Isaka, H., 1987. Adsorption of drugs on microcrystalline cellulose suspended in aqueous solutions. Chem. Pharm. Bull. 35, 761-768.

Padmadisastra, Y., Gonda, I., 1989. Preliminary studies of the development of a direct compression cellulose excipient from bagasse. J. Pharm. Sci. 78, 508-514.

Papirer, E., Brendle, E., Balard, H., Vergelati, C., 2000. Inverse gas chromatography investigation of the surface properties cellulose. J. Adhesion Sci. Tech. 14, 321-337.

Parikh, D.M., 1997. Handbook of Pharmaceutical Granulation Technology, Drugs and the Pharmaceutical Sciences Volume 81, 512pp.

Parker, M.D., Rowe, R.C., 1991. Source variation in the wet massing (granulation) of some microcrystalline cellulose. Powder Technol. 65, 273-281.

Pepin, X., Blanchon, S., Couarraze, G., 1999. Powder dynamic contact angle data in the pharmaceutical industry. Pharm. Sci. Tech. Today 2, 111-118.

Picker, K.M., Hoag, S.W., 2002. Characterization of the thermal properties of microcrystalline cellulose by modulated temperature differential scanning calorimetry. Drug Dev. Ind. Pharm. 91, 342-349.

Podczeck, F., Révész, P., 1993. Evaluation of the properties of microcrystalline and microfine cellulose powders. Int. J. Pharm. 91, 183-193.

Podczeck, F., Miah, Y., 1995. The influence of particle size and shape on the angle of internal friction and the flow factor of unlubricated and lubricated powders. Int. J. Pharm. 144, 187-194.

Qtaitat, M.A., Zughul, M.B., Badwan, A.A., 1988. Bromhexine hydrochloride adsorption by some solid excipients used in the formulation of tablets. Drug Dev. Ind. Pharm. 14, 415-429.

Raman, C.V., 1928. A change in the wave-length in light scattering. Nature 121, 619.

Raymond, S., Kvick, A., Chanzy, H., 1995. The structure of cellulose II - a revisit. Macromol. 28, 8422-8425.

Read, N.D., Jeffree, C.E., 1991. Low-temperature scanning electron microscopy in biology. J. Microscopy 161, 59-72.

Richardson, N.E., 1973. PhD Thesis, The interaction of some benzoic acid derivatives with polyamides, University of Bath.

Riddle, F.L., Fowkes, F.M., 1990. Spectral shifts in acid-base chemistry. 1 Van der Waals contributions to acceptor numbers. J. Am. Chem. Soc. 112, 3259-3264.

Ritger, P.L., Peppas, N.A., 1987. Transport of penetrants in the macromolecular structure of coals. 4. Models for analysis of dynamic penetrant transport. Fuel 66, 815-826.

Roberts, R.J., Rowe, R.C., 1993. The solubility parameter and fractional polarity of microcrystalline cellulose as determined by mechanical measurement. Int. J. Pharm. 99, 157-164.

Roberts, R.J., Rowe, R.C., York, P., 1991. The relationship between Young's modulus of elasticity of organic solids and their molecular structure. Powder Tech. 65, 139-146.

Rowe, R.C., 1977. The adhesion of film coatings to tablet surfaces – the effect of some direct compression excipients and lubricants. J. Pharm. Pharmacol. 29, 723-726.

Rowe, R.C., 1988. Interactions of lubricants with microcrystalline cellulose and anhydrous lactose – A solubility parameter approach. Int. J. Pharm. 41, 223-226.

Rowe, R.C., 1992. Interactions in powders and granules – a reappraisal. Int. J. Pharm. 79, 257-261.

Rowe, R.C., McKillop, A.G., Bray, D., 1994. The effect of batch and source variation on the crystallinity of microcrystalline cellulose. Int. J. Pharm. 101, 169-172.

Rowe, R.C., Parker, M.D., McKillop, A.G., 1993. The effect of particle size on the heat of immersion of microcrystalline cellulose. Int. J. Pharm. 91, 247-250.

Rulison, C., 1996. Wettability studies for porous solids including powders and fibrous materials. Technical Note #302, Krüss GmbH.

Sarko, A., 1976. Crystalline polymorphs of cellulose: prediction of structure and properties. Appl. Polymer Symp. 28, 729-742.

Savin, P.P., 2001. Cell-wall masses of conifer tree rings. Abstracts of the International Conference Tree Rings and People, Davos, Switzerland. Abstract 27.

Schultz, J., Laville, L, Martin, C., 1987. The role of the interface in carbon-fiber epoxy composites. J. Adhesion 23, 45-60.

Senderoff, R.I., Mahjour, M., Radebaugh, G.W., 1992. Characterization of adsorption behavior by solid dosage form excipients in formulation development. Int. J. Pharm. 83, 65-72.

Sharma, P.K., Rao, K.H., Forssberg, K.S.E., 2001. Surface chemical characterisation of Paenibacillus polymyxa before and after adaptation to sulfide minerals. Int. J. Miner. Process. 62, 3-25.

Sherwood, B.E., Becker, J. W., 1998. A new class of high functionality excipients: silicified microcrystalline cellulose. Pharm. Tech. 22, 78-88.

Sherwood, B.E., Hunter, E.A., Staniforth, J.N., 1996. Pharmaceutical excipient having improved compressibility. US Patent 5,585,115.

Smith, A.L., 1979. Applied Infrared Spectroscopy. Wiley International, London. 322pp.

Soltys, J., Lisowski, Z., Knapczyk, J., 1984. X-ray diffraction study of the crystallinity index and the structure of microcrystalline cellulose. Acta Pharm. Technol. 30, 174-180.

Staniforth, J.N., Chatrath, M., 1996. Towards a new class of high functionality tablet binders I: quasi-hornification of microcrystalline cellulose and loss of functionality. AAPS Annual Meeting, 1996.

Sterk, H., Sattler, W., Janosi, A., Paul, D., Esterbauer, H., 1987. Eisatz der Festkörper $^{13}$C-NMR-Spektroskopie für die Bestimmung der Kristallinität in Cellulosen. Das Papier 41, 664-668.

Suzuki, T., Nakagami, H., 1999. Effect of crystallinity of microcrystalline cellulose on the compactability and dissolution of tablets. Eur. J. Pharm. Biopharm. 47, 225-230.

Swaminathan, V., Kildsig, D.O., 2002. Polydisperse powder mixtures: Effect of particle size and shape on mixture stability. Drug Dev. Ind. Pharm. 28, 41-48.

Teeäär, R., Serimaa, R., Paakkari, T., 1987. Crystallinity of cellulose, as determined by CP/MAS NMR and XRD methods. Polymer Bull. 17, 231-237.

Ticehurst, M.C., Rowe, R.C., York, P., 1994. Determination of the surface properties of two batches of salbutamol sulphate by inverse gas chromatography. Int. J. Pharm. 111, 241-249.

Timofei, S., Kurunizi, L., Schmidt, W., Simon, Z., 1996. Lipophilicity in dye-cellulose fibre binding. Dyes Pigments 32, 25-42.

Tobyn, M.J., McCarthy, G.P., Staniforth J.N., Edge S., 1998. Physicochemical comparison between microcrystalline cellulose and silicified microcrystalline cellulose. Int. J. Pharm. 169, 183-194.

Tobyn, M.J., Edge, S., Steele, D.F., Staniforth, J.N., Chen, A., 2002. Physicochemical and mechanical evaluation of a novel high density grade of microcrystalline cellulose. *Submitted to* Drug Dev. Ind. Pharm.

Tomer, G., Patel, H., Podczeck, F., Newton, J.M., 2001. Measuring the water retention capacities (MRC) of different microcrystalline cellulose grades. Eur. J. Pharm. Sci. 12, 321-325.

Tshabalala, M.A., 1997. Determination of the acid-base characteristics of lignocellulose surface by inverse gas chromatography. J. App. Polymer Sci. 65, 1013-1020.

Uesu, N.Y., Pineda, E.A.G., Hechenleitner, A.A.W., 2000. Microcrystalline cellulose from soybean husk: effects of solvent treatment on its properties as acetylsalicylic acid carrier. Int. J. Pharm. 206, 85-96.

Vachon, M.G., Chulia, D., 1999. The use of energy indices in estimating powder compaction functionality of mixtures in pharmaceutical tableting. Int. J. Pharm. 177, 183-200.

van der Hart, D.L., Atalla, R.H., 1984. Studies of microstructure in native celluloses using solid-state $^{13}C$ NMR. Macromolecules 17, 1465-1472.

van Oss, C.J., Giese, R.F., Wu, W., 1997. On the predominant electron-donicity of polar solid surfaces. J. Adhesion 63, 71-88.

Vincent, J.F.V., 1999. From cellulose to cell. J. Experim. Biol. 202, 3263-3268.

Webster, C.E., Drago R.S., Zerner, M.C., 1998. Molecular dimensions for adsorptives. J. Am. Chem. Soc. 120, 5509-5519.

Wei, S., Kumar, V., Banker, G.S., 1996. Phosphoric acid mediated decrystallization and depolymerization of cellulose. Preparation of low crystallinity cellulose – a new pharmaceutical excipient. Int. J. Pharm. 142, 175-181.

Weise, U., 1998. Hornification - mechanisms and terminology. Paperi JA PUU - Paper and Timber 80, 110-115.

Weise, U., Maloney, T., Paulapuro, H., 1996. Quantification of water in different states interaction with wood pulp fibres. Cellulose 3, 189-202.

Westermarck, S., Juppo, A.M., Kervinen, L., Yliruusi, J., 1998. Pore structure and surface area of mannitol powder, granules and tablets determined with mercury porosimetry and nitrogen adsorption. Eur. J. Pharm. Biopharm. 46, 61-68.

Westermarck, S., Juppo, A.M., Kervinen, L., Yliruusi, J., 1999. Microcrystalline cellulose and its microstructure in pharmaceutical processing. Eur. J. Pharm. Biopharm. 48, 199-206.

Wiley, J.H., Atalla, R.H., 1987. Band assignment in the Raman spectra of celluloses. Carbohydrate Res. 160, 113-129.

Wu, W., Giese, R.F., van Oss, C.J. Change in surface properties of solids caused by grinding. Powder Technol. 89, 129-132.

Wu, J.-S., Ho, H.-O., Sheu, M.-T., 2001. A statistical design to evaluate the influence of manufacturing factors on the material properties and functionalities of microcrystalline cellulose. Eu. J. Pharm. Sci. 12, 417-425.

Yadava, K.P., Tyagi, B.S., Singh, V.N., 1991. Effect of temperature on the removal of lead(II) by adsorption on china clay and wollastonite. J. Chem Tech. Biotech. 51, 47-60.

Zisman, W.A, 1964. Relation of equilibrium contact angle to liquid and solid constitution. *In* Contact Angle, Wettability, and Adhesion; Advances in Chemistry Series 43, F.M. Fowkes (Ed), 1-51.

Zografi, G., Kontny, M.J., Yang, A.Y.S., Brenner, G.S., 1984. Surface area and water vapor sorption of microcrystalline cellulose. Int. J. Pharm. 18, 99-116.

Zografi, G., Kontny, M.J., 1986. The interaction of water with cellulose- and starch-derived pharmaceutical excipients. Pharm. Res. 3, 187-194.

## Publications

Adsorption of an amine drug onto microcrystalline cellulose and silicified microcrystalline cellulose samples
D. F. Steele, S. Edge, M.J. Tobyn, R.C. Moreton, J.N. Staniforth
*In Press*, Drug Development and Industrial Pharmacy

Directional strength in compacts of microcrystalline cellulose
S. Edge, D.F. Steele, M.J. Tobyn, J.N. Staniforth, A. Chen
Drug Development and Industrial Pharmacy (2001) 27, 613-621

The mechanical properties of compacts of microcrystalline cellulose and silicified microcrystalline cellulose
S. Edge, D.F. Steele, A. Cheng, M.J. Tobyn, J.N. Staniforth
International Journal of Pharmacy (2000) 200, 67-72

# ADSORPTION OF AN AMINE DRUG ONTO MICROCRYSTALLINE CELLULOSE AND SILICIFIED MICROCRYSTALLINE CELLULOSE SAMPLES

D. FRASER STEELE[1], STEPHEN EDGE[1], MICHAEL J. TOBYN[1],

R. CHRISTIAN MORETON[2,3], JOHN N. STANIFORTH[1]

[1]Pharmaceutical Technology Research Group, Department of Pharmacy & Pharmacology, University of Bath, Bath, BA2 7AY, UK

[2]Penwest Co., 2981 Route 22, Patterson, NY, 9970-2281, USA.

[3] Present Address: Idenix Pharmaceuticals Inc., 125 Cambridge Park Drive, Cambridge, MA 02140

Keywords: Microcrystalline cellulose, adsorption, amine drugs.

Short title: Amine adsorption on microcrystalline cellulose

Correspondence: D.F. Steele,

Pharmaceutical Technology Research Group,

Department of Pharmacy & Pharmacology,

University of Bath,

Bath,

BA2 7AY, UK.

Tel: +44 (0)1225 826826 ext 4831

Fax: +44 (0)1225 826114

email: d.f.steele@bath.ac.uk

ABSTRACT

The adsorption of a model amine drug (tacrine hydrochloride) from aqueous solution onto twenty--one microcrystalline cellulose (MCC) based samples has been investigated. The MCC source (manufacturer) affected adsorption. The adsorption appeared to be fully reversible. Adsorption was reduced by the use of high--density grade MCC, high--energy milling and silicification. Adsorption of the model drug was not affected by the particle size of the MCC. Significant variations of the adsorption characteristics between batches of certain MCC products were found. The primary mode of adsorption was by ion exchange.

## INTRODUCTION

The adsorption of drugs by excipients during *in vitro* testing is an ongoing concern in formulation science. As a result of its multifunctionality, microcrystalline cellulose (MCC) is very widely used as an excipient in solid dosage forms; however, the adsorption of some drugs is a barrier to its wider use. Within the pharmaceutical industry it has been observed that drugs containing amine functionalities are prone to adsorption onto MCC, with <100% release observed during dissolution tests. Because MCC is not digestible, the observed reduced release indicates that the total *in vivo* availability will be less than the amount of drug in the formulation.

Microcrystalline cellulose was introduced as a pharmaceutical excipient in the US National Formulary in 1966 under the trade name 'Avicel'. Recently, there has been an increase in the number of manufacturers marketing pharmaceutical grade MCC. It has been shown (1--3) that the differences in the source of pulp and the characteristics of the manufacturing processes used result in significant intermanufacturer variations in the observed functionalities and physico-chemical properties (4--7) of the MCCs.

Microcrystalline cellulose is the β--1,4 linked polymer of D--glucopyranose, partially depolymerised to yield a product with a mean degree of polymerisation of between 150 and 250. For pharmaceutical grade MCC products, the most commonly used raw material is high--quality timber pulp, as used in paper manufacture. The pulp feedstock is acid depolymerised, neutralised and the resulting slurry is dried to yield

aggregates of MCC fibrils with a volume diameter mean particle size in the range 40--200μm.

The inter--brand and batch--to--batch variations in drug--excipient interactions (3), drug release rates (8), drug adsorption (9--11), and water--MCC interactions (4, 12, 13) have been investigated by several researchers.

Variations in drug release in prednisone formulations made up with four different MCCs (8) suggested that significant differences can be expected for such formulation depending on the MCC product, and also the MCC batch, used. This was linked to the hydrophobicity of the samples, as indicated by lignin content, with higher lignin content tending to improve release efficiency.

In terms of drug sorption, El Samaligy et al. (9) and Qtaitat et al. (11) found that the volume diameter mean particle size of the MCC samples affected the adsorption of the drugs under investigation. A reduced degree of adsorption was observed for larger particle size grades, which the authors linked to the reduced specific surface area of the materials.

Okada et al. (10) compared the adsorption of four drugs onto a standard grade MCC with that of a high density grade MCC. They found that the standard grade of MCC had a lower adsorption capacity for three promazine derivatives than the high--density grade. The affinity of the promazine derivatives for MCC did not follow any steric trend, nor was there any relationship between drug pKa and adsorption. In contrast,

the adsorption of acrinol, an acridine derivative, was lower for the high--density grade MCC than for the standard grade.

The water--cellulose interaction is of interest for the possible consequences for adsorption from aqueous solution. Water retention values (WRV), an indication of hydrophilicity, have been determined for seven MCCs (12) using a centrifugation technique. Significant differences were observed between the WRV of different manufacturers' products, which may affect the release efficiency (8).

A previous study (13), comparing the adsorption of water onto MCC and silicified MCC (SMCC), found no significant difference in the enthalpy of water vapour sorption. SMCC is a patented MCC derivative, coprocessed with 2% w/w colloidal $SiO_2$ (14) showing improved resistance to loss of compactibility on wet granulation.

It is the purpose of this study to investigate inter--brand variations in the adsorption of a model amine drug and to explore the nature of the drug adsorption onto MCC. In addition, the adsorption of SMCC will be investigated for the first time.

The model drug used in this work is tacrine hydrochloride (tacrine, 9--amino--1,2,3,4--tetrahydroacridine; Figure 1). Tacrine is prescribed as a cholinesterase inhibitor for the alleviation of the symptoms of mild to moderate Alzheimer's type dementia (Cognex, 10 to 40mg dose). A previous study (15) demonstrated that tacrine adsorbs to a significant degree onto MCC. The flat structure and delocalised aromatic electron structure predicts that the molecule is a fast dye for cellulosic materials (16), hence

the significant adsorption observed. Tacrine is readily soluble in water with a pKa of 9.3, therefore at pH values below 7, tacrine will be fully protonated. Protonation occurs on the exocyclic nitrogen.

## MATERIALS AND METHODS

### Materials

Details of the twenty--one MCC products and derivatives used in this study are given in Table 1. They can be divided into six groups, each group having a single common feature, which is used to distinguish between the products. All groupings and descriptions for commercial products are based on the relevant supplier's literature, where available. In order to assess the adsorption of the material as used in general formulation work, samples were not particle size fractionated. The groupings into which the MCCs have been placed can be described thus:

#### 'Standard' grades from different manufacturers

These have a volume diameter mean particle size of approximately 50μm and are marketed as equivalent to Avicel 101 (FMC Inc, USA). A total of six MCCs were investigated, two US brands, two European, one Brazilian and one Japanese.

Batch--to--batch variation

Multiple batches of Avicel PH101, Emcocel 50M and Vivapur 101 were obtained in order to determine whether any observed inter-product variations fall within the range of batch--to-batch variability.

Larger particle size grades

Increased volume diameter mean particle size materials are manufactured by adjustment of the drying conditions. A lower specific surface area is to be expected for larger particle sizes. Three grades, each a commercial product from Penwest Co. (USA) are studied: the 'standard' grade and two large particle grades. According to product literature, the same feedstock as used for the 'standard' grade was used for each of these products, since they are designed to be interchangeable in all respects except for dry flow performance; hence any differences between these products will be due to the final drying conditions.

High density grades

Most standard grade MCCs are manufactured using softwood (evergreen) pulp as the feedstock. High density grades are normally manufactured from hardwood (deciduous) pulps, which have a higher bulk density, reflecting the lower porosity of the source timber (16).

Silicified MCC

The adsorption of SMCCs, patented co--processed MCCs containing 2% w/w colloidal silicon dioxide, were investigated to assess the effect on adsorption of the presence of $SiO_2$ in the particle surface. Standard (50μm volume diameter mean particle size), large particle (90μm) and high density grades were investigated.

Treated samples

Micronised MCC (Emcocel SP15, Penwest Co.) is used to investigate the effect of high--energy milling on the adsorption capacity of MCC. Emcocel 50M heated to 80°C for 16 hours was used to investigate the effect of the type of drying undergone during wet granulation on drug adsorption.

Other chemicals

Tacrine hydrochloride (BP grade, Aldrich, Gillingham, UK) was used without further purification. Water used in these studies was freshly purified by reverse osmosis (Millipore, Watford, UK) with conductivity in the range 650--700μS. Water was de--gassed by helium displacement (minimum 1 hour per litre). Sodium chloride was analytical grade (AR grade, Fisher, Loughborough, UK).

Adsorption of tacrine

Adsorption isotherms were obtained by batchwise thermostatic equilibration (10). A 1000mg sample of MCC was suspended in 40ml solution at each of fifteen drug concentrations in 50ml borosilicate volumetric flasks. This was then equilibrated for two hours at the required temperature in a shaking water bath (Gyrotory®, New Brunswick Scientific, Edison, USA) to ensure thorough mixing, maximum adsorption and thermal equilibrium. The time required for equilibrium adsorption was determined separately by extracting supernatant after equilibration for one half to five hours.

Supernatant was separated by centrifugation (1400*g*, 10 min) and analysed by UV spectrophotometry (Helios α, Unicam, Cambridge, UK) ($\lambda_{max}$ = 239nm, $\varepsilon_{tacrine}$ = 39 900 $mol^{-1}cm^{-1}$) after dilution to between 1 and 5$mgl^{-1}$ (4--20μM). Three controls were analysed: MCC in water, a tacrine solution of an appropriate concentration and water. These determine the UV absorbance of water--soluble extractives, possible thermolytic degradation or adsorption of the drug onto the glassware and levels of contaminants from the glassware, respectively. Replicate analyses (n = 5) of the water--soluble extractives indicated that UV absorbing material was released from all the MCC samples. This material may be the protein--like surface active solute previously described (18). The UV absorption of these extractives was reproducible to ±0.001 absorbance units at 239nm for each MCC, therefore the UV absorption of each diluted equilibrium tacrine solution was adjusted to account for the presence of these extractives. No significant thermolytic degradation or adsorption onto the

experimental apparatus was found. No significant contamination from the glassware was detected.

Tacrine concentration

Fifteen data points over the initial tacrine concentration range of 0.05 to 1.0 mM were collected for isothermal equilibration studies at 25°C.

Data interpretation

The Langmuir (L2, (19)) isotherm for monolayer adsorption was used to interpret the data obtained in the isotherm studies. The linear form of the Langmuir isotherm is given in equation 1, where $C_{eq}$ is the equilibrium concentration, $x$ is the amount of adsorbate adsorbed on $m$ mass of adsorbent, $k_1k_2$ is the affinity constant and $k_2$ is the capacity constant.

$$\frac{C_{eq}}{(x/m)} = \frac{1}{k_1 k_2} + \frac{C_{eq}}{k_2} \qquad \text{Equation 1}$$

A plot of $C_{eq}$ against $C_{eq}/(x/m)$ will yield a straight line if ideal adsorption has occurred. This indicates that monolayer adsorption is occurring in the concentration range under investigation. Adsorption sites are assumed to be energetically homogeneous and adsorption is independent of occupancy of adjacent sites. Residuals analysis showed no discernible trend and a normal distribution (Anderson--Darling test, $p>0.3$ in all cases) for the residuals about the line of best fit.

The adsorption data was also modelled using the Freundlich isotherm, used to interpret data from multi--layer adsorption. Although generally good correlation coefficients were obtained ($r^2 > 0.80$), residuals analysis yielded a quadratic trend, rather than the normal distribution of residuals observed for Langmuir fitting, indicating that this isotherm does not reliably describe the observed adsorption.

Least squares linear regression analyses were completed using Minitab 12 (Minitab Inc. USA) whereby slope, intercept and the standard deviations of the slope and intercept were computed for each linear isotherm. In addition to the raw data obtained from these isotherm plots, the surface area available for adsorption may be estimated from the amount of tacrine adsorbed per unit mass. Surface area values are estimated on the basis that the tacrine molecule has a molecular area of $2nm^2$, similar to that of anthracene ($= 2.05nm^2$) (20), using equation 2, where *sa* is the specific surface area ($m^2kg^{-1}$), $A$ is the area of the molecule ($= 2x10^{-18}\ m^2$), $(x/m)$ is the adsorption capacity in $molkg^{-1}$ and $N_A$ is Avogadro's constant.

$$sa = A.(x/m).N_A \qquad \text{Equation 2}$$

Reversibility of adsorption

The extent of the reversibility of the adsorption of tacrine from aqueous solution was assessed for Emcocel 50M by a re--equilibration technique. A 1000mg sample of MCC was thermostatically equilibrated with 40ml of a $150mgl^{-1}$ solution of tacrine at

25°C. The sample was then centrifuged as above and 20ml of the supernatant was removed for UV spectroscopic analysis to obtain the first equilibrium concentration ($C_{eq1}$). The MCC dispersion was then quantitatively returned to the original volumetric flask by washing with 20ml degassed water. The dispersion was then thermostatically equilibrated a second time and the supernatant extracted after centrifugation for UV spectroscopic analysis. From the previously obtained Langmuir isotherm and the equilibrium concentration after the second equilibration, the initial concentration prior to the second equilibration ($C_{in2}$) could be determined from equation 3, where $C_{eq2}$ is the second equilibrium concentration, $x_2$ is the amount of tacrine adsorbed in the second equilibration and $v$ is the total liquid volume (0.041 in this study).

$$C_{in2} = C_{eq2} + \frac{x_2}{v} \qquad \text{Equation 3}$$

The value of $x_2$ may be determined using the rearranged Langmuir isotherm in equation 4, where $m$ is the mass of MCC used and $k_1k_2$ and $k_2$ are values determined from the Langmuir isotherm (equation 1).

$$x_2 = \frac{C_{eq2}m}{\frac{1}{k_1k_2} + \frac{C_{eq2}}{k_2}} \qquad \text{Equation 4}$$

For the experiment described above, the extent of the reversibility of the adsorption may be determined *via* equation 5, where $f$ is the fraction of tacrine reversibly adsorbed.

$$f = \frac{v}{2x_2}\left(2C_{in2} - C_{eq1}\right) \qquad \text{Equation 5}$$

Ionic strength

In order to determine the effect of the ionic strength of the tacrine solution on adsorption, adsorption isotherms at 25°C were obtained using Emcocel 50M and Emcocel HD90 as adsorbate. These MCC samples were selected to compare the effect of increased salinity on softwood and hardwood MCCs. Isotonic solutions of NaCl (0.9% w/v, 0.154M) over the tacrine concentration range 1.5 to 50 $mgl^{-1}$ were used. Previous investigations (Figure 2; see also (11)) had established that adsorption decreased as salinity increased until a plateau of minimum absorption was reached at NaCl concentrations above 0.05M.

Surface area

Specific surface area was determined by 5--point BET $N_2$ adsorption (Gemini 2360, Micromeritics, Dunstable, UK) at 77K in triplicate. Samples were dried at 40°C to constant mass (usually sixteen hours) under a stream of dry nitrogen to remove surface moisture.

Particle size

Particle size distribution analysis by laser diffraction was performed using the Mastersizer 2000 (Malvern Ltd., Malvern, UK). Samples were presented as dry powders using the Scirocco 2000 automated dry powder feeder (Malvern Ltd., Malvern, UK) set to yield a pressure drop of 3bar across the sampling chamber. Each analysis is the mean of 10 000 scans over ten seconds. Sample feed rate was adjusted to give a laser obscuration of 0.5 to 2.0% during analysis. Results quoted are the means of three analyses. All results are quoted as volume diameter distributions.

RESULTS AND DISCUSSION

The data from the isotherms of all MCCs studied were described well by the Langmuir equation ($r^2 > 0.92$). Isotherm plots for Pharmacel 101, Emcocel 50M and Emcocel HD90 are compared in Figure 3, with a comparison of the linearised data in Figure 4. Data for all sixteen MCCs studied are summarised in Table 2 (single batch data) and Table 3 (batch--to--batch data).

Statistical treatment of adsorption results

The initial null hypotheses, that the mean affinities ($\chi^2$ test; $p<0.01$) and the mean capacities ($\chi^2$ test; $p<0.01$) of all MCCs studied were equal, were rejected. The well--known Fisher pairwise multiple comparison test for normally distributed data was adapted to establish statistically equivalent groups of MCCs, on the basis of affinity

and capacity. This test is based on the standard deviations of the slope and intercept calculated from the linear regression analyses. Using the Fisher treatment, a critical difference is obtained for affinity and capacity data, determined *via* the calculation of a pooled standard deviation. This means that within sample variations are taken to be equal for each MCC, irrespective of the individually calculated 95% confidence limits given in Table 2. Differences smaller than 56.5 for affinity constants and 0.81 $mmolkg^{-1}$ for capacities are not significant to within 95% confidence.

The groupings of the MCCs are used to simplify the discussion of the differences and similarities between the affinity constants and capacity values calculated for the adsorption isotherms measured.

Standard grades

Statistical analysis based on Fisher's pairwise comparison shows that there are significant differences ($p < 0.05$) between some of the standard grades.

The affinity constant for Tabulose 101 is significantly lower than the values obtained for the other five MCCs in the standard grade group, and Ceolus KG--802 has a significantly higher affinity than any other MCC sample. The capacities for tacrine of Avicel 101, Ceolus KG--802 and Pharmacel 101 are significantly higher than the other three MCCs, with Pharmacel 101 displaying a significantly higher capacity than Avicel 101 and Ceolus KG--802.

The difference between the affinity constants has a noticable effect on the adsorption observed at lower drug concentrations. This is illustrated in Figure 5, comparing tacrine adsorption against equilibrium concentration for Tabulose 101 and Ceolous KG--802. The Langmuir isotherms for these products predict that the saturation adsorptions differ by 16%. Taking a hypothetical formulation containing 250mg MCC and a release of 10mg (concentration of $11.1mgl^{-1}$ in a 900ml dissolution bath), a dose of 11.7mg would be required in a formulation using Ceolus KG--802 (15% adsorption). In contrast, an initial drug dose of 10.4mg is required to reach the same equilibrium concentration with Tabulose 101 (4% adsorption). Therefore, low affinity MCCs may be suitable for use in cases where a lower degree of adsorption is acceptable, since a 10.4mg dose is within Pharmacopoeial tolerances for formulations of this dosage.

From these results it may be concluded that Vivapur 101 and Emcocel 50M are equivalent products with respect to adsorption of tacrine. Also, the adsorption capacities of Avicel 101 and Ceolus KG--802 are statistically equivalent. The technique used to achieve a lower bulk density for Ceolus KG--802 does not have a significant effect on the adsorption capacity of the material. No correlation between affinity constant and capacity for these products was observed. These results indicate that variables such as pulp source, depolymerisation conditions and neutralisation techniques play an important role in affecting adsorption characteristics.

It should be emphasised that these comparisons are made on the basis of single, randomly selected batches from each manufacturer. The differences seen here may,

therefore, be a reflection of batch--to--batch variations within each manufacturer's product.

Final drying conditions are less likely to play a significant role, since Emcocel 50M is spray dried (Penwest product literature), in contrast to the air--stream drying technique employed in the manufacture of Vivapur 101 (Rettenmaier product literature). Furthermore, it is probable that different drying techniques are used in the final production of Avicel 101 and Ceolus KG--802, since these products have different bulk densities (Ceolos KG--802 = 0.24$gm^{-3}$, Avicel 101 = 0.31 $gm^{-3}$). Therefore, the equivalence in adsorption capacity between Avicel 101 and Ceolus KG--802 may be a result of the use of similar pulp and depolymerisation techniques.

Reversibility of adsorption

Quadruplicate analyses of the reversibility of the adsorption of tacrine from aqueous solution onto Tabulose 101 and Ceolus KG--802 indicated that the adsorption is fully reversible ($f = 1.01 \pm 0.01$ for both samples). These two MCC types were selected because they display the lowest and highest affinities for tacrine in the adsorption isotherm studies. These results indicate that the affinity of tacrine for MCC and the reversibility of the adsorption are not linked.

This finding confirms some previous work investigating the elution of some drugs from MCC using a pH 2.1 HCl solution, wherein complete elution of ampicillin, amoxycillin (9), fluphenazine and promethazine (21) was achieved. However, none of

these workers were able to fully elute either of these drugs using water as the elution medium. This would tend to confirm the assumptions made by Akaho & Fukumori (22) about the adsorption of drugs onto cellulose, who stated that adsorption tends to be irreversible. There is clearly a discrepancy between the results reported here for adsorption of tacrine and the previously published work. There remain as yet unresolved structure--dependent influences on the reversibility of the adsorption of different drugs.

The observed reversibility of the adsorption of tacrine onto MCC has important consequences for the expected *in vivo* adsorption of this drug, even though *in vitro* dissolution tests may indicate that there is a significant decrease in bioavailability due to adsorption. Constant absorption of the drug from the digestive tract will result in the release of adsorbed drug from the dosage form as the equilibrium between the amount adsorbed and the concentration of the drug is re--established. Therefore, although adsorption of the drug onto MCC may decrease the *in vivo* bioavailability, the decrease will be less than *in vitro* studies indicate if the adsorption is reversible to any degree.

Batch--to--batch variation

More than one batch of Avicel PH101, Emcocel 50M and Vivapur 101 were obtained from the manufacturers. These three products are marketed as equivalent products on the basis of particle size. Significant differences were established for all three products on a batch-to-batch basis (Table 3). However, repeating the statistical

analyses including all the adsorption experiments for each product irrespective of batch number (n = 45 for Emcocel 50M and Vivapur 101, n = 30 for Avicel PH101) still suggested that Emcocel 50M and Vivapur 101 are equivalent products and Avicel PH101 has a higher capacity than the other two products.

Some correlation of the time between analysis and manufacture and the adsorption was observed for Emcocel 50M and Avicel PH101 of the products. It may be, therefore, that storage time has a significant effect on the surface chemistry of these MCCs. The possibility that storage time has an effect on adsorption has previously been suggested from a study of the dissolution efficiencies of prednisone formulations (8), where the lowest batch number of three unspecified Emcocel products was found to have the best dissolution efficiency, implying a decreased adsorptivity.

Interestingly, no time dependence was observed for the three Vivapur 101 batches analysed. This product may be more stable, or any time--dependent trend may be masked by larger batch--to--batch variations in this product.

Further analysis of adsorption isotherms of the same batches after extended storage times will yield further information.

Large particle size

There are no significant differences in either the affinity constants or the capacities of Emcocel 50M, Emcocel 90M and Emcocel LP200. This indicates that the spray

drying conditions have no significant effect on the surface chemistry of the MCC products. It can be deduced that the nature of the fibrils forming the aggregates, rather than the size of the aggregates, is a primary determinant of the adsorption capacity.

The results presented here disagree with previous investigations into the effect of particle size of MCC on adsorption (11). This may be a result of steric factors affecting the ability of the large bromhexine (2--amino--3, 5--dibromo--N--cyclohexyl--N--methylbenzylamine HCl) molecules to occupy adsorption sites within small pores, which is not a significant factor in tacrine adsorption. Qtaitat et al. (11) presented no porosimetry data, however a difference in the pore size distribution and therefore the accessibility of the internal surfaces may be expected. Microcrystalline cellulose particles as measured by standard particle sizing methods are aggregates of smaller particles of MCC (23), the size of these aggregates being the measured particle size. On a mass--for--mass basis, less of the interior of the larger particles will be accessible to these larger drug molecules, if it is assumed that there are pores present small enough to block access to the interior of the agglomerate.

High density products

Microcrystalline celluloses manufactured from hardwood sources have a significantly lower adsorptive capacity for tacrine than softwood sourced MCCs. This is best observed when comparing hardwood and softwood products from the same manufacturer, because the similar techniques and manufacturing practices may be used for each product.

Use of a hardwood pulp source for product pairs based on manufacturer and pre--treatment show that there are significant differences in the capacities of these products (Table 2). Affinity is not affected for the Rettenmaier GmbH products (Vivapur 101 and Vivapur 302), but the two Penwest Co. pairs (Emcocel 90M and Emcocel HD90; Prosolv90 and Prosolv HD90) and the two FMC Co. products (Avicel PH101 and Avicel PH302) show significant differences within the pairs.

Okada et al. (10) found that a high density MCC (Avicel 301) has a lower capacity (from Freundlich multi--layer isotherm plots) for the acridine derivative acrinol (2--ethoxy--6, 9--diaminoacridine) than the standard grade Avicel 101. This was ascribed to slight variations in the cellulose microcrystallite and cluster structure. The mean size of softwood MCC aggregates is shown to be not significant in our study for tacrine adsorption. Therefore the known differences in microcrystallite structure between softwood and hardwood products (5) are shown to significantly influence the adsorption capacity of tacrine onto MCC.

Silicification

Silicified MCC products are shown to have a significantly lower capacity, but an unchanged affinity, for tacrine compared with the equivalent unmodified grade (Figure 3). This may be a consequence of the presence of $SiO_2$ in the surface of the product (24). Silicification reduces the adsorption of tacrine by 21% to 12%, due either to the replacement of cellulosic surface area by non--adsorbing silicon dioxide

or the preferential adsorption of silicon dioxide onto active sites in the surface of MCC.

The similarity of the affinity constants of the unmodified and silicified grades indicates that there is not a preferential adsorption of silicon dioxide in the surface. This reflects the previously reported similarity in the water vapour adsorption enthalpy (13) between MCC and SMCC. Preferential adsorption would reduce the affinity of tacrine by masking the most active sites, thus making adsorption more difficult. It is more likely that there is a net reduction in the surface available for adsorption, with any masking of adsorption sites occurring randomly.

Treated samples

Emcocel SP15 is a micronised (air--jet mill) grade of MCC. This high--energy treatment of the MCC significantly lowers the capacity for adsorption of tacrine, despite the increase in specific surface area as measured by BET $N_2$ adsorption. This may be evidence of mild dry hornification (25), a heat--induced reduction of the water retention capacity of cellulosic products. It is therefore possible that the water--cellulose interaction is an important factor in drug adsorption, with the ability of MCC to swell in water a factor in determining the area available for adsorption from aqueous solution.

The data obtained from the heated samples show significant reductions in both the adsorption capacity (decrease of 42 ± 3%) and affinity constant (decrease of 40 ±

10%) of Emcocel 50M on heating. This, again, may be evidence of hornification, with the surface structure of cellulose collapsing and the available adsorption sites destroyed by pyrolysis and intra cellular hydrogen bonding (25).

The observed changes in the adsorption capacity and affinity reflect a reduction in surface energy and a consequent increased hydrophobicity on heating. This, therefore, will mean that any measurements of surface energetics that involve heating cellulose samples will not yield surface energy results that are relevant to unheated samples.

Correlation of adsorption capacity with surface area

The correlation of surface area determined by BET $N_2$ adsorption with the capacity to adsorb tacrine from aqueous solution can be determined by examination of the data in Table 1. Only 'standard' and 'large particle' grades were considered to avoid the large increase of the BET surface area on silicification and the potential effects of using a hardwood pulp source. From these data it is observed that there is no apparent correlation between capacity for tacrine and surface area measured by BET $N_2$ adsorption (Table 2). The actual correlation coefficient ($r^2$) using the eight MCCs considered was 0.043, a strong indication that no correlation exists.

This finding is explicable with reference to nitrogen adsorption work conducted previously by Nakai et al. (26) and doRego et al. (27). Nakai et al. (26) measured high (80 000 $m^2kg^{-1}$) surface areas of cellulose samples after maceration in water. DoRego et al. (27) measured surface areas in a manner similar to that described here, using

cyanine dyes as probes. Working with ethanolic (slightly swelling) and dichloromethane (non--swelling) solutions, they obtained active surface areas of 2400 and 1200 $m^2kg^{-1}$, respectively, for an unspecified cellulose sample.

One possible explanation for these observations is water--induced swelling of the cellulose. In order to investigate the effect of solvent on the apparent surface area, a sample of Emcocel 50M was washed repeatedly with dry ethanol to remove water and then washed with *n*--pentane to remove the ethanol. The resulting powder was analysed using 5--point BET $N_2$ adsorption yielding a surface area of 2300 $m^2kg^{-1}$. By itself, this result could be interpreted as a more complete removal of water from the pores of the sample than is achieved by gentle heating under dry nitrogen. In conjunction with the results of doRego et al. (27) it would appear that swelling of the sample in ethanol is a more valid explanation of the observed increase in surface area than water removal.

This may also go some way to explaining the observed reduction in adsorption of the high--energy milled and heated MCC samples, since hornification reduces the ability of cellulose to swell and increase hydrophobicity may affect release efficiency (8).

Effect of ionic strength

Figure 2 compares the effect of NaCl concentration on the percentage tacrine adsorbed onto MCC from solutions containing 50 $mgl^{-1}$ (Emcocel 50M) and 15$mgl^{-1}$ (Emcocel HD90) tacrine.

The data obtained from this study can be discussed in three different ways:

First, the main mechanism for adsorption onto MCC is by ion exchange. Processing cellulose oxidises the surface hydroxyl groups to carboxyl groups (28), resulting in a pKa for cellulosic materials of 4.0--4.3 (29). This means that within the pH range 6--7, at which these experiments were conducted, the maximum potential for adsorption by ion exchange is expected for the tacrine – MCC system (30). The sodium cation, having a smaller radius than the protonated tacrine molecule, has a greater charge density. Therefore, sodium cations preferentially occupy the negative adsorption sites on the surface of MCC, eventually preventing tacrine from adsorbing on these sites. This confirms the findings of Okada et al. (10) and Qtaitat et al. (11) who determined that adsorption was mainly due to an ion--exchange mechanism, occurring by interaction with surface carboxyl groups.

Secondly, there appears to be a second, as yet unassigned, mode of adsorption in the softwood MCC. Approximately 10% of the available tacrine is adsorbed even at high NaCl concentrations. This might be due to a dipolar (Lifshitz – van der Waals) type interaction or H--bonding within the surface (10, 31). Spectroscopic (vibrational and NMR) investigations, currently in progress, may be able to resolve this issue (32).

Thirdly, there is a large, significant decrease in the adsorption observed at isotonic salinity (0.154M NaCl) compared with the adsorption in degassed purified water. As well as providing an insight into the adsorption mechanism, this observation shows

that *in vitro* testing conditions will have a marked effect on drug adsorption and the consequent bioavailability determined for a formulation. This last point has implications for the effect of adsorption on *in vivo* release. The higher osmolarity of physiological systems would decrease the tendency of MCC to adsorb tacrine and other drugs that adsorb through an ion exchange mechanism (21).

Analysis of the isotherms from the adsorption experiments was complicated by the very low adsorption and the consequent increase in experimental (type 1) error. This error led to a high degree of scatter about the line of best fit, with correlation coefficient ($r^2$) decreasing to 0.8. However, a rank similarity in the calculated adsorption capacities of Emcocel 50M and Emcocel HD90 from saline tacrine solution with the estimated capacities from the single concentration can be established. The 'non--ionic capacities' for these two materials are $0.49 \pm 0.12$ $mmolkg^{-1}$ (Emcocel 50M) and $0.12 \pm 0.58$ $mmolkg^{-1}$ (Emcocel HD90). These results are of the same order of magnitude as those estimated from observation of the effect of the ionic capacity on adsorption at a single initial drug concentration.

## CONCLUSIONS

The findings from these studies may be summarised in the following points:

Inter--manufacturer differences are demonstrated for the adsorption of tacrine from aqueous solution for the MCC batches used in this investigation. This may be an indication of batch--to--batch variations, with the single batches selected being

representative of the extremes of variation to be expected between manufacturers' products.

Significant differences in the capacities and affinities were determined between the batches investigated of Avicel PH101, Emcocel 50M and Vivapur 101. Some of this variation may be attributable to storage time. Despite the batch--to--batch variations, the conclusions from the single batch investigations still apply; Emcocel 50M and Vivapur 101 are similar and Avicel PH101 has a higher adsorption capacity than the other two products.

Surface area determined by BET $N_2$ adsorption is not an indicator of the adsorption capacity. It is therefore not possible to predict the adsorption of water--swollen MCC from dry state surface area determinations.

The adsorption of tacrine onto MCC from an aqueous solution is fully reversible.

High--density grades of MCC display a lower adsorption capacity and reduced affinity for tacrine than standard grades.

The nature of the primary particles that constitute the aggregates of MCC is a critical factor in determining the adsorption capacity of the product. The size of the aggregates is not a significant factor.

Silicified MCC samples show a reduced adsorption capacity due to reduction in the cellulosic surface area, replaced by non--adsorbing $SiO_2$. High density SMCC (Prosolv™ HD90) has the lowest capacity for adsorption of tacrine of all the samples studied.

The water -- cellulose interaction may be an important factor in determining the adsorption capacity of cellulosic materials from aqueous solution.

The main mechanism for adsorption is by ion--exchange. A secondary interaction, either H--bonding or a dispersion force interaction, is a minor but significant adsorption mode for softwood MCCs. The ion exchange mode is quickly saturated under test conditions by solubilised ions. Testing conditions for *in vitro* dissolution and bioavailability analyses will, therefore, significantly affect the observed drug release.

Therefore, a change in the brand of MCC used in a formulation may have a significant effect on the observed *in vitro* adsorption, and potentially affect drug bioavailability.

ACKNOWLEDGEMENTS

We thank Penwest Co. (USA) for financial support (DFS, SE) and provision of MCC and SMCC samples. We also thank Dr. Ray Cox for providing the Mastersizer 2000 data.

Table 1. Summary of the twenty one microcrystalline cellulose samples studied. All groupings are based on descriptions from manufacturer's literature. Standard grade MCCs marked with an asterisk are additional samples used for batch--to--batch comparison.

| MCC | Batch | Supplier | Country | Group |
|---|---|---|---|---|
| Avicel PH101 | 6902C | FMC Inc. | USA | standard grade |
| Avicel PH101 | 1113 | FMC Inc. | USA | standard grade* |
| Ceolus KG-802 | H0134 | Asahi Kasei Corp. | Japan | standard grade |
| Emcocel 50M | E5D8C17X | Penwest Co. | USA | standard grade |
| Emcocel 50M | E5D7E21 | Penwest Co. | USA | standard grade* |
| Emcocel 50M | E5B1E48 | Penwest Co. | USA | standard grade* |
| Pharmacel 101 | 90971 | DMV International | The Netherlands | standard grade |
| Tabulose 101 | 113/99 | Blanver Ltda. | Brazil | standard grade |
| Vivapur 101 | 5610193529 | J. Rettenmeier GmbH | Germany | standard grade |
| Vivapur 101 | 5610104629 | J. Rettenmeier GmbH | Germany | standard grade* |
| Vivapur 101 | 5610110714 | J. Rettenmeier GmbH | Germany | standard grade* |
| Emcocel 90M | E9B8A01X | Penwest Co. | USA | large particle |
| Emcocel LP200 | 2S6003X | Penwest Co. | USA | large particle |
| Avicel PH302 | Q918C | FMC Inc. | USA | high density |
| Emcocel HD90 | HD9B5K3X | Penwest Co. | USA | high density |
| Prosolv HD90 | K9S9040X | Penwest Co. | USA | high density, silicified |
| Vivapur 302 | 5630280112 | J. Rettenmeier GmbH. | Germany | high density |
| Prosolv 50 | P9B9B11X | Penwest Co. | USA | silicified |
| Prosolv 90 | P5B7D26X | Penwest Co. | USA | silicified |
| Emcocel SP15 | SPD7C01X | Penwest Co. | USA | treated |
| Heated E50M | E5D8C17X | Penwest Co. | USA | treated |

Table 2. Summary of surface area data from BET $N_2$ adsorption, volume diameter mean particle size (d (v, 0.5)) and analysis of Langmuir adsorption isotherms for single batches of the MCCs studied. The affinity constants ($k_1k_2$) and adsorption capacities ($k_2$) are presented together with the 95% confidence intervals of the individual analyses, determined from standard deviation calculations. Tacrine surface areas are based on a molecular surface area of 2 $nm^2$ for tacrine.

| MCC | BET surface area ($m^2kg^{-1}$) | d (v, 0.5) (μm) | $k_1k_2$ | $k_2$ ($mmolkg^{-1}$) | Tacrine surface area ($m^2kg^{-1}$) |
|---|---|---|---|---|---|
| Avicel PH101 | 1200 | 54 | 219 ± 47 | 11.4 ± 0.4 | 13700 ± 500 |
| Ceolus KG-802 | 1200 | 52 | 439 ± 65 | 11.6 ± 0.6 | 14000 ± 700 |
| Emcocel 50M | 1270 | 57 | 172 ± 46 | 10.5 ± 0.4 | 12600 ± 400 |
| Pharmacel 101 | 1300 | 57 | 219 ± 16 | 12.5 ± 0.2 | 15100 ± 200 |
| Tabulose 101 | 1340 | 70 | 42.4 ± 6.9 | 10.0 ± 1.6 | 12000 ± 1900 |
| Vivapur 101 | 1450 | 93 | 217 ± 40 | 10.5 ± 0.3 | 12600 ± 300 |
| Emcocel 90M | 1250 | 109 | 183 ± 63 | 10.5 ± 0.3 | 12700 ± 400 |
| Emcocel LP200 | 1100 | 184 | 157 ± 73 | 10.5 ± 0.9 | 12700 ± 1000 |
| Avicel 302 | 610 | 104 | 93.2 ± 35.0 | 6.93 ± 0.46 | 8300 ± 600 |
| Emcocel HD90 | 680 | 123 | 109 ± 46 | 5.30 ± 0.59 | 6400 ± 700 |
| Vivapur 302 | 1220 | 110 | 220 ± 90 | 8.24 ± 0.44 | 9900 ± 500 |
| Prosolv 50 | 4920 | 55 | 190 ± 79 | 8.30 ± 0.41 | 10000 ± 500 |
| Prosolv 90 | 5490 | 109 | 209 ± 54 | 9.28 ± 0.46 | 11200 ± 600 |
| Prosolv HD90 | 4320 | 124 | 124 ± 31 | 4.33 ± 0.22 | 5200 ± 300 |
| Emcocel SP15 | 3320 | 14 | 167 ± 63 | 8.68 ± 0.63 | 10500 ± 800 |
| Heated E50M | 1260 | 55 | 116 ± 47 | 4.76 ± 0.25 | 5800 ± 300 |

Table 3. Analysis of Langmuir adsorption isotherms from the study of batch--to--batch variations of Avicel PH101, Emcocel 50M and Vivapur 101. The first given batch number is that of the batch used for interproduct comparison (Table 2).

| MCC | Batch No. | $k_1k_2$ | $k_2$ (mmolkg$^{-1}$) | Tacrine surface area (m$^2$kg$^{-1}$) |
|---|---|---|---|---|
| Avicel PH101 | 6902C | 219 ± 47 | 11.4 ± 0.4 | 13700 ± 500 |
| Avicel PH101 | 1113 | 285 ± 11 | 9.27 ± 1.13 | 11200 ± 1400 |
| Emcocel 50M | C17X | 172 ± 46 | 10.5 ± 0.4 | 12600 ± 400 |
| Emcocel 50M | E21 | 230 ± 4 | 8.43 ± 0.88 | 10200 ± 1100 |
| Emcocel 50M | E48 | 295 ± 7 | 9.39 ± 1.08 | 11300 ± 1300 |
| Vivapur 101 | 3529 | 217 ± 40 | 10.5 ± 0.3 | 12600 ± 300 |
| Vivapur 101 | 4629 | 276 ± 6 | 8.72 ± 1.04 | 10500 ± 1300 |
| Vivapur 101 | 0714 | 290 ± 5 | 7.84 ± 0.93 | 9400 ± 1100 |

REFERENCES

(1) Doelker, E., Mordier, D., Iten, H., Humbert-Droz, P. Comparative tableting properties of sixteen microcrystalline celluloses. Drug Dev. Ind. Pharm. **1987,** *13* 1847-1875.

(2) Dittgen, M., Fricke, S., Gerecke, H. Microcrystalline cellulose in direct tabletting. Manuf. Chem. **1993**, *64,* 17-21.

(3) Maincent, P. L'interchangeabilité des excipients en formulation et ses consequences éventuelles. Thérapie **1999**, *54*, 5-10.

(4) Landín, M., Martínez-Pacheco, R., Gómez-Amoza, J.L., Souto, C., Concheiro, A., Rowe, R.C. Effect of country of origin on the properties of microcrystalline cellulose. Int. J. Pharm. **1993**, *91*, 123-131.

(5) Landín, M., Martínez-Pacheco, R., Gómez-Amoza, J.L., Souto, C., Concheiro, A., Rowe, R.C. Effect of batch variation and source of pulp on the properties of microcrystalline cellulose. Int. J. Pharm. **1993,** *91*, 133-141.

(6) Rowe, R.C., McKillop, A.G., Bray, D. The effect of batch and source variation on the crystallinity of microcrystalline cellulose. Int. J. Pharm. **1994**, *101*, 169-172.

(7) Ardizzone, S., Dioguardi, F.S., Mussini, P.R., Mussini, T., Rondinini, S., Vercelli, B., Vertova, A. Batch effects, water content and aqueous/organic solvent reactivity of microcrystalline cellulose samples. Int. J. Biol. Macromolecules **1999,** *26,* 269-277.

(8) Landín, M., Martínez-Pacheco, R., Gómez-Amoza, J.L., Souto, C., Concheiro, A., Rowe, R.C. Influence of microcrystalline cellulose source and batch variation on the tabletting behaviour and stability of prednisone formulations. Int. J. Pharm. **1993,** *91,* 143-149.

(9) El-Samaligy, M.S., El-Mahrouk, G.M., El-Kirsh, T.A. Adsorption - desorption effect of microcrystalline cellulose on ampicillin and amoxycillin. Int. J. Pharm. **1986,** *31,* 137-144.

(10) Okada, S., Nakahara, H., Isaka, H. Adsorption of drugs on microcrystalline cellulose suspended in aqueous solutions. Chem. Pharm. Bull. **1987,** *35,* 761-768.

(11) Qtaitat, M.A., Zughul, M.B., Badwan, A.A. Bromhexine hydrochloride adsorption by some solid excipients used in the formulation of tablets. Drug Dev. Ind. Pharm. **1988,** *14,* 415-429

(12) Tomer, G., Patel, H., Podczeck, F., Newton, J.M. Measuring the water retention capacities (MRC) of different microcrystalline cellulose grades. Eur. J. Pharm. Sci. **2001**, *12*, 321-325.

(13) Buckton, G., Yonemochi, E., Yoon, W.L., Moffat, A.C. Water sorption and near IR spectroscopy to study the differences between microcrystalline cellulose and silicified microcrystalline cellulose before and after wet granulation. Int. J. Pharm. **1999**, *181*, 41-47.

(14) Sherwood, B.E., Becker, J.W. A new class of high functionality excipients: silicified microcrystalline cellulose. Pharm. Tech. **1998**, *22*, 78-88.

(15) Davies, J.L. PhD Thesis, Electrorheological fluids as smart medicines with potential in controllable drug delivery, University of Bath (1999).

(16) Morita, Z., Tanaka, T., Motomura, H. Diffusion/adsorption model of cellulose dyeing II. Ordinary cellulose-direct dye system. J. App. Polym. Sci. **1985**, *30*, 3697-3705.

(17) Kotelnikova, N.E., Petropavlovsky, G.A. Preparation of microcrystalline cellulose form cellulose of deciduous wood species and its properties In *Cellulose Sources and Explotation*; Kennedy, J.F., Phillips, G.O., Williams, P.A. Eds.; Ellis Howood: London, 1991; 21-31.

(18) Ardizzone, S.; Dioguardi, F.S.; Quagliotto, P.; Vercelli, B.; Viscardi, G. Microcrystalline cellulose suspensions: effects on the surface tension at the air-water boundary. Colloids Surfaces A: Physicochem. Engin. Aspects **2001,** *176,* 239-244.

(19) Giles, C.H., MacEwan, T.H., Nakhwa, S.N., Smith, D. Studies in adsorption. Part XI. A system of classification of solution adsorption isotherms, and its use in diagnosis of adsorption mechanisms and in measurement of specific surface areas of solids. J. Chem. Soc. **1960,** 3973-3993.

(20) Narbonne, J.F.; Djomo J.E.; Ribera, D; Ferrier, V.; Garrigues, P. Accumulation kinetics of polycyclic aromatic hydrocarbons adsorbed to sediment by the mollusk Corbicula fluminea. Ecotox. Environ. Safety **1999,** *42,* 1-8.

(21) Franz, R.M., Peck, G.E. In vitro adsorption – desorption of fluphenazine dihydrochloride and promethazine hydrochloride by microcrystalline cellulose. J. Pharm. Sci. **1982,** *71,* 1193-1199.

(22) Akaho, E., Fukumori, Y. Studies on adsorption characteristics and mechanism of adsorption of chlorhexidine mainly by carbon black. J. Pharm. Sci. **2001,** *90,* 1288-1297.

(23) Ek, R., Alderborn, G., Nyström, C. Particle analysis of microcrystalline cellulose: Differentiation between individual particles and their agglomerates. Int. J. Pharm. **1994,** *111*, 43-50.

(24) Edge, S., Potter, U.J., Steele, D.F., Tobyn, M.J., Chen, A., Staniforth, J.N. The location of silicon dioxide in silicified microcrystalline cellulose. Pharm. Pharmacol. Commun. **1999,** *5*, 371-376.

(25) Weise, U. Hornification - mechanisms and terminology. Paperi JA PUU - Paper Timber **1998**, 80, 110-115.

(26) Nakai, Y., Fukuoka, E., Nakajima, S., Hasegawa, J. Crystallinity and physical characteristics of microcrystalline cellulose. Chem. Pharm. Bull. **1977,** *25*, 96-101.

(27) doRego, A.M., Pendo Pereira, L., Reis, M.J., Oliveira, A.S., Vieira Ferreira, L.F. X-ray photoelectron, UV-vis adsorption and luminescence spectrophotometric studies of 2,2'-cyanines adsorbed onto microcrystalline cellulose. Langmuir **1997,** *13*, 6787-6794.

(28) Michell, A.J., Higgins, H.G. The absence of free hydroxyl groups in cellulose. Cellulose **1999,** *6,* 89-91.

(29) Krässig H.A. *Cellulose. Structure, Accessibility and Reactivity.* Gordon and Breach Science Publishers, Amsterdam, 1993; 360pp.

(30) Senderoff, R.I., Mahjour, M., Radebaugh, G.W. Characterization of adsorption behavior by solid dosage form excipients in formulation development. Int. J. Pharm. **1992,** *83,* 65-72.

(31) Jorgensen B.S., Dye R.C., Pratt L.R., Gomez, M.A., Meadows, J.E. Concentrating low-level tritiated water through isotope exchange. Fusion Technol. **2000** *37,* 124-130

(32) Burkhanova, N.D., Yugai, S.M., Khalikov, S.S., Turganov, M.M., Muratova, S.A., Nikonovich, G.V., Aripov, K.N. Interaction of drugs with microcrystalline cellulose at the molecular and supermolecular levels. Chem. Nat. Compounds **1997,** *33,* 340-346.

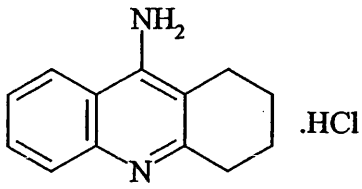


Figure 1. Conformational structure of tacrine hydrochloride

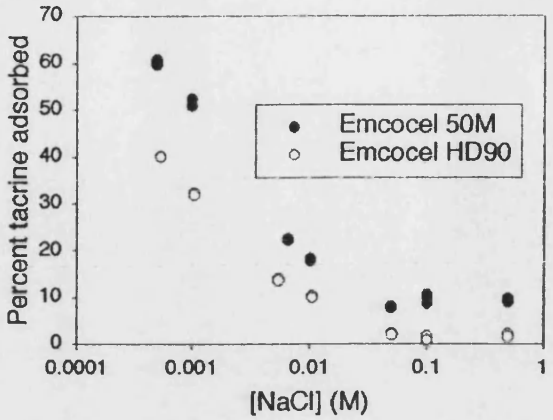


Figure 2. Effect of ionic strength on the adsorption of tacrine by a softwood (Emcocel 50M) and a hardwood (Emcocel HD90) MCC. Three repeats at each of seven NaCl concentrations. These results indicate that the primary adsorption mode is by ion exchange. A secondary adsorption mode is of importance for Emccoel 50M.

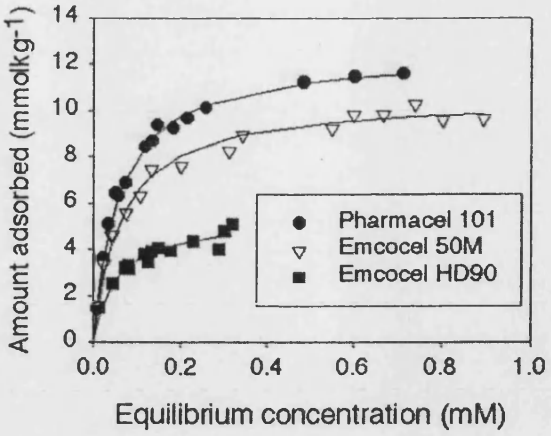


Figure 3. Adsorption isotherms of tacrine onto Pharmacel 101, Emcocel 50M and Emcocel HD90.

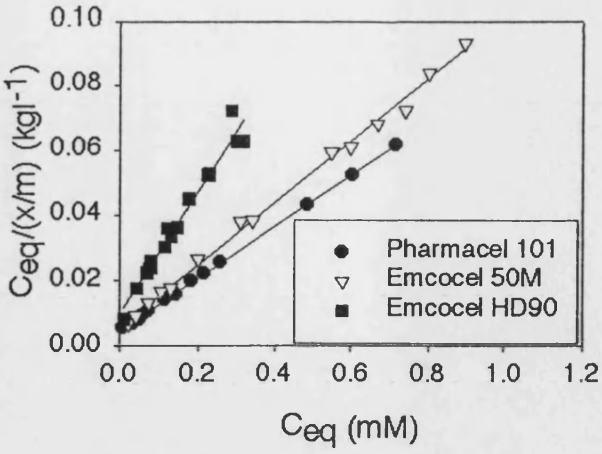


Figure 4. Langmuir plots for the adsorption of tacrine onto Pharmacel 101, Emcocel 50M and Emcocel HD50. The data presented in Figure 3 have been linearised according to the Langmuir isotherm (Equation 1).

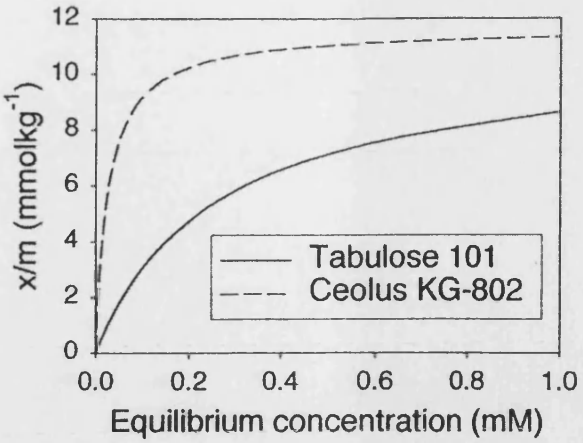


Figure 5. The effect of affinity constant on the amount of tacrine adsorbed from aqueous solution at 25°C, where x/m is the amount of tacrine adsorbed at equilibrium per unit mass of adsorbate. Comparison of Tabulose 101 and Ceolus KG-802. The capacity of Tabulose for tacrine is 85% that of Ceolus, but the affinity constant for Tabulose 101 is 10% that of Ceolus KG-302.

Drug Development and Industrial Pharmacy, 27(7), 613–621 (2001)

RESEARCH PAPER

# Directional Bonding in Compacted Microcrystalline Cellulose

S. Edge,[1,*] D. F. Steele,[1] M. J. Tobyn,[1]
J. N. Staniforth,[1] and A. Chen[2]

[1]*Pharmaceutical Technology Research Group, Department of Pharmacy and Pharmacology, University of Bath, Bath, BA27 7AY, UK*
[2]*Department of Materials Science and Engineering, University of Bath, Bath, BA2 7AY, UK*

## ABSTRACT

*The mechanical properties of compacts of microcrystalline cellulose (MCC) and silicified microcrystalline cellulose (SMCC) were evaluated by tensile testing, diametric compression testing, and compression testing. For tensile and compression testing, cubic specimens were carefully machined from MCC and SMCC compacts, and the tensile and compression strengths were evaluated both normal and parallel to the compaction direction. The cubic tensile strengths were compared to values obtained from the diametric compression test. The results obtained using the diametric compression test suggested compacts of SMCC exhibit greater strength than those of MCC. In addition, the cubes machined from compacts of MCC and SMCC exhibited directional strength; the direction normal to the compaction direction displayed the greater tensile strength; and the parallel direction had greater compression strength. The diametric compression test afforded strength values with reduced spread compared to the values collected from the cubic tensile test, suggesting that the errors involved in collecting diametric compression test data of compacts are less than those for the cubic tensile test. Analysis of the cubes using X-ray diffraction (XRD) suggested that they display directional structural anisotropy, with the direction normal to the compaction direction being more crystalline than the parallel direction. However, it is not clear whether the difference in the directional strength is solely a consequence of the increased crystallinity or a culmination of crystallographic and mechanical keying effects.*

*Corresponding author. Fax: 01225 826114; E-mail: prssje@bath.ac.uk

*Key Words:* *Crystallinity; Directionality; Mechanical strength; Microcrystalline cellulose; Silicified microcrystalline cellulose*

## INTRODUCTION

Microcrystalline cellulose (MCC) is used as a filler/binder in the manufacture of pharmaceutical solid dosage tablets. The material has been extensively studied to understand its tableting behavior. For example, the compaction properties of mixtures of MCC with other pharmaceutical materials, such as drugs and other excipients like dicalcium phosphate, have been reported (1–3). However, due to the complexity of tablet formulations, the characteristics of compacted pure MCC and MCC in the presence of lubricants have also been investigated to understand the functionality of the material (4–6).

In tableting technology, MCC is considered to be a plastically deforming excipient. Another description of MCC is as a particulate aggregate of fibrils of a semicrystalline cellulose polymer. The mechanical properties of MCC are more complex than typical fabricated polymer systems in that the samples (compacts) invariably consist of compressed particles. This results in a large interfacial surface area that is responsible for tablet strength (7). This is a crucial characteristic of MCC compacts.

In addition, when considering the potential failure modes of pharmaceutical compacts, it is important to remember that, in general, materials fail under an applied load due to crack propagation. The stress associated with a crack or flaw in a matrix is described as the critical stress intensity factor (8). In contrast to typical polymer systems, pharmaceutical compacts are usually composed of compressed powder. This invariably results in failure by brittle fracture under an applied load, which occurs through the rupture of the interparticle bonding rather than intraparticle failure.

The mechanical strength of polymeric materials is usually determined by the tensile testing of dumbbell-shaped samples. These homogeneous test pieces are typically prepared by molding of the polymer samples. The tensile strength is determined by applying a tensile load to the sample via grips. The plastic flow of ductile materials allows compensation for any misalignment of the sample grips. Pharmaceutical tablets differ from typical polymer systems in that the samples are invariably inhomogeneous noncontinuous matrices of compressed powders. These samples tend to be brittle, making the determination of tensile strength using the conventional mechanical test difficult: Stress concentration occurs in the gripped portion of the sample, and the samples are susceptible to shear stresses that are induced by nonalignment of the test grips. To overcome these difficulties, the mechanical properties of compressed pharmaceutical powders have been determined using flexural tests (9,10) (three- and four-point bending) and the diametric compression test (11). The diametric compression test involves the application of a load normal to the compaction direction. A "true" tensile test involves the application of a tensile stress in which no load is applied to the sample normal to the tensile stress.

The important difference between these two techniques for measuring the tensile strength of materials is that, in the diametric compression test, the tensile failure is limited to the stress plain induced by the applied load; the true tensile test produces a tensile failure that reflects the weakest area in the sample. Even though these two tensile tests would be expected to afford different tensile strength values, the true tensile test may afford information concerning the directional strength of compacted pharmaceutical powder via the testing of compressed powder of similar geometry using an apparatus that reduces experimentally induced shear stresses.

The radial and axial tensile strengths of pharmaceutical compacts have been reported (12). However, possible sources of differences in apparent strengths of reported axial and radial tensile strength data of pharmaceutical samples are the presence of shear stresses in the test configuration and differences in the geometries of the test pieces. One way to overcome the problem of test piece geometry is to prepare samples of similar geometry, preferably cubes. The directional tensile strength of cubic tablets of MCC (Avicel PH-101, a 50-μm particle size grade) prepared using a single-punch tablet machine at a relatively small compression load has been previously investigated (13). The study reported that the direction parallel to the compaction direction exhibited significantly greater strength

than the normal direction. However, the samples were tested using a method that did not employ a mechanism to minimize sheer stresses that can be induced during the mounting and testing of the samples. Cubes of compacted MCC have also been previously prepared for tensile testing (using the transverse compression technique); however, no directional strength data were reported (14).

As previously stated, the mechanical properties of polymers are affected by crystallinity. This will be true for the mechanical properties of MCC. If MCC is considered as a homogeneous bulk polymer, then the crystallinity would have a profound effect on strength. However, MCC compacts consist of compressed discrete particles. Our unpublished previous investigations of the failed surfaces of samples (after diametric compression testing) using scanning electron microscopy (SEM) suggested that MCC compacts fail primarily at the particle interfaces rather than within the particles, although some evidence for intraparticle failure was identified. It would be expected that any small changes in the crystallinity of MCC would not affect this interparticle mode of failure. However, mechanical testing involves the application of a load to a material. It will be the way in which a material (of a particular geometry) copes with the applied stress that will affect the apparent strength. It would be expected that the compaction of an anisotropic material (in terms of particle size and particle shape) would result in an anisotropic compact, and that this will affect any apparent mechanical properties.

The relationship among source, compactibility, and crystallinity of MCC powders is complex (15). The apparent crystallinity of MCC depends on the method of determination: both X-ray diffraction (XRD) and infrared spectroscopy have been used to study the crystallinity of MCCs (16,17). Nuclear magnetic resonance spectroscopic and photoacoustic infrared spectroscopic studies of MCC compaction suggest that the axial and radial crystallinity develops differently during MCC compression, with the radial tensile strength always being greater than the axial values (18). In addition, the crystallinity was reported to be lower on the tablet perimeter (far from the compacting surfaces) than the top and bottom flat faces, emphasizing the importance of geometry and compression conditions.

Even though MCC is a highly compactible tableting excipient, manufacturers have continued to try to improve its functionality. Recently, a new modified MCC, silicified microcrystalline cellulose (SMCC), was introduced. This material is reported to exhibit improved compactibility in wet granulation and direct compression tableting (19). Low-speed powder compaction studies also suggested that the material does exhibit improved compactibility compared to unmodified MCC (20). To investigate any anisotropic mechanical properties and the apparent benefits of silicification, cubes were machined from compacts of MCC and SMCC, and the compression and tensile strengths were evaluated in two directions, parallel and normal to the compaction direction. The crystallinity of the cubes was also studied using wide-angle XRD.

## EXPERIMENTAL

### Materials

MCC (Emcocel 90M, Penwest Pharmaceuticals Co., New York) and SMCC (based on Emcocel 90M, SMCC90, 2% w/w silicon dioxide, Penwest Pharmaceuticals) were used as supplied.

### Preparation of Compacts

Compacts were prepared by compacting powders (6 g) in the absence of lubricant in a die (25 mm diameter heat-treated silver steel) using a load of 100 kN at compression and decompression rates of 10 mm/min and a dwell time of 1 min using an Instron 1185. Powders were stored at ambient conditions; the temperature and humidity were monitored during compaction and testing.

### Preparation of Cubes

Cubes (8.45 mm ± 0.1 mm) were machined from the central part of the MCC and SMCC compacts using a milling machine. Compacts were milled using a slow speed; the size of the cutting volume was reduced as the required compact dimensions were approached when the time between each cut was lengthened to reduce any heating effects. All of the samples were examined visually to detect any macroscopic cracks. None were detected in any of the samples, and all the samples survived the machining stage apparently intact.

### Tensile Testing of Compacts and Cubic Specimens

Diametric compression testing and cubic tensile testing were performed using an Instron 1125 using a crosshead speed of 1 mm/min. The tensile strength was calculated from the failure load (21). The tensile stresses were derived from the applied load divided by the original cross-sectional area of the corresponding cubic specimens. The deflection in compression and elongation in tension were monitored and were used to generate stress/strain data for the respective tests. The elastic (Young's) modulus is defined as the ratio of the stress to the strain data and can be represented by the slope of the stress/strain data (22). The greater the slope, the greater the apparent modulus.

$$E = \frac{\sigma}{\varepsilon}$$

where $E$ is the elastic (Young's) modulus, $\sigma$ is the stress, and $\varepsilon$ is the strain.

The specially designed tensile test apparatus is shown diagrammatically in Fig. 1. The sample cubes were glued (Araldite™ epoxy resin, Ciba-Geigy, Stafford, UK) into aluminum mounts. To reduce the possibility of inducing shear stresses, $9 \times 9 \times 0.5$ mm recesses were machined into the center of the aluminum mounts. The aluminum mounts, with the specimen glued in between, were carefully screwed into the steel mounts. The top mount was fixed into the load cell. The bottom mount was attached to the test machine via a chain mechanism to reduce pretest loading from the specimen gripping procedure. The samples were tensile tested by increasing the load on the steel chain. Three specimens were fabricated and tested for each testing procedure. All samples failed within the gauge length of the cubes; no samples failed in the glue/sample region.

### Compression Testing of Cubic Specimens

Compression testing was performed using an Instron 1125 using a crosshead speed of 0.05 mm/min. The compressive stresses were derived from the applied load divided by the original cross-sectional area of the corresponding cubic specimens. The deflection in compression and elongation in tension were monitored and used to generate stress/strain data for the respective tests.

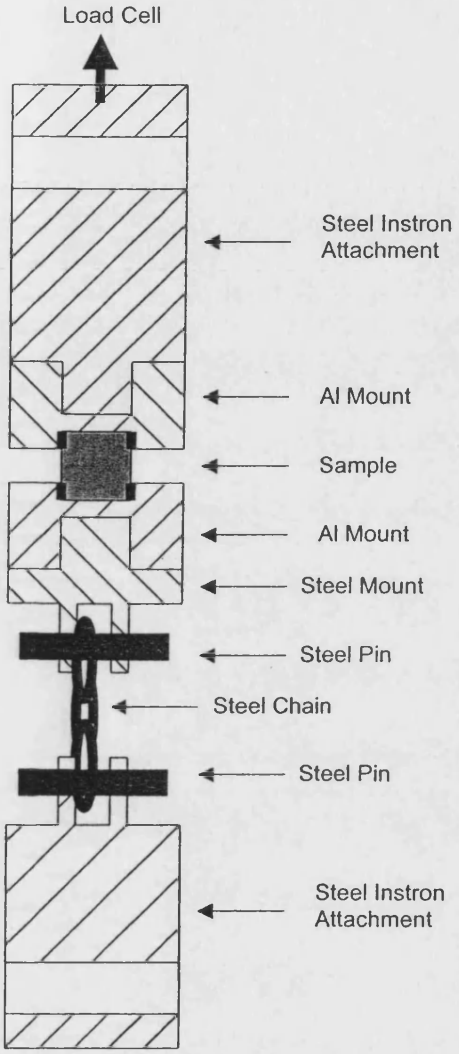


**Figure 1.** Representation of cubic tensile test apparatus.

### X-ray Diffraction

Spectra were obtained using an X-ray powder diffraction system (Phillips X-ray analytical, Cambridge, UK). Each sample was analyzed by a single $2\theta$ sweep at a rate of 0.02 degrees $2\theta$, step time 13 s.

### Scanning Electron Microscopy

SEM was performed after gold coating (Edwards Sputter Coater, UK) using a Jeol 6310 (Jeol Instruments, Tokyo, Japan) system.

## RESULTS AND DISCUSSION

Particles of MCC consist of nonhomogeneous fibrils or small agglomerates of a semicrystalline polymer (23). The compression of MCC would therefore be expected to produce anisotropic compacts. Machined cubes of MCC and SMCC were tested normal and parallel to the compaction direction. The directions of analysis are represented in Fig. 2. The data obtained from the cubic tensile test were compared to tensile strengths obtained from the diametric compression test.

### Tensile Testing

The tensile strengths of MCC and SMCC obtained using the cubic tensile test and the diametric compression test are presented in Table 1. Tensile strengths obtained using the diametric compression test for compacts of SMCC and MCC were typical for these compaction and testing protocols (20). Samples were tested on the same day to reduce effects of aging and conditions on the apparent strength.

It can be seen from Table 1 that cubes and compacts of MCC and SMCC appear to exhibit similar mechanical behavior, although the strength of SMCC appears to be greater than that of MCC in both directions. The sets of data were subjected to the Student $t$ test. The normal direction data were compared to the parallel data for each material. These comparisons had a significance of $P < .05$. The diametric compression test data between MCC and SMCC also had a significance of $P < .05$. However, when the normal direction data of MCC and SMCC and the parallel data of MCC and SMCC are compared, values of $P > .05$ were obtained. These observations suggest that the direction normal to the compaction direction appears to exhibit greater tensile strength than the parallel direction in the cubic tensile test, and compacts of SMCC exhibit greater tensile strength than those of MCC when evaluated using the diametric compression test. This is in contrast to a previous study of the directional tensile strength of cubic MCC tablets, which reported that the parallel direction exhibited the greatest strength (13).

The stress/strain data obtained from the tensile testing of cubes of MCC and SMCC are shown in Fig. 3. It can be seen from Fig. 3 that, again, MCC and SMCC cubes display similar mechanical behavior in terms of different stress/strain levels in the different directions. The elastic modulus is comparable for each material in the same direction; however, the direction normal to the compaction direction displays a greater elastic modulus than the parallel direction, which is represented by the increased slope of the stress/strain data for the normal direction samples.

The diametric compression test data, in Table 1, appear to give more reproducible strength values than the cubic tensile test. This probably reflects the cumulative errors associated with the two testing procedures and the differences in fracture areas; the diametric compression test restricts failure to the load line between the platens, whereas the cubic tensile test can result in failure sites within the entire gauge section of the specimen. In all cases, the samples failed in the central portions of the cubes. Invariably, the parallel direction gave a relatively even fracture surface in the center of the

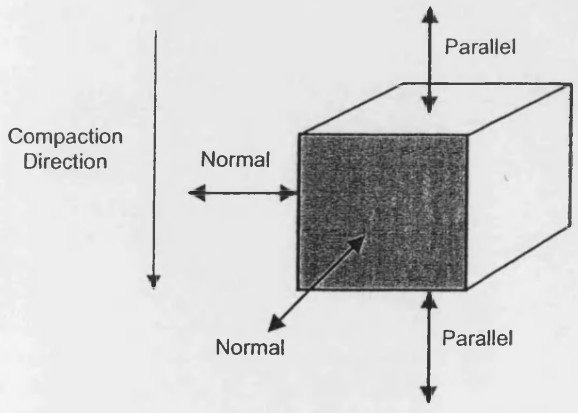


**Figure 2.** Representation of mechanical testing directions.

Table 1

*Comparison of the Tensile Strengths of Cubes and Compacts of Silicified Microcrystalline Cellulose (SMCC) and Microcrystalline Cellulose (MCC)*

| | | Tensile Strength (MPa) | |
|---|---|---|---|
| Sample | Test | Parallel | Normal |
| SMCC | Tensile | 4.7, 4.7, 4.1 | 11.2, 10.4, 8.8 |
| SMCC | Diametric tensile | — | 10.5, 10.4, 10.4 |
| MCC | Tensile | 3.9, 3.6, 3.9 | 9.6, 7.5, 9.1 |
| MCC | Diametric tensile | — | 8.3, 8.3, 8.5 |

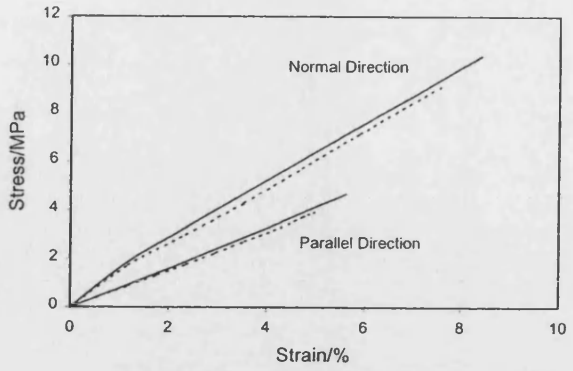


**Figure 3.** Stress/strain curves from the cubic tensile test for MCC (broken line) and SMCC (solid line) tested normal and parallel to the compaction direction.

cubes; the normal direction samples showed a rougher fracture surface. There was no evidence for failure in the glue or glue/sample interface using this procedure. Our previous experimental design did produce such failures, presumably due to nonalignment of the grips, which resulted in shear stresses applied onto the samples. These observations also suggest that the apparent reproducibility of the failure modes of the cubic samples is not an artifact of the machining process.

## Compression Testing

To evaluate further the mechanical properties of MCCs, the compression strength was studied in the directions normal and parallel to the compaction direction. Cubes of MCC and SMCC were compression tested at 0.05 mm/min. The resulting load/deflection data were converted into stress/strain data. The stress/strain data for the compression testing of cubes of MCC and SMCC are shown in Fig. 4. It can be seen from Fig. 4 that all the materials behave similarly in that the direction parallel to the compaction load exhibits greater compression strength than the normal direction. The actual compression strengths were not calculated from these experiments.

## Fracture Surfaces

The failed samples were studied visually and by SEM to assess any differences in failure modes. In the cubic tensile test, the failed surfaces obtained from cubes tested normal to the compaction direc-

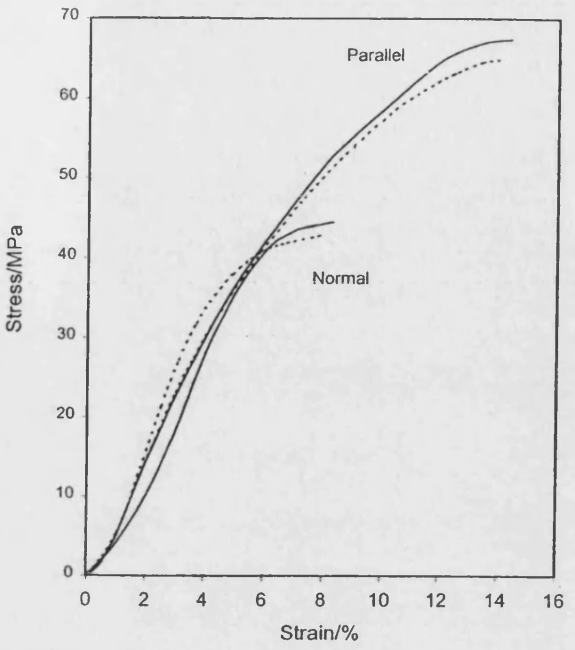


**Figure 4.** Stress/strain curves from the compression test of cubes of MCC (broken line) and SMCC (solid line) tested normal and parallel to the compaction direction.

tion were rougher in appearance than those tested parallel to the compaction direction. Typical low magnification scanning electron micrographs of fracture surfaces from samples tensile tested in the normal direction and parallel direction are shown in Figs. 5 and 6, respectively. Again, these suggest that the fracture modes in the two directions are different.

There were distinct cracks in the samples tested normal to the compaction direction (Fig. 5). These cracks were normal to the compaction direction. No similar cracks were identified in the samples tested parallel to the compaction direction (Fig. 6). The topographies of the parallel direction fracture surfaces were relatively smoother in appearance and appeared to consist of flattened discrete MCC particles. Analysis of the cubes from compression testing (micrographs not shown) using SEM suggested that cracks were more pronounced in the cubes tested normal to the compaction direction (weakest compression, greatest tensile strength): The cracks were normal to the compaction direction. The presence of these cracks normal to the compaction direction is similar to that observed for the failed surfaces of the cubic tensile test. Compression testing of

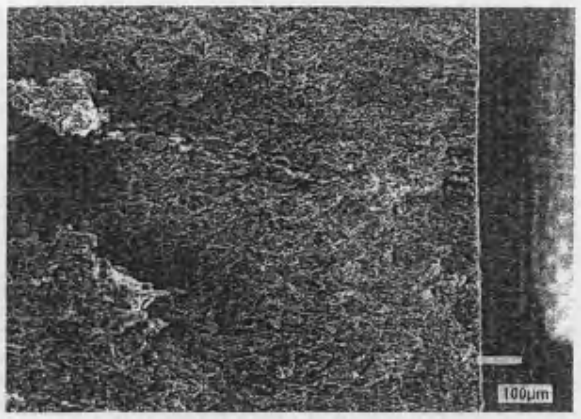


**Figure 5.** SEM image of fracture surface from cubic tensile test for SMCC tested normal (↔) to compaction direction (×100).

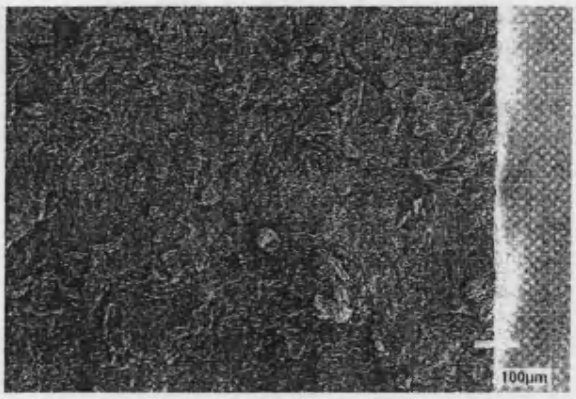


**Figure 6.** SEM image of fracture surface from cubic tensile test for MCC tested parallel (↕) to compaction direction (×100).

samples parallel to the compaction direction also resulted in cracks that were mainly normal to the compaction direction.

Obviously, the presence of decompression (post-compaction) cracks would reduce the parallel strength of MCC compacts. However, it is difficult to study the internal morphology of compacts. To try to resolve this issue, the fracture surfaces of the samples from the diametric compression test were studied using SEM. This suggested that microcracks, normal to the compaction direction, may be present in the compacts. This suggests that the presence of decompression microcracks may affect the parallel tensile strength. The compression test data suggest that the normal direction exhibits the lowest compression strength, which together with the tensile test observations, indicates the presence of weaker bonding in the parallel direction. Examination of the surfaces from the tensile test at higher magnifications showed that some intraparticle fracturing may have occurred in the normal direction, which suggests that mechanical keying may be an important factor for the strength of compacts in the normal direction.

The mechanical testing of cubes of MCC and SMCC has suggested that compacts of MCCs exhibit directional strength. The tensile strengths, as determined using the diametric compression test, suggest that compacts of SMCC exhibit greater tensile strength than those of MCC. In addition, tablets and compacts of SMCC are reported to exhibit enhanced tensile strength compared to compacts of MCC (19,20). However, the reasons for these observations are unclear.

Possible reasons for any apparent differences in the tensile strengths of compacted powders are particle size distribution and crystallinity effects. It has previously been reported that MCC and SMCC exhibit comparable crystallinity and particle size distributions, as well as similar porosities and macroscopic structures (24). To investigate the possibility that orientation of the crystallinity of the powders was occurring during compaction, the faces of the cubes were studied using XRD.

### X-ray Diffraction

Examination of the XRD patterns of MCC and SMCC powders suggested that, as previously demonstrated, there were no significant differences in crystallinity between the two materials (24). X-ray diffraction patterns obtained in the normal and parallel directions from the cubes are shown in Figs. 7 and 8. It can be seen from Figs. 7 and 8 that the data obtained from each direction for MCC and SMCC were similar, suggesting that orientation, in terms of crystallinity, is not significantly affected by the presence of silicon dioxide (in SMCC) during compaction. This is in agreement with previous studies into the crystallinity of MCC and SMCC powders (24). In addition, there appear to be changes in ratios of the diffraction lines at 20.5° 2θ and 22.5° 2θ.

It is not clear whether the reduced strength of the parallel direction is a consequence of reduced crystallinity or changes in the crystalline orientation. The

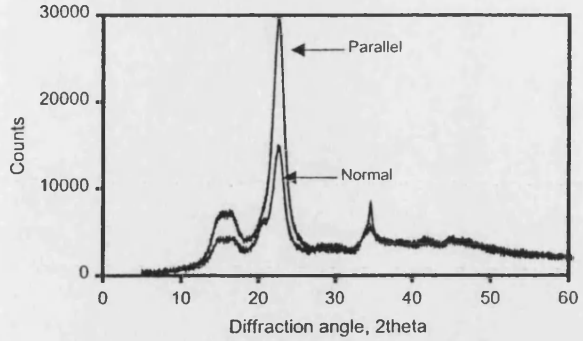


**Figure 7.** XRD patterns of SMCC machined cube.

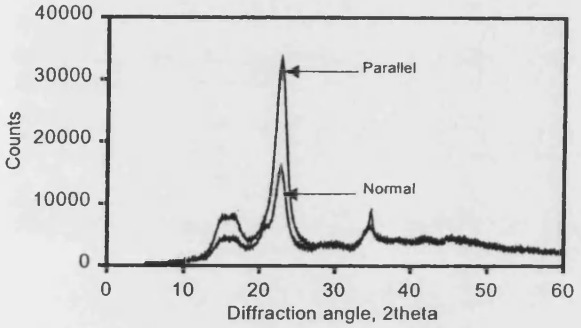


**Figure 8.** XRD patterns of MCC machined cube.

compacts exhibit anisotropic structure (in terms of amorphous/crystalline regions) and anisotropic crystallinity in terms of apparent polymorph (cellulose II 110 plane exhibits a diffraction angle at 19.8° 2θ) (25) or crystal plane orientation ratio. This suggests that the cellulose polymorphs (if cellulose II is present) are not randomly distributed in MCC, or there is some further reordering of the cellulose on compaction. If MCC and SMCC compacts were continuous matrices, then the apparent orientation of the cellulose crystallinity would be expected to result in anisotropic mechanical properties since the elastic properties of polymer crystals are reported to exhibit directional modulus (22, p. 273). However, compacted powders are more complex in that they are noncontinuous. Therefore, any direct relationship between degree of crystallinity and apparent strength is difficult to identify. However, it would be expected that, if the interparticle bonding is sufficiently strong, a direction that exhibits greater apparent crystallinity would be expected to show greater stiffness when a load is applied as described in Fig. 4.

## CONCLUSIONS

Overall, these results suggest that compression of MCC and SMCC produces anisotropic compacts in terms of strength and crystallinity. Testing of compacted MCC and SMCC using the diametric compression test suggest that SMCC compacts exhibit greater strength than those of MCC. In terms of the "true" tensile test, the directions normal to the compaction direction appear to exhibit the greatest strength for MCC and SMCC, which is in contrast to a previous study that reported that the parallel direction was stronger (13). This may reflect the speed of compression or the MCC grade used. However, the larger particle size grade in the present study would be expected to orientate during compression so that the parallel direction exhibited the lower strength. The tensile strength data obtained from mechanical testing appear to be more reproducible for the diametric compression test than for the cubic tensile test. This probably represents the errors involved in these mechanical testing procedures; the cubic tensile test involves gluing and mounting of the specimen. In terms of compact crystallinity, it would be expected that, for this system, the crystallinity (crystal structure and degree) would be unaffected as long as dissolution and/or chemical modification of the crystalline regions did not occur during the silicification process.

The present data suggest that this is the case, and that the apparent differences in strength between MCC and SMCC are not due to any significant changes in bulk directional crystallinity. However, the large apparent difference in directional strength in both MCC and SMCC compacts may be a consequence of the anisotropic structure of the compacts, which includes crystallographic, mechanical keying, and possible decompression cracking effects.

## ACKNOWLEDGMENT

We thank Penwest Pharmaceuticals Company for financial support (S. E., D. F. S.) and the provision of MCC and SMCC. We also thank a referee for useful comments.

## REFERENCES

1. Akande, O.F.; Ford, J.L.; Rowe, P.H.; Rubinstein, M.H. J. Pharm. Pharmacol. **1998**, *50*, 19.

2. Inghelbrecht, S.; Remon, J.P. Int. J. Pharm. **1998**, *161*, 215.
3. Castillo-Rubio, S.; Villafuerte-Robles, L. Eur. J. Pharm. Biopharm. **1995**, *41*, 309.
4. Zouai, O.; Thomas, C.; Pourcelot-Roubeau, Y. Drug Dev. Ind. Pharm. **1996**, *22*, 1253.
5. Lahdenpää, E.; Niskanen, M.; Yliruusi, J. Eur. J. Pharm. Biopharm. **1997**, *43*, 315.
6. Buckton, G.; Yonemochi, E.; Yoon, W.L.; Moffat, A.C. Int. J. Pharm. **1999**, *181*, 41.
7. Nyström, C.; Alderborn, G.; Duberg, M.; Karehill, P.-G. Drug Dev. Ind. Pharm. **1993**, *19*, 2143.
8. Roberts, R.J.; Rowe, R.C.; York, P. Int. J. Pharm. **1993**, *91*, 173.
9. Baie, S.B.; Newton, J.M.; Podczeck, F. Eur. J. Pharm. Biopharm. **1996**, *43*, 138.
10. Bassam, F.; York, P.; Rowe, R.C.; Roberts, R.J. Int. J. Pharm. **1990**, *64*, 55.
11. Davies, P.N.; Newton, J.M. In *Pharmaceutical Powder Compaction Technology*; Alderborn, G., Nyström, C., Eds.; Marcel Dekker: New York, 1996; 171.
12. Karehill, P.G.; Glazer, M.; Nyström, C. Int. J. Pharm. **1990**, *64*, 35.
13. Newton, J.M.; Alderborn, G.; Nyström, C. Powder Technol. **1992**, *72*, 97.
14. Williams, R.O., III; McGinity, J.W. J. Pharm. Sci. **1989**, *78*, 1025.
15. Whiteman, M.; Yarwood, R.J. Powder Technol. **1988**, *54*, 71.
16. Rowe, R.C.; McKillop, A.G.; Bray, D. Int. J. Pharm. **1994**, *101*, 169.
17. Doelker, E.; Gurny, R. Powder Technol. **1987**, *52*, 207.
18. Ek, R.; Wormald, P.; Östelius, J.; Iverson, T.; Nyström, C. Int. J. Pharm. **1995**, *125*, 257.
19. Sherwood, B.; Becker, J. Pharm. Technol. **1998**, *22*, 78.
20. Edge, S.; Steele, D.F.; Chen, A.; Tobyn, M.J.; Staniforth, J.N. Int. J. Pharm. **2000**, *201*, 67.
21. Fell, J.T.; Newton, J.M. J. Pharm. Sci. **1972**, *59*, 688.
22. Young, R.J. *Introduction to Polymers*; Chapman and Hall: London, 1983; 216.
23. Khan, F.; Pilpel, N.; Ingham, S. Powder Technol. **1988**, *54*, 161.
24. Tobyn, M.J.; McCarthy, G.P.; Staniforth, J.N.; Edge, S. Int. J. Pharm. **1998**, *169*, 183.
25. Isogai, A. In *Cellulosic Polymers Blends and Composites*; Gilbert, R.D., Ed.; Hanser Verlag: Munich, 1994; 4.

ELSEVIER

International Journal of Pharmaceutics 200 (2000) 67–72

international journal of pharmaceutics

www.elsevier.com/locate/ijpharm

# The mechanical properties of compacts of microcrystalline cellulose and silicified microcrystalline cellulose

Stephen Edge [a], D. Fraser Steele [a], Ansong Chen [b], Michael J. Tobyn [a], John N. Staniforth [a,*]

[a] *Pharmaceutical Technology Research Group, Department of Pharmacy and Pharmacology, University of Bath, Bath BA2 7AY, UK*

[b] *Department of Materials Science and Engineering, University of Bath, Bath BA2 7AY, UK*

Received 9 July 1999; received in revised form 19 December 1999; accepted 7 January 2000

**Abstract**

The mechanical properties of compacts of unlubricated microcrystalline cellulose and silicified microcrystalline cellulose were evaluated using the diametric tensile test. The results suggested that, under comparable testing conditions, compacts of silicified microcrystalline cellulose exhibited greater strength than those of microcrystalline cellulose. In addition to enhanced strength, silicified microcrystalline cellulose compacts exhibited greater stiffness and required considerably more energy for tensile failure to occur. Comparison of the data with that obtained for a dry blend of silicon dioxide/microcrystalline cellulose suggested that the functionality benefits of silicification were not due to a simple composite material model. © 2000 Elsevier Science B.V. All rights reserved.

*Keywords:* Silicified microcrystalline cellulose; Mechanical property; Strength

## 1. Introduction

Microcrystalline cellulose (MCC) is a widely used tableting excipient. In terms of tableting technology, the material is described as a 'filler/binder' in that it is usually added to formulations to enhance compactibility. Recently, a new, modified MCC, silicified microcrystalline cellulose (SMCC), has been developed that is reported to exhibit improved binding functionality in both direct compression and wet granulation (Sherwood and Becker, 1998).

When considering any apparent improved strength benefits of an excipient, it is important to understand the mechanisms of bonding in a compacted material. The reported data for the improved functionality of SMCC was obtained using high-speed tableting. However, these data do not explain the reasons for this improved performance; in particular, whether it is solely a SMCC interparticle interaction or some synergistic effect is occurring in the presence of lubricant.

In terms of materials categorisation, MCC can be considered to be a semicrystalline polymer. It would be expected that the mechanical properties of the polymer would be dominated by the crys-

* Corresponding author. Fax: +44-1225-826-114.
*E-mail address:* prsjns@bath.ac.uk (J.N. Staniforth)

0378-5173/00/$ - see front matter 
PII: S0378-5173(00)00343-4

talline domains. This is particularly true for semicrystalline polymers such as polyethylene. In these types of 'plastic' polymer systems, processing is achieved by thermally induced flow, i.e. heating to the melting point ($T_m$) of the crystallites; the glass transition ($T_g$) behaviour is of little importance (in terms of processing). This is in part due to the fact that even though these types of systems can be considered to be random block copolymer chains (crystalline/amorphous), the microscopic structure is essentially isotropic. This is not true for MCC. Indeed, the structure of MCC is complex but it can be considered to consist of particulate aggregates of cellulose (Chatrath, 1992). It is generally accepted that the material contains amorphous and crystalline regions as well as other ordered structures (Doelker et al., 1987). In terms of processing, MCC is treated very differently from other polymer systems in that $T_m$ and $T_g$ are not considered; the material is simply compressed into a desired shape. As it is unlikely that $T_m$ will be reached, it will be the properties of the cellulose structures (as particles and polymers) that will dictate the compression and compaction behaviour of the material. The amorphous regions will be important in terms of chemistry and $T_g$, especially when processing, storage and testing conditions are considered. It has been reported that silicification of MCC results in no discernible modification of MCC in terms of primary structure (Buckton et al., 1999), as well as particle size and distribution, porosity and crystallinity (Tobyn et al., 1998). These latter three particle characteristics will be crucial factors in MCC compactibility. In order to try to understand the mechanisms by which the functionality of SMCC is enhanced, the materials (MCC and SMCC) were studied as simple powders and compacted in the absence of lubricants at a relatively slow compression rate.

## 2. Materials and methods

### 2.1. Materials

Microcrystalline cellulose (Emcocel 90M, MCC90 and Emcocel 50M MCCO50; Penwest Pharmaceuticals Co., NY) and silicified microcrystalline cellulose (based on Emcocel 90M, SMCC90, 2% w/w silicon dioxide content and Emcocel 50M, SMCC50, 2% w/w silicon dioxide content; Penwest Pharmaceuticals Co., NY) were used as supplied. A 'dry' mix consisting of 9.80 g Emcocel 90M and 0.20 g dried colloidal silicon dioxide (15% dispersion w/v Cab-o-Sperse; Cabot Corporation, USA) was prepared by low shear mixing (Turbula). Powders were stored under ambient conditions; the temperature and relative humidity were regularly monitored.

### 2.2. Preparation of compacts

Compacts were prepared by compacting powders (6 g) in a die (25 mm diameter, heat-treated silver steel) using a load of 100 kN (200 MPa), at a rate of 10 mm/min and a dwell time of 1 min using an Instron 1185 test machine. Compacts were tested on the same day as preparation, typically 3 h after compaction. This allows compaction and testing to be performed under comparable ambient conditions (temperature and relative humidity).

### 2.3. Testing of compacts

Diametric tensile testing was performed at 5 and 0.05 mm/min using an Instron 1125 test machine. Tensile strength was calculated using the failure load over the diametric area of the compacts (Fell and Newton, 1972). Stress was calculated by dividing the applied load by the compact cross-sectional area (diameter × height). Strain was calculated as a percentage of the deformation divided by the original diameter.

## 3. Results

There are many variables that need to be considered when comparing experimental data obtained for materials. This is especially true for compacted powders. When pharmaceutical powders are compacted, data such as crushing strength or tensile strength is often reported to describe the integrity of the compact. It is impor-

ant to remember that the compaction and testing conditions will affect the resulting test data of the same material under investigation, which makes comparisons with literature values difficult. In general, there are three main sets of variables that need to be considered when comparing the mechanical properties of compacted powders:

1. compact preparation and testing conditions;
2. powder and compact storage conditions;
3. powder and compact characteristics.

Compaction and testing conditions can be controlled, and it is the interpretation of the 'sample characteristics' that are likely to be the key to understanding the properties of compacted materials. This is a complex subject area and covers: particle size, distribution and shape, chemical composition, surface area, porosity, crystallinity, batch-to-batch variability, etc.

In the case of the present study, the base material in MCC and SMCC is similar in that the cellulose polymers will have comparable characteristics, i.e. molecular weight ($M_w$) and molecular weight distribution (polydispersity); these two characteristics will affect melt viscosity. As previously stated, it has been reported that there are no significant differences in the particle size and distribution, porosity and crystallinity of the cellulose in MCC90 and SMCC90 (Tobyn et al., 1998). This alleviates some of the problems discussed previously concerning quantifying apparent differences in properties of materials. It has been reported that silicification of MCC results in a marked difference in surface topography and that silicon dioxide appears to be primarily located in the surface of SMCC particles (Edge et al., 1999). This would be expected to have an effect on the compactibility of MCC since surface roughness is reported to influence interfacial adhesion in MCC/MCC laminates (Karehill et al., 1990). In order to evaluate the effect of this apparent surface modification, compacts of MCC and SMCC were prepared and mechanically tested using the diametric tensile test. One important aspect of pharmaceutical mechanical testing is to prepare and test samples using the same protocols. Additionally, it is essential that compacts of comparable density are prepared since porosity (as in relative density) has a marked effect on strength. Indeed, relative density can be a more useful representation of the total stress that a powder bed has experienced during the compaction cycle.

### 3.1. Determination of suitable compaction and testing protocols

Before the mechanical properties of compacted powders can be compared, it is important that reproducible compaction and testing protocols are used. Not only will this produce reproducible data, but the evaluation of suitable conditions may allow any apparent differences in properties to be magnified. For our powder compaction studies, many compression rates and testing conditions, including the effect of variations in ambient temperature and humidity, were studied until satisfactory protocols were identified.

### 3.2. Diametric tensile testing

A variety of techniques have been used to investigate the mechanical properties of compacted pharmaceutical powders (Davies and Newton, 1996). The diametric tensile test is an indirect method of determining the tensile strength of homogeneous disk-shaped materials. The test is widely employed for testing the strength of pharmaceutical (Karehill and Nyström, 1990; Elamin et al., 1994) and ceramic (Thoms et al., 1980) compacts. In this test, tensile failure is a result of the application of a compression load normal to the compaction direction. This is in contrast to a 'true' tensile test, where materials are tested in tension and no compression load is applied to the sample in the direction normal to the tensile stress.

### 3.3. Tensile strength

The tensile strength of compacts of SMCC and MCC were determined using the diametric tensile test at 5 mm/min. Eight replicate samples of each excipient were tested. The results are shown in Table 1. It can be seen from Table 1 that, as expected, MCC50 produces stronger compacts than MCC90 (Bolhuis and Chowhan, 1996). Silicification appears to produce compacts of similar

strength, at comparable silicon dioxide contents, for the two typical grades tested. In addition, the apparent strength benefit of silicification appears to be greater for the larger particle-sized MCC90, under these specific conditions, possibly reflecting increased surface coverage of silicon dioxide of the larger particle sized 90 μm grade.

### 3.4. Toughness

Tensile strength (or crushing strength) is often used to describe the strength of a compact. However, this measurement does not fully reflect inter- and intraparticle cohesion within a compact. The cohesion (integrity or binding capability) in a compact may be further represented by the energy of failure. The energies of failure during diametric tensile testing at 5 mm/min (Table 1) were calculated by integration of the area under the load/deflection curve of the tensile test. The results for MCC90, SMCC90 and a dry blend of MCC90 and silicon dioxide (2% w/w), together with the maximum deflection data, are given in Table 2. It can be seen from Table 2 that silicification produces compacts of greater ductility (deflection under load) than MCC. However, the effect on the energy of failure is even more pronounced, with an increase of over 50% in value (under these conditions). In addition, the tensile strength, energy of failure and ductility of compacts of a dry blend of MCC90 and silicon dioxide (2% w/w) were less than those for pure MCC90.

Table 1
Tensile test data for compacts of MCC, SMCC and a blend of MCC90 and dried colliodal silicon dioxide[a]

| Sample | Tensile strength (MPa) | Density (g/cm$^3$) |
|---|---|---|
| MCC50 | 11.5 ± 0.3 | 1.45 ± 0.03 |
| SMCC50 | 13.0 ± 0.3 | 1.42 ± 0.02 |
| MCC90 | 10.5 ± 0.2 | 1.45 ± 0.02 |
| SMCC90 | 12.7 ± 0.2 | 1.45 ± 0.02 |
| Blend[b] | 9.1 ± 0.2 | 1.44 ± 0.02 |

[a] Powder (6 g) compressed using a load of 100 kN at 10 mm/min, with a dwell time of 1 min. Tested at a rate of 5 mm/min. Values after ± represent the range of measurements ($n = 8$).
[b] MCC90 and dried colloidal silicon dioxide (2% w/w).

Table 2
Mechanical properties of compacts of MCC90, SMCC90 and a blend of MCC90 and dried colliodal silicon dioxide[a]

| Sample | Deflection (mm) | Tensile strength (MPa) | $E_f$ (J) |
|---|---|---|---|
| MCC90 | 0.86 ± 0.01 | 10.5 ± 0.2 | 1.6 ± 0.1 |
| SMCC90 | 1.11 ± 0.02 | 12.7 ± 0.2 | 2.6 ± 0.1 |
| Blend[b] | 0.70 ± 0.03 | 9.1 ± 0.2 | 1.2 ± 0.1 |

[a] Powder (6 g) compressed using a load of 100 kN at 10 mm/min, with a dwell time of 1 min. Tested at a rate of 5 mm/min. Values after ± represent the range of measurements ($n = 8$).
[b] MCC90 and dried colloidal silicon dioxide (2% w/w).

### 3.5. The effect of test rate

The values describing the mechanical properties of materials are usually strain rate dependent, i.e. they vary according to the rate at which the stress is applied to the sample (test rate). This phenomenon has previously been reported for MCC-based tablets (Rees et al., 1970). Our preliminary investigations to determine compaction and testing protocols confirmed this for MCC. In order to understand more fully the effect of test rate on apparent mechanical properties, compacts of MCC and SMCC were tested at the slower rate of 0.05 mm/min. The tensile test data was integrated to calculate the energies of failure, and the results are shown in Table 3. It can be seen from Table 3 that, again, silicified MCCs produce compacts which exhibit greater tensile strength, greater ductility and greater energies of failure than their respective unmodified MCCs, in agreement with the data in Table 2. The values of tensile strength are apparently lower than values obtained at the rate of 5 mm/min, which suggests that, as expected, the apparent mechanical properties of MCCs are strain rate dependent. It is also clear that the strain rate dependence of the mechanical behaviour of MCC has not been changed by the silicification process.

### 3.6. Effective stiffness

The slopes of the load/deflection and stress/strain curves can give an indication of the resis-

Table 3
Mechanical properties of compacts of MCC and SMCC[a]

| Sample | Test rate (mm/min) | Deflection (mm) | Tensile strength (MPa) | $E_f$ (J) | Density (g/cm$^3$) |
|---|---|---|---|---|---|
| MCC90 | 5 | 0.88 ± 0.02 | 10.3 ± 0.2 | 1.7 ± 0.1 | 1.45 ± 0.01 |
| MCC90 | 0.05 | 0.73 ± 0.02 | 8.9 ± 0.3 | 1.2 ± 0.2 | 1.44 ± 0.01 |
| SMCC90 | 5 | 1.13 ± 0.03 | 12.7 ± 0.3 | 2.6 ± 0.1 | 1.44 ± 0.01 |
| SMCC90 | 0.05 | 0.96 ± 0.04 | 11.1 ± 0.4 | 2.0 ± 0.2 | 1.45 ± 0.01 |

[a] Powder (6 g) compressed using a load of 100 kN at 10 mm/min, with a dwell time of 1 min. Tested at a rate of 5 and 0.05 mm/min. Values after ± represent the range of measurements ($n = 4$).

tance of a material to deformation, i.e. the effective stiffness or stiffness. The data (load/deflection), for compacts of SMCC90 and MCC90 that were subjected to diametric tensile testing (at 0.05 and 5 mm/min), were converted to stress/strain curves. A typical set of stress/strain curves is shown in Fig. 1. The data in Fig. 1 suggest that silicification produces a material which, when compacted, exhibits a slightly greater stiffness normal to the compaction direction when tested at the slow test rate of 0.05 mm/min. Testing at 5 mm/min resulted in similar load/deflection and stress/strain curves for both sets of materials. All the samples tested exhibited this mechanical behaviour. In addition, the similarity in stiffness of the different materials suggests the presence of similar bonding mechanisms (under these conditions).

### 3.7. Reinforcement mechanisms

Simple compaction and testing of powders of SMCC and MCC has suggested that SMCC exhibits enhanced tensile strength compared with MCC. If SMCC was a simple composite of MCC and silicon dioxide then, under comparable testing conditions, its maximum strength (in tension and compression) can be very roughly approximated to:

$$\sigma_{composite} = \sigma_{MCC} v_{MCC} + \sigma_{SD} v_{SD}$$

where $\sigma$ is the strength and $v$ the volume fraction.

The tensile test data for SMCC, MCC and a blend of MCC and silicon dioxide suggest that the strength of compacts of SMCC is greater than would be expected for a simple composite, given that compacted silicon dioxide is a very brittle material. However, the preparation and testing of a homogeneous blend that contains silicon dioxide particles of similar size to those in SMCC would address this hypothesis. This probably reflects the method of silicification in that the size and distribution of silicon dioxide aggregates and the MCC/silicon dioxide interfacial adhesion determines the compactibility of SMCC. The strength enhancement in SMCC compacts may be as a consequence of mechanical reinforcement.

## 4. Conclusions

The compaction of MCC and SMCC at a relatively slow compression rate results in compacts of comparable relative density, suggesting that the two materials exhibit comparable compression behaviour. The tensile strength (diametric tensile test) of compacts of SMCC was found to be greater than that of the respective MCC, the

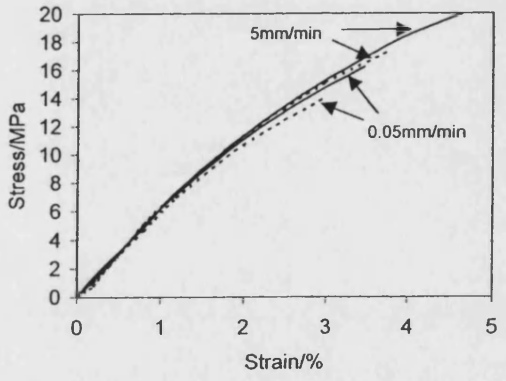


Fig. 1. Stresss/strain data of compacts of MCC90 (– – –) and SMCC90 (——) from the tensile test experiments of Table 3. Tested at 5 and 0.05 mm/min.

apparent enhancement being greater for the larger 90 μm particle-sized grade. The effect on compact toughness was even more pronounced, the energies of failure being significantly greater for compacts of SMCC. Again, the effect was greater for the larger particle-sized 90 μm grade. These apparent differences in mechanical strength cannot be satisfactorily explained in terms of modifications of the particle size, porosity or crystallinity of SMCC. Our examination of the failure surfaces using scanning electron microscopy suggested that when compacts of MCC fail during testing, the failure primarily occurs at the interparticle interfaces. The mechanical data together with the comparable densification characteristics of MCC and SMCC suggest that this apparent strength enhancement may be a consequence of an interfacial interaction rather than modification of bulk MCC properties. These data are in agreement for data reported for lubricated SMCC and MCC tablets in that silicification of MCC appears to produce materials with greater binding capability. In the test rate regimes used, it has also been shown that the higher the rate, the higher the apparent strength.

## Acknowledgements

We thank Penwest Pharmaceuticals Co. for financial support (S.E.) and the provision of MCC and SMCC.

## References

Bolhuis, G.K., Chowhan, Z.K., 1996. Materials for direct compression. In: Alderborn, G., Nyström, C. (Eds.), Pharmaceutical Powder Compaction Technology. Marcel Dekker, New York, pp. 419–500.

Buckton, G., Yonemochi, E., Yoon, W.L., Moffat, A.C., 1999. Water sorption and near IR spectroscopy to study the differences between microcrystalline cellulose and silicified microcrystalline cellulose before and after wet granulation. Int. J. Pharm. 181, 41–47.

Chatrath, M., 1992. The effect of wet granulation on the physico-mechanical characteristics of microcrystalline cellulose. PhD Thesis. University of Bath.

Davies, P.N., Newton, J.M., 1996. Mechanical strength. In: Alderborn, G., Nyström, C. (Eds.), Pharmaceutical Powder Compaction Technology. Marcel Dekker, New York, pp. 165–191.

Doelker, E., Gurny, R., Schurz, J., Jånosi, A., Matin, N., 1987. Degrees of crystallinity and polymerisation of modified cellulose powders for direct tableting. Powder Technol. 52, 207–213.

Edge, S., Potter, U.J., Chen, A., Steele, D.F., Tobyn, M.J., Staniforth, J.N., 1999. The location of silicon dioxide in silicified microcrystalline cellulose. Pharm. Pharmacol. Commun. 5, 371–376.

Elamin, A.A., Alderborn, G., Ahlneck, C., 1994. The effect of pre-compaction processing and storage conditions on powder and compaction properties of some crystalline materials. Int. J. Pharm. 108, 213–224.

Fell, J.T., Newton, J.M., 1972. Determination of tablet strength by diametrical compression test. J. Pharm. Sci. 59, 688–691.

Karehill, P.G., Nyström, C., 1990. Studies on direct compression of tablets. XXII. Investigation of strength increase upon aging and bonding mechanisms for some plastically deforming materials. Int. J. Pharm. 64, 27–34.

Karehill, P.G., Glazer, M., Nyström, C., 1990. Studies on direct compression of tablets. XXIII. The importance of surface roughness for the compactibility of some directly compressible materials with different bonding and volume reduction properties. Int. J. Pharm. 64, 35–43.

Rees, J.E., Hersey, J.A., Cole, E.T., 1970. The effect of rate on the strength of tablets. J. Pharm. Pharmacol. 22 (Suppl.), 64S–69S.

Sherwood, B.E., Becker, J.W., 1998. A new class of high functionality excipients: silicified microcrystalline cellulose. Pharm. Technol. 22, 78–88.

Thoms, M.B., Doremus, R.H., Jarcho, M., Salsbury, R.L., 1980. Dense hydroxyapatite: fatigue and fracture strength after various treatments, from diametral tests. J. Mater. Sci. 15, 891–894.

Tobyn, M.J., McCarthy, G.P., Staniforth, J.N., Edge, S., 1998. Physicochemical comparison between microcrystalline cellulose and silicified microcrystalline cellulose. Int. J. Pharm. 169, 183–194.